Non-man-entry sewer renovation robot characteristics.

BROADHURST, Simon John.

REFERENCE

Fines are charged at 50p per hour

Non-Man-Entry Sewer Renovation

Robot Characteristics

Simon John Broadhurst

A thesis submitted in part fulfilment of the requirements of

Sheffield Hallam University

for the degree of Doctor of Philosophy

October 2000

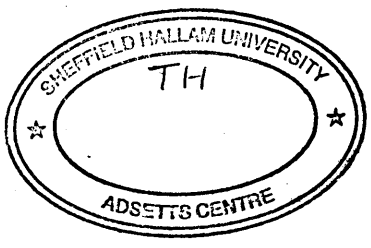
SHEFFIELD HALLAM UNIVERSITY
TH
ADSETTS CENTRE

The reported work lies in the area of automation in the construction industry, and involves multi-disciplinary engineering studies. In particular, sewer renovation methods, computer vision (CV) and robotics are all included. More specifically, the key objective of the research programme was to investigate the characteristics of retrofit components suited to mounting on an industrial / proprietary sewer tractor. The overall aim was the provision of a non-man-entry (NME) sewer renovation robot to undertake reconnection of lateral junctions, following a cured-in-place (CIP) relining process. The programme primarily involved theoretical studies of the requisite sensory and kinematic components, incorporation of a novel computer vision sensing system and production of a chainage measurement system and robotic drill task arm. The theory was supported by laboratory testing using a modified proprietary tractor, with emphasis placed on promoting applications of information technology driven systems (i.e. CV) to construction-industry tasks within hazardous environments involving significant health issues. The use of such techniques in the construction industry is rare.

Chapter 1 reviews the context and history of sewer maintenance/dereliction in the UK. NME sewers are the most common type and are, by definition, difficult to maintain. Renovation, typically employing CIP liners, is therefore a cost-effective alternative to replacement. Lateral connections are, inevitably, blocked off during the relining process; it is suggested that application of a robust robotic system to the task of reconnecting them is novel and offers clear potential within such a hazardous environment.

Chapters 2 and 3 develop the underlying theoretical models of the CV and kinematic systems respectively. The novel CV work (provided by third party specialists employing the TINA CV research environment) was incorporated by the author to provide detection and classification of lateral junctions, crucially noting the particular properties of direct and reflected illumination. Classification aspects include estimation of lateral / NME intersection angle and closure-to-target distance from the robot. The author proposes a separate procedure for estimating lateral diameter. A chainage measurement system, using a rotary encoder and inclinometer, was developed to determine invert path distance travelled. This allows for the inevitable wander and thereby gives the system robustness. The novel application of GRASP (a robotic modelling and simulation design tool) to NME environments, provided the ability to model arm designs without the need for the production of more than one expensive physical prototype. A mathematical solution for determining the requisite arm kinematics is presented.

Chapter 4 details the hardware requirements of the robotic system components, whilst Chapters 5 and 6 present the laboratory evaluation results for the kinematic and CV systems respectively. The abilities of the CV system qualitatively to detect laterals under reflected illumination, and to provide quantitative classification data, are demonstrated. The chainage measurement system is assessed under a variety of initialisation conditions to determine suitability to task, and the ability of the robotic arm to physically simulate lateral reconnection is investigated.

Chapter 7 discusses the specification for an industrially-applicable prototype, based on the findings herein. Appropriate comparisons with the pre-prototype system are made, including cost. Finally, Chapter 8 draws conclusions and makes suggestions for further work. Supporting documentation is provided in Chapter 9 and the Appendices.

ACKNOWLEDGEMENTS

The author would like to thank Dr N Taylor, Prof. G Cockerham and Dr T Pridmore, supervisors of this research programme, for their continued guidance and support throughout this work.

Thanks must also be given to J Stanley Esq. for his technical help regarding the learning and implementation of GRASP and to the many technicians involved with the construction of the robot for their invaluable help; although too numerous I would particularly like to mention K Wells Esq., S Tunnard Esq., R Wilkinson Esq. and B Palmer Esq. Thanks are also given to Dr S Fu and to K Soar Esq. for much needed support regarding the programming aspects of this work.

The author wishes to draw attention to the fact that distinct 'external' party input was received regarding certain specialist computer vision aspects of the work reported herein. This input centres on Dr T Pridmore and use of the TINA Vision Research Environment made available by the Artificial Intelligence Vision Research Unit (AIVRU), University of Sheffield; this is specifically identified as appropriate in the text.

Appreciation must also be given to the following industrialists, M Shaw Esq. of NUFLOW Systems Ltd, N Bunting Esq. and R Chapman Esq. of Sub Tech Limited and to G Milward Esq., Consultant, for their technical advice regarding Non-Man-Entry sewer renovation. The author would like to express thanks to Hepworths Building Products, UK, for provision of the 'Pipe Rig' materials.

The author is especially grateful to his parents, Kathleen and Peter, and to his wife Lisa for their continued support and encouragement throughout the period of this work.

CONTENTS

CHAPTER 1

INTRODUCTION

"Man is borne to thrive with pure air to breathe, pure water to drink and pure soil to live on. The impurities which tend to render air, water, and soil unfavourable for his best development are the products of his own life. The removal of the source of this impurity must be effected by his own act." - George E Waring Jr, 1880, [1].

1.1 THE SEWER ENGINEERING PROBLEM

1.1.1 Context

Until the 19th Century, no public underground network for the distribution of clean fresh drinking water nor the transportation/disposal of waste (in the form of suspended solids) existed. It was not until during the Industrial Revolution of the late 18th/19th Century that the need for systems of water sanitation in the newly developing large conurbations became evident [2]. Large increases in industrial and domestic waste polluted water supplies such as wells and streams which continued to be used as sources of fresh drinking water. Consequently high mortality from the then unknown water borne diseases of typhoid, cholera and dysentery was widespread. No link between them was discovered until 1854, when Dr John Snow first applied what is now known as Epidemiology. Dr Snow correlated the cases of a violent cholera outbreak with the use of a particular communal water pump after 500 people living in close proximity to, and drawing their water from it, died [3]. The work of the then Secretary To The Poor Law Commission, Edwin Chadwick, who, realising the link between consuming polluted water and early death, commissioned the report of 1841 concerning the

Sanitation Of Towns [2], led to the introduction of the first Public Health Act of 1841. Subsequent revisions developed into the embodiment of sewerage schemes first proposed by Chadwick. Construction of large brick sewers in major cities was to become the basis of the present sewerage network in the United Kingdom.

The initial development of the water supply industry throughout the UK was slow, and the shortage of sufficient drinking water supplies provided the incentive for constructive and progressive action to rectify this. Even so, at the beginning of the nineteenth century no great schemes of water supply had been initiated, and until the Industrial Revolution had well passed its first half-century, there were practically no piped supplies of water and no sewerage systems. However, by 1961 every town and nearly every village had a constant piped supply of wholesome water, together with a water-borne sewerage system [4]. This country has one of the oldest and most extensive sewer systems in the world , and since our Victorian forefathers helped to build similar systems in many other countries, the dereliction encountered in this country also has implications overseas; many sewers dating back to Victorian times are still in use today [5].

From the above it may be suggested that through the provision of fresh drinking water supply and waste water removal the Civil Engineer has done more for Public Health than the Medical Profession has ever achieved. The provision of such a sewerage system was at the time considered to be a major engineering achievement, though inadequate maintenance measures have left a legacy of disrepair for today's engineers.

1.1.2 Sewer Maintenance Considerations

In the early 1980's an estimated 2500-5000 sewer collapses were occurring in Britain every year [6], Between 1978 and 1981 Manchester, one of the worst hit areas, suffered 45 sewer collapses necessitating many road closures and restrictions to public access, resulting in much disruption to traffic and commerce and presenting risk to public health [7], The problems of sewer dereliction, refer to Figures 1.1 and 1.2, exist to varying extents throughout the industrial areas of the North West in particular and in other locations throughout the country, and are in general attributable to infrequent maintenance resulting in general disrepair [8, 9], Statistics relating to current sewer dereliction are elusive at best though figures relating to 1985 data would not be considered outlandish today [10], The structural condition of these sewers, where known, is assigned a grade. Grade 1 indicates sound structural integrity whereas grade 5 points to likely imminent collapse of the sewer system if rehabilitation works are not soon initiated.

Figure 1.1: Sewer Dereliction - Example 1

'Complete loss of sewer structural integrity' [5]

Figure 1.2: Sewer Dereliction - Example 2

'Sewer cross-section defonned and approaching collapse' [5]

At the time of study approximately 95% of the UK population were connected to the main drainage system, which is the highest proportion by world standards. Of the 260,000km of sewer existing, in the region of 5% was of man-entry classification which as the name suggests are of large enough internal diameter to admit manned inspection (i.e. greater than lm). Approximately 95% of sewers are therefore of non-man-entry (NME) dimensions and limited access to these must be obtained directly from manhole locations, or from within man-entry systems with which they intersect. Consequently, most maintenance operations involve NME sewers and lack of human access clearly complicates matters. Sewers inherently transport media which are hazardous to the health of any operative associated with, or working within, this environment. Numerous fatalities have occurred directly associated with the industry, due to disease or from poisonous gas inhalation. However, the industry has enforced safety training equipment, now in general use, and this has significantly reduced the number of reported accidents occurring in recent times. Information obtained from the Health and Safety Executive

indicates a provisional figure of 1159 reported injuries, to sewerage disposal employees, over the period 1985/92 [11].

The dangers aside, man-entry sewers are relatively straightforward to maintain, subject to economic considerations. Little is known concerning the structural integrity and flow performance of the more numerous NME types, due to their comparative inaccessibility. Moreover, the actual location of many of these sewers is unknown due to incomplete and/or out of date council records. Usually a problem is only first recognised when a collapse, blockage or flood situation occurs, i.e. reactive maintenance.

Statistics [10] indicate that 2% of all UK sewers were in critical need of repair in 1985, accounting for over 5000km of NME sewer pipe requiring immediate attention. It would not be unreasonable to assume, based on the general lack of funding for purposes such as maintenance, that the current percentage exceeds the 1985 estimate and that the problem of sewer maintenance is growing. Proposed EC legislation demands a reversal of this situation; the research program would therefore appear timely.

Until the advent of 'closed circuit television' (CCTV) sewer inspections in the 1960's, very little was known about the condition of the majority of the nation's sewerage system; incomplete information on sewer location and integrity present maintenance difficulties for every local authority, though many are currently in the process of updating their records through the service of specialist CCTV surveying contractors. Further, many authorities felt that there was serious neglect of even those man-entry

accessible sewers that it was possible to inspect, principally due to the low priority put on pre-emptive sewer rehabilitation [5].

Sewer surveys are generally initiated on behalf of the presiding Water Authority (the client), or by the clients agents (typically a local Council Authority or Consultant) as either part of a rolling programme of sewer network inspection, or following a report of a network failure. The failure may present itself as a flooding problem or surcharge of the sewer system. In any event, such a failure indicates that either a sewer collapse or localised blockage has occurred on the system. A specialist contractor is then employed to undertake a routine CCTV sewer survey. A camera, generally mounted on a motorised tractor unit remotely driven along the sewer, is conveyed along the sewer under consideration in the direction of flow. The CCTV signal is relayed in real time and monitored; problem areas are identified and logged.

In the case of a rolling programme of sewer inspection, many of these surveys not only serve to identify and locate potential trouble spots requiring basic maintenance, but also provide basic locations of manholes and lateral connections with other sewers. Information provided by these surveys allows decisions to be made regarding what remedial measures are required for particular sewer sections. Any decision to replace or renovate cannot simply be based upon the extent of sewer deterioration found. Replacement, involving ground-works is an invariably costly exercise, especially in urban and inner-city areas, due in part to the resulting disruption to local industry and commerce and is generally only considered when complete structural collapse of the existing sewer is imminent or has already occurred. Otherwise, as many of the materials used in the varying renovation processes, when in composite with the existing sewer,

restore if not exceed the required structural capacity of the sewer system, the option of renovation provides a cost effective alternative [12].

This research programme is therefore primarily concerned with aspects of renovation of NME sewers.

1.1.3 Renovation

Renovation is defined as methods by which the performance of a length of sewer is improved by incorporating the original sewer fabric, but excluding maintenance operations such as isolated local repairs and root or silt removal [5].

Sewer renovation is not a new area of public health engineering. Preventative maintenance and renovation in one form or another have taken place from the earliest days of sewer construction. Repointing of brick sewers certainly used to find more favour than in recent times. Whilst a wider variety of renovation methods and materials is available for man entry systems [5], insertion of a liner into the length to be rehabilitated is predominantly the only cost effective renovation solution for NME sewers. The four most significant issues to be addressed therefore, when considering the option to renovate, are economic, hydraulic capacity, material characteristics and strength;

(i) Economic - generally, renovation of a sewer length by lining can be undertaken for less than 75% of the equivalent open cut, i.e. in trench, renewal cost.

(ii) Hydraulic capacity - with the exception of slip-lining (see later), lining techniques, in general, do not significantly reduce the hydraulic capacity of the sewer. The thickness of the liner material introduces a reduction in the cross sectional area of the renovated sewer when compared to the pre-renovated one, however, the resulting improvement in hydraulic performance of the renovated sewer far outweigh this slight disadvantage.

(ii) Material considerations - factors such as durability, chemical and abrasion resistance, and strength are of importance. It may be concluded that, when used within their known limitations, established renovation lining materials can be assigned a minimum design life of at least 50 years.

(iii) Strength - lining systems can be confidently designed to at least be equal to a new sewer in structural capacity.

Lining techniques can therefore be used to improve the structural strength of the sewer, to improve the hydraulic characteristics, to reduce infiltration or to provide an improved abrasion or chemical resistance. For NME sewer renovation only two suitable lining systems are currently available, these being 'slip-lining' and 'cured-in-place' (CIP) lining.

Traditional slip lining systems generally involve the insertion of butt fusion welded or screw jointed polypropylene pipes into the sewer length to be renovated. These rigid pipes are drawn and/or jacked inside the sewer providing a relatively rapid renovation method. However, a lead-in trench to the sewer invert is required. As many sewers' invert depths are between 3.5m and 6m, the excavation costs and likely need for expensive service diversions are likely to be both disruptive and prohibitively

expensive. Moreover, the maximum liner pipe diameter used is dependent upon the minimum clearance available within the existing sewer; localised structural deformations can therefore vastly reduce the entire renovated sewer diameter, and therefore its new hydraulic capacity. The void left between the existing sewer and liner also requires grouting to maintain structural integrity.

For CIP renovation systems, liners are typically inserted from existing manhole locations and therefore avoid the need for lead in trench excavation. The liner material is non rigid and is inserted into the sewer under water pressure. The liner moulds itself to the existing sewer profile and overall sewer renovated diameter is unaffected by minor localised structural deformations of up to 10% of existing sewer cross-sectional area (CSA); 'uncollapsed' localised deformations exceeding 10% CSA may be lined following sewer 're-rounding' where a metal clip is remotely inserted at the point of deformation and expanded in-situ to reform sewer profile. Following insertion, the water is heated to cure the liner and the liner achieves 90% of its structural rigidity typically within three to six hours dependent upon liner length and diameter. Negligible void between liner and exiting sewer is formed avoiding the need for post lining grouting. Liner thickness is small compared to sewer diameter and the reduction in hydraulic capacity of the renovated sewer is generally negligible. Accordingly, information obtained from industrial sources indicates that the most common lining material used, for NME applications of the diameter under consideration, is of the 'soft' CIP liner type.

For the purposes of this research programme, therefore, the CIP liner renovation of NME sewers is of prime interest.

1.1.4 Cured In Place Lining Implications

The renovation process associated with CIP liners offer a rapid and relatively inexpensive solution to structural degradation of the sewer network. Access to the sewer system is obtained using existing manholes and the sewer need only be off line typically for a matter of hours. Lining methods requires the insertion of a flexible lining material into the sewer to be rehabilitated, utilising an inversion process, with in-situ curing. The liner material used and lining process are now further discussed.

The liner generally consists of what can be described as a polyester needle felt bag, impregnated with a thermosetting polyester or epoxy resin. The thickness of the liner is dependent on the diameter of the sewer to be lined and may be increased by adding layers of felt, generally in 3mm layers; a 225mm diameter sewer may be required to have a liner wall thickness of around 6mm, whereas a sewer of 600mm diameter would require a liner with wall thickness of a approximately 19 to 24mm. Liner thickness are determined by the lining contractor and based on a finite design brief depending on parameters which include length of sewer to be lined and depth from ground level to sewer invert. A final skin of polyurethane is bonded to the felt to prevent washout of resin, and to contain the water used for inversion and curing. The lining is usually impregnated with resin in the factory and immediately transported to site where it is installed in the sewer. The liner is inserted via existing manholes, by a specialist contractor, under pressure of water, and cured by circulating water at temperatures between 70 and 90°C. Curing is typically achieved within 3 to 6 hours dependent upon liner length and diameter by which time the liner will have attained 90% of its final

structural rigidity, the remainder being achieved up to three months post lining. The process is illustrated in Figures 1.3a to c.

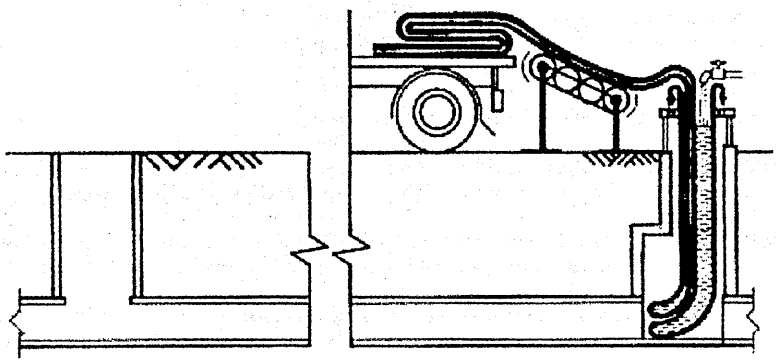

Figure 1.3a: Commencing Insertion

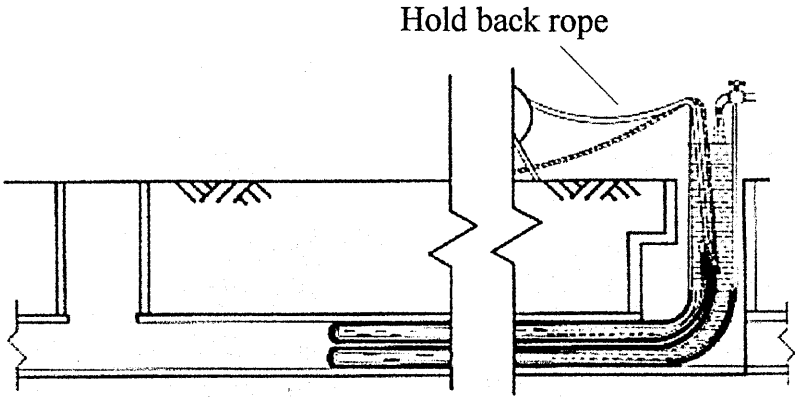

Figure 1.3b: Insertion Half Completed

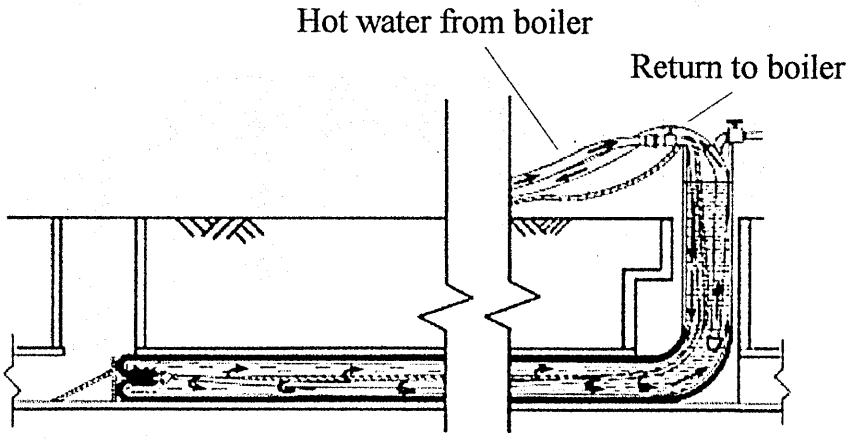

Figure 1.3c: Insertion Completed - Curing By Hot Water

Depending upon the diameter of the sewer to be renovated, sewer lengths of up to 300m may in certain instances be installed in a single insertion. However, insertions lengths in the range of 50 to 150m are more common. As there is generally no annulus, or void between the liner and existing sewer wall, grouting is very rarely required and the reduction in hydraulic capacity of the sewer is negligible as the liner thickness compared to overall sewer diameter is small; an example of a CIP lined sewer is shown in Figure 1.4.

Figure 1.4: A CIP lined sewer.

A key issue, however, is the post lining reconnection of laterals; i.e. the smaller diameter pipes which discharge the flow from, for example, domestic dwellings into the NME sewer.

Prior to a sewer being lined, an initial CCTV pipe survey is carried out to log the lateral positions by, (a) chainage via a cable dispensing distance measurement device attached to the motorised tractor and, (b) clock positions; please refer to Figure 1.5 and Table

1.1. The parametric values shown in the latter are amongst the most common encountered in practice.

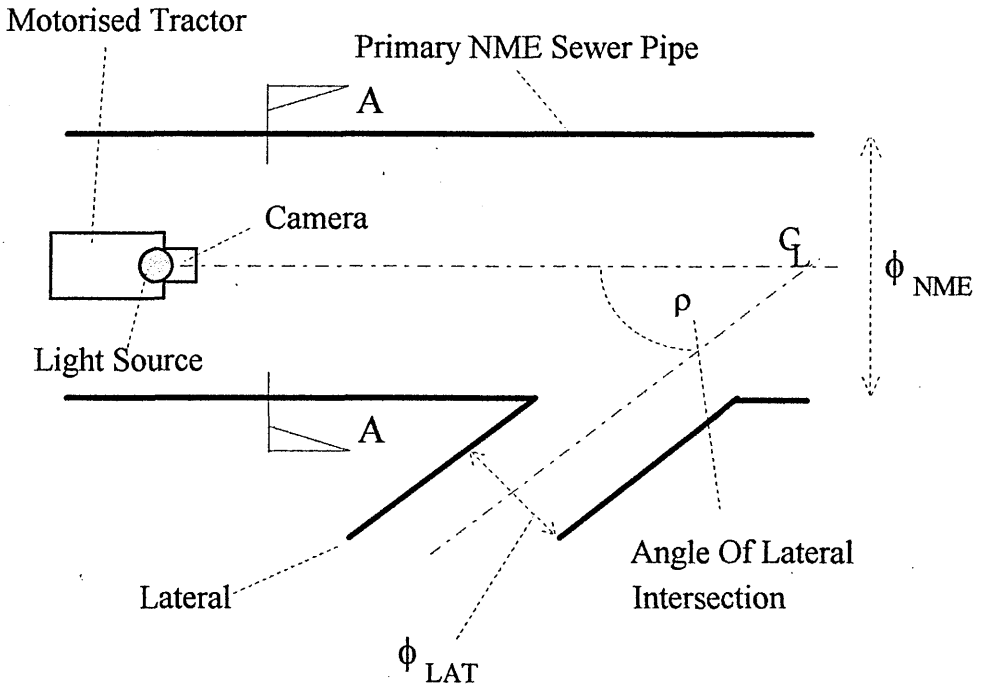

SLICE THROUGH NME AT $\frac{\phi_{NME}}{2}$

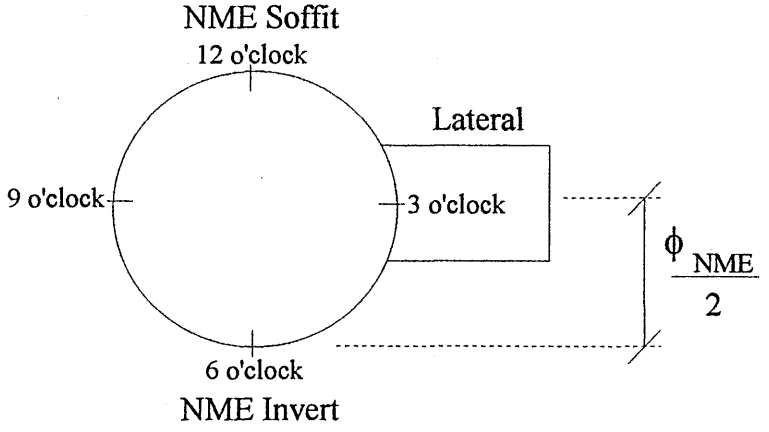

SECTION A - A

Figure 1.5: NME Topology.

Parameter.	Key Value.
NME Diameter ϕ_{NME} (Known a priori)	225mm,300mm,375mm,450mm 500mm or 600mm
Lateral Diameter ϕ_{LAT}	150mm, 225mm or 300mm
Intersection angle ρ	45° or 90°
Intersection 'hour'	3 o'clock or 9 o'clock

Table 1.1: Key Parametric Values

Following lining, this information is used to re-position a cutting rig adjacent to all the laterals that require reopening given the now featureless 'landscape' (note Figure 1.4). Table 1.2 provides an overview of the requisite survey, lining and lateral re-location procedure common to most CIP lining operations.

Stage.	Task.	Comments.		
1	Investigative CCTV Survey of NME by Specialist.	Undertaken as a rolling programme component or as reactive maintenance; deterioration noted and lateral junctions identified.		
2	Follow-up CCTV activity by sewer contractor.	NME cleaned and jet-washed to remove obstructions (e.g. tree roots) as first stage of contract. NME surveyed to log lateral clock positions and chainage.		
3	Set-up overpumping (if required).	NME length to be lined overpumped, from upstream to downstream manhole, to divert sewer flows for duration of operation.		
4	Liner insertion.	Inserted employing water pressure.	NME laterals blocked for 6 to 10 hours dependant on length of sewer being lined, and its diameter.	System 'off-line' for approximately 2 days.
5	Liner curing.	Cured by circulating hot water.		
6	Upstream and downstream breakouts.	Cured liner opened up at both ends to permit NME flow.		
7	Initial, small bore holes drilled at lateral junctions.	Relief of blocked lateral pipe flows using a wire brush tipped drill under remote CCTV surveillance.		
8	Complete drilling of lateral junctions.	Full drilling to match lateral junction geometry.		
9	Post renovation CCTV survey for client.	provide visual evidence that all laterals have been reconnected, and liner is structurally sound.		
10	Remove overpumping	Flow from upstream manhole to downstream manhole permitted through rehabilitated NME length.		

Table 1.2: Typical NME cured-in-place sewer renovation procedure

Figure 1.6, provides an example of a simple yet cost effective (non-motorised) cutting rig employed by many small CCTV survey companies. More recent sewer rigs take the form of motorised tractors (refer to Chapter 4). The rig is required to be of sufficient mass to act as an anchor during the cutting operation, to stabilise the equipment. Liner cutting is achieved using a variety of drilling heads; often, the speed and action of the 'grinding' cone drill can cause the clay pipe walls to become victims of the tool, damaging both wall and tool as a result. More popular wire brush type cutters are now becoming widely used and appear to result in far less damage to both existing sewer and to installed liners. These wire brushes come in a variety of bristle arrangements and can be used for initial puncturing and grinding of the lateral connection to a gentler polishing action for finishing off the edges around the lateral profile. Visual feedback of how an operation is progressing can be restricted to the monitoring operative's view of the proceedings; i.e. the limited pan-and-tilt parameters of the camera can in certain situations reduce the field of view that can be reasonably monitored during cutting, and the heavy vibration induced during this operation causes interference on the vision system. Further, accurate relocation of the drill head at the required drilling position relative to some convenient datum is difficult to obtain in practice by winch methods and dead reckoning.

At present, the correct location and relocation of lateral entry points is determined by the camera monitor operative and as such is open to subjective human error. Incorrect relocation has often resulted in lateral holes being miss-cut; the outcome of mistakes may be a partially opened joint, or more significantly a hole in the liner with no lateral behind it. The quality of the cut can also be of great concern; if the cut leaves jagged liner edges or a lip to the lateral connection, then blockages may be a likely result. In

these cases further remedial measures are needed to correct the damage, paid for at the contractor's own expense.

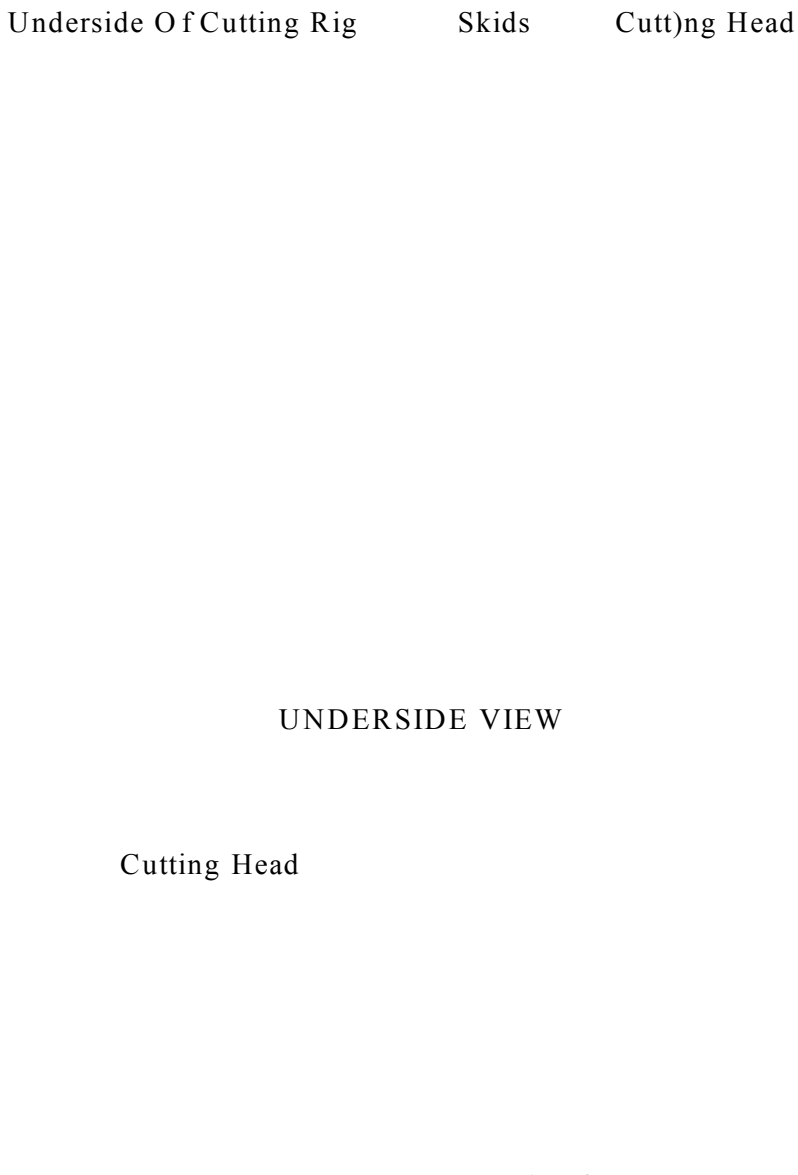

Figure 1.6: Typical Remote Lateral Reconnection Cutter

Clearly, the relocation and reconnection of laterals intersections blocked and obscured by lining is problematic. The lengthy drill-based cutting techniques that are employed to reinstate these can be crude and mistakes occur. The relocation and reconnection of

laterals in the featureless landscape of the NME sewer post lining is therefore a major consideration of this research programme.

1.1.5 Engineering Task Specification

Given that current methods for lateral reconnection are problematic, it is considered that the control of such a repetitive task would be better suited to, and carried out more objectively by a computer controlled, automated system.

Recalling Table 1.2, it is anticipated that any such automated system will employ a three pass strategy; i.e. survey, task and check. Table 1.3 summarises the elements of these passes respectively.

Task	System Requirements.
SURVEY PASS	To inspect the NME sewer for lateral connections and identify; 1) Laterals' longitudinal positions with respect to some datum, 2) Laterals' angles of intersection with the NME centre line, and 3) Diameters of the laterals.
TASK PASS	To return to each lateral location and reconnect the lateral to the main NME sewer by drilling.
CHECK PASS	To provide video evidence, that; 1) All laterals are reconnected to the NME system, and 2) Quality of reconnection is acceptable and not likely to lead to future maintenance problems itself.

Table 1.3: Automated Tasks Employing Three Pass Strategy.

It suggested that automation of this three 'pass' system may be achieved by the implementation of a stand alone robotic system, operating under autonomous fire-and-forget-status. Similar proposals have been investigated elsewhere [13]. Robotic surveying and lateral cutting methods will reduce operation time and be more accurate, improving the whole quality of the operation and its procedure. It is the opinion of industrial contacts that;

a) Automation of the described process would have great potential with regard to their current mode of operation and reduction in errors arising from human operator subjective judgement.

b) Though remote repair systems such as the AMTEC KATE robot are currently available [14], prohibitive purchase costs (of approximately £600,000) exceed the budget of many smaller concerns. As many contractors already possess motorised CCTV 'tractor' units, the ability to 'retro-fit' the requisite components of the proposed robotic system will provide a more cost effective alternative.

c) Automation will lead to a reduction in the present size of the work force currently exposed to the hazardous sewer environment. Overheads will consequently also be lowered, in turn allowing the company to be more competitive.

Clearly, there is potential for the application of automation technology to the task of lateral reconnection for NME sewers lined by CIP liner methods. The following section will address the requirements of such a robotic system.

1.1.6 Research Program Proposals.

This research programme is primarily concerned with providing an automated solution to the problem of reconnecting lateral connections blocked during the CIP lining of NME sewers.

Production of a fully working prototype including integration of discrete sensing and task components under digital control (i.e. 'fire and forget') is currently considered beyond both the academic scope and financial constraints of this project. The ability to provide the discrete sensing and task components, which may be retro-fitted to existing CCTV tractors, is considered more feasible (and cost effective). It is therefore the aim of this programme to investigate the pre-prototype requirements of such a lateral reconnection 'robotic' system.

Attempting to ensure that automation introduces more than simple mimicry of present manual practice, the ultimate goal would take the form of a three pass robotic system as suggested by Table 1.3. This would be based upon a proprietary sewer inspection tractor unit and incorporate task specific modular systems capable of retro-fit; these include a Chainage Measurement System (CMS) for determining the invert line distance travelled by the robot, a novel Computer Vision System (CVS) for both detecting and classifying laterals and an actuator driven robotic arm capable of lateral reconnection.

Referring to Figure 1.7 and recalling Table 1.3, primary aspects of the research programme of study therefore include;

1) Development of a mainly kinematic chainage measurement system which will be able to determine the robot's real-time position within the NME sewer during both survey and task passes.

2) Incorporation of a Knowledge Based CVS capable of detecting laterals during the survey pass.

3) Incorporation of a Knowledge Based CVS capable of providing quantitative data for the laterals detected in (2) during the survey pass. Classification data will include distance from lateral to camera position, intersection angle of the lateral with the NME sewer centre-line and diameter of lateral.

4) Development of a kinematic robotic arm and end effector capable of describing the required cutting profiles for lateral reconnection during task pass.

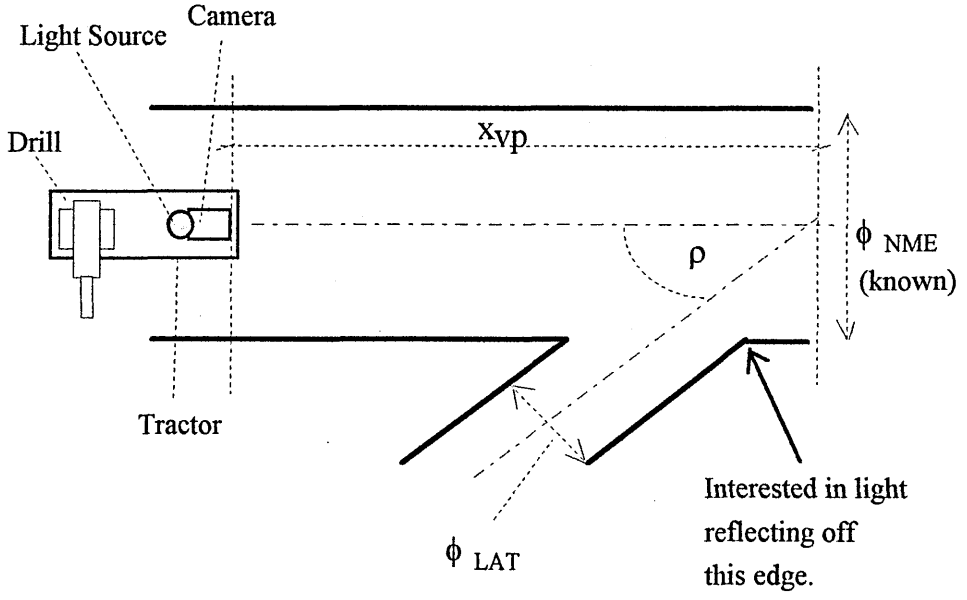

nb; chainage acquisition to involve additional inclinometer and rotary encoder (refer to Chapter 3)

Figure 1.7: Plan Showing Primary Unknowns; x_{vp}, ρ and ϕ_{LAT}

Due consideration will be made of the necessary factors concerned with the integration of these modules under overall digital control. It is envisaged that the proposed pre-prototype modular system would greatly improve both the accuracy and quality of the current working practice.

The following section will discuss the recent advances of automation technology to the construction industry.

1.2. AUTOMATION

1.2.1 Automation And Robotics - Context

Long before the industrial concept of robotics became a reality, the idea for a robotic creature was popularised in 1920 through the play, "Rossum's Universal Robots", by Karel Capeck. In the play, small artificial and anthropomorphic creatures strictly obeyed their master's orders. Capeck first coined the phrase 'robot' in 1917 from the Czech 'Robota', a Russian word for work [15]. A modern definition of a robot may be suggested as a device that responds to designer-perceived stimuli.

In the latter half of the 20th Century, Japan has been responsible for many of the technological developments that have forwarded the field of robotics. A machine which is both automatic and autonomous may be considered to be robotic, though many of Japan's 'robots' would be termed 'advanced automation devices' or 'telerobots' as they are remotely controlled and utilise umbilical support for power and control requirements. European perception, however, is of the former view, defining robotics as the theory and practice of automation of tasks which, because of their nature, were previously

thought to be reserved for man alone [16]. Such work is characterised by an almost permanent interaction between the robotic device and the operational environment. Implicit in such interaction is some kind of pre-appointment of task. It would appear that adaptive execution of this kind would call for the use of an operators reflexes and intelligence. This is why the term 'robotic' is often linked with the notion of Artificial Intelligence. Brady defines robotics to be "the intelligent connection of perception to action" [17].

To date, the vast proportion of commercial robotic/autonomous devices have been employed within the context of industrial manufacturing situations. These are largely static based and function in a structured environment. Present industrial robots are actually mechanical handling devices manipulated under computer control. Consequently, products using standardised components and manufactured in bulk are prime candidates for robotization, and is one reason for the widespread integration of them into the world's automotive industry. Component design has therefore become substantially controlled by, and tailored to, robotic assembly and finishing operations [18].

Of late, a restricted number of robotic applications have out grown the confines of structured manufacturing to be employed within more hostile environments. One example is that of the nuclear industry. Disasters at Three Mile Island and at Chernobyl highlighted the desperate need for remote/telerobotic machines to explore contaminated areas of nuclear plants. One such device used at Three Mile Island Unit 2 was 'Rover', a six wheeled motorised platform originally developed for high speed all-terrain

operation. An onboard video and telescopic detector system allowed collection of radiation data from within the containment basement [19].

Similar machines were used at Chernobyl after the explosion there in 1986. Teleoperated drones have also been used for the inspection and repair of deep sea gas pipelines and oil rig support legs. Application to construction tasks is one of the latest industries in which Japanese innovation has led to the development of telerobots, this time for application to material handling and finishing operations, [18, 20]. Contemporary research projects in the UK have recently been inaugurated.

Whilst many construction tasks may appear suited to automation developments, the environment of the construction site clearly presents many difficulties to the designer. The environment has a major impact upon appropriate proposed robotic designs.

1.2.2 Applications In The Construction Industry

The construction industry currently constitutes approximately 10% Gross Domestic Product in the UK [21]. The varying tasks carried out in the industry often require the site operative to work under difficult environmental conditions, sometimes involving heavy, noisy or potentially dangerous activities. In the UK alone between 1981 and 1985 there was a 45% rise in deaths and major injuries on construction sites [22]. As recent studies indicate [23, 24], construction activities are often performed in readily accessible areas, are repetitive and monotonous in nature, and as such appear favourable to robotic work methods. However, fixed based machines are in reality pre-programmed automatic devices performing repetitive operations within structured

environments. For an autonomous construction robot to function on site, cognitive skills will be required to overcome environmental navigational problems including the rough terrain and the ever changing environment; high level sensing and control features will be required to navigate and operate without causing undue hazard to their human counterparts [18]. Perhaps the standardisation of key construction areas will provide one possible solution [25, 26,] with, understandably, computer application effecting changes in the way tasks are undertaken [27].

Development of such devices has already been achieved to some extent in Japan; largely these are teleoperated by design. Japanese advancement and acceptability of such machines has been most impressive in comparison with the contrary attitude of many European industrial and academic institutions. Companies such as the Shimzu Corporation, Tokyo, have reported large scale investment in such 'robots' [18, 20], particularly in the fields of Steel Erection, Finishing and Inspection operations. In the UK, research is reported regarding production of a robotic excavator [28], and the automation of building inspection tasks [29, 30].

1.2.3 Pre-Prototype Key Robotic Components

As noted in Section 1.1.6, it is considered that the development of a fully working prototype robot is beyond the current scope of this study. Given that such a prototype system would consist of both kinematic and Computer Vision (CV) aspects integrated under digital processor control, then the current study of pre-prototype form is to concentrate on the kinematic and CV sensing task activities as discrete items.

Clearly, during the study of these items attention will be paid to how overall integrated control could be duly developed. Furthermore, the CV work will be largely dependent on substantial technical assistance provided from specialist parties (please refer to Acknowledgements). That is, the project is essentially concerned with the derivation, design and testing of the kinematic components and incorporation of a new technology sensing system developed by third parties to a specification drawn up by the candidate.

For sewer lengths found to contain no lateral connections the operation of the system will default to chainage assessment only which will be fully kinematic (please refer to Section 3.1). For cases where laterals are present, the usual case, CV is to provide for both the detection and classification of lateral connections. Whilst detection is primarily a qualitative task, classification affords estimations of lateral intersection angle (ρ) and lateral diameter (ϕ_{LAT}) together with determination of close-to-target distance chainage increment (x_{vp}) to be added to the kinematically acquired chainage recorded at some convenient location when in close proximity to the lateral. Lateral reconnection is to be achieved by drilling, again fully kinematic (refer to Section 3.2). Computer Vision is a relatively new science and an introduction now follows.

1.3. COMPUTER VISION CONSIDERATIONS

1.3.1 Context

Vision aims to describe the real world. Images provide the input from which the vision system must produce a symbolic representation of the viewed scene. Information implicit in the image is therefore made explicit. There is a huge psychological and physiological literature describing biological vision systems, though at present most visual processes are at best only partly understood.

Computer Vision is a relatively new science which aims to understand the processes and representations underlying vision in sufficient detail that they may be implemented on a computer. Workers in computer vision seek both to gain a better understanding of the principles underlying vision, and to make computers more useful [31].

Computer vision systems obtain their world data via digitised images. Light is focused onto an array of light sensitive CCD (charged coupled device) cells, which produce electrical signals proportional to the intensity of light falling upon them. A finite number of cells produces a finite number of intensities, and these are represented as a 2D array of integers, known as picture elements or pixels. Together these form a grey level image representing the real world. Typically 512 x 512 arrays are used with each pixel distinguishing 256 grey levels [31]. Colour is rarely employed at present due to the associated complexity.

The apparent ease with which the human vision system processes images belies the complexity of the vision problem and the inherent difficulties to be overcome. The

image representation of a given scene is determined by a complex function of four parameters; the surface reflectance of objects within the world and their surface geometry both have affect. Scene illumination and the vision system viewpoint can produce shadows or occlusions which complicate the image. The effects of these parameters are effectively compiled into each pixel value. Unanalysed images therefore do not provide explicit information on all the parameters required for solution of a problem; basic assumptions and/or *a priori* knowledge is/are additionally required [31].

1.3.2 Computer Vision Approaches

Image understanding problems can generally be classified according to the amount of a priori information available. There are three broad classes of computer vision problem: Model-Based, Knowledge-Based and Pure Vision.

For Model Based Vision, the computer vision system has access to a full description (a model) of at least an object's 3D shape. Given this knowledge and one or more grey level images, Model-Based Vision usually provides 3D positional and orientation information, though it may be employed purely for recognition or as a component of a larger system performing, for example, inspection or navigational tasks [32]. A Pure Vision problem does not provide any *a priori* hard knowledge about the world being viewed. Its goal is to extract general world features such as depth and orientation. Much work in this area has been inspired by components of biological vision systems, e.g. binocular stereo [31, 33].

Knowledge Based vision is of far more import to the current research programme. Here the computer vision system possesses knowledge of the class of object expected, e.g. plane faced blocks, but not details of specific objects. Unlike model based vision systems which extract features from image data and match idealised models to them to find model parameters, knowledge-based systems extract features from the image and segment them into groups corresponding to objects. These groups must satisfy constraints derived from knowledge of the object class expected. Each group obtained is effectively a hypothesis that a member of that class is visible in the image. As there is no model available recognition is impossible. Objects can only be described to the best ability of the system, which relies on the level of knowledge available. Through the evolution of computer vision algorithms and resulting systems, several computer vision system prototyping tools have been developed to enable the investigation/development of suitable computer vision systems. One such tool is TINA [34, 35].

TINA is a computer vision development environment containing much of the general image processing/vision software associated with common-place computer vision techniques such as thresholding, edge detection and image smoothing for example. For the application programmer therefore, TINA is intended to provide a platform for research and development of new vision code without having to start from scratch, allowing the user to inherit as much or as little of the existing standard TINA modules, graphics, code and programming style as is required. TINA provides a hierarchy of image processing, display and interactive manipulation modules specifically designed for the recovery and representation of 2D and 3D geometrical primitives. The TINA interface comprises a collection of graphical 'tools' which is easily extended by the

vision system developer. TINA has been used to develop all the computer vision techniques reported herein.

1.3.3 Applicability Of Computer Vision To the Sewer Inspection Task

Other established sensor technologies are currently employed within sewer environments. Structured light methods have been investigated and a technique based on a light ring has been patented [36]. Radar systems are under investigation [37]. Although they provide accurate measurements, the uptake of these technologies is often problematic. Special purpose, sometimes expensive, equipment is required and existing video records cannot normally be exploited. While structured light methods incorporate a 'Closed Circuit Television' camera, the lighting conditions imposed restrict the use of any images obtained.

The performance of present computer vision techniques does not match that of comparable biological systems. However, in some circumstances computer vision techniques may be better suited to the task at hand. One crucial difference is that biological vision systems do not provide their users with easily accessible, quantitative descriptions of world geometry. A human observer may know where viewed objects are to a high degree of precision and be able to use that information internally to pick up or navigate between objects. S/He is however unlikely to be able to state verbally *inter alia* the exact distance to a viewed surface. It would appear that sewer surveys require quantitative measurements; the more qualitative results now provided by human operators leave something to be desired.

To date machine vision systems have been successfully employed in industrial inspection tasks, bin picking exercises and for robotic guidance. Most systems operate within structured environments where the data to be assessed is minimised; object(s) of interest are typically machine manufactured and occupy only a small proportion of the viewed world, the actual environment being generally clean and well-illuminated. Conversely, the NME sewer environment is comparatively unstructured, generally dirty and often poorly-illuminated; mist and/or spray, within the sewer, can further obscure features of interest. Objects within the sewer are not so geometrically perfect and perhaps damaged. The application of machine vision to such an environment requires the ability to operate with reduced *a priori* knowledge whilst assimilating data from the full visual field.

A computer vision approach is likely to be both economically viable and stable. Images captured under standard lighting remain the norm, so records of survey operations may be used in other contexts. No special hardware is needed, so little modification to current equipment is expected. However, should equipment standards change it is anticipated that closed circuit television cameras will continue to be employed; many clients insist on the production of a survey video. It may be suggested that the use of computer vision in sewer survey will both provide a robust basis for automation within this hostile environment and force new developments within the field.

1.3.4 Potential Use Of Vision Systems In The Construction Industry

Currently, the application of computer vision techniques within the construction industry is relatively rare. For example, the robotic inspection of external building surfaces using a single uncalibrated camera and image processing techniques provides a visual survey for finding cracks, and resulting staining due to reinforcement corrosion, in high rise concrete structures and for aiding robot navigation [38]. The use of computer vision for the monitoring and interpretation of structural deformation of masonry vaults utilising edge detection techniques regarding the assessment of arch bridge deformation under load is also currently under investigation [39, 40]. A robot, equipped with a computer vision based navigation system, for the location and inspection of air conditioning ducts is also under development [41].

The application of computer vision techniques to sewers has, to date, been very limited; some work has been conducted regarding the detection of pipe joints, but this was only part of a study which relied heavily on the use of laser-range finding technology [36].

1.3.5 Problem Definition Regarding Sensing Requirements of Sewer Study

Based on the research aims expressed earlier, the proposed CVS will incorporate two stages; these being lateral detection and description/classification.

Recalling Figure 1.7, this vision system must initially be able to detect a lateral connection from a series of images during an initial survey pass. Through investigation of optimum light source/camera positioning, laterals will be detected from step edge intensity profiles [31], edge detection being a key feature of the CVS employed; that is,

edges generally generate significant brightness contours in images. Figure 1.8 indicates how this is assessed in intensity (Ia, Ib) terms; further discussion is given in Section 2.1.2.

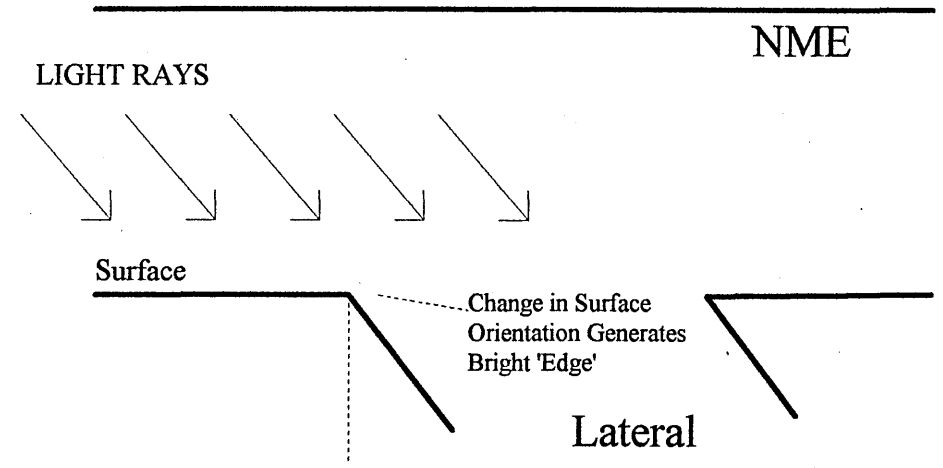

a) Illuminated Physical Edge

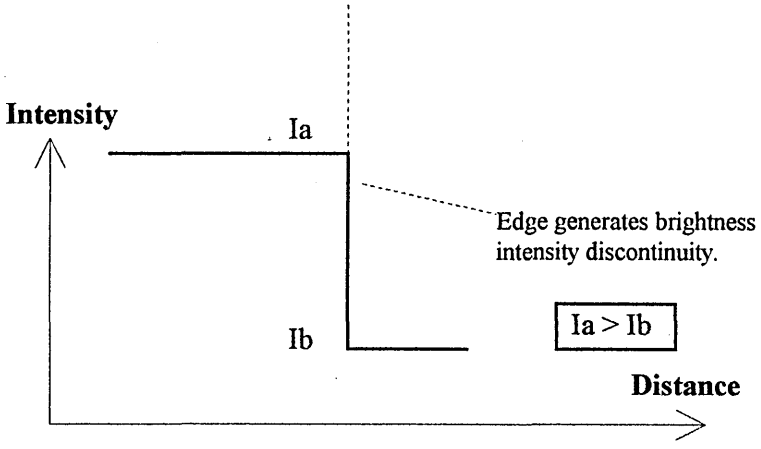

b) Intensity Plot

Figure 1.8: Step Edge Intensity Profile

Upon confirmed lateral detection, adapted photometric stereo techniques are to be employed using an initial reflected illumination image and a second image obtained under direct light to provide estimates of;

(a) closure to target distance x_{vp}, (Figure 1.7)

(b) lateral orientation ρ, (where ρ is usually 45^{o} or 90^{o}) and

(c) lateral diameter φ_{LAT}, (usually 150mm, 225mm or 300mm).

Based on the estimated closure to target distance combined with the CMS derived invert line chainage, lateral positions will be logged for reference for relocation after the primary sewer pipe has been lined. Lateral orientation and diameter data will determine the correct cutting profile for the robotic drill arm to initiate when reconnecting the lateral to the lined NME sewer.

1.4 Summary Of Research Objectives

The nature and importance of maintaining the UK's sewer infrastructure and the desirability of applying information technology-based automation procedures to improve current practice, provides for the need to study the necessary characteristics of a task-dedicated robot of sufficient robustness to operate in a hazardous environment. The renovation of NME sewers offers clear potential for development of such. This research programme is therefore primarily concerned with providing an automated solution to the problem of reconnecting lateral connections blocked during the CIP lining of NME sewers.

Recalling Section 1.3.5, a three pass strategy is proposed based upon a proprietary sewer inspection tractor unit incorporating task specific modular systems, these being capable of retro-fit for cost effective practice. During the initial survey pass, a novel Computer Vision System is to provide both for the detection and classification of laterals. Once detected, the latter component linked with a Chainage Measurement System (for determining invert line distance travelled) will provide the ability to accurately re-position the actuator driven robotic arm and drill adjacent to the lateral during the second, or drill, pass where classification data relating to lateral intersection angle and diameter will be recalled and provide for optimum cutting profile to be chosen and implemented. The third pass purely provides documentary evidence that all laterals have been satisfactorily reconnected.

Figure 1.9 shows a diagrammatic sketch identifying the proposed key modular components of the proposed laboratory robotic model.

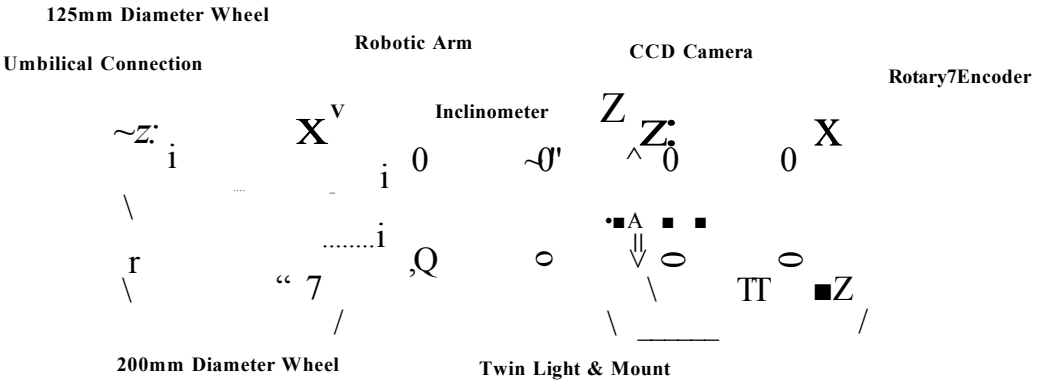

Figure 1.9: Diagrammatic Sketch Of Proposed Retro Fit Sewer Robot

Whilst alternatives to a tractor based system have been considered, for example modular systems retro-fitted to chain driven sleds, impracticalities regarding their employment within NME sewer environments have discounted further investigation.

Regarding the retro fit units required to provide for the robotic systems, the drill is self-explanatory, the light sources and camera relate to the CV system, the inclinometer and rotary encoder are used for kinematic chainage acquisition whilst a remote CPU provides the requisite hardware and software support to the kinematic task components; financial constraints negate the preferred option of onboard processing. Note, the position and orientation of the camera and twin lights employed here is fixed whilst in practice the use of more expensive pan and tilt systems is not uncommon. It is considered that as well as being more cost effective, a fixed camera system is both robust and adequate to afford the requirements of the CV system as shown in Chapter 6.

It is considered logical to address the sensing aspects of the study prior to presenting the crucial kinematic factors. Accordingly, Chapter 2 discusses the proposed CV system to be employed.

CHAPTER 2

COMPUTER VISION MODEL DEVELOPMENT

2.1 INTRODUCTION

2.1.1 Lambertian Reflectance

It is a general assumption herein that the reflectance properties of the sewer pipe correspond to that of a Lambertian reflector [31]. With the reflecting material of matt finish, all points on a sewer wall illuminated from a point light source of intensity I (lux) are taken to emit light of equal intensity E (lux) in all directions (Figure 2.1). An expression for the reflected light intensity E is given in Equation 2.1.

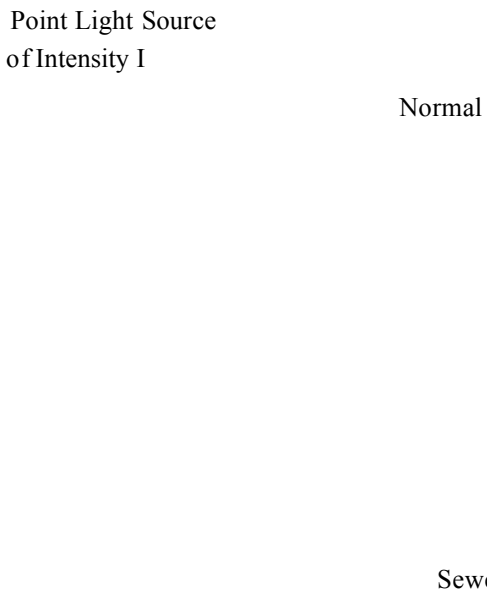

Figure 2.1: Lambertian Reflectance Characteristics

$$\_ \; klzosO \qquad \text{(Equation 2.1)}$$

where k denotes the surface reflectivity (0< k <1), 0 defines the angle between the incident light ray and the surface normal, N, and r is the distance the ray travels between light source and target surface.

Self-evidently, the illumination model employed is a critical feature of any proposed system and is discussed in more detail in Section 2.1.3.

2.1.2 Edge Detection

A vital step in the design of a machine vision system is the determination of relations between the interesting features of the viewed world and measurable properties of the image; this often involves objects' 'edges'.

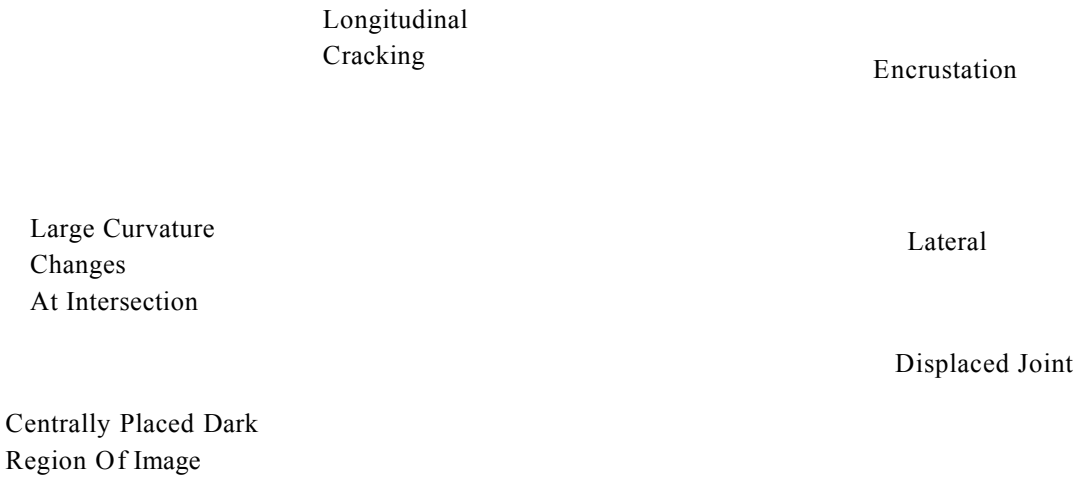

Figure. 2.2. Typical Grey Level Image of A Clay NME Sewer

Figure 2.2 shows a typical grey-level digital image, obtained from a field CCTV survey, of an NME sewer. Wall encrustation gives rise to a dappling effect while displaced joints appear as bright crescent shaped regions; longitudinal cracks are usually represented by connected series of near-random line segments. Lateral intersections generate light image regions, usually smaller and less bright than those arising from similarly distant displaced joints. Lateral profiles are smooth, elliptical and frequently complete with relatively high curvatures occurring at the top and bottom of the intersection profile. Such real-world occurrences usually give rise to sharp changes in

image intensity or 'edges', providing easily detectable features which may therefore be used as cues to the image location of lateral intersections.

Edge detection algorithms or operators typically employ the first derivative of image intensity, and significant peaks, which correspond to edge locations (Figure 2.3), are marked [31]. Canny has proposed an operator which has become the *de facto* industry standard and is derived from an optimisation procedure seeking good detection, good localisation and minimal response [42]. The Canny algorithm involves removal of image noise by Gaussian smoothing, factor (σ), followed by differentiation and a search for significant peaks. Two thresholds assess the height, and therefore significance, of peaks in the first derivative of intensity while a single threshold places a lower limit on acceptable edge length. A low σ value provides for minimal smoothing while a high σ value gives greater noise reduction but may lose significant structures. Thresholding anticipates targeted edge length.

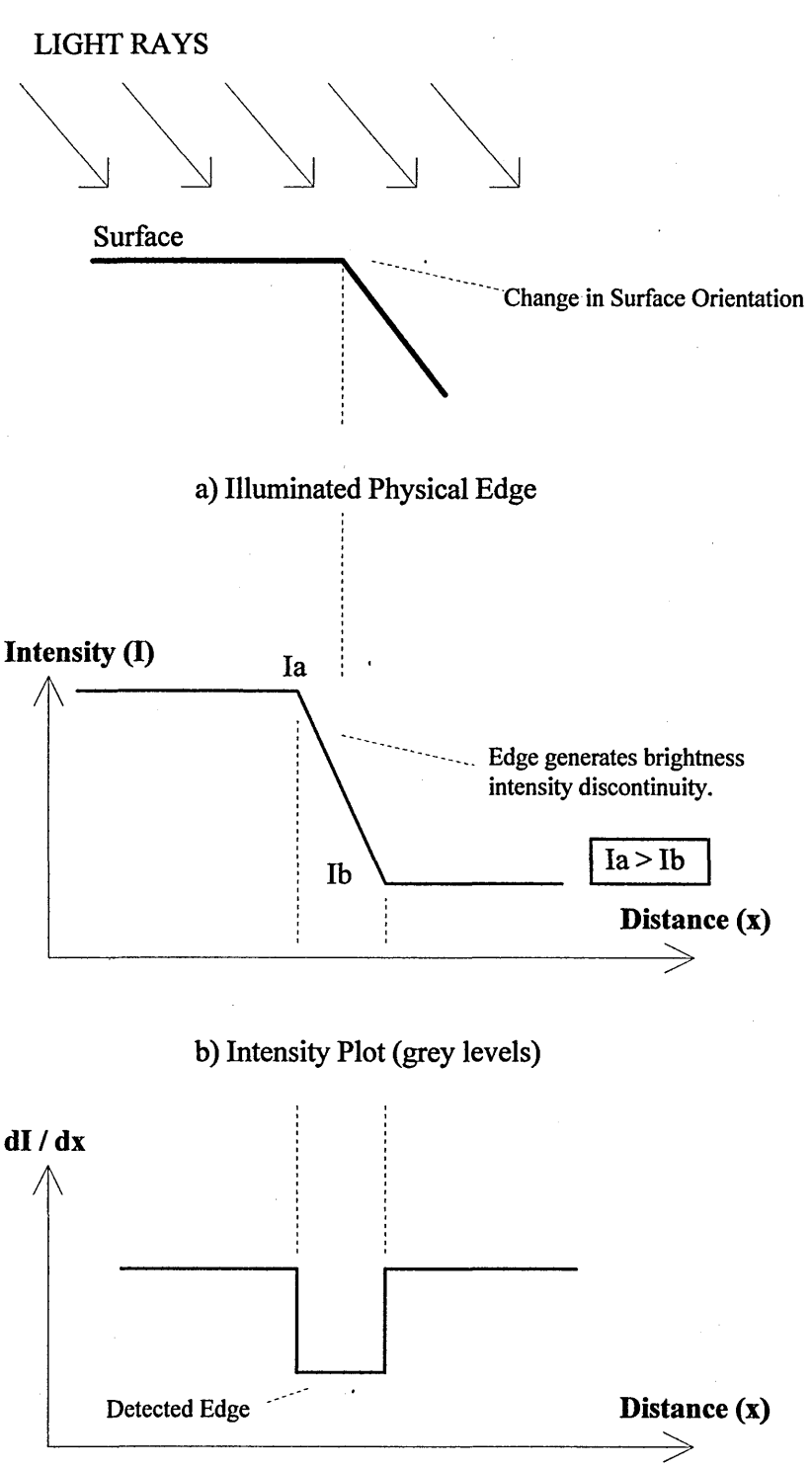

Figure 2.3: Step Edge Intensity Profile

Figure 2.4 shows the result of applying a Canny operator to the image of Figure 2.2. It is evident that the lateral profile, although represented in some detail, is masked by the rogue edges attributable to wall encrustation in its vicinity. Apparently surprising, as the surface discontinuities introduced by encrustation are relatively small, suspicion of the lighting conditions is aroused with regard to this magnification of effect.

Lateral Profile Masked
By Rogue Edges

Spurious Edges Due To Wall Encrustation

Figure 2.4: Canny Edge Detection Algorithm Applied to Figure 2.2

2.1.3 Illumination Conditions

Current CCTV surveys are generally conducted under effectively arbitrary illumination conditions. While 'pan and tilf camera technology is not unfamiliar, more usually, a single light source is mounted on a fixed position on a winched sled or tractor unit which may wander within the pipe, due, *inter alia,* to imperfections of sled lie under

tow and/or the presence of physical objects. When the image shown in Figure 2.2 was captured, the light source was directed, approximately, towards the lateral intersection. It is considered that such 'direct' illumination disproportionately emphasises edges arising from noise elements. Further, current CCTV camera practice includes the notion of averting the illumination source away from the feature under consideration, primarily to avoid glare from the often-wet pipe surface obscuring the operator's view.

Figure 2.5 accordingly depicts a further lateral intersection image obtained under 'reflected' light whereby the spot lamp is pointed at the wall opposite the lateral connection. The lateral intersection is thereby bathed in a more diffuse light of lower intensity. When the edges obtained from this image, as illustrated in Figure. 2.6, are compared with those shown in Figure 2.4, it can be appreciated that the lateral profile is much easier to distinguish. Noise is much reduced and the lateral edge profile is complete and unbroken. Although Figures 2.2 and 2.5 relate to distinct surveys, the sewers concerned are of similar diameter and viewing distances are comparable.

Light intensity profiles taken longitudinally across the lateral intersections of Figures 2.2 and 2.5 serve to clarify this improvement in lateral definition; these profiles are shown in Figure. 2.7 and 2.8 respectively. Noise intensity is dramatically reduced under reflected illumination and some investigation of this counter-intuitive phenomenon is warranted.

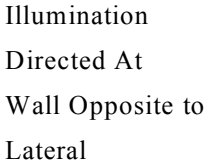

Figure 2.5: Grey Level Image Obtained under Reflected Illumination

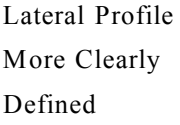

Figure 2.6: Canny Edge Detection Algorithm Applied to Figure 2.5

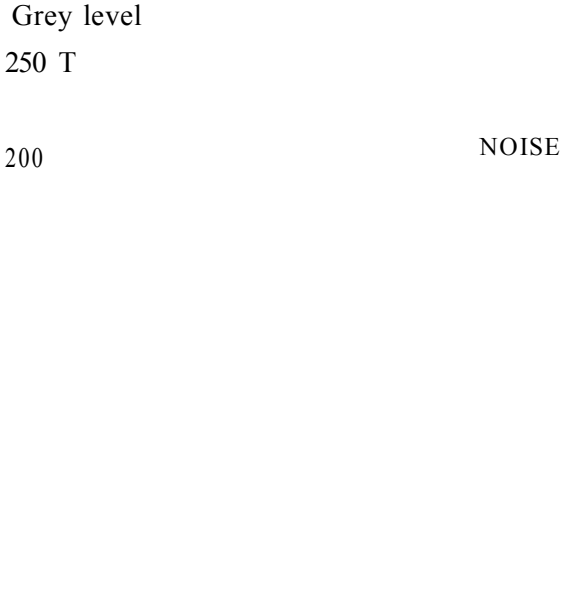

Figure 2.7: Intensity Profile Crossing The Directly Illuminated Lateral Intersection of Figure 2.2

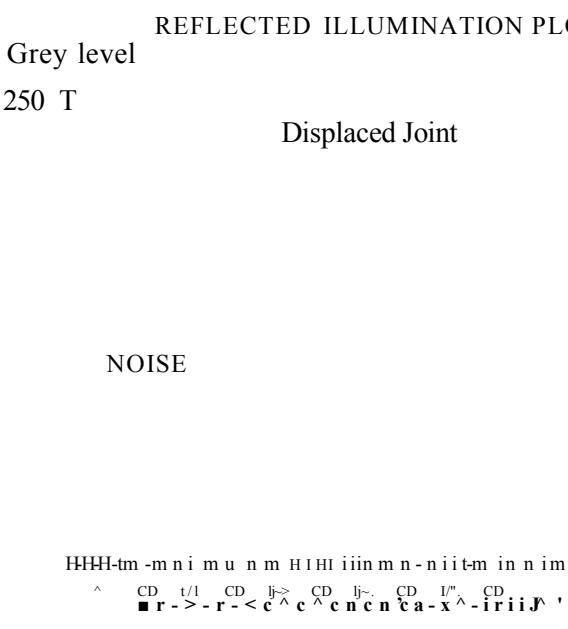

Figure 2.8: Intensity Profile Crossing The Directly Illuminated Lateral Intersection of Figure 2.5

Sewer encrustation or structural damage typically gives rise to surface distortions, which may be modelled by small 'blips'. Under direct illumination (Figure 2.9) a shadowed area is produced behind the blip. The contrast between the illuminated blip and the shadowed area produces a step edge of a magnitude not too dissimilar to those associated with lateral profiles.

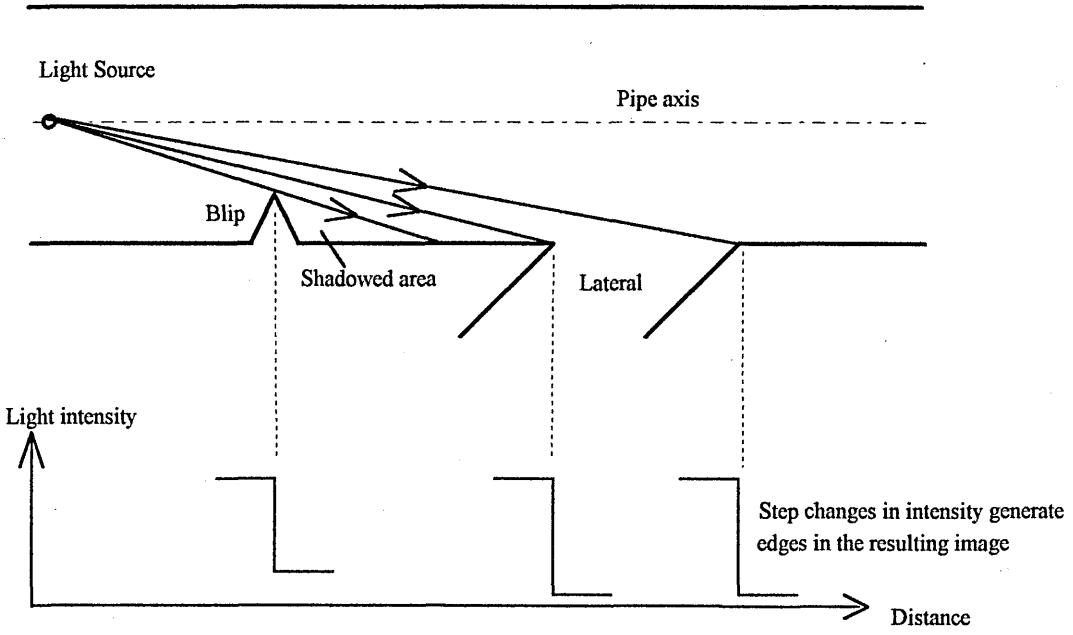

Figure 2.9: Direct Illumination within the NME Sewer

Under reflected illumination (Figure 2.10) and noting the Lambertian reflectance model employed, recall Figure 2.1, the blip is fully illuminated so that no, or a vastly reduced, shadowed area is produced. This results in a smaller step edge.

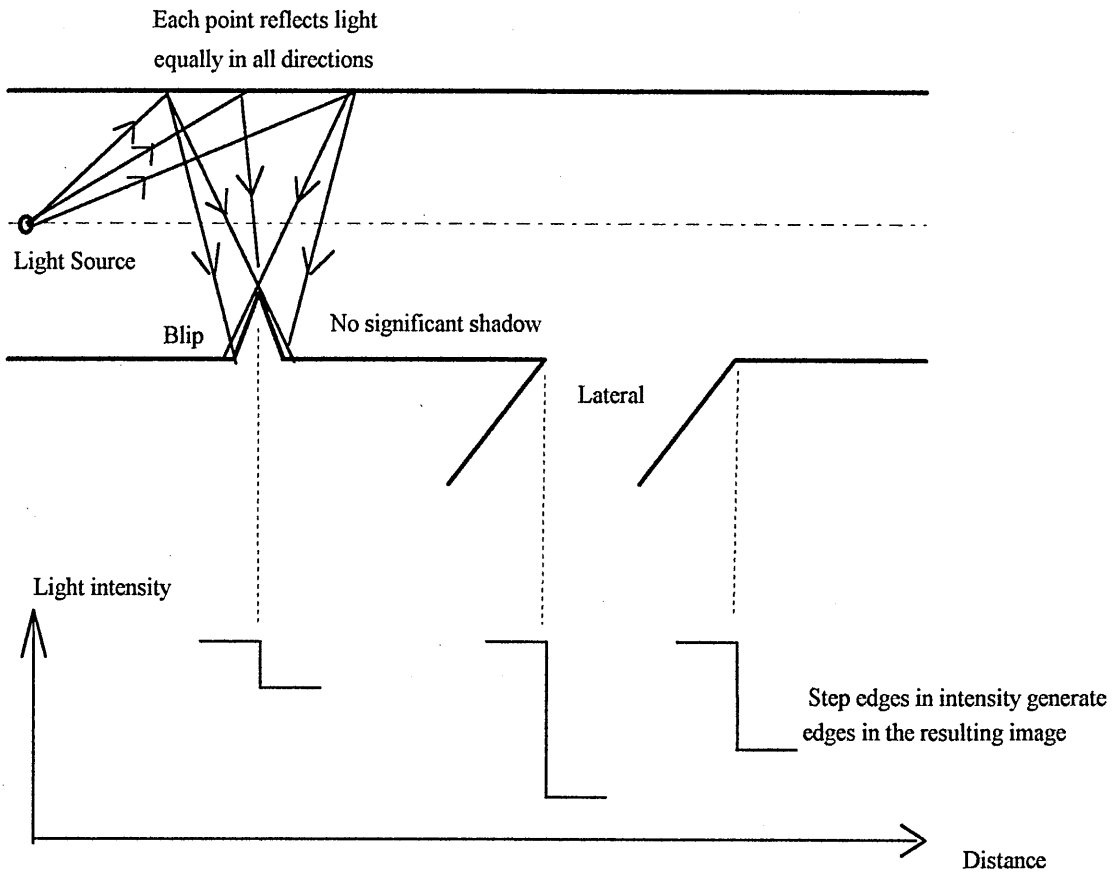

Figure 2.10: Reflected Illumination within the NME Sewer

Chantler has analysed the properties of direct light in some detail, finding that this form of illumination acts as a directional filter for three-dimensional texture during image acquisition [43].

2.1.4 Image Processing

Inadequate lighting typically underlies the poor image quality associated with many commercially produced CCTV surveys available today. A solution would be to increase the power of light source included in the survey rig, however, problems of associated glare and introduced image noise are likely to result in wet and/or light coloured pipes. An alternative is to enhance the captured image.

A wide variety of image enhancement techniques exist, with median filtering and histogram equalisation being particularly suited to the task in hand. Median filtering is particularly effective for images where noise patterns consist of strong, spike like components, and where the characteristic to be preserved is edge sharpness [44]; the filter replaces the grey level of each pixel by the median of the neighbouring grey levels. To determine the median value, the neighbourhood or window size must be chosen; a window size of 3, for example, calculates the median value from a 3 x 3 area centred on the pixel under consideration. Histogram equalisation is particularly suitable for increasing image contrast and hence overall image definition. The technique utilises a histogram of grey levels to provide a global description of the appearance of an image. Image enhancement may be achieved by modifying the histogram of a given image. Histogram equalisation modifies the appearance of image by controlling the probability density function of its grey levels via a transformation function. Again, when applying such a technique, a window size is assigned (a value of 55 would not be considered in-appropriate). In general, the technique increases the dynamic range of pixel distribution, considerably altering the appearance most images.

Experimental investigation of the above is discussed later in Section 6.1.4. Whilst image enhancement can result in an overall more robust system, it cannot always compensate for problems introduced by direct lighting (please refer to Section 2.2.3).

2.1.5 Knowledge Based Engineering

Having established that computer vision, with particular respect to edge detection and illumination, can provide useful engineering data interspersed amongst a larger collection of (visual) signals and noting that field engineers employ heuristically derived procedures that can, with effort, be explained, it is logical to attempt to sieve the

surfeit of visual data provided employing knowledge-based engineering (KBE) decision making criteria. That is, qualitative characteristics provide clues to the nature of NME / lateral intersections regardless of their measurable features including, inter alia, their dimensions, orientation and position. Awareness of such characteristics can be considered as a priori heuristic knowledge - i.e. based upon experience and thereby known from the outset.

Field operators can typically identify laterals in commercial survey videos at a distance of 2 to 3m from the camera, although accurate measurement of these distances is not currently possible in general situations as all are gauged from the on screen chainage readout supplied by the contractor. As a result, laterals are expected to be observed towards the centre of the image (as the camera nears the intersection, the lateral appears closer to the image boundary). Attention is therefore focused upon a centrally placed region of interest. Further, the corresponding edge strings arising from a variety of lateral intersections enable an estimate of the likely length of the desired strings to be made such that short, irrelevant edge strings may be eliminated by applying a simple line length threshold.

A final factor concerns the intersection edge string shape. Generally, regions of high curvature may be found at the top and bottom of the peanut-shaped string (see Figures 2.3 and 2.5). Accordingly, any sufficiently long and appropriately placed edge string displaying two clear curvature maxima is taken to arise from a lateral intersection. As intersection strings may appear incomplete in practice, robustness demands the possibility of a lateral being detected on the basis of just one curvature peak, but rejected if more than two are located.

The above criteria form the core of the proposed lateral identification system, which has been implemented under the TINA Vision Research Environment software [34]. Strict numerical quantitative precision is not required for lateral detection purposes which is in effect a qualitative procedure.

2.1.6 Frame Of Reference

An estimation of the vanishing point (VP) of a sewer image is to be employed to establish a frame of reference; a previous procedure exploiting the courses present in brick sewers has been previously proposed [45]. Here, a more general image analysis procedure is required which assumes the presence of an approximately centralised and circular darkened region appertaining to a locally straight run of pipe – note Figure 2.2. Limiting each pixel to be black or white, dependent upon its shade of grey therefore produces a simplified image (Figure 2.11); grey scales are in the range of 0 (black) to 255 (white) and a threshold of 100 was chosen empirically. All grey levels below a value of 100 are turned to 0, all of 100 or above are turned to 255. The resulting binary image is scanned to determine the centroid, taken as the VP, of the centralised 'black hole' (Figure 2.12).

Figure 2.11: Thresholded Image of Figure 2.2

Figure 2.12: Estimated Vanishing Point

Provided that this centralised region is sufficiently large, small errors in its placement will have no effect on the performance of the method. Moreover, the centroid provides a reasonable estimate of the location of the vanishing point, even in the presence of large scale distortions in the form of inter alia mist in the pipe, Figure 2.13.

Figure 2.13 Vanishing Point Estimation - Misty Image

A limiting assumption made here is that the pipe under consideration is locally straight. Should a bend occur, as may be the case in any NME sewer, the vanishing point would degenerate to a curve. The centroid of the 'black hole' should, however, lie on or very near to this curve and so, as long as size of the region of interest is not underestimated, the method proposed here is not expected to fail.

2.1.7 Consideration

Essentially, the key issue of the Computer Vision Model Development study was to incorporate the relevant CV models within the overall engineering task specification rather than to develop the modelling itself. However, the specification that the modelling meets has been prescribed to respective third party specialists and the resulting testing has been directly undertaken. For this reason, certain CV modelling details are attached in Appendix C.

2.2 LATERAL DETECTION

2.2.1 Proposed Procedure

As proposed in Section 1.4, the tractor unit is to be fitted with one fixed CCD camera and two fixed light sources. The first light source is fixed so that its principal axis is directed towards the left-hand sewer wall as is the second light source towards the right hand sewer wall. The direction of the principal axes of the lights is at approximately 30 degrees about the NME sewer centre line, derived empirically. During the survey pass until a lateral has actually been detected, the CVS is to sample images of both sides of the pipe wall alternatively under reflected illumination (noting the assumption that laterals will occur at either 3 or 9 o'clock). This is to be achieved by alternating which light source is illuminated at any one time; left light source for the detection of laterals located at 3 o'clock and right for laterals at 9 o'clock.

The engineering specification provided in Chapter 1 therefore demands the following;

(a) Acquisition of an appropriate digital image under reflected illumination.

Initial survey pass to be employed utilising digital camera and twin light system; lamps approximately level with axis of NME sewer, positioned so that direction of their principal axes are nominally 30 degrees about sewer centre line. Lamps are sequentially illuminated to provide cyclic reflected illumination of both sides of the pipe. Laterals anticipated intersecting with the NME sewer at either 3 or 9 o'clock and being of either 150, 225 or 300mm diameter. Laterals are to be detected under reflected illumination. For each cycle, images of the sewer digitised prior to enhancement if required.

(b) Application of image processing to enhance the image – but only when necessary

It is likely that some image noise will lead to some otherwise long point strings being broken up into a number of shorter sections. This problem is to be partly addressed by applying median filtering and histogram equalisation to the initial grey scale sewer image; image features are therefore expected to be smoothed, implying a reduction in edge break up without a significant reduction in image detail.

(c) Determination of approximate vanishing point

It is expected that laterals will be detected from a distance of approximately 2 to 3m; laterals are therefore expected to be observed mid-image (note (a)). The volume of edge data to be considered can therefore be reduced by considering only an elliptical region of interest centred about the sewer vanishing point, as discussed in Section 2.1.5. In most cases, e.g. Figures 2.1 and 2.4, the camera is approximately aligned with the central axis of the pipe, the vanishing point is therefore near to the image centre and the region is approximately circular.

(d) Application Of Edge Detection

The Canny algorithm is then applied employing a Gaussian smoothing σ value of 2.0, determined empirically.

(e) Institution of application specific selection criteria to detect the lateral

Short, insignificant edge strings, which are anticipated to be a product of noise, are then to be eliminated by applying a line length threshold of 50 pixels. This value is again determined empirically. The ideal lateral curvature plot incorporating 2 high curvature peaks (figure 2.14) is to be used to identify their profiles. Noting that profile sections

may unfortunately be broken or missing, a more robust identification algorithm will accept the possibility of a lateral being detected on the basis of just one peak, but rejected if more than two are located. If necessary, as the 'detected' lateral is further approached, the curvature may be re-checked and lateral detection confirmed if 2 peaks are identified.

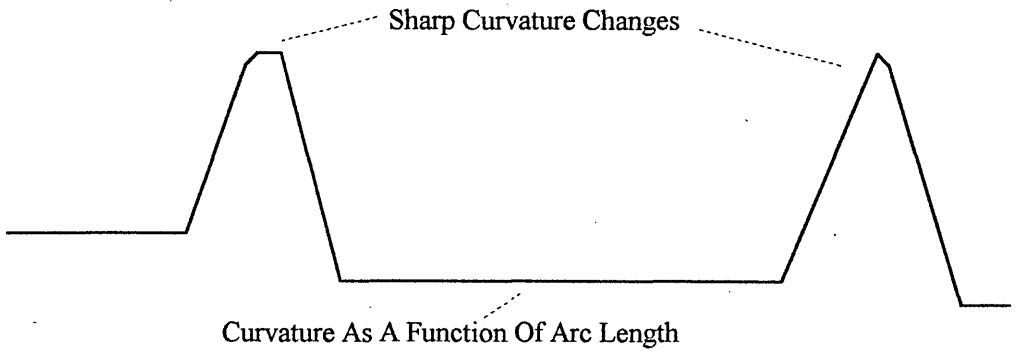

Figure 2.14: Lateral Curvature Profile

2.2.2 Preliminary Investigation

Whilst Chapter 6 deals with the experimental assessment of lateral detection, an initial case study is used here to establish the proposed procedures.

Figure 2.15a shows, for ease of reference, the edges of Figure 2.5 overlaid on the image of Figure 2.4, captured under reflected illumination. Note that in this case image enhancement prior to edge detection was not required; the walls of the pipe are quite wet and the lamp employed quite bright. As a result there is sufficient light in this environment to allow immediate application of the Canny operator. The result of thresholding the image is shown in Figure 2.15b, while the estimated vanishing point is shown in Figure 2.15c. The large dark region to the right of the image severely disrupts the vanishing point location process. Two points should, however, be noted. First, this is an extreme example. Second, this effect will always shift the vanishing point estimate

away from the directly illuminated wall and towards the region where laterals are to be sought. Hence, while the vanishing point estimates obtained may be inaccurate, the region of interest will still be appropriately placed; the effect is unlikely to cause laterals to be missed.

Figure 2.15d shows the result of applying the proposed detection criteria to the edge data of Figure 2.15a.. The lateral mouth is again correctly identified; Figure 2.15e shows the curvature plot of the corresponding edge string. Two other strings are, however, also considered likely to represent lateral intersections. One arises from the colour-coding bar superimposed on the video frame and is easily discounted. The second is located on the far wall of the sewer; on the opposite side of the vanishing point from the true lateral. Since the use of reflected illumination is key to the proposed method no intersections would be sought in this part of the image, which depicts a directly illuminated wall. Hence this additional 'false positive' may also be discarded without effort.

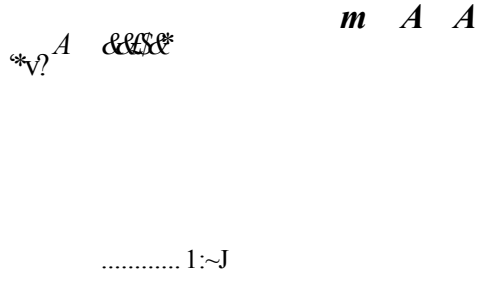

Figure 2.15: Application of Proposed Lateral Detection System - Reflected Illumination

2.2.3 Support For Counter Intuitive Assertion

A critical feature of the CV based sensory system has been the use of reflected illumination for lateral detection. If the facility is to be automatic by nature, this decision dominates the entire procedure and is based on engineering judgement. That is, practitioners employ a procedure which has been justified scientifically in Figures 2.8 and 2.10.

Figure 2.16 shows the outcome of applying the proposed detection system to the directly illuminated lateral of Figure 2.2. Note that, in general, direct illumination leads to a more clearly defined 'black hole' and so eases the vanishing point estimation stage of the process. As can be seen, however, several edge strings possessing only one curvature peak have been identified in the lateral vicinity. The true lateral profile has not been identified and the system has therefore failed to detect the lateral.

c. d.

Figure 2.16: Application of Proposed Lateral Detection System - Direct Illumination

2.2.4 Other Factors

Recalling Figure 2.15, whilst the CVS reports a lateral has been successfully detected within the image, it is difficult to prove by any scientific method that a lateral actually exists. Rather, confirmation that a lateral exists within the image at all relies on the word and engineering judgement of the operator who initially supplied the video. Formal experimental (laboratory testing) study is given in Section 6.1.3. With reference to the detection 'rules' presented in Section 2.2.1, it should be noted the decision as to whether or not to enhance images gathered from a given pipe run would be made by a fully automatic system. Image enhancement is also addressed in Section 6.1.4.

Lateral classification with respect to assessment of angle of lateral intersection to NME sewer, ρ, lateral diameter, φ_{LAT}, and closure to target distance x_{vp} is to be undertaken immediately following detection during the survey pass (recall Table 1.3).

Having demonstrated the applicability of CV to the qualitative detection of lateral intersections, and noted the different properties of direct and reflected illumination, consideration is now turned to a CV based quantitative approach to lateral classification.

2.3 LATERAL CLASSIFICATION

2.3.1 Proposed Procedure

Figure 2.17, provides an overview of the topology associated with lateral classification.

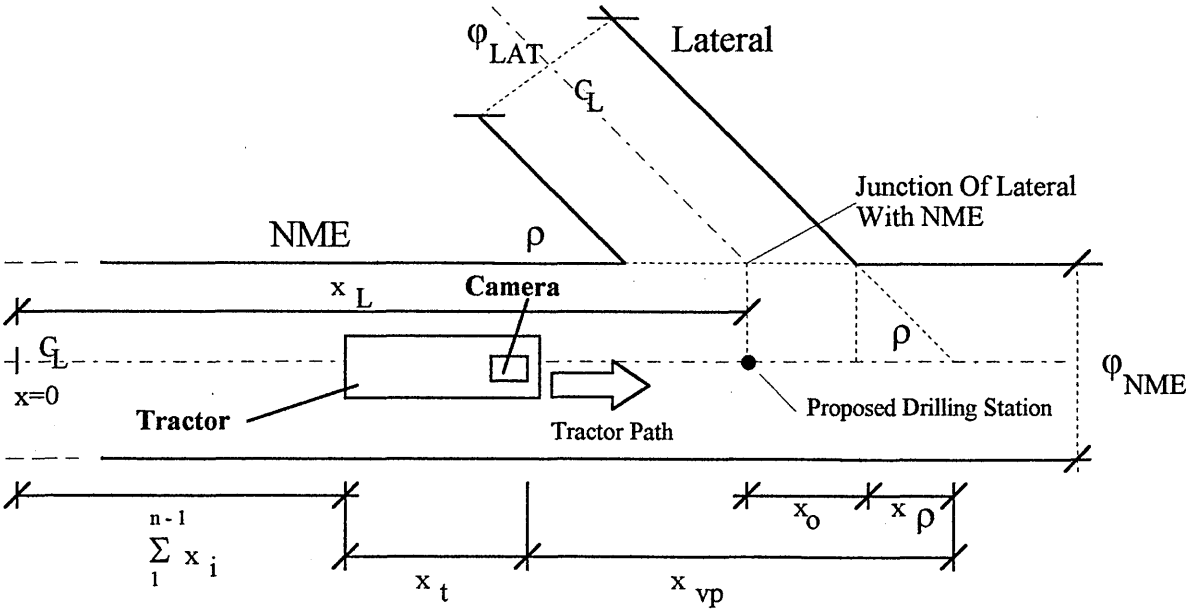

WHERE;

φ_{NME} = NME diameter

φ_{LAT} = Lateral diameter

ρ = Angle of lateral to NME intersection

'x' is general invert chainage such that (refer to Chapter 3);

x_{vp} = Closure to target distance between camera and lateral back wall projection

x=0 = Datum chainage position - arbitrary

$\sum_{1}^{n-1} x_i$ = Culmative distance travelled by tractor - kinematically aquired; ref Chapter 3

x_L = Chainage to drilling station position - primary chainage requirement for task pass

x_t = Offset from rear of tractor to camera CCD Chip (300mm)

x_ρ = Geometrical offset for lateral wall

x_o = Geometrical offset for drilling station

Figure 2.17: Classification Topology

Recalling Table 1.1, laterals intersect the NME at either 45 or 90 degrees, occurring at either 3 or 9 o'clock (recall Figure 1.5); the topology represented in Figure 2.17 accordingly corresponds to a horizontal slice through the NME at ϕ_{NME} / 2. NME diameter (ϕ_{NME}) is known *a priori* whilst the likely set of discrete values of φ_{LAT} are 150, 225 or 300mm

The proposed lateral classification system is therefore to estimate the following three key parameters;

1) Closure to target distance, from camera to lateral, x_{vp}, (for incorporation in x_L),

2) Angle of lateral and NME intersection, ρ and

3) Lateral diameter, φ_{LAT}.

where only x_{vp} is to be 'accurately' specified as the other two parameters are to be compared to a discrete data set of likely values which are distinct.

Evaluation of both x_{vp} and ρ is to be provided by Reflective Photometric Stereo, a development of the existing CV technique known as Photometric Stereo (PS). The principles underlying Photometric and Reflective Photometric Stereo (RPS) and the relationships between them are now discussed. Evaluation of φ_{LAT} is obtained from a separate procedure, discussed later in Section 2.3.4.

Photometric Stereo is similar in some respects to more widely known stereo techniques such as binocular stereo, Figure 2.18. Binocular stereo computes the 3D position of an object by triangulation after comparing two images of the object, obtained from different viewpoints but under the same illumination conditions. If it can be determined that image features, which are most commonly edges, extracted independently from the two views arise from the same object features, then the location of those object features can be recovered.

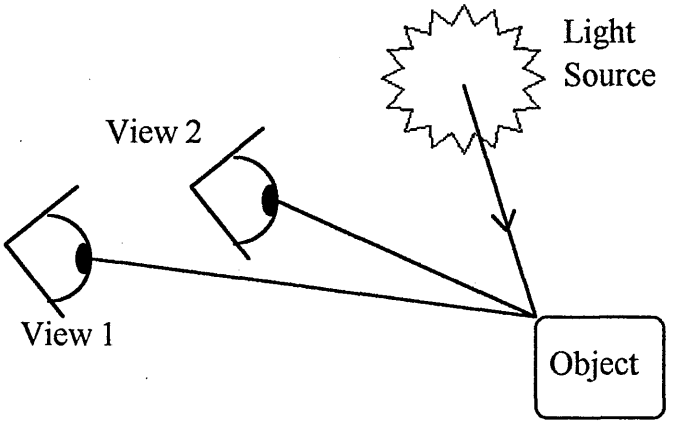

Figure 2.18: Binocular Stereo

Photometric Stereo [46, 47] also exploits differences between images captured under different circumstances, however, viewing position is kept constant and multiple images are obtained by varying the illumination considerably, Figure 2.19. The PS method relies upon the ability to measure differences in image intensity at corresponding locations within each image under varying illumination conditions to obtain 3D measurements. For each lighting configuration, all possible image intensity values and their relationship to surface properties, usually surface orientation, are stored in look-up tables termed a reflectance maps (RM's) [48]; please refer to Section 2.3.3.

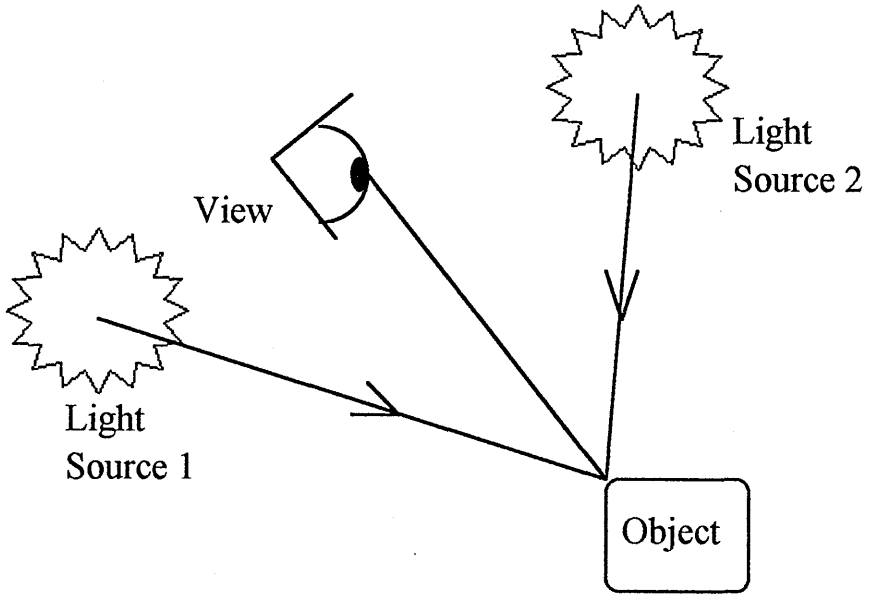

Figure 2.19: Photometric Stereo

In general PS techniques are not widely used, as a requisite key initial assumption is that the illumination conditions under which the images are taken must vary significantly and in a known manner between successive images. Even in open environments such as offices and factories for example, it is often not possible to control illumination conditions to the extent required. In the enclosed environment of the NME sewer these conditions are even more unlikely to be achievable as there is simply not enough space to allow such widely different light source positions.

However, recalling the concept of direct and reflected illumination already proposed in Section 2.2, a variant of photometric stereo which utilises these forms of illumination to produce the necessary differences in illumination source positions for as NME sewer classification, is achievable and has been developed by third parties. This variant is termed Reflective Photometric Stereo (RPS) with the underlying notion that in enclosed environments radically different lighting conditions may be obtained by careful positioning of two fixed light sources.

Upon confirmed lateral detection under reflected light, a second image is taken of the lateral from the same tractor position under direct illumination and the classification process is initiated employing RPS. From these two images, by modelling both the radiometry and geometry of the environment, equations may be derived that estimate the amount of light emitted from the target surface under direct and reflected illumination: E_d and E_r respectively. From these equations, look-up tables termed Reflectance Maps are generated which are used to interpret image pairs to elicit surface orientation, ρ, and target distance, x_{vp}. Theoretical models, which describe E_d and E_r respectively, are now proposed.

2.3.2 Mathematical Model

Recalling Section 2.1.1 and Figure 2.17, the proposed objectives of the procedure are to determine relationships for intersection angle ρ and the distance between the tractor and the image vanishing point represented by x_{vp}, figure 2.17. For these two unknowns, two simultaneous equations are provided, one employing direct illumination, the other, reflected.

Considering the former case initially and recalling Equation 2.1, the direct illumination ray of initial intensity I travels a distance r from the tractor, at an angle α_d to the NME centreline, to the distant junction or laterals intersection edge as illustrated in Figure 2.20. It makes an angle θ with the normal to the lateral's wall and returns towards the camera along the same path; other light rays are reflected off this wall, but the camera does not collect these. It is to be noted that the light source is assumed to generate a spreading beam (Figure 2.20). The one illuminating the target edge being directed

relative to the NME centre line corresponds to angle α_d as per the return ray. The fact that the light source and camera are not completely coincident gives rise to a relatively negligible offset error (approximately 5%).

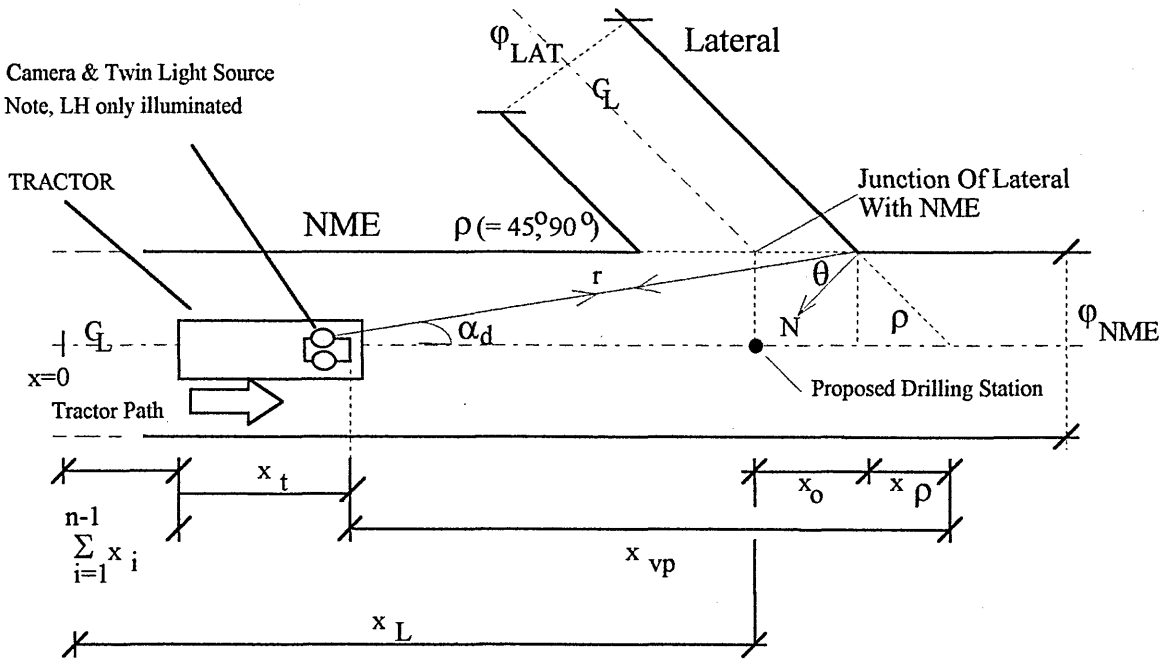

Note; $x_L = \sum_{i=1}^{n-1} x_i + x_t + x_{vp} - x_o - x_\rho$

and, $x_o = \frac{\varphi_{LAT}}{2\sin\rho}$ $x_\rho = \frac{\varphi_{LAT}}{2\tan\rho}$ for $\rho = 45$

and, $x_o = \frac{\varphi_{LAT}}{2}$ $x_\rho = 0$ for $\rho = 90$

Figure 2.20: Classification Topology – Direct Illumination

Recalling Equation 2.1, incorporation of incident light ray angle α_d requires appreciation that the angle subtended at the illuminated junction edge by x_{vp} shows;

$$90 + \theta = 180 - (\rho + \alpha_d) \qquad \text{(Equation 2.2)}$$

Rearranging Equation 2.2 gives,

$$\theta = 90 - (\rho + \alpha_d) \qquad \text{(Equation 2.3)}$$

By inspection, emittance angle α_d is available from,

$$\tan \alpha_d = (\frac{\varphi_{NME}}{2})(x_{vp} - \frac{\varphi_{NME}}{2 \tan \rho}) \qquad \text{(Equation 2.4)}$$

From Figure 2.20 and incorporated formulae,

$$r \cos \alpha_d = x_{vp} - \frac{\varphi_{NME}}{2 \tan \rho} \qquad \text{(Equation 2.5)}$$

If Equations 2.3 to 2.5 are now incorporated within Equation 2.1, then a final expression for Ed may be obtained Equation 2.6.

$$E_d = kI \left[\frac{\sin\left(\rho + \tan^{-1}\left(\frac{\varphi_{NME}}{2\left(x_{vp} - \frac{\varphi_{NME}}{2 \tan \rho} \right)} \right) \right)}{\frac{\left(x_{vp} - \frac{\varphi_{NME}}{2 \tan \rho} \right)}{\left(\cos \frac{\varphi_{NME}}{2\left(x_{vp} - \frac{\varphi_{NME}}{2 \tan \rho} \right)} \right)^2}} \right] \qquad \text{(Equation 2.6)}$$

E_d denotes the intensity of light returned / reflected off the directly illuminated junction edge.

This complex expression may be written,

$$\frac{E_d}{Ik} = f_1(\rho, x_{vp}) \qquad \text{(Equation 2.7)}$$

For the reflected illumination case, the light ray incident upon the junction edge travels a distance r1 + r2 as shown in Figure 2.21.

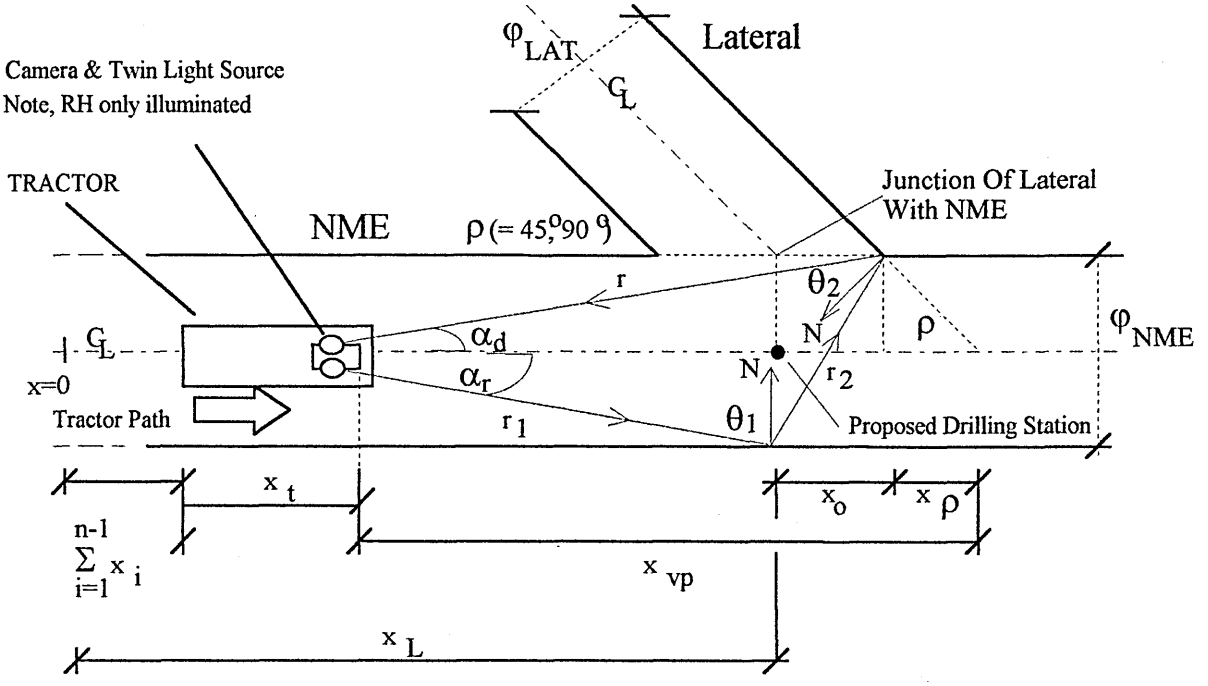

Note; $x_L = \sum_{i=1}^{n-1} x_i + x_t + x_{vp} - x_o - x_\rho$

and, $x_o = \frac{\varphi_{LAT}}{2\sin\rho}$ $x_\rho = \frac{\varphi_{LAT}}{2\tan\rho}$ for $\rho = 45$

and, $x_o = \frac{\varphi_{LAT}}{2}$ $x_\rho = 0$ for $\rho = 90$

Figure 2.21: Classification Topology – Reflected Illumination

Again employing Equation 2.1, the intensity of light reflected off the far NME wall is given by,

$$I_1 = \frac{kI\cos\theta_1}{r_1^2} \qquad \text{(Equation 2.8)}$$

From the geometry of Figure 2.21 this becomes,

$$I_1 = kI\sin\alpha_r\left(\frac{2\sin\alpha_r}{\phi_{NME}}\right)^2 \qquad \text{(Equation 2.9)}$$

or

$$I_1 = kI\sin^3\alpha_r\left(\frac{2}{\phi_{NME}}\right)^2 \qquad \text{(Equation 2.10)}$$

This reflected light illuminates the junction edge having travelled a further distance r_2 such that the light returned from the junction edge to the camera, noting α_d is common return angle to direct and reflected rays, is given from Equation 2.1 by,

$$E_r = I_1 = k\left(\frac{kI\cos\theta_1}{r_1^2}\right)\cos\left(\frac{\theta_2}{r_2^2}\right) \qquad \text{(Equation 2.11)}$$

or

$$E_r = I_1 = \frac{k^2 I\cos\theta_1\cos\theta_2}{(r_1 r_2)^2}) \qquad \text{(Equation 2.12)}$$

Geometric manipulation similar to that used in Equations 2.2 to 2.5 leads to substitution for α_r θ_2 and r_2, such that an expression results from Equation 2.12.

(Equation 2.13)

More formal details are provided in Appendix C.

Simultaneous solution of Equations 2.7 and 2.13 should therefore provide for values of p and x_{vp} noting k and I (and (P_{nme}) are known *a priori* whilst Ed and Er are established from appropriate grey-level images.

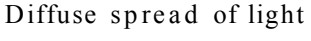

Figure 2.22: Reflected Illumination - 'Elongated Light Source'

Unfortunately, development of the model resulted in poor results being obtained and inspection of typical sewer images employing reflected light indicated why this was the case. As shown in Figure 2.22, reflected light tends to be diffuse, and whilst it is considered reasonable to use single ray light illumination for a nominal distant point source, it is clearly unacceptable in the reflected case.

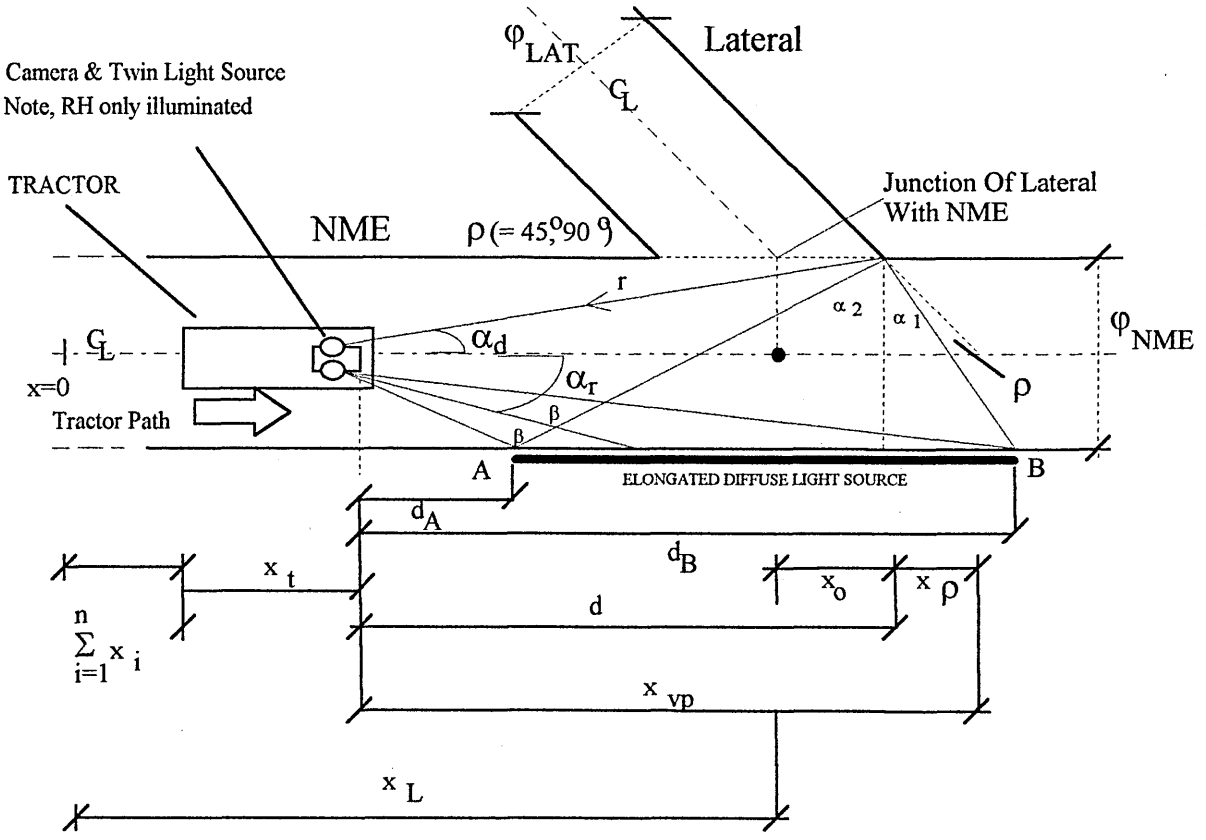

Note; $x_L = \sum_{i=1}^{n} x_i + x_t + x_{vp} - x_o - x_\rho$

and, $x_o = \frac{\varphi_{LAT}}{2\sin\rho}$ $x_\rho = \frac{\varphi_{LAT}}{2\tan\rho}$ for $\rho = 45$

and, $x_o = \frac{\varphi_{LAT}}{2}$ $x_\rho = 0$ for $\rho = 90$

● = Proposed Drilling Station

Figure 2.23: The Geometry of 'Diffuse' Linear Light Approximation For Reflected Illumination

Figure 2.23 shows the updated geometry of the diffuse reflected illumination situation superimposed on the single ray model of Figure 2.21. Illumination of the target is produced by integration of the light emitted from the diffuse light source.

A non point source illuminator, such as that proposed by Keitz [49], is therefore considered to best describe the illumination provided. It is assumed that the diffuse effect produced along the reflecting wall approximates to a simple linear source, which emits light uniformly along its length. The illumination reflected from the NME sewer wall, opposite the lateral junction, effects a linear light source produced over a determinate extent of the wall denoted by points A and B.

The derivation proceeds by first calculating the contribution dI_1 of a cylindrical surface element of AB, dl in length. Integration of dI_1 between the angles α_1 and α_2 then provides an estimate of total illumination. It is assumed that the 'reflecting' light source lying mounted on the tractor is directional, with its principal axis oriented α_r degrees from the pipe axis. It is further assumed that the light source only emits light in directions lying within +/-β degrees of its principal axis. Both the position and length of the linear source are then functions of α_r, β and φ_{NME}.

If points A and B mark the endpoints of the linear source and d_A and d_B are the distances, measured in the direction of the pipe axis, from the light source to A and B respectively, then the illumination reflected from the lateral wall intersection is given by Equation 2.14; this is a revised version of Equation 2.13 where it is $f_2(\rho, x_{vp})$ that is revised. Note E_r is the total intensity of illumination at the target junction edge.

$$E_r = I_1 k \cos\left[\rho - \tan^{-1}\left[\frac{\left(d - \left(d_A - \left(\frac{d_B - d_A}{2}\right)\right)\right)}{\varphi_{NME}}\right]\right] \qquad \text{(Equation 2.14)}$$

As a result, Equation 2.13 given in general form remains valid though the precise nature of the right hand side differs from that provided by the direct ray model. Formal details of the appropriate formulae and derivations are again given in Appendix C.

The procedure employing reflectance maps for the simultaneous solution of equations 2.7 and 2.14 is now discussed.

2.3.3 Reflectance Maps

As noted previously, because the equations describing direct and reflected illumination are highly non-linear, solution for the desired parameters of ρ and x_{vp} cannot be obtained directly [46]. By generating Reflectance Maps, which are simply a table of intensity values (Figure 2.24), for both direct and reflected model cases for a range of ρ and x_{vp} values, reflectance maps for successive viewing conditions may then be compared. This assumes that the irradiance of a common point can be measured, to solve for the required parameters.

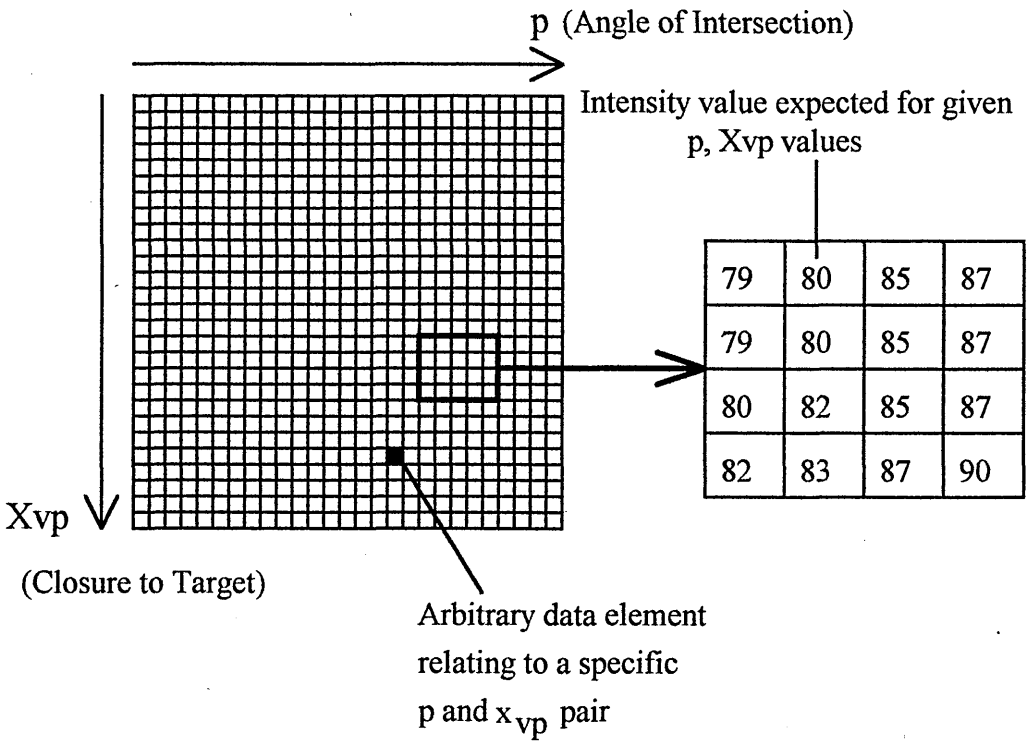

Figure 2.24: A Reflectance Map

An illustrative example is now provided.

Consider Figure 2.25, which provides two arbitrary reflectance maps generated by theoretical equations corresponding to direct and reflected illumination respectively. The grey scale levels, which comprise each RM, are particular to a set of determinate parameters and are valid for a discrete range of ρ and x_{vp} values.

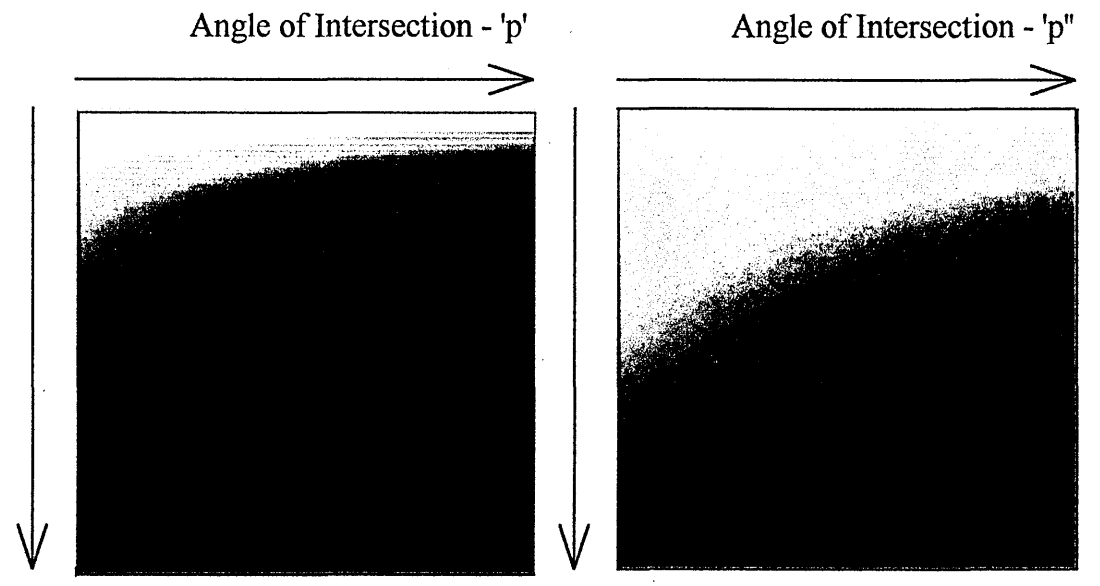

Figure 2.25: Reflectance Maps (Grey Scale)

The irradiance of a point of interest, at a common location in a pair of images captured under both illumination conditions with the same determinate parameters, may be obtained by simply reading off the grey level values in the image – say E_d/Ik and E_r/Ik^2. If all the intensity elements equal in value to E_d/Ik are now identified and highlighted in the reflectance map, an isoluminance contour is produced. This is also repeated for E_r/Ik^2 (Figure 2.26).

Closure to Target - 'x Vp

Isoluminance Contour

Associated with Direct Elimination Reflectance Map

Closure to Target - 'x Vp

Isoluminance Contour

Associated with Reflected Illimination Reflectance Map

Figure 2.26: Isoluminance Contours

'p'

Intersection point

Closure to Target - 'Xy '

Figure 2.27: Estimation of p and x vp by Interpolation

Each reflectance map constrains the surface parameters at the point of interest to a curve in ρ, x_{vp} space. To determine which single ρ and x_{vp} data set describes the point of interest, the isoluminance contours are overlaid and their intersection point found. By interpolation, the values of ρ and x_{vp}, corresponding to this intersection may be estimated, Figure 2.27.

In many real applications there may be more than one point of intersection, and hence solution, for ρ and x_{vp}. In these circumstances further images, and hence illumination conditions are required to provide a unique solution [50].

Of the three classification parameters required, the above application of the Photometric Stereo derivative method allows for the estimation of ρ and x_{vp}. Determination of the final parameter, φ_{LAT}, is considered in the following section.

2.3.4 Determination of Lateral Diameter φ_{LAT}

A method has been derived by the author to provide an estimate for the lateral diameter from an image obtained under direct illumination with known vanishing point. The method proposes that by direct comparison of the image size of the lateral junction diameter to that of the NME radius, an estimation for the lateral diameter can be obtained and compared to the known discrete sets of diameters available (i.e. 150, 225, and 300mm). Recall that the radius of the NME sewer is expected to be known *a priori*; determined empirically at the time of survey.

Referring to figure 2.28, it is assumed that the image vanishing point has already been determined by the method proposed earlier in Section 2.1.6. Initially, a straight line is projected from the vanishing point to the top of the lateral profile. A second straight line is then projected from this point to the bottom of the lateral profile.

Figure 2.27: Estimation of lateral diameter

The two image line lengths are then measured noting that their ratio corresponds to that of lateral diameter / NME radius, Equation 2.15.

$$\frac{\varphi_{LAT}}{\left(\frac{\varphi_{NME}}{2}\right)} = \frac{b}{a} \qquad \text{(Equation 2.15)}$$

where

a = scaled length of straight line connecting top and bottom of lateral profile, and

b = scaled length of straight line connecting vanishing point to top of lateral profile.

By inspection therefore,

$$\varphi_{LAT} = \left(\frac{b\varphi_{NME}}{2a} \right) \qquad \text{(Equation 2.16)}$$

2.4 SUMMARY

The applicability of CV to the qualitative detection of lateral intersections has been introduced and the different properties of direct and reflected illumination together with a method for determination of a frame of reference been noted and tested on field data. A CV based quantitative approach to lateral classification, employing an adaptation of the exiting CV technique of Photometric Stereo, has been proposed exploiting the simultaneous solution of mathematical models base on both illumination conditions to afford the estimation of both angle of lateral intersection (ρ) and closure to target distance (x_{vp}). Whilst it is to be noted that external specialist support has provided the lateral detection routines and mathematical models underlying the lateral classification system to a specification drawn up by the candidate, a simple yet effective approach has been proposed by the author for the estimation of lateral diameter (φ_{LAT}). Formal testing of both detection and classification systems is investigated using laboratory-sourced data with equipment / testing strategy discussed in Chapter 4 and results provided in Chapter 6.

Consideration is given to the qualitative kinematic study of both chainage measurement and drill task arm theory, now presented in Chapter 3, with primary concern placed on the development of a chainage measurement system for determining invert chainage or distance travelled. The characteristics and mathematical solution of kinematic attributes of a 3 degree of freedom (DOF) robotic arm for lateral reconnection are investigated, with use made of GRASP - a robot design and simulation software package

CHAPTER 3

KINEMATIC MODEL DEVELOPMENT

3.1 CHAINAGE MEASUREMENT SYSTEM (CMS)

3.1.1 Context

Given that the NME sewer presents an essentially featureless environment post-lining – only sometimes will a 'dimple' form in the lining due to the pressure curing to betray the presence of a blocked-off lateral junction - a record of the lateral's location and characteristics is to be obtained during the pre-lining survey pass. Referring to Figure 3.1 and recalling the symbol definition provided in Figure 2.17, the co-ordinate value of invert chainage x_L, the location of the drilling station, is a primary requirement.

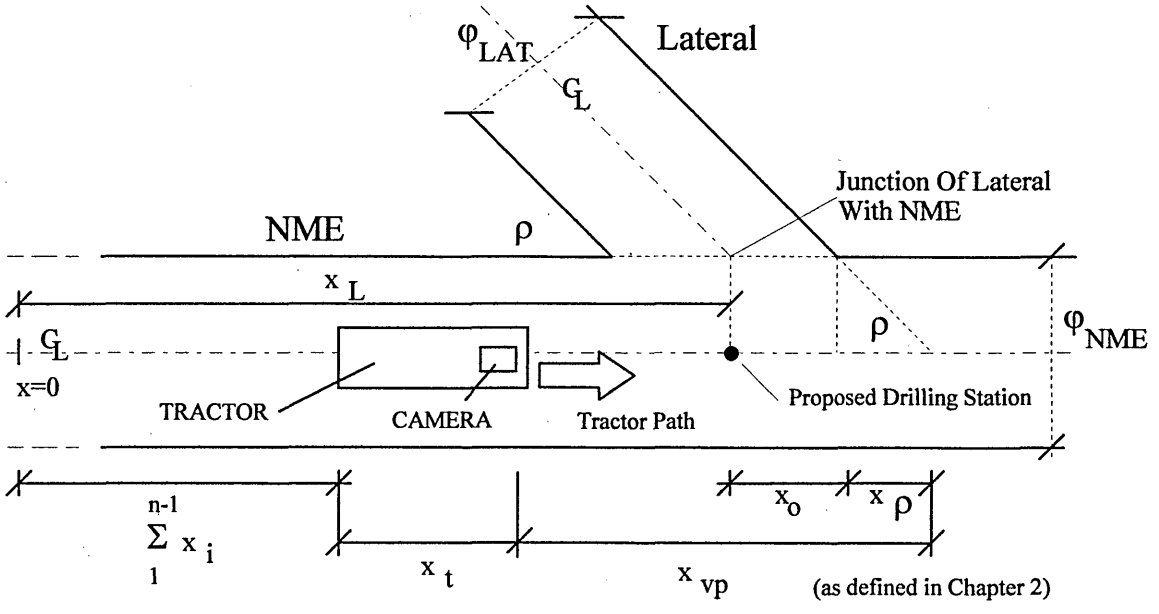

Figure 3.1: Overview of Parametric Requirements

The position of the drilling station has been chosen such that, in the vertical plane, the dimension / size of φ_{LAT} limits the extent of drilling required and to exploit symmetry of cut. It should be noted that it is the drill arm mount (i.e. revolute joint 1 noted in Section 3.2.2) that is to be centred on the drilling station (nb x_L) during the task pass. (Further, revolute joint 2 is coincident with NME centreline).

A three-pass strategy has been proposed as discussed in Chapters 1 and 2. A mechanical system will first provide appropriate chainage data to within approximately 2 to 3.5m of the lateral junction (i.e. Σx_i), whilst following detection the computer vision procedure, as noted in Section 2.3.1, will then be employed to provide the remaining classification data (i.e. closure to target chainage x_{vp}). For cost effective research, both the CMS and CVS programmes are to be implemented employing a remote PC

3.1.2 Associated Matters

Current motorised tractor practice, as previously noted in Section 1.1.4, employs a cable dispensing digitally monitored drum sited (at datum) remote to the tractor, which provides umbilical support to the CCTV and power systems. Minimising the umbilical requirements is obviously advantageous. Referring to Figure 3.2, the proposed system is to employ a rotary encoder and a laterally mounted inclinometer.

The rotary encoder acts as a 'rev' counter to the front axle such that for one complete revolution of the encoder shaft, and hence wheel, a set number of digital pulses is output by the encoder. The rotary encoder thereby provides direct digital read out of number of pulses and hence complete rotations of the wheel achieved. From *a priori* knowledge of the tractor wheel diameter the encoder provides for total distance travelled. The

inclinometer is provided to record the inevitable and necessarily non-horizontal wander up the NME sewer wall from the desired invert path. This wander is due to debris within the pipe and general wear and tear of the tractor drive components. The inclinometer therefore allows for an imperfect path being taken thereby giving the system robustness. The inclinometer provides an analogue voltage output proportional to the degree of inclination, which must be then converted into a more appropriate angle of rotation.

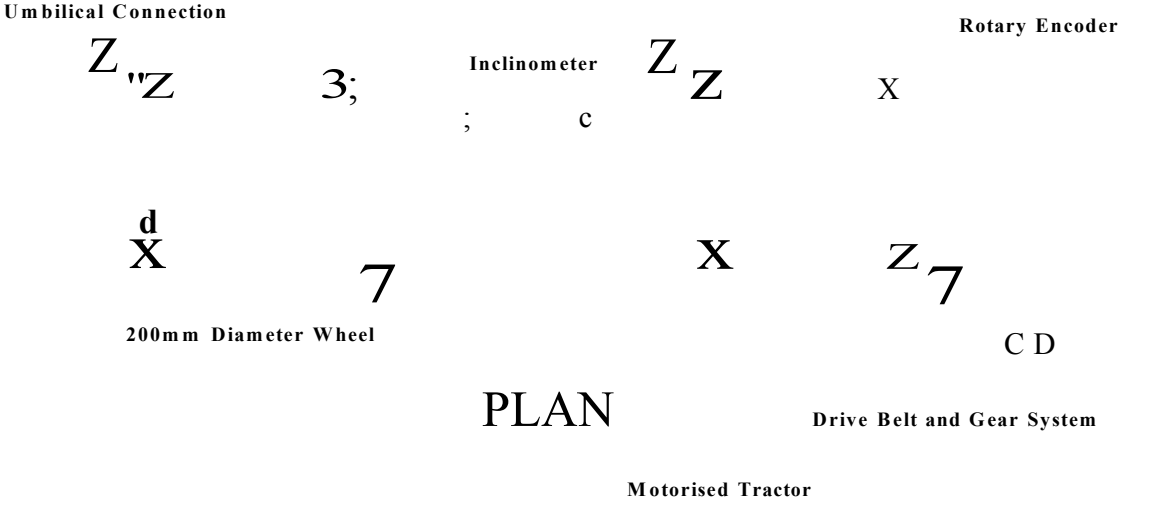

Figure 3.2: Rotary Encoder and Inclinometer System Components

Assessment of the mathematics underlying the integration of the rotary encoder and inclinometer is now addressed.

3.1.3 Mathematical Theory

Referring to Figure 3.3, typical tractor locations i and j (and k) lie a presumed straight distance travelled Δ apart. These locations represent discrete stations whose position is differentiated by the pre-set 1 second time interval (i.e. real time control) at which both Δ and the inclination or wander angle θ are effectively acquired by the encoder and inclinometer respectively. Geometry provides for the required invert chainage increment x_i by, typically, either

$$x_i = \Delta_i \cos\left\{\sin^{-1}\left[R\left(\frac{\sin\theta_i - \sin\theta_j}{\Delta_i}\right)\right]\right\} \qquad \text{(Equation 3.1)}$$

Or

$$x_i = \left(\Delta_i^2 - R^2\left[\sin\theta_i - \sin\theta_j\right]^2\right)^{1/2} \qquad \text{(Equation 3.2)}$$

And

$$O_i = R\sin\theta_i \qquad \text{(Equation 3.3)}$$

$$\alpha_i = \sin^{-1}\left(\frac{O_j - O_i}{\Delta_i}\right) \qquad \text{(Equation 3.4)}$$

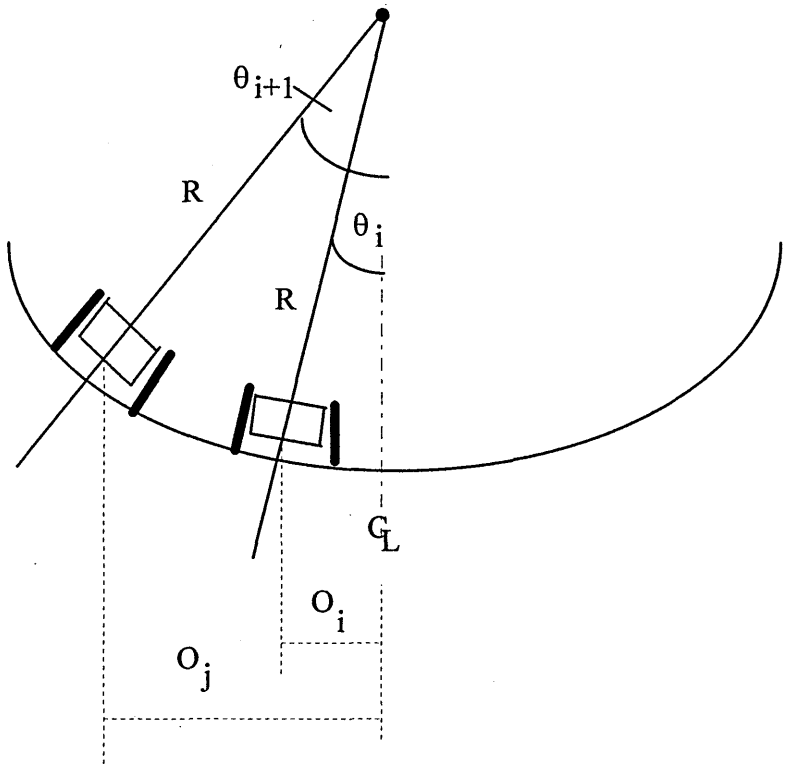

a) SECTIONAL VIEW

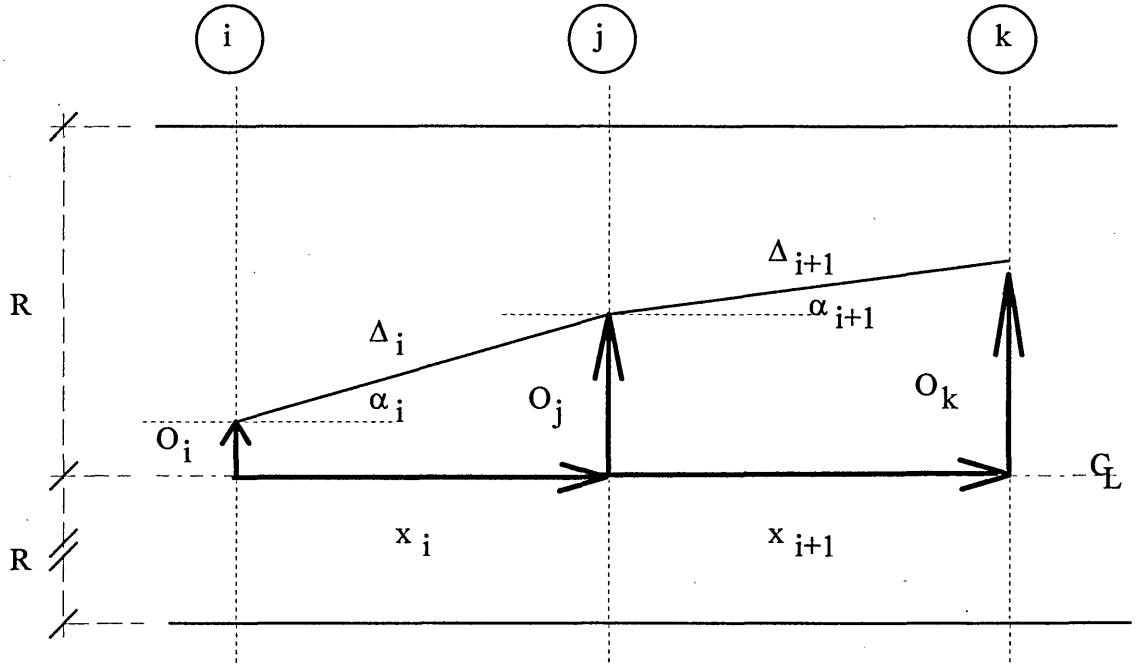

b) PLAN VIEW

Figure 3.3: Chainage Measurement System Topology

where;

O_i Horizontal offset of tractor from invert at increment i.

O_j Horizontal offset of tractor from invert at increment j.

O_k Horizontal offset of tractor from invert at increment k.

R Radius of main sewer pipe

x_i Invert line distance travelled by tractor between increments i and j.

x_{i+1} Invert line distance travelled by tractor between increments j and k.

Δ_i Distance measured by Rotary Encoder at between increments i and j.

Δ_{i+1} Distance measured by Rotary Encoder at between increments j and k.

α_i Angle of Δ_i vector relative to pipe centre line at increment i.

α_{i+1} Angle of Δ_{i+1} vector relative to pipe centre line at increment j.

θ_i Inclinometer reading at increment i.

θ_{i+1} Inclinometer reading at increment j.

Accuracy is proportional to sampling rate, which as previously mentioned is to be monitored in real time at one-second intervals. For n samples therefore, overall distance travelled as measured by the rotary encoder is $\Sigma\Delta_i$, for samples 1 to n, whilst the resolved invert chainage referring to either Equations 3.1 or 3.2 is $\Sigma x_{i,}$, for (n-1) increments of x_i.

Sampling rate is time dependent. With small time intervals (i.e. circa 1 second) and an effectively constant tractor speed (typically of the order of 0.08m/s – Section 5.1.3), then not only is Δ_i directly proportional to tractor speed but it is reasonable to assume

that α_i is constant and small through Δ_i. [Large α_i values would infer that non-parallel, with reference to the invert axis of the sewer, tractor trajectories were being obtained. Consequently, the inclinometer-derived inclination of the tractor with respect to sewer invert would not be considered accurate without undergoing some transformation.]

The assumption that α_i is small and that substantially parallel trajectories are achievable are proved later in Section 5.1.4, wherein the inaccuracies associated with potentially large α_i are also investigated.

When invert chainage Σx_i results in the tractor being within 2 to 3.5m of a lateral junction, this junction should be in 'view' of the computer vision system as noted in Chapter 2. Total chainage from datum to the drilling station is thereby acquired by adding an assessment of the distance between the lateral and the tractor's current chainage x_{vp}.

Recalling Figure 3.1, the distance along the NME invert between some convenient datum (nb manhole access) and drilling station is denoted by x_L. The chainage is taken to correspond to the distance from the datum to the intersection of the lateral's centre-line and the projection across the junction of the NME sewer wall. The CVS assessed closure to target chainage x_{vp} is the distance from the tractor to the projection of the lateral's furthest edge, as seen from the cameras perspective, i.e. lateral back wall, to its intersection with the NME sewer centreline. A correction therefore has to be made to resolve the estimated distance to drilling station as defined in Equation 3.5.

$$x_L = \sum x_i - (x_{vp} - x_\rho - x_O) \qquad \text{(Equation 3.5)}$$

where

$$x_O = \frac{\varphi_{LAT}}{\sin \rho} \qquad \text{(Equation 3.6)}$$

and from geometry

$$x_\rho = \frac{\varphi_{NME}}{\tan \rho} \qquad \text{(Equation 3.7)}$$

Note that Equations 3.6 and 3.7 will require values for φ_{LAT} and ρ from the CV system.

3.1.4 Programming Factors

The CMS computer programme, written in QBASIC and provided in Appendix B, is based on the flow diagram of figure 3.4. As discussed in Section 3.2.2, in order to keep α_i small the programme samples the outputs of both the rotary encoder and inclinometer based on a time increment of 1 second. Keeping tractor speed low and constant ensures that the assumptions used in the CMS mathematical theory are valid. At each sampling station both the incremental distance covered by the tractor, Δ_i, and tractor inclination, θ_i, are calculated. The incremental distance x_i is determined (recalling Equations 3.1 and 3.2), and overall invert line distance travelled from datum Σx_i calculated and stored until next loop. For each time increment Σx_i is updated until the end of the survey pass.

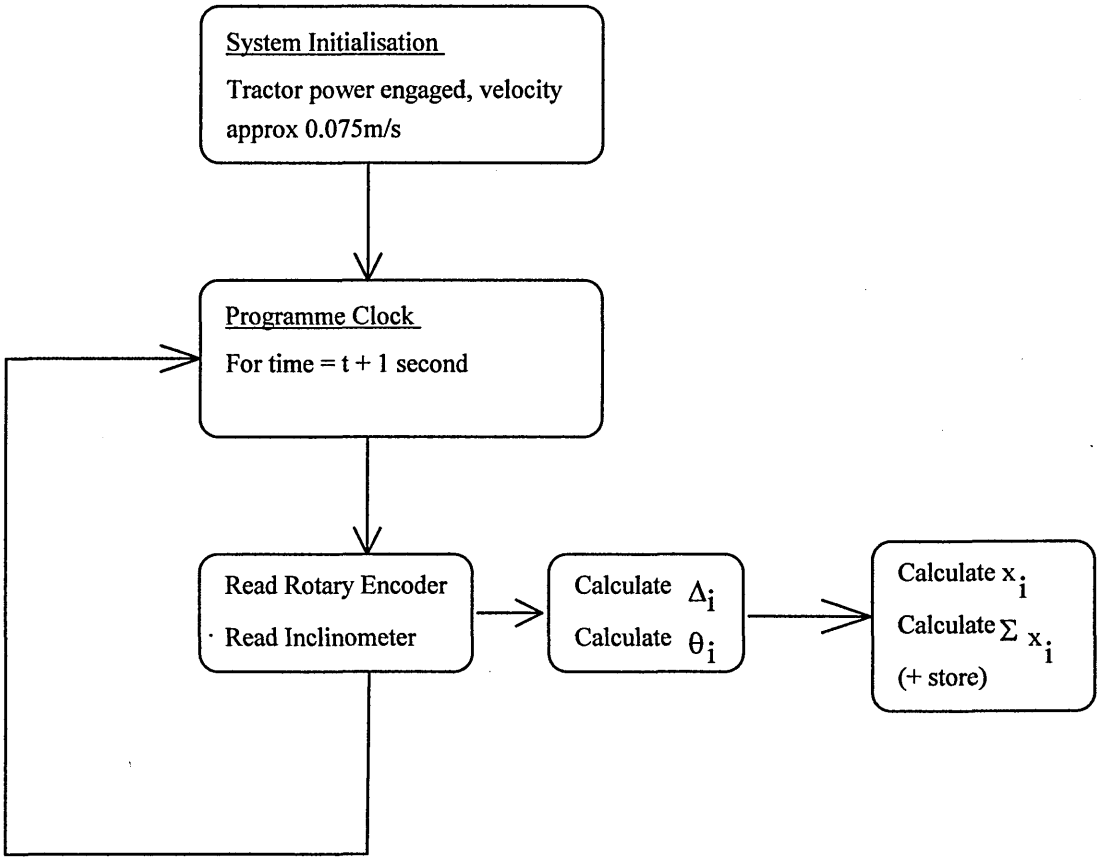

Note; n 't' readings give $\sum_{1}^{n-1} x_i$ for (n - 1) distance increments

Figure 3.4: CMS Programme Flow Diagram

As previously noted, a fuller explanation of both the software and hardware requirements of the system are presented in Section 4.3 with the laboratory investigation and evaluation of the CMS system presented in Section 5.1. Consideration is now given to the design and development of the robotic drill task arm.

3.2 ROBOT ARM KINEMATICS

3.2.1 Context

Further to initial investigations regarding the design of robotic arms [51, 52], it is considered that a 3 degree of freedom (DOF) robotic arm will satisfy the requirements of the kinematic lateral reconnection system as discussed in Section 1.4. The benefits of kinematic simulation are discussed with regard to the development of a robotic model through GRASP [53], an interactive, 3 dimensional (3D), off-line, graphical, computer simulation package, and anticipated outcomes of the study are discussed. The revised objectives of the GRASP study, in light of limitations found through the course of the research, are considered and the attainable benefits of the GRASP simulation work and resulting finalised arm design are presented. A corresponding mathematical model forming the basis for defining the trajectories that the drill must follow to undertake reconnection is derived, and equations defining the requisite arm kinematics defined. Hardware requirements are addressed and programming factors discussed.

3.2.2 Proposed Mechanism

An arm design similar to that presented in Figure 3.5a to c was initially considered to posses the required number of DOF to perform the task lateral reconnection following CIP lining of an NME sewer in line with the drill task pass strategy proposed earlier in Section 1.1.6. As can be seen from the figure, the proposed mechanism comprises two revolute and 1 prismatic joints totalling three DOF in all. A fourth DOF will be required for the anticipated drill twist located at the arm's end effector (EE); however, as will be discussed later in Section 4.3.3, the cost effective research programme presented herein necessitated a fixed rather than dynamic drill substitute for this relatively simple DOF.

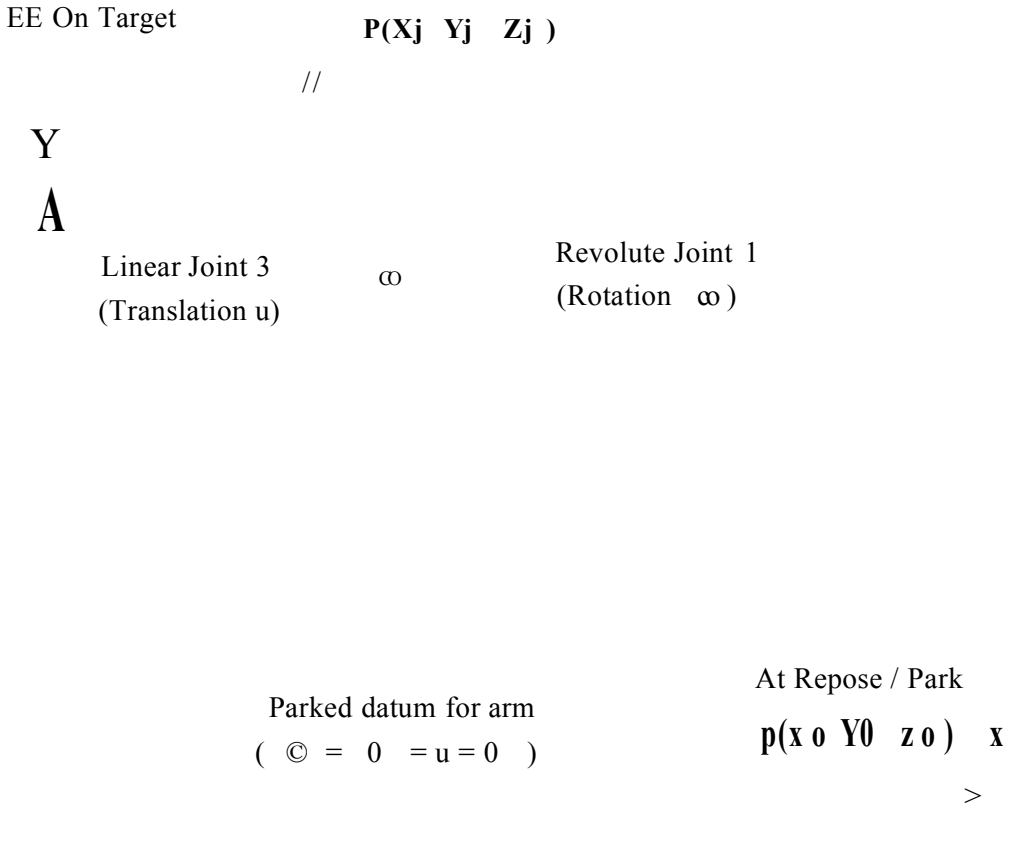

Figure 3.5a: Proposed Arm Configuration - Plan

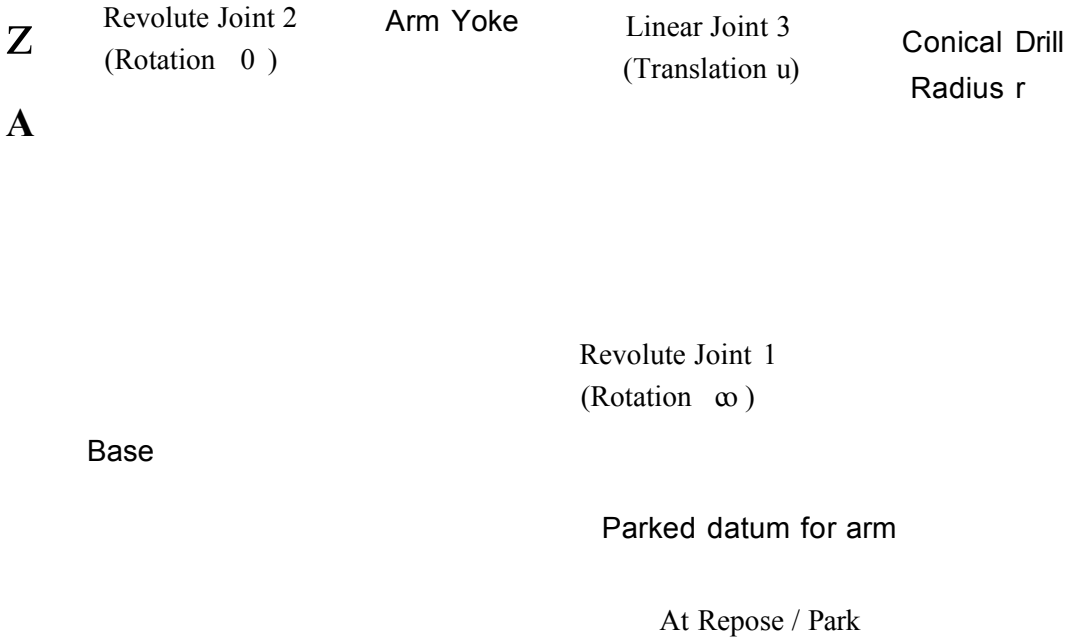

Figure 3.5b: Proposed Arm Configuration - Repose / Park Elevation

With reference to Figure 3.5a to c, assuming that the robot employs a conical grinding tool of radius r_d and that the robotic arm during transit to drill location point, i.e. lateral, is in repose, then rotational movements are required in both the horizontal and vertical planes. These are provided for in both the horizontal plane, ω (joint 1), and in the vertical plane, θ (joint 2). Together with arm extension u (joint 3), these kinematic parameters provide for reaching the furthest part of the lateral to be cut. The procedure employed for lateral reconnection is now addressed.

The arm as noted above is initially at repose so that the arm lies longitudinally along the centre of the tractor unit base. With the tractor located such that the centroid of joint 1 is located at the drilling station, the cone drill is placed on the liner surface at a position close (i.e., within r_d) to the centre of the lateral to be drilled through rotation of joints 1 and 2 and translation of joint 3. The required action of the conical drill will be to grind the liner away rather than cut out an actual solid section, which could otherwise cause an obstruction elsewhere in the sewer. Following emplacement therefore, thrust is applied (u) and the drill grinds away a curve of intersection, or inter-penetration, path. Upon completion of the path the cone drill continues grinding whilst the end effector / drill is retracted and then stepped out radially a distance not greater than r_d. Thereupon, this stepping out of curve of inter-penetration cycle continues until the last step reaches $\leq (\varphi_{LAT})/2 - r_d$ whereupon a final circular grinding loop is made. The arm is then withdrawn and returned to repose by means of a linear trajectory.

Noting that within current practice the problem of damage to the lateral pipe itself during liner drilling is not uncommon, it is envisaged that a prototype device might employ a spring tensioned universal joint mechanism at the EE, to allow the drill to

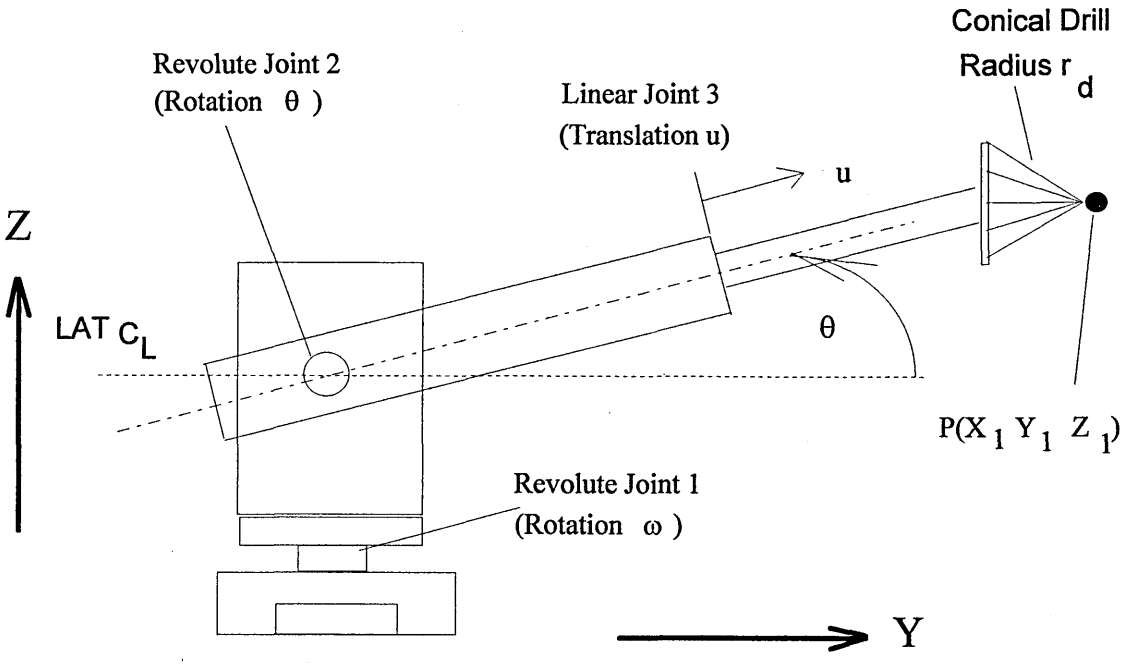

Figure 3.5c: Proposed Arm Configuration – On Target Elevation

The kinematic procedures concerning movement of the EE for lateral reconnection can be considered to entail three separate procedures:

a) Move EE from repose / park (say X_0, Y_0, Z_0) to drill initiation location (say initial X_1, Y_1, Z_1 values).

b) Commence drilling / grinding of determined curves of interpenetration defined by ensuing values of X_2, Y_2, Z_2 etc.

c) Return EE to repose.

In each case, however, the principle is common, to use kinematic increments $\Delta\theta$, $\Delta\omega$ and Δu to move through prescribed spatial increments ΔX, ΔY and ΔZ.

With reference to Figure 3.5a to c, assuming that the robot employs a conical grinding tool of radius r_d and that the robotic arm during transit to drill location point, i.e. lateral, is in repose, then rotational movements are required in both the horizontal and vertical planes. These are provided for in both the horizontal plane, ω (joint 1), and in the vertical plane, θ (joint 2). Together with arm extension u (joint 3), these kinematic parameters provide for reaching the furthest part of the lateral to be cut. The procedure employed for lateral reconnection is now addressed.

The arm as noted above is initially at repose so that the arm lies longitudinally along the centre of the tractor unit base. With the tractor located such that the centroid of joint 1 is located at the drilling station, the cone drill is placed on the liner surface at a position close (i.e., within r_d) to the centre of the lateral to be drilled through rotation of joints 1 and 2 and translation of joint 3. The required action of the conical drill will be to grind the liner away rather than cut out an actual solid section, which could otherwise cause an obstruction elsewhere in the sewer. Following emplacement therefore, thrust is applied (u) and the drill grinds away a curve of intersection, or inter-penetration, path. Upon completion of the path the cone drill continues grinding whilst the end effector / drill is retracted and then stepped out radially a distance not greater than r_d. Thereupon, this stepping out of curve of inter-penetration cycle continues until the last step reaches $\leq (\varphi_{LAT})/2 - r_d$ whereupon a final circular grinding loop is made. The arm is then withdrawn and returned to repose by means of a linear trajectory.

Noting that within current practice the problem of damage to the lateral pipe itself during liner drilling is not uncommon, it is envisaged that a prototype device might employ a spring tensioned universal joint mechanism at the EE, to allow the drill to

pivot about its attachment point. This will ensure that when liner drilling is undertaken in close proximity to the lateral inner wall, the cutting surface of the drill will be aligned with the lateral thereby producing least abrasion to its surface.

Whilst the two revolute joints and one prismatic joint are to be powered by stepper motors, it is anticipated that the drill twist action required for the EE would be achieved by using the existing tractor drive. Noting that liner drilling is to be undertaken with the tractor statically positioned, it is envisaged that some simple clutch mechanism could be designed to redirect the motor drive from the chain driven tractor wheels to the drill.

Having decided on an initial design for the robot arm, a computer simulation of the envisaged fire-and-forget robotic system was initially proposed. This was to allow the continuous updating and refinement of the robotic drill arm design and to address methods by which its task control could be achieved (i.e. possibly employing inverse kinematics for EE movements) and integrated with that of the computer vision system. It was anticipated that during this design stage, problems could be minimised without incurring expenditure on expensive physical prototypes. Therefore, as a first stage in the robot design process, predictive modelling was implemented employing an industry standard robot design package, GRASP.

3.2.3 GRASP – Research Objectives

GRASP, is an interactive, 3D, off-line, graphical, computer simulation package originally intended for the design and modelling of 3D industrial robots and their structured environment [53, 54]. The investigation of the proposed robot kinematic and control requirements, for application to NME sewer renovation seeks to apply GRASP to the more demanding environments appropriate of the construction industry. Prior to the implementation of this study the use of GRASP within the university had been minimal, and the author was the first key user.

The GRASP computer workplace is a hierarchical structure based on object ownership. Given a predefined or user generated robot, the programming required to perform any specific action with a simulation may be investigated using discrete 'step' positioning comparable to conventional walk through techniques employed in industry. The individual step functions may be compiled into continuous operational 'tracks' processes and saved as such. A robotic 'process' then may be developed and animated in real time from this track information, and the robot interaction with the environment monitored. Once a simulated process is considered finalised and ready for evaluation using a real robot, GRASP has the provision of downloading all the inverse kinematics necessary for the simultaneous joint movement to achieve the required point to point movement contained within the process. This information is contained within what is termed a GRDATA file. The abilities of GRASP to produce and to download such complex inverse kinematics are powerful features. The provision allowing directly loading of the GRDATA FILE into a compatible real robotic control program eliminates teaching robots using traditional 'walk through' modes. GRASP is equipped with the ability to down load a GRDATA file to virtually any *commercially* available robot.

It was proposed therefore to use GRASP as a non-physical modelling tool to simulate both the robot and NME sewer environment and evaluate the kinematic model employed for lateral reconnection and assess interaction within the NME environment and hence its suitability to the task prescribed in Section 1.1.5; the main goal of which was the production of a downloadable GRDATA file. Further, the CV aspects of camera and lighting were to be investigated towards integration within the simulation.

Modelling aspects will now be considered.

3.2.4 Robotic Modelling Employing GRASP

Figure 3.6 illustrates a simple 3 DOF robot arm generated using GRASP referenced here as MOD1.

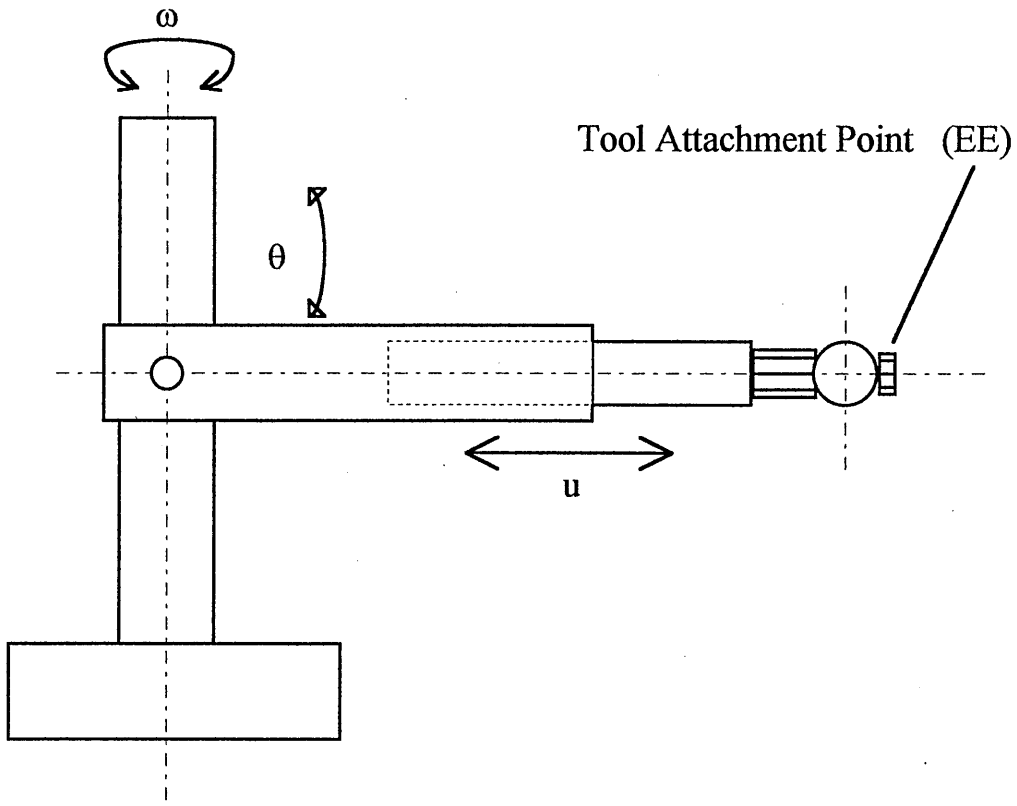

Figure 3.6: Robot Structure – MOD1

Similar to the arm design proposed in Figure 3.5, rotational movements are again provided in both the horizontal and vertical planes, ω (joint 1) and θ (joint 2), together with arm extension u (joint 3).

1. ROBOT MOD1 NEW TYPE A
2. JOINT 1 (SHIFT Z 250) REVOLUTE Z
3. JOINT 2 (SHIFT Z 1000) REVOLUTE Y
4. JOINT 3 (SHIFT X 650) PRISMATIC X
5. TAP (SHIFT X 125)
6. MINIMUM -180 -45 -70
7. MAXIMUM 180 45 750
8. INITIAL 0 0 150
9. PARK 0 0 -50
10. VELOCITY 60 60 500
11. ACCELERATION 160 160 1500;

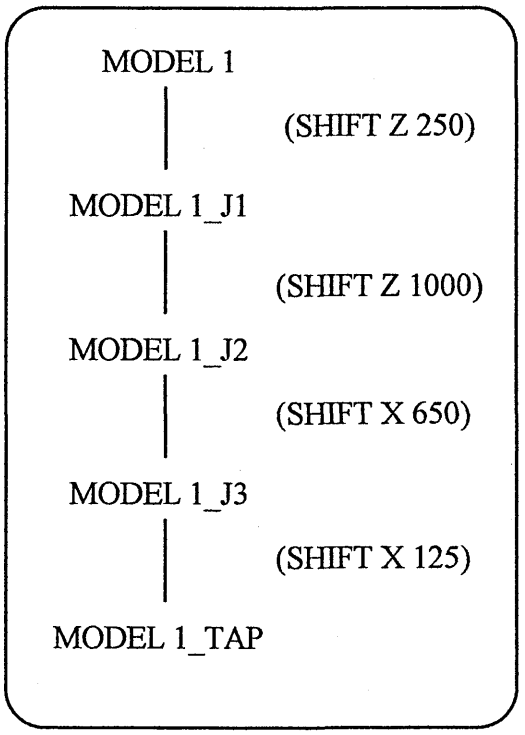

Robot Input Statement

Robot Structure

3 DOF Arm

Figure 3.7: GRASP Robot Input Configuration Statement

Figure 3.7 details the underlying data structure used by the software package to define the robot structure of Figure 3.6; the geometry and available kinematic movement of the arm 'joints' of the model are defined in what is termed a 'robot input statement'. This statement details the robots configuration, shape in 3D space, and joint type, whether prismatic or revolute. Functional parameters of the robot, corresponding to initial joint positioning, maxima and minima of attainable joint movement and allowable joint

velocities and acceleration. All these may be pre-defined at design and adjusted at any later development stage during the design or simulation process. Table 3.1 provides a brief summary of the input statement provided in Figure 3.7;

Input Statement	**Purpose**
ROBOT MOD1 NEW TYPE A	Creates New robot called MOD1 with geometric structure referenced TYPE A.
JOINT 1 (SHIFT Z 250) REVOLUTE Z	Defines joint 1 as revolute, offset 250mm from the XYZ datum (0, 0, 0) along the Z axis.
JOINT 2 (SHIFT Z 1000) REVOLUTE Y	Defines joint 2 as revolute, offset 1000mm from Joint 1along the Z axis
JOINT 3 (SHIFT X 650) PRISMATIC X	Defines joint 3 as prismatic, offset 650mm from joint 2 along the X axis.
TAP (SHIFT X 125)	Defines the Tool Attachment Point (i.e. EE position) offset 125mm from Joint 3 along the X axis.
MINIMUM	Defines minimum allowable joint movement; i.e. joint 1 –180 degrees, joint 2 –45 degrees and joint 3 –70mm.
MAXIMUM	Defines maximum allowable joint movement for the joints
INITIAL	Defines the joint positions for the robot when it is first loaded into a GRASP simulation.
PARK	Defines the joint positions when the robot is instructed to PARK, i.e. assume repose position.
VELOCITY / ACCELERATION	Define the maximum velocity and acceleration with which joint may move.

Table 3.1: Explanation Robot Input Configuration Statement (Figure 3.7)

A full input statement such as that shown in Figure 3.7 is only required when a new robot structure is being defined. If a simulation requires a number of duplicate TYPE A robots then these can be quickly created employing a much-simplified robot input statement; e.g. ROBOT MOD2 NEW TYPE A which would create a duplicate robot called MOD2.

The physical structure of the robot is added to the already defined configuration in terms of specifying simple geometric shapes. These are then attached to the structure of the robot specifying suitable XYZ co-ordinate offsets to produce a complete robot design (recall Figure 3.6).

Following initial exploration of software and the possibilities that simulation under GRASP affords to robot design, as mentioned in the preceding section it was intended that GRASP be used to provide the following;

1) The ability to produce a design for the robot arm without the need for expensive physical trial prototypes,
2) The ability to animate the robotic model produced provides the ability to analyse and assess their suitability to the task requirements that they have been designed for and, including for example, the compatibility of performance envelopes within environmental constraints,
3) The ability to test the CVS on GRASP generated geometry to assess the performance of the detection and classification system, proposed in Chapter 2, on theoretical image data; during the course of the research programme, later versions of GRASP provided the ability to control illumination constraints and observe simulations from a user specified camera perspective.

4) The control algorithms produced within a GRASP simulation can be directly downloaded to an industrial robot in the form of a GRDATA file. This file provides all the inverse kinematics necessary to obtain simultaneous joint movement for complex point to point movement; involving simultaneous movement of all required joints resulting in a direct path from initial to final position, involving the shortest and therefore quickest path for the EE.

Whilst staggered movement of individual motor joints to achieve the desired final position achieves the same end result, the chosen path is longer both in distance and duration. GRASP provides a cost effective solution to the problem.

5) The ability to integrate all aspects of the robot system with the intention of defining the integration of the full robotic system under GRASP.

Throughout the research program, the GRASP system at the university was methodically updated both in terms of accessing the most recent software version available given the hardware affordable to run it. Advancement of the in-house expertise of GRASP was achieved through in house consultancy arrangements with BYG Systems Ltd of Nottingham responsible for developing GRASP, and by attending workshops and open days. Through this collaboration, the research objectives regarding GRASP were more clearly targeted offering clear potential for the integration of the complete robotic system under GRASP.

Unfortunately, after considerable time during which the prototype itself was fabricated, it became apparent that the promise of downloading the inverse kinematics generated within GRASP to the robot was not going to be feasible in a viable timescale; downloading being only possible to commercially available robots and not to research tool robot designs. Further, although GRASP provides the ability to model light sources, the necessary computing power which could produce both realistic shading in real time and useable camera perspective was beyond the financial constraints of the research programme. The option of prototyping the CVS on GRASP generated theoretical sewer images could not be achieved.

The usefulness of GRASP was therefore limited but GRASP could still be used as an initial design and development tool for the robot arm's structure and joint configuration. The kinematics required for arm control was investigated separately employing direct mathematical modelling, and the control programs required providing the requisite control data developed away from GRASP (please refer to Section 3.2.6).

In light of the above, short comings of the application of GRASP to the solution of the envisaged robot control and system integration, GRASP was used to provide the following, reduced, aspects of study;

1. To model an idealised sewer environment incorporating both 45 and 90 degree lateral connections, and
2. To model a suitable arm and end effector for the task of lateral reconnection, and
3. Integration of the above to assess the suitability of the arm kinematics to the task of lateral reconnection.

The following kinematic solution for the robot arm was therefore addressed by two methods;

a) Simulation using GRASP to assess performance characteristics within the envisaged sewer environment, and

b) In the absence of any aforementioned GRDATA file, derive equations that allow the kinematics of the arm movements required to be determined.

The revised GRASP model, simulation and associated simulated control produced are now addressed.

3.2.5 Revised GRASP Study

As discussed in the preceding section, GRASP was used to produce a model of the task environment, including typical NME sewer diameters of 375, 450 and 600mm, incorporating lateral connections and robot. A robotic arm and associated conical drilling tool were initially modelled, as was the proprietary tractor unit already acquired, Figure 3.8.

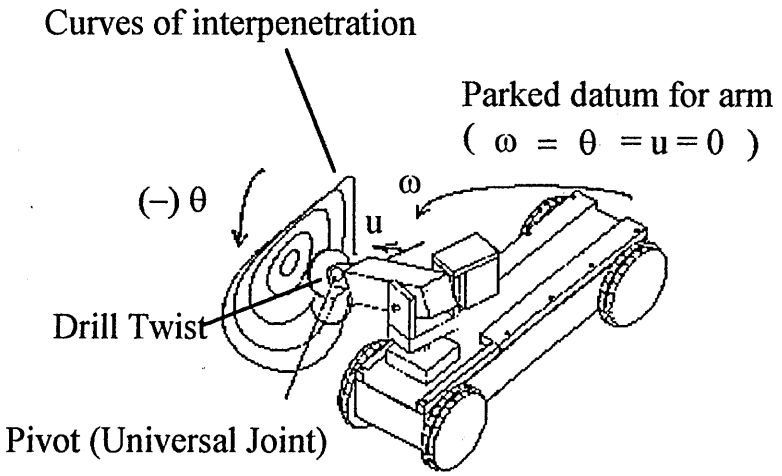

Figure 3.8: GRASP Generated Tractor/Arm Model and Target

Based on the reconnection procedure discussed in Section 3.2.2, the following provides a summary of the kinematic procedures employed within the simulation.

With the arm initially at repose and positioned at the drilling station, through rotation of joints 1 (co) and 2 (0) and translation of joint 3 (u) the cone drill is placed on the liner surface at the centre of the lateral to be drilled within a tolerance r^. Following emplacement, thrust is applied (u) and the drill follows a curve of intersection, or inter-penetration, path. Upon completion of the path the cone is stepped out radially a distance not greater than r^. Thereupon, this stepping out of curve of interpenetration cycle continues until the last step reaches < Rj - r^ whereupon a final circular loop is made. The ami is then withdrawn and returned to repose by means of a linear trajectory.

Figure 3.9: GRASP Generated Tractor/Arm Model and Target

The GRASP simulation employed shows well in this action, Figure 3.9, as the respective 3D linear path described by the end effector is simply generated, employing inverse kinematics, despite the complex interaction required between u, ω and θ to achieve this aim.

In GRASP, dynamic movements are programmed using the TRACK facility. This facility provides for the animation of the reconnection process, i.e. a simulation. It was envisaged that tracks could be post-processed to the actual prototype robot avoiding the need for explicit mathematical modelling, and subsequent programming. However, the inability to download a useable GRDATA file has necessitated both the mathematics and programming to be assessed independently, refer to Sections 3.2.5 and 3.2.7. The GRASP analysis still affords the study of GRASP generated algorithms for arm control

The GRASP simulation produced can be thought to essentially contain two TRACKS or grouped operations which employ field data (pipe radii, lateral joint intermittancy distances, intersection angles) as program variables but during simulation given common values; the interaction of which is illustrated in the flow diagram of Figure 3.10. It is to be noted that the reference to CVS derived classification data and CMS recalled chainage to target.

- MOVE_TRACTOR; This positions the tractor in the vicinity of the lateral relative to some arbitrary datum, and
- DRILL_LATERAL_N (N relates to the particular non man entry sewer / lateral incidence angle); This concerns the drilling task per se, with return to the above upon completion.

Interest is currently centred upon the latter TRACK; it consists of three key GRASP procedures;

- PARK; This checks the repose status.
- CURVE_START; This initially moves the end effector (drill) to the target (lining-covered lateral entry orifice) employing the PATH facility.
- CURVE_FOLLOW; A POLYLINE facility is used to grind out a curve of interpenetration path. A C programme generates a series of POLYLINE intersection profiles employing the geometrical models derived in Section 3.2.6, based upon the requisite geometry of the lateral profile. The profiles radiate from the lateral intersection centreline in steps of r_d, such that the final profile radius is not greater than $R_l - r_d$.

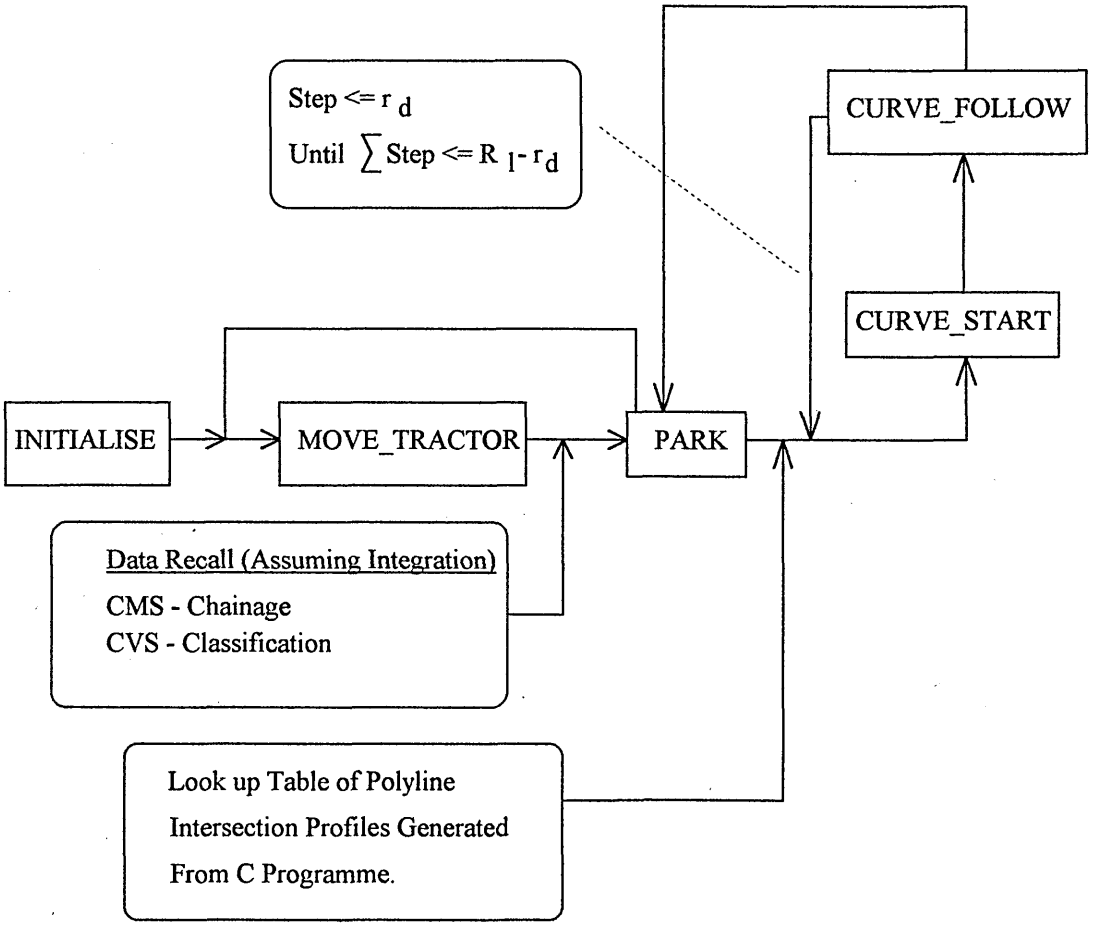

Figure 3.10: GRASP Simulation - Flow Diagram

Upon completion of the first POLYLINE activity, CURVE_START is recalled to step the end effector out to the next POLYLINE, on this occasion drilling as it moves through the lining material. CURVE_FOLLOW is then reactivated and the procedure continues until the lateral has been fully reconnected whereupon PARK is recalled to achieve repose; control is then passed back to MOVE_TRACTOR in order to locate the next lateral.

In the absence of a GRDATA file, the following section now determines analytically the task kinematic model performance criteria from considering the task environment, and deriving equations which describe it.

3.2.6 Interpenetration Curve Arm Kinematics – A Mathematical Solution

As discussed in Section 1.1.4, lateral connections to the NME main sewer are most commonly aligned at either $\rho = 45^{o}$ or 90^{o} and generally occur centreline-to-centreline. Laterals usually intersect the main sewer between 9 and 3 o'clock about the NME centreline and may, therefore, also possess some fall (γ) - any angle of fall would be acquired by inspection of an appropriate (CV) grey scale image. As noted in Table 1.1, however, concentration is placed on laterals at 3 and 9 o'clock (i.e. no lateral fall, γ=0). However bearing in mind for possible future development, an algorithm for lateral fall is herein theoretically included.

The geometrical model of such an intersection between lateral and sewer is as illustrated in Figures 3.11 to 3.13. Initially and noting the above, the model pre-supposes a horizontal lateral lie ($\gamma = 0$) at the joint itself in conjunction with a general value of lateral intersection angle to the NME sewer centre line, ρ.

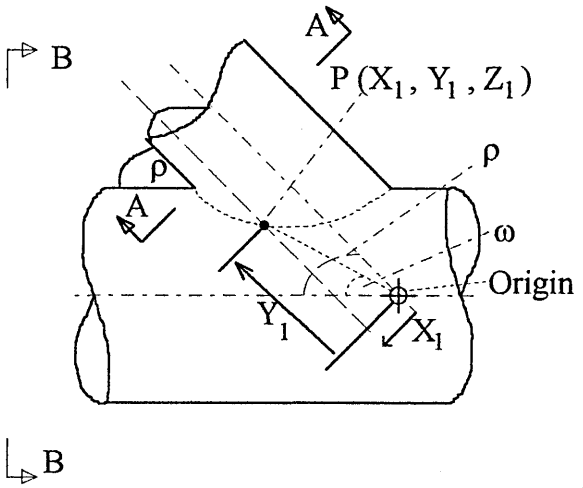

Figure 3.11: Plan View on Sewer Intersection

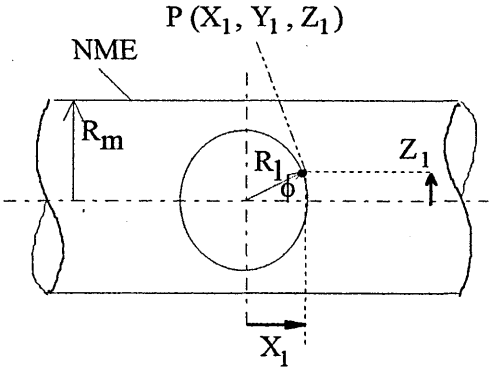

Figure 3.12: Section A – A

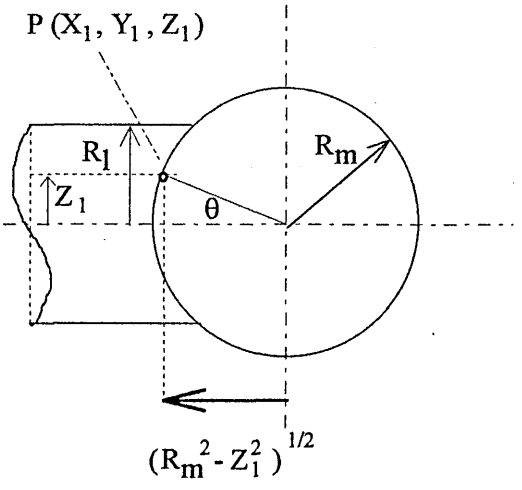

Figure 3.13: Section B – B

To determine the kinematic arm movements required, equations defining the 3D co-ordinates of the expected intersection profiles are to be computed from known pipe geometry, as suggested by Figures 3.11 to 3.13. Considering an arbitrary point P(X_1, Y_1, Z_1) on the intersection profile of the connection - note the co-ordinate system is oriented about the lateral centreline - the typical spatial co-ordinates are given by the following Equations 3.8 to 3.10;

$$X_1 = R_l \cos\phi \qquad \text{(Equation 3.8)}$$

$$Y_1 = \frac{\sqrt{R_m^2 - Z_1^2}}{\sin\rho} + \frac{X_1}{\tan\rho} \qquad \text{(Equation 3.9)}$$

$$Z_1 = R_l \sin\phi \qquad \text{(Equation 3.10)}$$

Where R_m ($=\phi_{NME}/2$) and R_l ($=\phi_{LAT}/2$) represents the radii of the main sewer and lateral intersection pipes respectively, ϕ denotes the angle about lateral centre line incremented from 0 to 360^o in 1^o steps and ρ, the angle of pipe intersection.

Given the tractor's co-ordinate frame, it is useful to transform the lateral co-ordinates X_1, Y_1, Z_1 into X_2, Y_2, Z_2 based upon the non man entry centreline as illustrated in Figure 3.14. Accordingly,

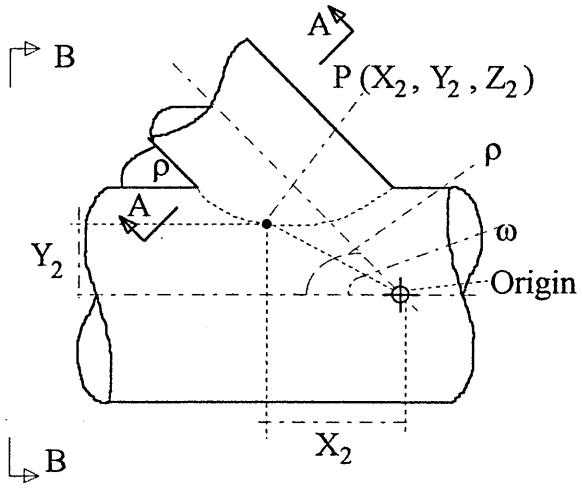

Figure 3.14: Co-ordinate Frame Transformation

Hence;

$$X_2 = R_1 \cos\phi \sin\rho \left(1 + \frac{2}{\tan^2\rho}\right) + \frac{\sqrt{R_m^2 - Z_2^2}}{\tan\rho} \qquad \text{(Equation 3.11)}$$

$$Y_2 = \sqrt{R_m^2 - Z_2^2} \qquad \text{(Equation 3.12)}$$

$$Z_2 = R_1 \sin\phi \qquad \text{(Equation 3.13)}$$

For generality, now introducing fall γ provides for a second transformation involving co-ordinates X_3, Y_3, Z_3 as illustrated in figure 3.15,

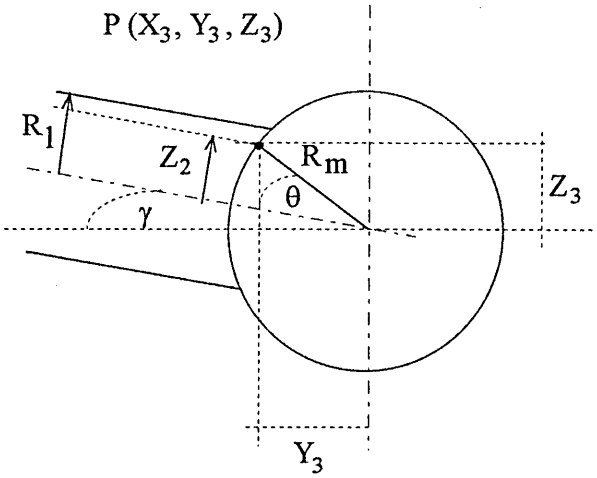

Figure 3.15: Lateral Fall Co-ordinate Transformation

Therefore;

$$X_3 = R_l \cos\phi \sin\rho \left(1 + \frac{2}{\tan^2\rho}\right) + \frac{\sqrt{R_m^2 - Z_3^2}}{\tan\rho} \qquad \text{(Equation 3.14)}$$

$$Y_3 = R_m \cos\gamma \sqrt{1 - \frac{R_l^2 \sin^2\phi}{R_m^2}} - R_l \sin\phi \sin\gamma \qquad \text{(Equation 3.15)}$$

$$Z_3 = R_l \sin\phi \cos\gamma + R_m \sin\gamma \sqrt{1 - \frac{R_l^2 \sin^2\phi}{R_m^2}} \qquad \text{(Equation 3.16)}$$

For each point on any given intersection profile, the spatial co-ordinates may be determined from Equations 3.13 to 15. The kinematic movements required to place the end effector at any given point must now be derived.

Recalling Figure 3.8, kinematic expressions therefore employ;

$$\theta = \tan^{-1}\left(\frac{Z_3}{Y_3}\right) - \gamma \qquad \text{(Equation 3.17)}$$

$$\omega = \tan^{-1}\left(\frac{Y_3}{X_3}\right) \qquad \text{(Equation 3.18)}$$

$$u = \sqrt{X_3^2 + Y_3^2 + Z_3^2} - u_0 \qquad \text{(Equation 3.19)}$$

where ω and θ represent the orthogonal arm rotations of joints 1 and 2 and u and u_0 denote the arm extension required (to reach the desired point on a lateral intersection profile) and the reposed arm length respectively. The algorithms expressed in Equations 3.17 to 3.19 are responsible for control of the robotic arm.

3.2.7 Associated Matters

Whilst Section 3.2.6 covers the kinematics associated with procedure b) defined in Section 3.2.2, i.e. the primary drilling /grinding stage, it remains to define the mathematics associated with the EE attaining target from repose / park and thereafter returning to park. These are simple procedures involving drive commands;

$\theta = 0,$

$$\omega = -90 + \left[\tan^{-1} \left(\frac{r_d}{\frac{\phi_{NME}}{2}} \right) \right] \qquad \text{(Equation 3.20)}$$

$$u = -u_0 - l_d \qquad \text{(Equation 3.21)}$$

and

$\theta = 0,$

$$\omega = +90 + \left[\tan^{-1} \left(\frac{x_L - \left(\frac{\phi_{LAT}}{2\sin\rho} \right)}{\frac{\phi_{NME}}{2}} \right) \right] \qquad \text{(Equation 3.22)}$$

$$u = \left(\sqrt{\phi_{NME}^2 + \left(x_L - \left(\frac{\phi_{LAT}}{2\sin\rho} \right) \right)^2} \right) - l_d \qquad \text{(Equation 3.23)}$$

respectively, where l_d is the distance from the EE to the axis of revolute joint 1.

The first set of controls move the EE to point $P(X_1, Y_1, Z_1)$ described in Section 3.2.6.

Given the lack of inverse kinematics and the associated synchronous joint movements, actual programmed drive is piecewise, simple and robust with any $\Delta\theta$ being followed by any $\Delta\omega$ and then by any Δu in turn. The finalised arm design is suggested by Figure 3.16.

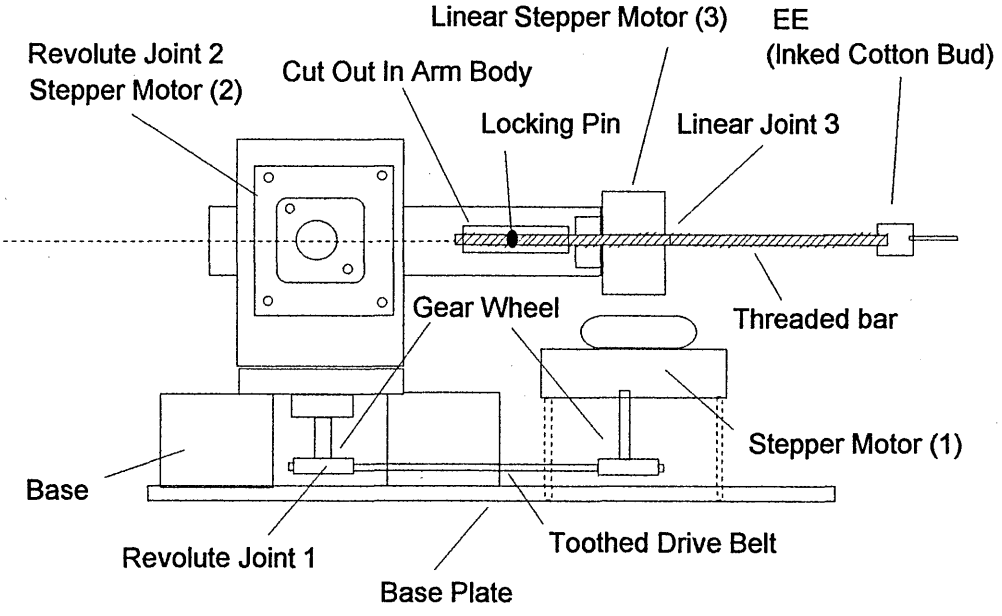

Figure 3.16: Overall Arm & Motor Configuration - Elevation

In line with above the GRASP design, two revolute joints powered by geared stepper motors and one prismatic joint powered by a linear actuator are provided. The EE chosen for the laboratory testing, in the absence of providing a 4^{th} DOF and active drill head, comprises a cotton bud which when loaded with a suitable marker (such as paint or ink) will allow the cut profiles generated to be marked on drawing paper.

3.2.8 Programming Factors

The arm control computer programme, written in QBASIC and provided in Appendix B is based on the lateral reconnection procedure described in Section 3.3.2. Figure 3.17 provides a flow diagram for the programme associated with procedure b) defined in Section 3.2.2. Speed of action is hardware dependent and, as noted above, joint movement is necessarily non-synchronous. Full explanation of both the software and hardware requirements of the system are given in Section 4.3 together with the laboratory investigation and evaluation of the arm control system in Section 5.2.

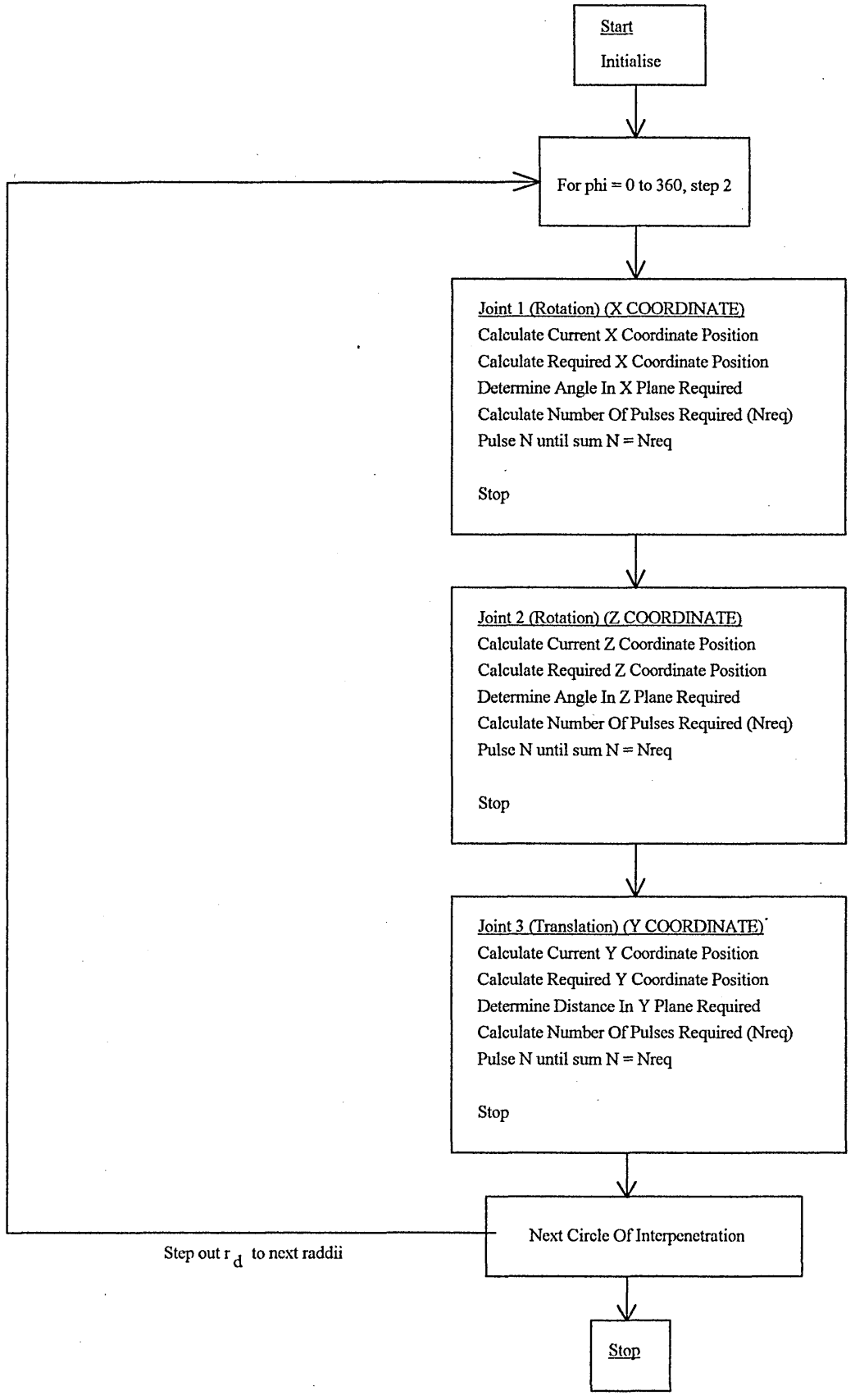

Figure 3.17: Arm Control Programme Flow Diagram, Associated with Procedure b) Defined in Section 3.2.2.

3.3 SUMMARY

Within this chapter, the kinematic aspects of a robotic system for the relocation / reconnection of lateral connections to a main sewer pipe, in the context of a cured in place lining renovation process, has been proposed incorporating a chainage measurement system and robotic task arm. The mathematical theory underlying each system had been presented together with a brief overview of the system components and control structure, noting that the ultimately proposed retro-fit system would feature on-board processing to minimise umbilical requirements, remote PC studies are employed to minimise costs.

Chapter 4 now provides an introduction to the laboratory testing employed to assess the performance of both the kinematic and CV systems, with test results provided in Chapters 5 and 6 respectively.

CHAPTER 4

EXPERIMENTAL CONSIDERATIONS

4.1 TESTING OBJECTIVES

Recalling Section 1.1.5, a three pass strategy has been proposed based upon a proprietary sewer inspection tractor unit and incorporating task specific, discrete, computer based modular systems, these being capable of retro-fit to existing NME tractor units for cost-effective practice. The objective of the testing phase of the research programme was to provide, in the absence of formal integrated control, a cost effective testing strategy which will allow the discretised testing of the kinematic and computer vision modular systems, whose models were developed in Chapters 3 and 2 respectively.

The experimental objectives for the kinematic systems were,

1) to evaluate the accuracy of the chainage measurement system (CMS) in determining invert chainage travelled by the tractor whilst allowing for wander within the pipe, and
2) to assess the ability of the robotic arm and computer control programme to describe the drill path profiles necessary for lateral reconnection for both the 45 and 90 degree lateral intersection.

The experimental objectives for the computer vision system (CVS) were,

1) to detect laterals junctions during an initial sewer survey pass, and
2) to classify the detected junction in terms of both angle of lateral intersection (ρ) and closure to target distance (x_{vp}); a separate procedure provides estimation of lateral diameter (φ_{LAT}).

At this level of development, laboratory testing was considered appropriate as it provided the ability to enable close control over experimental factors and to measure the systems performance, which would otherwise be difficult given the restrictive and hazardous nature of the NME sewer. Field tests are considered more appropriate for an ensuing prototype.

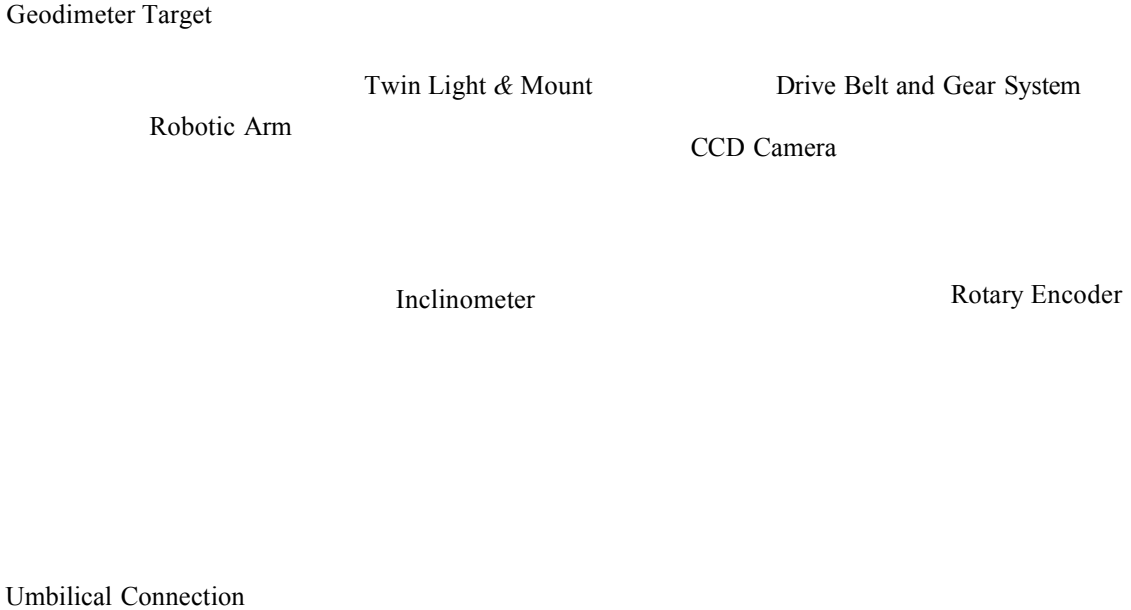

Figure 4.1: Retrofit Proposals for Cost Effective Sewer Robot

Figure 4.1 provides a diagrammatic sketch, identifying the key modular components of the proposed laboratory robotic model to be retrofitted to a standard tractor base, whilst Figure 4.2 shows the pre-prototype tractor unit incorporating the retro fit units deemed necessary to satisfy the requirements of both systems, noting that remote PC control is provided. The tractor employed here is a reconditioned unit used in practice and therefore subject to wear and tear, an assessment of which is carried out by means of ancillary testing outside the pipe rig on the laboratory floor as discussed in Section 5.1.2.

Rotary Encoder

Figure 4.2: Tractor Unit & RetroFit Modules

Consideration is now given to the testing strategy employed.

4.2 TESTING STRATEGY

4.2.1 Laboratory Set-Up

Test data for both kinematic and vision based systems was obtained using a 10m long, 450mm diameter laboratory based NME sewer pipe rig as shown in Figure 4.3

Figure 4.3: Laboratory Based Pipe Testing Rig

The rig comprises four 2.5m long sections incorporating 45 and 90 degree, 300mm diameter, lateral junctions. The pipe rig sections were arranged as shown in Figure 4.4. The diameters of the NME sewer and laterals pipes were taken as nominally specified by the pipe rig manufacturer as were the angles of lateral intersections.

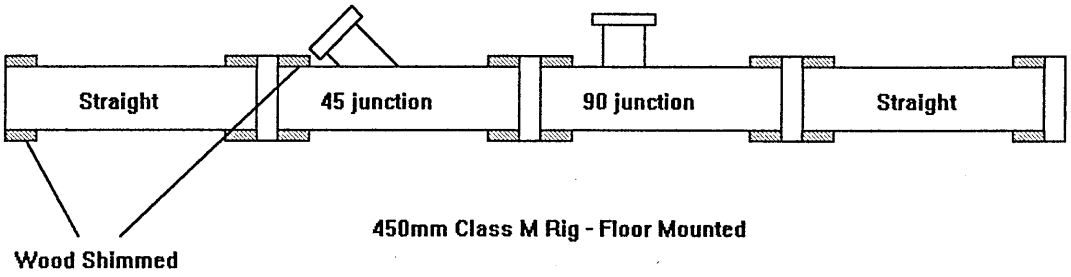

Figure 4.4: Pipe Rig Layout Plan

The pipe sections were positioned in line on the laboratory floor, levelled using a spirit level and shimmed with wooden blocks to prevent the sections rolling out of line. The lateral junctions were positioned at 9 o'clock and supported by concrete blocks; for testing purposes no lateral fall was required.

A key element of the laboratory set-up was to determine the topology of the pipe rig in particular the chainage locations of the lateral intersections with respect to the NME sewer centre line; a prerequisite for the evaluation of the CV based classification system. A geodimeter survey was carried out employing the following procedure.

By siting the geodimeter along the NME centreline with a geodimeter target inserted centrally through each lateral junction so as to be located at the point of NME / lateral centre line intersection, the chainage to these points could be measured. This therefore required the geodimeter to be positioned so as to sight down the NME axis.

The geodimeter, located on a horizontally and vertically adjustable base plate was positioned in front of the pipe rig. At both ends of the NME rig, 2 lengths of orthogonally opposed string were taped across the mouths, forming cross hairs with their intersection coincident with the pipe axis. The geodimeter position was adjusted so that when siting down the sewer pipe both cross hairs were coincident in the geodimeter viewfinder. The geodimeter was therefore sited along the centre line of the main pipe.

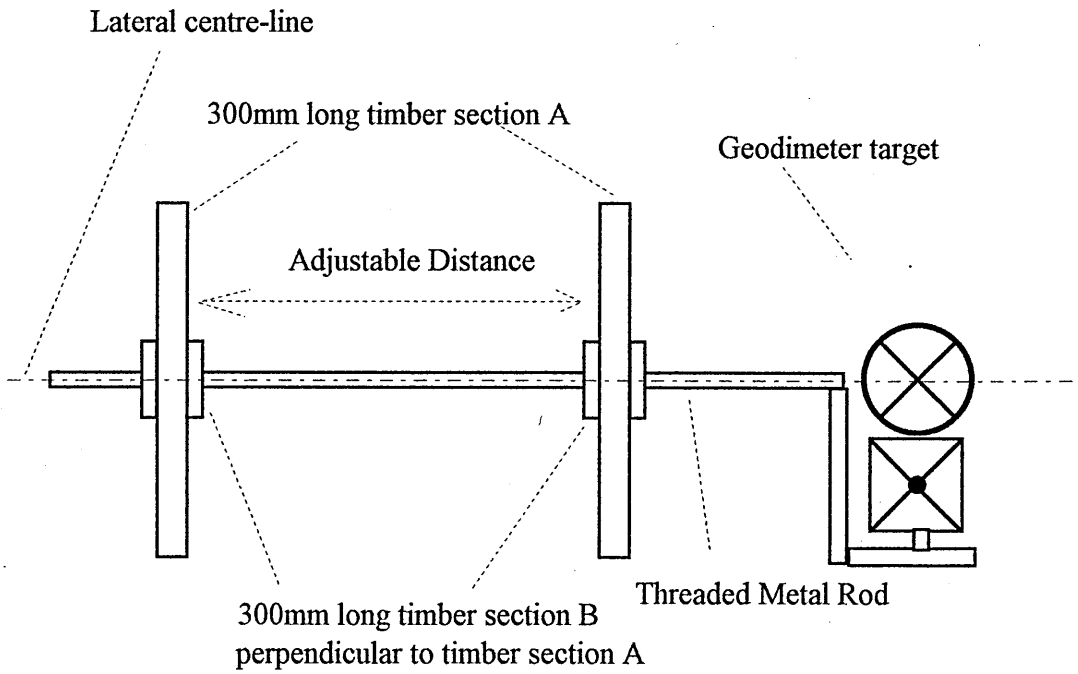

Figure 4.5: Target Location Frame

As illustrated in Figure 4.5, a 'target location frame' comprising 2 sets of 300mm long timber cross members centrally linked by a threaded metal rod was constructed. A geodimeter target was bolted to the end of the rod. Provision of a locking mechanism allowed the distance between cross member to be adjustable to for optimum placing within each lateral. The timber members were shaped to snugly fit within each lateral whilst maintaining position of the metal rod, and target, on the lateral centreline axis. By adjusting the frame within the lateral, and monitoring the audible 'on target' signal

sounded by the geodimeter, the target prism was positioned coincident with the intersection of lateral and NME centre lines and distance relative to geodimeter position were measured; please refer to Figure 4.6.

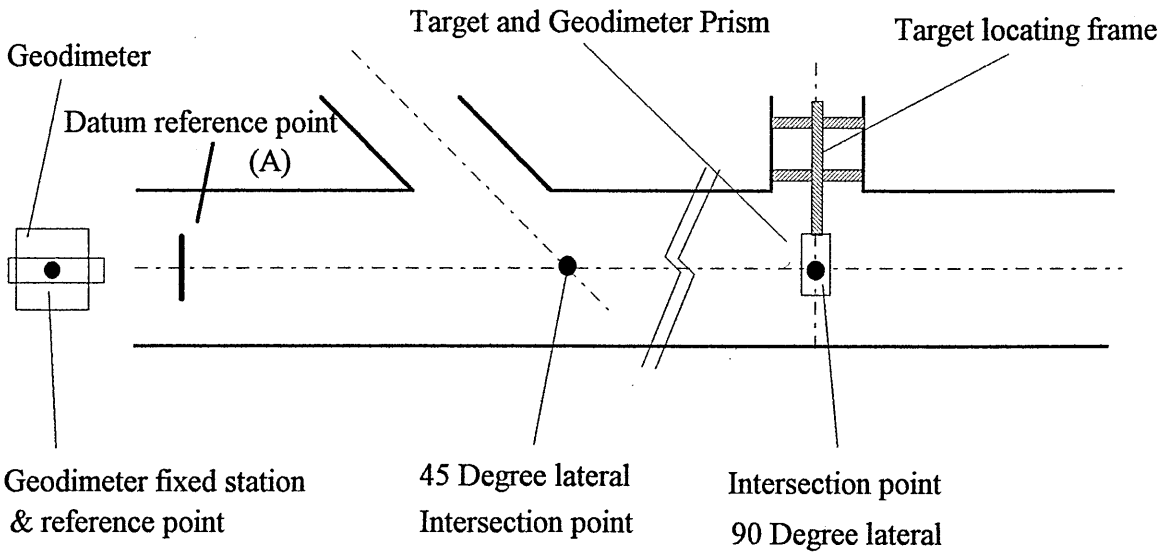

Figure 4.6: Geodimeter Evaluation of NME Topology

A datum position was permanently marked just inside the pipe rig at position (A). With target located at A, its horizontal distance from the geodimeter was measured. By subtracting this distance from that measured from the geodimeter to both lateral intersections, the individual chainage positions for each relative to datum A were determined; as noted in the CVS study of Section 2.3.1, the CV classification system determined closure to target distance x_{vp} based on the projected intersection point of the lateral back wall with the NME centre line as illustrated in Figure 4.7. Considering pipe geometry, a correction was made to allow for this and lateral chainages are as presented in Table 4.1.

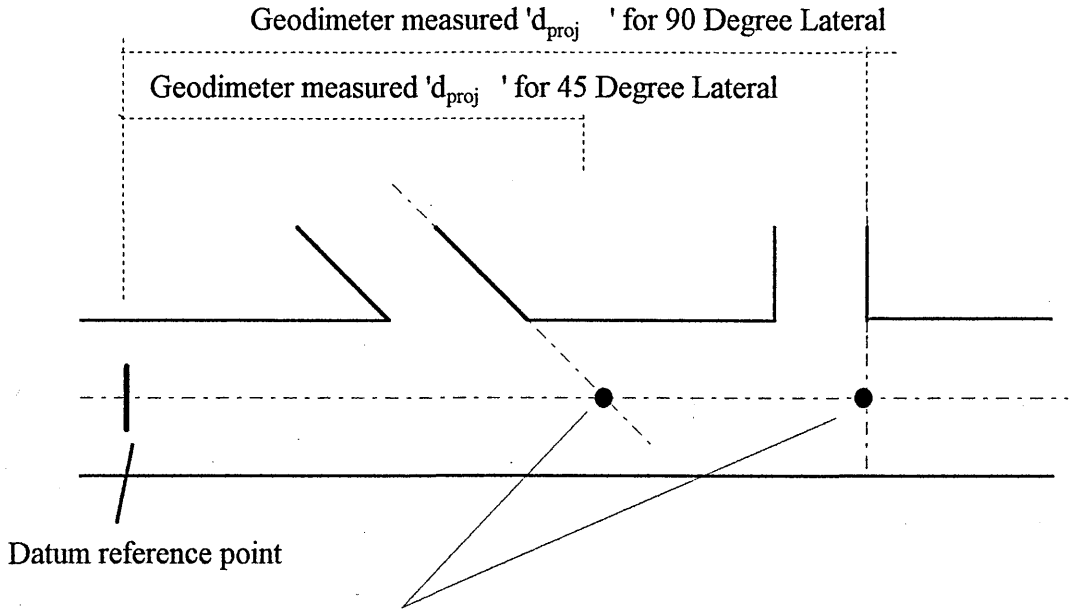

Figure 4.7: - Reference to Intersection of Lateral Back Wall

Lateral	Chainage Distance 'd_{proj}', Of Lateral Back Wall Intersection With Sewer Centre Line (m)
45 Degree	3.487
90 Degree	5.641

Table 4.1: Geodimeter Measured Distances (Corrected) Of Laterals From Datum

With pipe rig geometry determined, consideration is now turned to the testing of the mechanical aspects.

4.2.2 Mechanical Testing Factors

Recalling Section 4.1, the experimental objectives for the kinematic systems were,

1) to evaluate the accuracy of the chainage measurement system (CMS) in determining invert chainage travelled by the tractor whilst allowing for wander within the pipe, and

2) to assess the ability of the robotic arm and computer control programme to describe the drill path profiles necessary for lateral reconnection for both the 45 and 90 degree lateral intersection.

Whilst the laboratory pipe rig employed for testing purposes provides an idealised environment dry, clean, and relatively free from imperfections, the real sewer environment is far from ideal. For robust chainage assessment, the CMS system must be able to cope with all the imperfections likely to be encountered in the real NME environment, including worn /damaged tractor, not being correctly placed in the pipe invert and being deflected by objects in the invert away from the invert path. Chainage evaluation therefore comprises two phases; initial tests were conducted on the laboratory floor to assess the degree of bias / wander from a prescribed straight-line path exhibited by the tractor, attributable to general wear and tear form its use in the sewer inspection industry with a geodimeter being used to measure the distance travelled and determine the degree of wander. Secondly with attention turned to in pipe testing, the accuracy of the CMS was assessed for a series of differing initial tractor orientations to mimic imperfect lie and deflection by debris. Tests were first carried out with the tractor placed in the invert parallel to NME centre line then with increasing degrees of body rotation about the NME centreline to assess the impact on accuracy of non invert lie. To simulate deflection from path, the tractor was placed through varying degrees of skew to NME centreline and effect on accuracy determined.

Evaluation of the robotic drill arm was undertaken with the tractor statically placed in the NME invert. With drawing paper attached at 9 o'clock to the inside NME wall, the suitability of the robot arm and control programme, based on the mathematical model derived in Section 3.2.6., described drill profiles suitable for the reconnection of both 45 and 90-degree lateral junctions was monitored and performance assessed. This was achieved by overlaying computer generated, three dimensional, idealised cutting profiles, over the plots produced by the robotic arm end effector. Whist the profiles appear circular in situ, when removed from the pipe in 2D they are elliptical. A spreadsheet was used to generate an idealised set of ellipses corresponding to curves of interpenetration for both the 90 and 45 degree lateral cases. By superimposing idealised profiles over those experimentally obtained, the performance of the robotic arm system was assessed.

Please refer to Chapter 5 for full mechanical system testing methodology and test results.

4.2.3 Computer Vision Testing Factors

Recalling Section 4.1, the experimental objectives for the computer vision system (CVS) were,

1) to detect laterals junctions during an initial sewer survey pass, and
2) to classify the detected junction in terms of both angle of lateral intersection (ρ) and closure to target distance (x_{vp}); a separate procedure provides estimation of lateral diameter (φ_{LAT}).

Vision system testing required CCTV surveys to be carried out within the pipe rig using the tractor mounted camera and lights. Employing a geodimeter and geodimeter target

located on the tractor rear at a fixed offset from the camera, the tractor was driven along the pipe invert to within 3.5m (confirmed by geodimeter) of the 45 degree lateral junction. The tractor was stopped and chainage measured by geodimeter relative to datum to ensure within correct distance range and value noted for future reference, please note Section 4.2.1. Recording camera signal directly to a VCR, whist monitoring images on a connected TV, images sequences of the lateral were recorded under both direct and reflected illumination; the left hand light source was illuminated for 30 seconds then following manual remote switching the right hand light was illuminated respectively. The tractor was then moved nearer to the lateral and the above procedure repeated. In all, five image pairs (one obtained under direct and the other under reflected illumination) taken at known invert chainage were obtained for each lateral; noting the topology determined in 4.2.1, experimentally derived closure to target distance x_{vp} were determined from these. These images were later digitised in a remote IT laboratory prior to computer vision processing and evaluation. Images taken under reflected illumination were used to test the lateral detection system, whilst both direct and reflected illumination image pairs were used to evaluate the classification components of the vision system, (ρ, x_{vp} and φ_{LAT}).

Please refer to Chapter 6 for full testing methodology and test results.

4.3 EQUIPMENT EMPLOYED

4.3.1 Laboratory Inventory

In addition to the pipe rig and proprietary tractor unit, Table 4.2 provides an inventory of the major items involved in the testing programme.

Item	Components
Chainage Measurement System (CMS)	Rotary encoder and mechanical drives. Inclinometer Power supplies
Robotic Drill Arm	Prototype arm 2 No. stepper motors Linear actuator Drive cards, buffers and power supplies End effector
Computer Vision System	CCD camera and lens 2 No. 50W dichromatic lights + manual switch TV monitor and VCR Remote SUN SPARC workstation and TINA computer vision research tool Remote PC and frame grabber
Remote PC Control	IBM Compatible 386 PC Digital input / output signal cards Analogue signal input card CMS and Robotic Arm System Software Umbilicals

Table 4.2: Laboratory Testing Inventory

Discussion of the key items with particular regard to their incorporation within the testing programme now follows.

4.3.2 Chainage Measurement System (CMS)

The chainage measurement system comprises a rotary encoder, and inclinometer connected by umbilicals to a remote IBM compatible 386 PC to provide remote control in the absence of on-board processing. The PC houses the necessary drive cards for reading the output data from the rotary encoder and inclinometer and the software written to determine the invert path distance travelled by the tractor. The system components are now described in more detail.

Rotary Encoder

A rotary encoder is a mechanical device that produces an output voltage signal for each incremental step that its drive shaft rotates. Within the encoder housing, a calibrated and graduated disc is attached to the drive shaft with fixed optical readers being located to either side of it. As the shaft rotates the disc turns and the optical sensors read a cycle of on / off signals for each graduation passing the readers which are output as 5V pulses. These are interpreted by a DEVA Electronics digital encoder interface card housed in the remote PC to enable the real-time sampling of the incremental encoder signals.

The rotary encoder used here is a British Instruments model having a resolution of 1800 increment steps per full shaft rotation and therefore can detect angular change to 0.2 of a degree. The encoder was fixed to the tractor unit as shown in Figures 4.8 and 4.9.

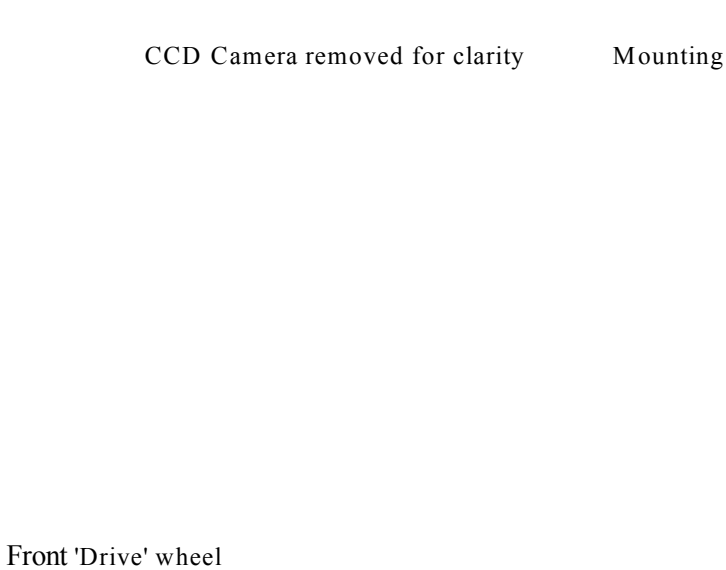

Figure 4.8: British Instruments Rotary Encoder - Plan View

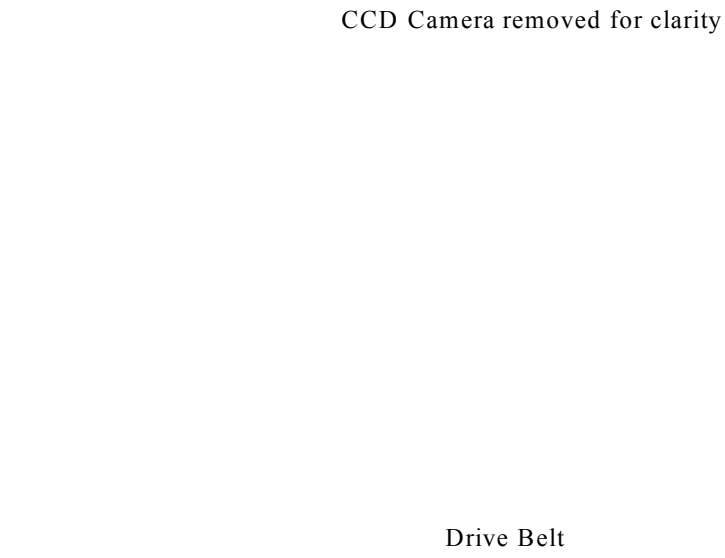

Figure 4.9: Rotary Encoder and Drive System - Elevation

As illustrated, the encoder is a sizeable device and engineering judgement was required to determine its optimum positioning. This was achieved by attaching a custom built mount for the encoder to the front of the tractor and fixing similarly sized gear wheels, pinned to both the encoder output shaft and front tractor axle. A toothed pulley belt connected the gear wheels providing drive to the encoder such that one revolution of the

200mm diameter tractor wheel produced one revolution of the encoder output shaft. For each wheel rotation the tractor covers 628.32mm and, noting the encoder resolution as given above, the rotary encoder provides an accuracy of 0.35mm per shaft increment. Given that most industrial CCTV chainage systems are approximately accurate to 0.1m, the accuracy obtained here is a significant improvement.

Inclinometer

The CMS theory presented in Section 3.1 requires the ability to assess tractor inclination to determine the invert distance travelled. A DS Europe SERVO Inclinometer capable of measuring inclinations in the range of $\pm$ 45 degrees to an accuracy of 0.001% was considered suitable and located on the tractor as shown in Figure 4.10.

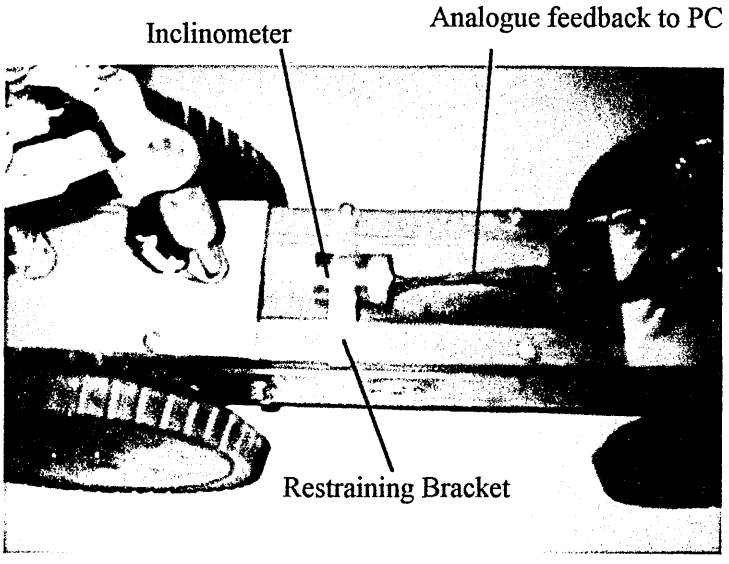

Figure 4.10: DS Europe SERVO Inclinometer

The inclinometer, powered by a stand alone 15V DC power supply, produces an output voltage relative to the degree of inclination experienced; + 5V for +45 degrees of inclination and –5V for –45 degrees of inclination.

The degree of inclination relative to output signal voltage (V_{out}) produced is expressed in Equation 4.1;

$$Inclination(\text{deg}\,rees) = Vout * 0.142965328 * \left[\frac{180}{\Pi}\right] \qquad \text{(Equation 4.1)}$$

An analogue control card housed in the 386 PC monitors the output signal, V_{out}. The aforementioned Chainage Measurement Program monitors Vout in real time, and determines in real-time the tractor inclination from the above equation. A computer program has been written in collaboration with others to sample both devices and provide the necessary computing power to calculate the straight-line distance from the mathematics derived in Section 3.1.3 and is provided in the Appendix B

4.3.3 Robotic Task Arm (Drill)

The design of this modular item was a principal feature of the research programme. A physical pre-prototype robotic arm was constructed and retrofitted to a proprietary tractor unit. The tractor unit itself weighs in the region of 40kgf so problems regarding robot stability during liner cutting are obviated. The robotic simulation carried out earlier, employing GRASP, allowed a simple yet effective arm design to be evaluated without the need for costly physical models to be built. Based upon the simulation, an aluminium mock up was fabricated in-house by the School Of Construction Technicians.

As described in detail in Section 3.2.2, the necessary kinematic attributes of the proposed robotic arm require two revolute and one prismatic joint. The ability to drive these joints, however, proved more problematic than initially thought. During the initial design stages, many motor concepts were discussed and varying motor emplacements

determined then dismissed for reasons of practicality and / or cost. At this pre-prototype research stage open loop control was employed. It was envisaged that the fourth degree of freedom (DOF) would take the form of a twisting drill end effector. For pre-prototype research purposes, a 'paint brush' for target marking was considered adequate and substituted. Further discussion of the arm is considered in terms of three joints identified in Figure 4.11.

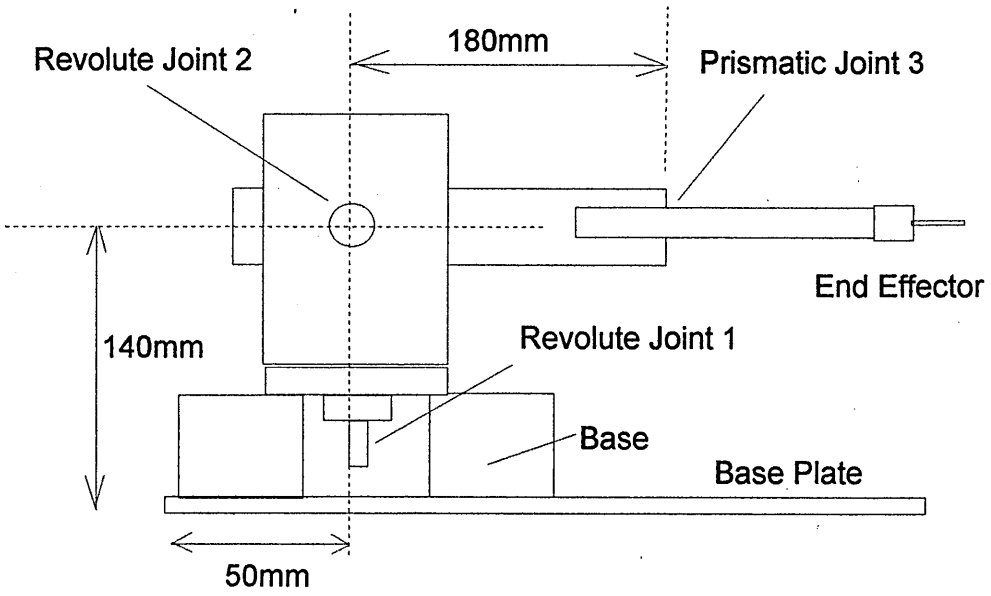

Figure 4.11: Robot Arm Design; 3 DOF Configuration

JOINT 1(ω)

A stepper motor system incorporating motor control drive card and buffer was chosen to drive this revolute joint enabling the motor to be digitally controlled; for each digital signal received the motor increments one step. After careful consideration of all possible motor emplacements, for practicality optimum positioning was determined be in front of the arm; drive to the joint was provide by a drive belt connecting identically sized gear wheels attached to motor gearbox drive shaft and directly to joint 1; please refer to Figure 4.12

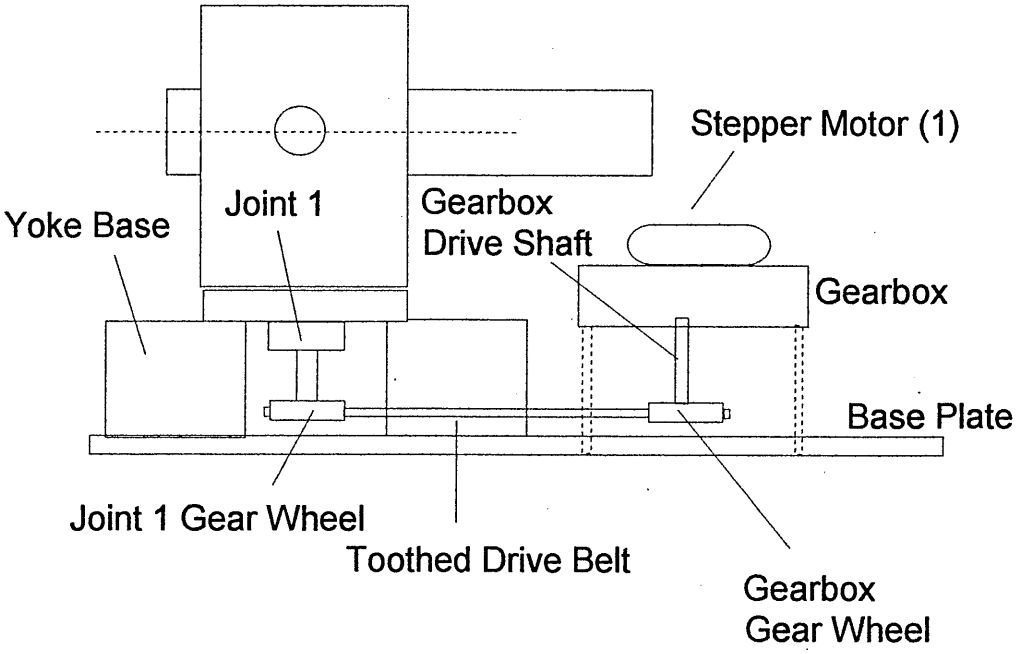

Figure 4.12: Joint 1 Configuration Details

The technical specification for the joint 1 drive system is now summarised.

The stepper motor used to drive joint 1 is a McLennan ID35 motor combined with a G17 50:1 gearbox, refer to Figure 4.13. The motor drives the joint via a toothed drive belt / gear pulley wheel configuration. Geared pulley wheels are pinned to both joint and gearbox spindles. The motor by itself has a resolution of 7.5 degrees per input pulse, giving 48 steps per one complete motor shaft revolution. Combined with the gearbox, 2400 steps are required to produce 360 degrees of revolution of the joint.

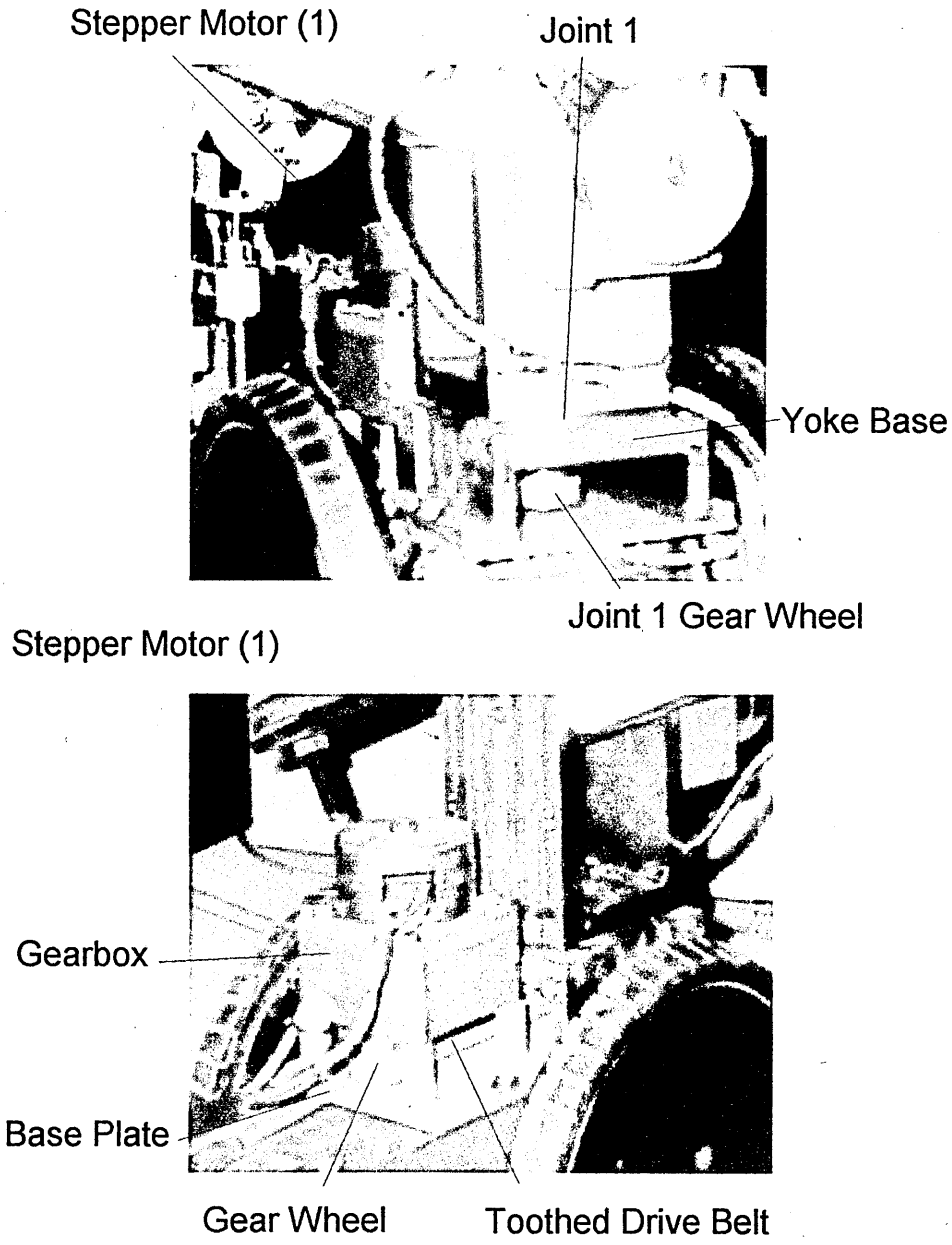

Figure 4.13: Motor Drives To Joint 1

JOINT 2 (θ)

The design of the arm and yoke allowed easy motor placement to drive the revolute joint 2. Simply, a geared stepper motor could be directly attached the pinned joint holding the main arm body in the yoke. The gearbox drive shaft was secured by a screw through a hole fashioned in the end of the arm pinion. The motor and gearbox body could then bolted directly to the arm yoke. A direct drive for this joint was thereby afforded, Figure 4.14.

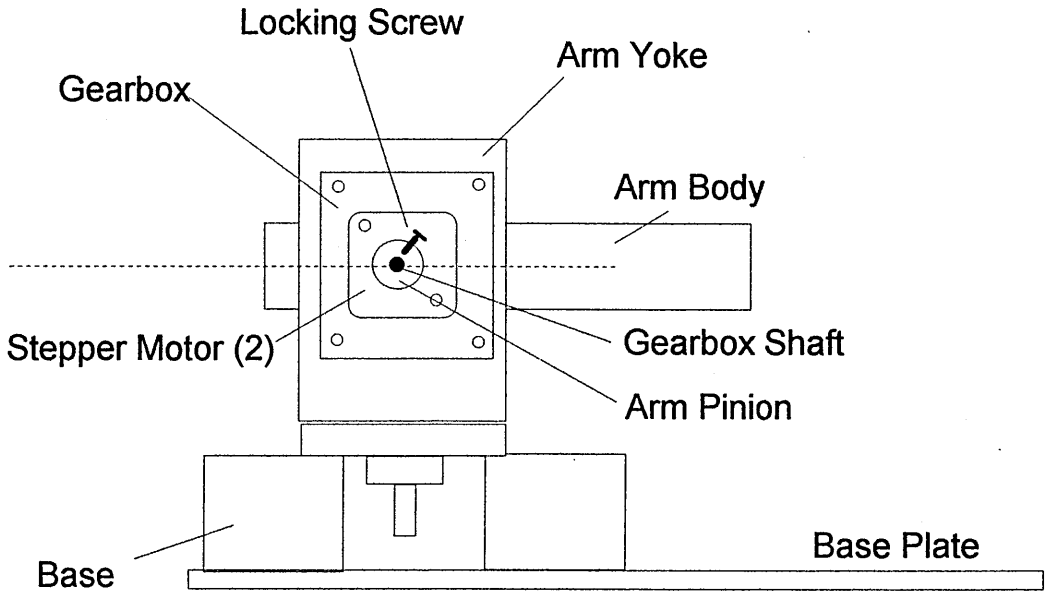

Figure 4.14 Joint 2 Configuration Details

The stepper motor used to drive joint 2 is again a McLennan ID35 motor combined with a G17 50:1 gearbox, Figure 4.15. The motor drives the joint directly; the motor / gearbox spindle is screwed directly to the joint pin. Motor resolutions are as given previously for joint 1.

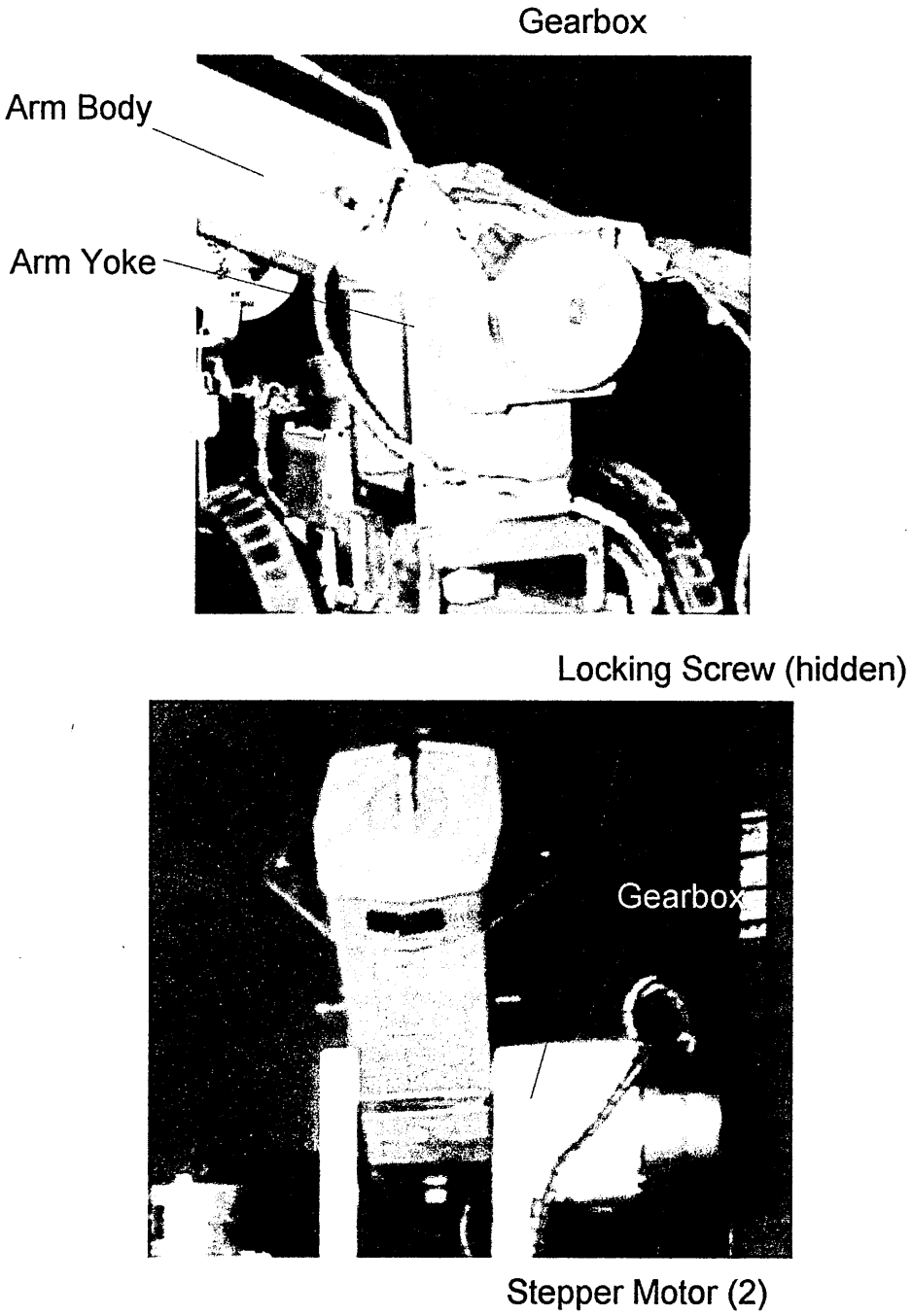

Figure 4.15: Joint 2 Motor Configuration

Please note that during set up and initial testing of the arm, both revolute joints exhibited a certain degree of play or backlash in their drive systems resulting in a loss of motor 'steps' when undertaking changes of direction. Although new gearboxes were acquired and fitted to the original motors the problem persisted, the implications of which are reported in Section 5.2.3.

JOINT 3 (u)

For the prismatic joint (joint 3), initial considerations focused on placing a stepper motor to the back of the arm and driving the end effector in and out of the main arm body on a geared pulley system. However, this design was complex and therefore likely to be problematic. Technicians from the School Of Engineering who were heavily involved in the set up of all the robot mechanics and electronics, provided information regarding linear stepper motors which were currently available and which could basically extend and retract a threaded bar.

Similar in operation to the geared stepper motors of joints 1 and 2, for each pulse sent to the motor via its own drive card, the linear actuator could drive the end effector to the target - as directed by the control program. Such a linear stepper motor was acquired and attached to the end of the main arm body. In order for the motor to drive the threaded bar, a clamping arrangement was required to prevent the bar from rotating; without being secured, the driving force of the motor would tend just to spin the bar about its longitudinal axis. With the bar clamped and no longer free to spin, the action of the motor is to pull or push it in the direction required.

The existing arm body therefore had to be modified; a horizontal cut out was fashioned along part of the length of the arm to provide access to the bar. A small metal block was manufactured which would fit inside the arm body and with a central hole for the bar to pass through. A threaded hole was provided right through the block perpendicular to that of the bar. Locking pins could therefore be screwed into the block to secure the bar to the block. The lengths of the securing pins were sufficient so that they extended outside of the arm through the slots. The bar was thereby unable to rotate in either

direction about its axis, and the linear stepper motor could drive the end effector both in and out in relation to its position on the arm refer to Figure 4.16.

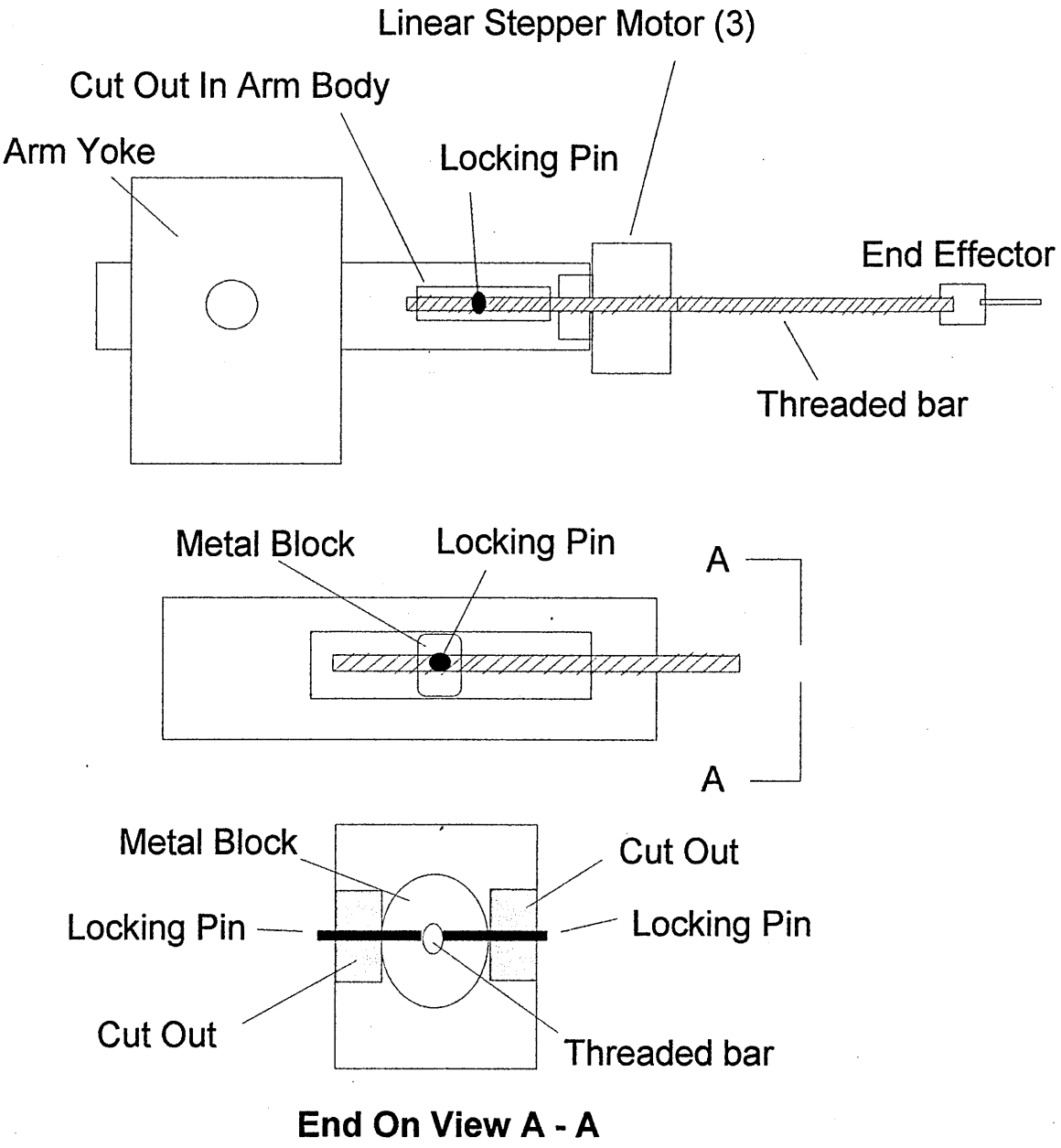

Figure 4.16: Joint 3 Configuration and Details

The weight of the linear stepper motor combined with the cantilever action from the joint 2 fulcrum, produced instability in the arm. When the power to the joint 2 stepper motor was switched on, the motor provided sufficient resistance to the weight of the

linear motor. However with power turned off, the arm would not hold position and gravity would effectively cause the arm to be displaced downwards. An upgraded counterweight system was therefore developed to overcome this and can be seen in Figure 4.17 which shows the linear stepper motor system.

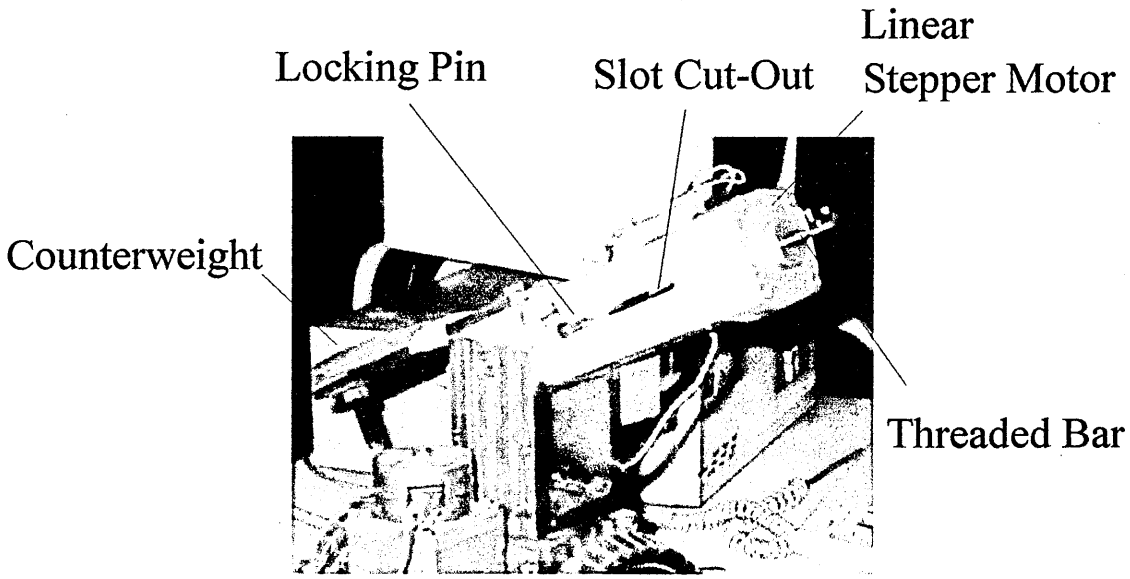

Figure 4.17: Linear Stepper Motor Configuration

As noted earlier in this section, a simple cotton bud was clamped at the end effector position to allow the robot to trace the lateral profile during the testing summarised in Section 5.2. The technical specification for the joint 3 drive is now summarised;

RS components direct drive linear stepper motor

Resolution – 2400 steps producing mm of travel

Drive direct to screwed bar which extend and retracts as directed.

The schematic for the overall robot arm is illustrated in Figure 4.18 and the actual arm and motor drives in complete is shown in Figure 4.19.

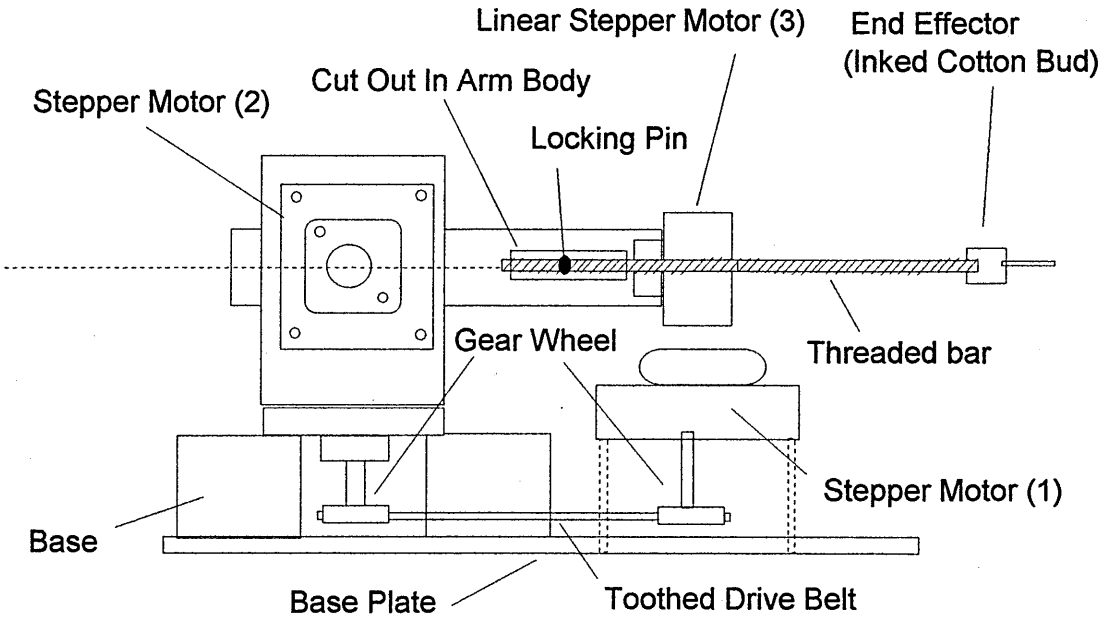

Figure 4.18: Overall Motor Configuration – Elevation

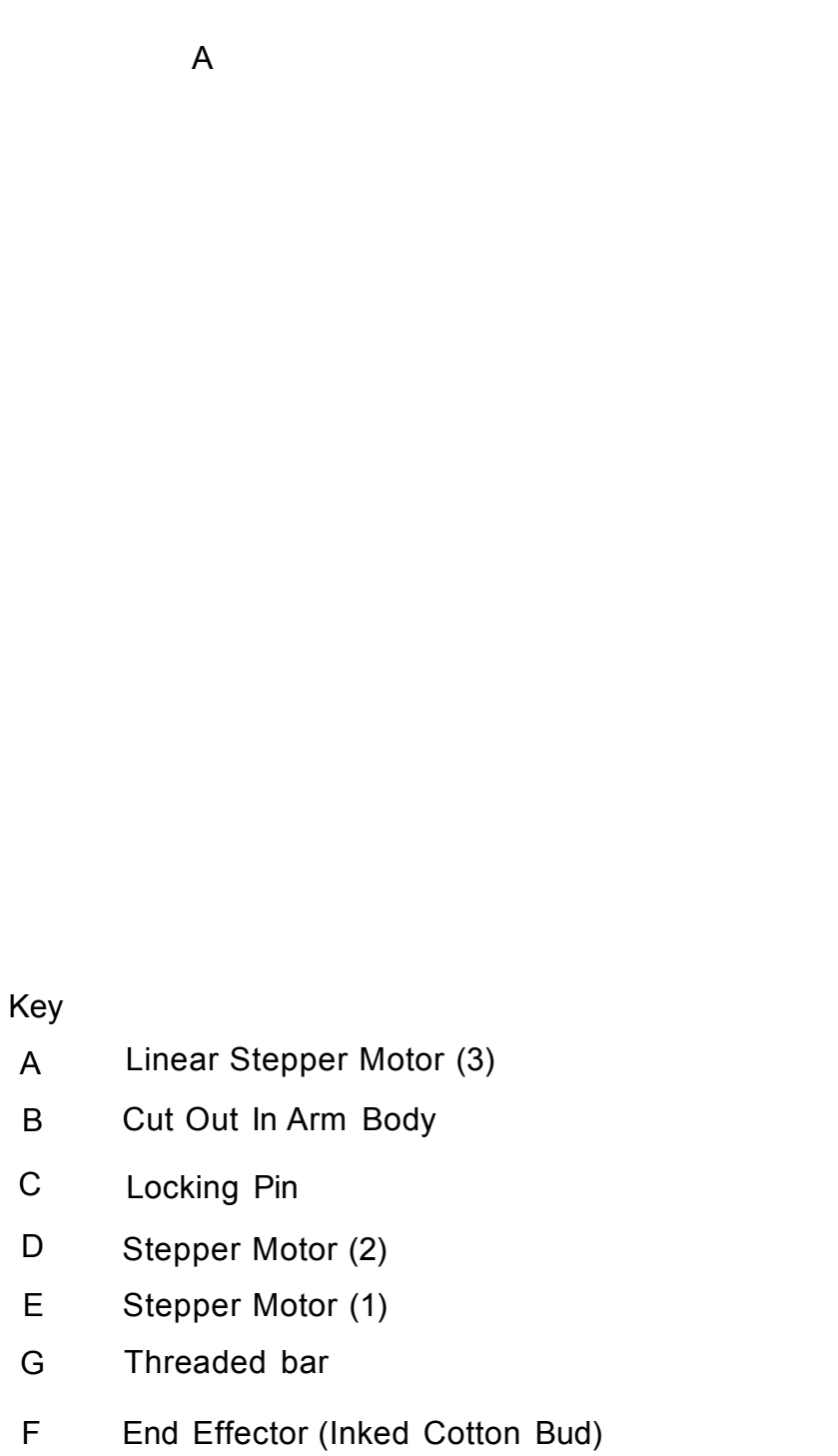

Figure 4.19: Prototype Configuration Arm & Motors

The requisite control system and hardware necessary are now addressed.

As discussed previously, kinematic algorithms have been suggested based on a mathematical model derived earlier in this chapter. By determining the 3D spatial co-ordinated of each point on the anticipated lateral cut profile, the kinematic movements required to move the end effector incrementally to each location can be determined by the kinematic algorithms produced.

Based on the motor dive unit specifications as summarised in the preceding section, a computer program was written which calculates both the spatial co-ordinates for any given lateral size and intersection angle and determines the joint movements required to correctly place the end effector on target. For each calculation performed the required number of step pulses that each motor must receive in order to drive it, are computed and output to the stepper motor drive cards. The drive cards are linked to a buffer system so if the motors are anticipated to work at a high rate then step information will not be lost or overwritten in transit from computer to motor. However, slow arm movement is preferable so as to avoid any possibility of over shooting the target. The arm control program is given in Appendix B.

Figure 4.20 provides an overview of the components of the robotic arm control system.

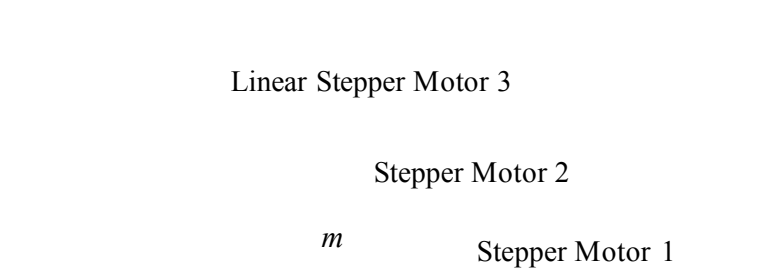

Figure 4.20: Arm Control Modules & Overview

The components of the robotic arm control system therefore comprise;

1) controlling computer housing digital output card to drive stepper motors,

2) stepper motor drive cards combined with power supply and signal buffers for driving joints 1 and 2, and

3) stepper motor drive card and power supply for linear actuator.

The equipment used is shown in Figure 4.21.

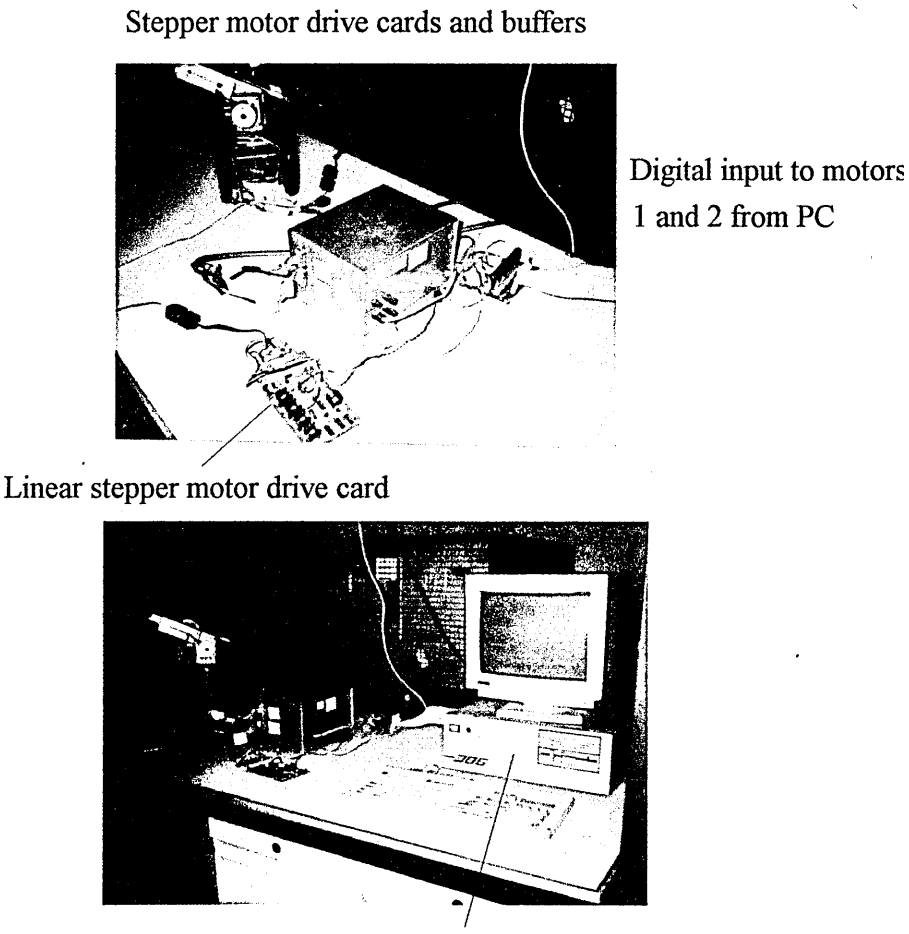

Figure 4.21: Stepper Motor Drive & Control

4.3.4 Lateral Detection and Classification System

For the lateral detection and classification study, a Watec CCD digital camera was employed with twin 50 W dichromatic lights to provide both direct and reflected illumination. These components are shown in Figure 4.22

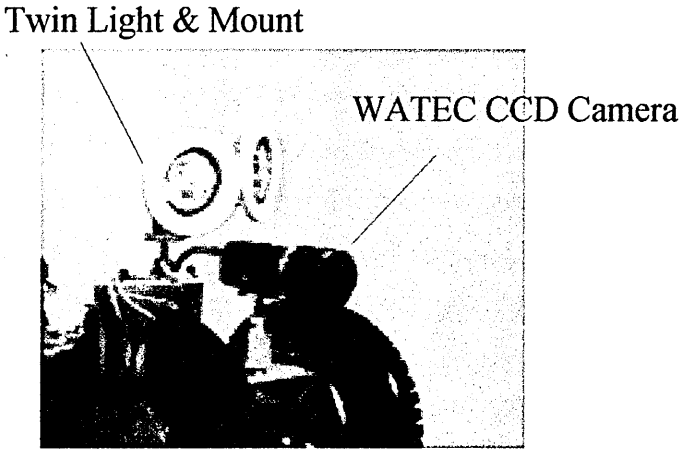

Figure 4.22: Computer Vision System Equipment

During CCTV survey employing the above equipment, images were relayed from the camera via umbilical support to an industry standard video recorder with image sequences being recorded and observed on a TV monitor in real time. An electrical switch box was used to manually alternate power to either lamp thereby providing both direct and reflected illumination. Images were captured on VHS tape and, using a frame grabber and dedicated PC, were digitised prior to CV processing. The TINA software environment as previously noted was used to develop the CVS modules, by a specialist party and employed on a SUN SPARC workstation in a remote IT laboratory.

4.4 SUMMARY

Within this chapter, the objectives and testing strategy for the evaluation of both the mechanical and vision systems have been addressed. The hardware and software comprising each system have been discussed. Proprietary testing and evaluation of the mechanical and computer vision systems, developed in Chapters 3 and 2 respectively, are presented in Chapters 5 and 6 respectively

CHAPTER 5

MECHANICAL SYSTEM TESTING

5.1 CHAINAGE MEASUREMENT SYSTEM (CMS)

5.1.1 Testing Strategy Employed

Whilst testing is primarily centred on the assessment of the CMS accuracy in calculating the actual invert chainage travelled as opposed to the distance measured by the rotary encoder, initial testing is concerned with assessing the tractor's tendency to wander from a straight path due to component wear and tear. Tests were then carried out within the pipe rig to assess the accuracy of the CMS under differing initial conditions. Primary evaluation was concerned with the assessment of the effect on accuracy of placing the tractor at varying degrees of inclination to the invert path whilst maintaining nominally parallel orientation of the tractor with respect to NME centre line. Orientations from 0 to $\pm$ 70 degrees, in 10 degree steps, as measured by the inclinometer, were considered. CMS determined distances were compared to geodimeter measured data to assess accuracy, refer to Section 5.1.3.

Secondary testing considered the effect on CMS determined accuracy by placing the tractor skew to the NME centreline, noting that from such initial positioning the tractor would climb the sewer wall to some degree before returning towards the invert path under the influence of gravity. Again, CMS determined distances were compared to those measured by geodimeter, refer to Section 5.1.4.

5.1.2 Assessment Of Tractor Bias

The tractor unit used here had previously been employed within the sewer inspection industry and an assessment of the degree of resulting wear and tear of the drive components was required. Any bias or wander exhibited by the tractor would need to be quantified to determine if any effect on CMS accuracy was attributable to this during the actual pipe tests.

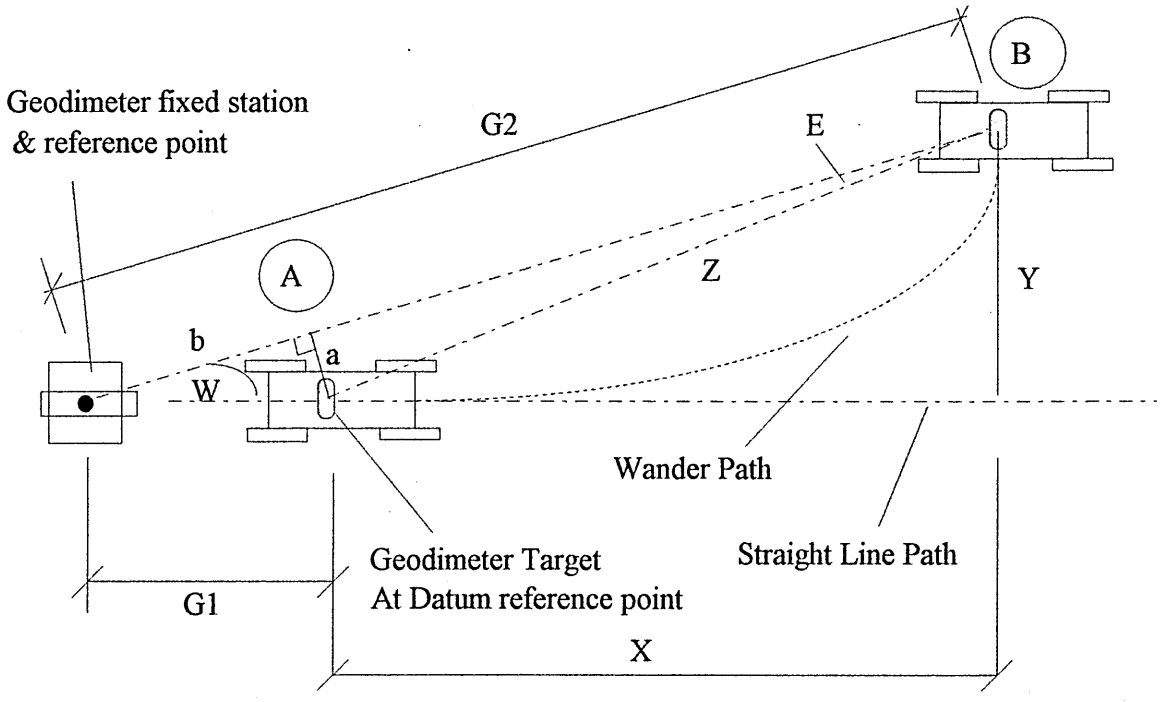

Figure 5.1: Assessment of Tractor Bias - Topology

With reference to the topology as illustrated in Figure 5.1, the assessment of tractor bias was conducted on the laboratory floor with the tractor initially statically placed at a convenient position 'A' parallel to a horizontal line marked on the laboratory floor. A target array of geodimeter prisms was bolted to the tractor top plate. Measurement of target position with respect to some arbitrary tractor feature is unnecessary as its position is fixed

throughout all the exterior tests employed. The geodimeter, Figure 5.2, was positioned on a set base plate and remained at this datum position throughout the testing. The tractor was placed approximately 2 to 3m beyond the geodimeter and an initial distance reading was taken to fix this start position; horizontal and vertical angles of the target in relation to the geodimeter were also measured.

Figure 5.2: Geodimeter - Measuring Initial Datum Position

Power was then supplied to the tractor drive motor and the tractor set in motion. A noticeable bias to the left was observed over the distance travelled as illustrated in Figure 5.1 by the 'wander path' trajectory. After covering a distance similar to that expected within the pipe rig, the tractor power was manually disengaged and the tractor stopped at position 'B \ Again the geodimeter was used to measure the distance and horizontal angles

of this position. The ability to measure the horizontal angular difference between initial and final target locations, W, is of particular import when assessing the degree of wander exhibited.

Recalling Figure 5.1, by consideration of the trigonometry employed it is possible, from the geodimeter measured distances to position A and B, G1 and G2 respectively, and the angular horizontal difference between each location, that the actual straight line distance from point A to point B, Z, be determined.

By inspection,

$$a = G1\sin W \qquad \text{(Equation 5.1)}$$

and,

$$b = G1\cos W \qquad \text{(Equation 5.2)}$$

Hence,

$$Z = \sqrt{\left(a^2 - (G2 - b)^2\right)} \qquad \text{(Equation 5.3)}$$

Having obtained an expression for Z, the degree of wander 'Y' with respect to horizontal distance 'X' is to be determined. Again by inspection,

$$E = \tan^{-1}\left(\frac{a}{G2 - b}\right) \qquad \text{(Equation 5.4)}$$

and,

$$\varphi = 90 - W \qquad \text{(Equation 5.4)}$$

$$\theta = 90 - E \qquad \text{(Equation 5.5)}$$

$$\gamma = 180 - (\theta + \varphi) \qquad \text{(Equation 5.6)}$$

Therefore,

$$Y = Z \sin \gamma \qquad \text{(Equation 5.7)}$$

$$X = Z \cos \gamma \qquad \text{(Equation 5.8)}$$

Hence wander Y expressed as a percentile of horizontal distance covered X is given by Equation 5.9,

$$Wander(\%) = \left(\frac{Y}{X}\right) * 100\% \qquad \text{(Equation 5.9)}$$

In all, five test runs were undertaken to assess the degree of wander exhibited by the tractor. In each test run the tractors trajectory whilst initially roughly parallel to its starting position showed gradual left-hand bias which, over the distances covered, resulted in a significant left hand deviation (wander) from its initial trajectory. A total of five test runs was employed and the results are summarised in Table 5.1.

Test Run	Geodimeter Measurement G1 (m)	Geodimeter Measurement G2 (m)	Angular Diff' W (deg)	Straight Line Dist' X (m)	Offset From Path Y(m)	Error (%)
1	3.429	10.064	5.30	6.592	0.929	14.10
2	3.320	11.540	6.09	8.155	1.224	15.01
3	3.191	11.662	6.45	8.397	1.311	15.07
4	2.793	10.915	5.91	8.064	1.124	13.94
5	2.591	11.081	6.48	8.149	1.251	14.86
Av'	**3.065**	**11.052**	**6.05**	**7.925**	**1.168**	**14.70**

Table 5.1: Assessment of Tractor Bias Test Results

From the results presented in Table 5.1, it is clear that the range of wander observed, 13.94 to 15.07% of projected horizontal distance, is significant. Clearly the tractor has undergone some mechanical wear or damage during its use in industry. For any application over flat surfaces this degree of bias would be pose serious problems for recovering accurate straight line chainage measurement; whilst a rotary encoder would record total distance covered by the tractor, use of inclinometer data would be in appropriate. However, it is anticipated that for sewer application, pipe curvature and influence of gravity will overcome the bias and maintain it within, or near to, the prescribed invert path. In any event, the provision of the inclinometer to assess tractor inclination will provide for any wander from the invert path to be determined and enable invert path chainage to be accurately calculated by the CMS.

Following assessment of tractor bias, evaluation now turns to the assessment of the accuracy of the CMS to determine invert chainage distance within the laboratory pipe rig. Using a worn tractor presents a more realistic engineering situation.

5.1.3 Parallel Chainage Runs

Tests were undertaken to determine what effect if any, not placing the tractor directly in the pipe invert, but parallel to the NME centreline, at the start of a chainage run would have upon the accuracy of the results produced. Commonly in practice, the tractor is manually placed roughly in the invert of the pipe though deviations of up to $\pm$ 15 degrees about the NME centreline would not be uncommon. Test runs were undertaken with the tractor placed initially in the pipe invert (at approximately 0 degrees inclination) and then with the tractor inclined up to $\pm$ 70 degrees relative to pipe invert as illustrated in Figure 5.2.

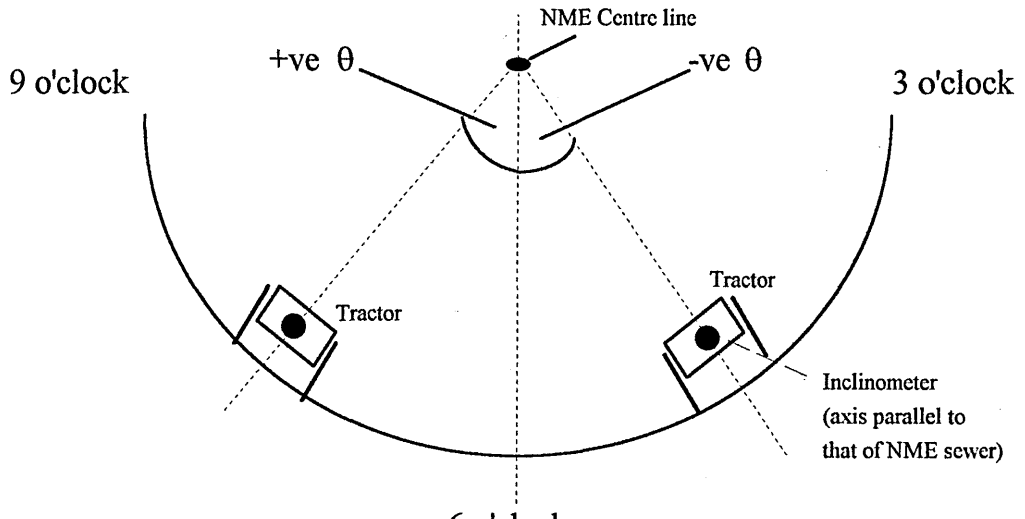

Section Through NME Sewer

$70^{\circ} \leq \theta \geq -70^{\circ}$

Figure 5.2: Inclinations about NME Centre Line – Parallel Tests

On screen readout of tractor inclination from the PC employed to run the CMS, provided for the tractor to be accurately positioned. Examples of typical initial tractor inclinations achieved are shown in Figures 5.3 and 5.4.

Figure 5.3: Parallel Inclination, 0 degrees

Figure 5.4: Parallel Inclination, + 30 degrees

With reference to Figure 5.5 and as noted in Section 4.2.1, a geodimeter was set up so that its range finder is roughly sited parallel and directly behind the tractor, sighting along the direction which it will travel. With a geodimeter target attached to a convenient location on the rear of the tractor body, the tractor was then initially positioned at the required degree of inclination. Employing the geodimeter the distance from it to the tractor is measured, as are the horizontal and vertical angles of the target in relation to the geodimeter.

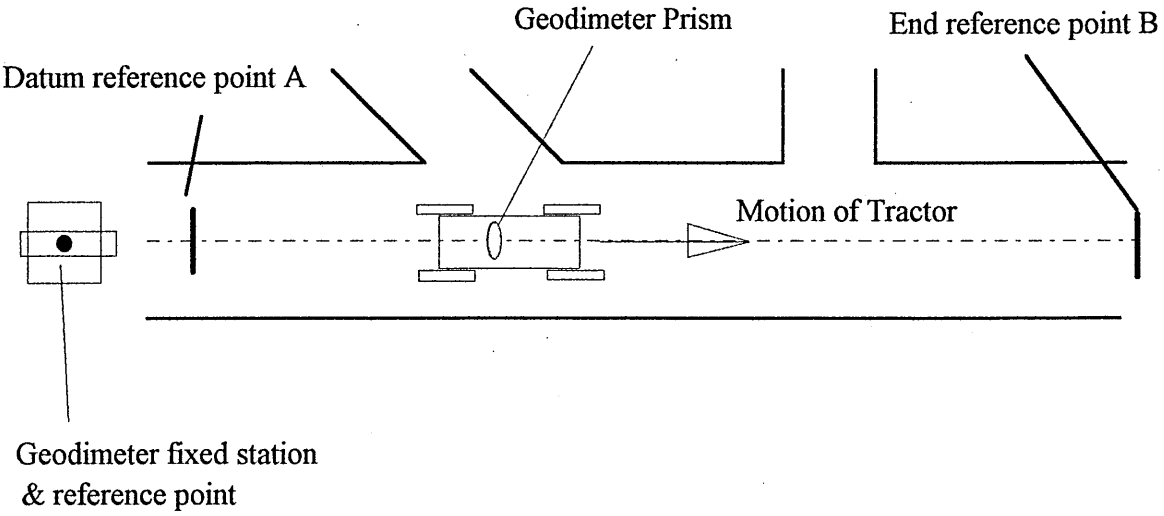

Figure 5.5: Geodimeter Chainage Evaluation – Parallel Tests

The CMS programme was then initiated with rotary encoder and inclinometer readings sampled at one-second intervals. With power supplied to the tractor drive motor, the tractor (i.e. geodimeter prism) was observed to travel from datum position (A) along the length of the pipe. During the chainage measurement run, the CMS continued to monitor at one second intervals the outputs of both the inclinometer and rotary encoder, whilst computing culmative straight-line distance travelled. After travelling a suitable distance, typically 8 to 8.5m, power to the tractor drive was manually switched off and the tractor immediately came to rest (position B). At this juncture the CMS programme was also terminated and data saved. The geodimeter was then again employed to

measure distance to position B, as are the horizontal and vertical angles of the target in relation to the geodimeter. Taking into account the vertical and horizontal angular difference measured by the geodimeter between points A and B and their corresponding measured distance readings, recalling the mathematical method employed in the previous section, the true invert path distance travelled by the tractor was calculated. The geodimeter precision is limited to the accuracy of current laser range finding devices and over the short distances considered here, an assumed accuracy of $\pm$ 1mm would not be considered inappropriate. The invert chainage calculated by the CMS was then compared to that measured by the geodimeter and the accuracy of the CMS determined.

Tables 5.1 to 5.3 provide the CMS data output for one of the test runs conducted with initial inclination of +30 degrees. Further examples are presented in Appendix D.

Time (s)	Culmative Distance (Rotary Encoder) (m)	Inclination (degrees)	Velocity (m/s)	Incremental Offset (m)	Culmative Invert Path Distance (m)
0	0.000	30.000	0.000	0.000	0.000
1	0.000	30.000	0.000	0.000	0.000
2	0.060	30.568	0.061	0.002	0.060
3	0.136	29.905	0.078	-0.002	0.136
4	0.216	28.391	0.082	-0.005	0.216
5	0.288	28.770	0.074	0.001	0.288
6	0.365	28.297	0.078	-0.002	0.364
7	0.447	27.445	0.084	-0.003	0.447
8	0.525	27.066	0.080	-0.001	0.525
9	0.603	27.350	0.080	0.001	0.603
10	0.680	28.391	0.079	0.004	0.680
11	0.757	27.350	0.079	-0.004	0.757
12	0.841	26.215	0.086	-0.004	0.840
13	0.920	26.025	0.081	-0.001	0.919
14	0.993	25.552	0.076	-0.002	0.993
15	1.070	24.795	0.079	-0.003	1.070
16	1.154	24.038	0.086	-0.003	1.154
17	1.238	25.457	0.086	0.005	1.237
18	1.311	25.931	0.075	0.002	1.310
19	1.390	25.079	0.081	-0.003	1.389
20	1.471	23.943	0.083	-0.004	1.470
21	1.548	23.470	0.079	-0.002	1.547
22	1.633	22.902	0.087	-0.002	1.632
23	1.717	22.429	0.086	-0.002	1.716
24	1.799	22.429	0.084	0.000	1.798
25	1.877	23.565	0.081	0.004	1.876
26	1.953	23.281	0.077	-0.001	1.952
27	2.032	22.524	0.081	-0.003	2.031
28	2.109	22.145	0.079	-0.001	2.108
29	2.192	21.577	0.085	-0.002	2.190
30	2.274	20.631	0.084	-0.003	2.273
31	2.364	20.063	0.092	-0.002	2.362
32	2.433	20.536	0.071	0.002	2.431
33	2.512	22.050	0.081	0.006	2.510
34	2.592	21.483	0.082	-0.002	2.590
35	2.671	20.536	0.081	-0.003	2.669
36	2.753	21.388	0.084	0.003	2.751

Table 5.2: CMS Data Output For Parallel Chainage Run, Nominal Tractor Inclination of 30 Degrees – Time Increments 0 to 36 Seconds

Time (s)	Culmative Distance (Rotary Encoder) (m)	Inclination (degrees)	Velocity (m/s)	Incremental Offset (m)	Culmative Invert Path Distance (m)
37	2.832	20.442	0.081	-0.003	2.830
38	2.910	19.401	0.080	-0.004	2.908
39	2.992	18.738	0.084	-0.002	2.990
40	3.070	19.779	0.081	0.004	3.068
41	3.149	21.483	0.081	0.006	3.147
42	3.230	20.347	0.083	-0.004	3.227
43	3.306	19.401	0.078	-0.003	3.303
44	3.384	19.211	0.081	-0.001	3.382
45	3.462	18.927	0.080	-0.001	3.459
46	3.546	18.265	0.086	-0.002	3.543
47	3.622	17.697	0.077	-0.002	3.619
48	3.697	18.927	0.077	0.005	3.694
49	3.773	19.306	0.078	0.001	3.771
50	3.849	18.265	0.078	-0.004	3.846
51	3.931	17.792	0.083	-0.002	3.928
52	4.004	17.697	0.075	0.000	4.001
53	4.080	17.508	0.079	-0.001	4.077
54	4.157	17.035	0.079	-0.002	4.154
55	4.234	16.278	0.079	-0.003	4.231
56	4.310	17.508	0.078	0.005	4.307
57	4.384	18.454	0.075	0.004	4.380
58	4.454	17.886	0.073	-0.002	4.451
59	4.532	17.697	0.080	-0.001	4.529
60	4.614	17.792	0.084	0.000	4.611
61	4.694	17.319	0.082	-0.002	4.691
62	4.773	16.562	0.081	-0.003	4.770
63	4.847	16.183	0.076	-0.001	4.844
64	4.918	15.615	0.073	-0.002	4.915
65	5.003	17.129	0.087	0.006	5.000
66	5.084	16.751	0.083	-0.001	5.080
67	5.160	16.562	0.078	-0.001	5.156
68	5.235	16.278	0.077	-0.001	5.231
69	5.312	15.521	0.080	-0.003	5.309
70	5.393	14.858	0.083	-0.003	5.390
71	5.469	15.237	0.077	0.001	5.465
72	5.544	16.562	0.077	0.005	5.540
73	5.618	16.751	0.076	0.001	5.614

Table 5.3: CMS Data Output For Parallel Chainage Run, Nominal Tractor Inclination of 30 Degrees – Time Increments 37 to 73 Seconds

Time (s)	Culmative Distance (Rotary Encoder) (m)	Inclination (degrees)	Velocity (m/s)	Incremental Offset (m)	Culmative Invert Path Distance (m)
74	5.690	16.278	0.074	-0.002	5.686
75	5.772	15.710	0.084	-0.002	5.768
76	5.847	15.710	0.077	0.000	5.844
77	5.923	15.142	0.078	-0.002	5.919
78	6.000	14.385	0.079	-0.003	5.996
79	6.075	14.480	0.076	0.000	6.071
80	6.150	15.615	0.077	0.004	6.146
81	6.222	16.088	0.075	0.002	6.218
82	6.291	15.426	0.070	-0.003	6.287
83	6.364	14.763	0.075	-0.003	6.360
84	6.436	14.574	0.074	-0.001	6.432
85	6.514	14.763	0.080	0.001	6.510
86	6.588	14.196	0.076	-0.002	6.584
87	6.661	14.006	0.074	-0.001	6.657
88	6.733	14.763	0.074	0.003	6.728
89	6.799	15.710	0.068	0.004	6.794
90	6.874	15.710	0.077	0.000	6.869
91	6.945	14.574	0.073	-0.004	6.940
92	7.012	14.385	0.069	-0.001	7.008
93	7.088	11.073	0.078	-0.013	7.083
94	7.167	12.208	0.081	0.004	7.162
95	7.243	12.114	0.078	0.000	7.238
96	7.316	13.155	0.075	0.004	7.310
97	7.387	15.047	0.073	0.007	7.381
98	7.464	16.278	0.079	0.005	7.458
99	7.543	14.385	0.081	-0.007	7.537
100	7.620	13.912	0.078	-0.002	7.613
101	7.696	13.722	0.079	-0.001	7.689
102	7.770	13.533	0.075	-0.001	7.763
103	7.847	12.965	0.079	-0.002	7.840
104	7.927	13.249	0.082	0.001	7.920
105	7.998	14.669	0.073	0.005	7.991
106	8.072	14.953	0.076	0.001	8.065
107	8.144	14.006	0.073	-0.004	8.137
108	8.219	13.344	0.077	-0.003	8.211
109	8.293	13.060	0.077	-0.001	8.286
110	8.363	12.587	0.072	-0.002	8.356
111	8.434	12.397	0.072	-0.001	8.427
112	8.484	12.019	0.051	-0.001	8.477

Table 5.4: CMS Data Output For Parallel Chainage Run, Nominal Tractor Inclination of 30 Degrees – Time Increments 74 to 112 Seconds

The CMS calculated invert chainage travelled of 8.477m compares well with the geodimeter measured distance of 8.436m, providing an accuracy of within 0.48% of that of the geodimeter.

In all, for each initial inclination case three test runs were conducted. It was observed during the tests that for all initial +ve inclinations the inclinometer readings indicated that although the tractor would tend towards the invert path, it was neither achieved nor did the tractor exhibit –ve inclination or +ve inclination greater than that at which the tractor was initially placed. The tractor was not observed resuming a climb at any stage and at all times maintained a steady descent towards the pipe invert. For the –ve inclinations, however, the bias of the tractor unit ensured that the invert path was always achieved, if only for a briefly, before climbing to +ve inclination.

Test results and accuracies obtained are now provided in Tables 5.5, 5.6 and 5.7 with average results summarised in Table 5.8.

Nominal Inclination of Tractor θ (deg)	Maximum Value of θ (deg)	Minimum Value of θ (deg)	Geodimeter Measured Invert Path Distance (m)	CMS Calculated Invert Path Distance (m)	Error (%)
70	70.79	13.25	8.314	8.402	1.05
70	70.01	15.32	8.189	8.298	1.31
70	71.69	11.18	8.062	8.156	1.16
Average	**70.83**	**13.25**	**8.188**	**8.285**	**1.17**
60	60.38	11.17	8.325	8.400	0.89
60	60.02	12.55	8.197	8.277	0.96
60	61.07	9.79	7.900	7.976	0.95
Average	**60.49**	**11.17**	**8.141**	**8.218**	**0.93**
50	50.35	13.91	8.468	8.538	0.82
50	50.17	13.00	8.356	8.423	0.80
50	50.56	13.41	8.216	8.287	0.86
Average	**50.36**	**13.44**	**8.347**	**8.416**	**0.83**
40	40.13	14.20	8.443	8.486	0.50
40	39.80	12.45	7.610	7.667	0.74
40	41.64	15.38	7.808	7.861	0.68
Average	**40.52**	**14.01**	**7.954**	**8.005**	**0.64**
30	30.00	12.02	8.436	8.477	0.48
30	30.97	9.21	8.304	8.356	0.62
30	30.77	14.83	8.192	8.239	0.57
Average	**30.58**	**12.02**	**8.311**	**8.357**	**0.56**

Table 5.5: Summary of Parallel Test Runs Inclinations +70 to +30 Degrees

Nominal Inclination of Tractor θ (deg)	Maximum Value of θ (deg)	Minimum Value of θ (deg)	Geodimeter Measured Invert Path Distance (m)	CMS Calculated Invert Path Distance (m)	Error (%)
20	21.15	10.93	8.354	8.392	0.45
20	20.86	9.72	7.842	7.876	0.43
20	22.25	10.54	8.070	8.108	0.47
Average	**21.42**	**10.53**	**8.089**	**8.125**	**0.45**
10	10.60	8.80	8.408	8.440	0.38
10	11.21	7.99	7.645	7.673	0.37
10	10.35	5.92	7.946	7.976	0.37
Average	**10.72**	**7.57**	**8.000**	**8.030**	**0.37**
0	8.19	-1.61	8.464	8.479	0.18
0	6.77	-5.71	8.256	8.271	0.18
0	6.64	-3.93	7.448	7.462	0.19
Average	**7.20**	**-3.75**	**8.056**	**8.071**	**0.18**
-10	7.38	-11.60	8.405	8.466	0.72
-10	6.74	-10.72	8.296	8.367	0.85
-10	5.91	9.39	8.348	8.432	1.00
Average	**6.68**	**-10.57**	**8.350**	**8.422**	**0.86**
-20	7.86	-20.06	8.223	8.327	1.25
-20	6.10	-21.09	8.411	8.522	1.30
-20	5.31	-20.54	7.882	7.997	1.43
Average	**6.42**	**-20.56**	**8.172**	**8.282**	**1.33**

Table 5.6: Summary of Parallel Test Runs Inclinations +20 to -20 Degrees

Nominal Inclination of Tractor θ (deg)	Maximum Value of θ (deg)	Minimum Value of θ (deg)	Geodimeter Measured Invert Path Distance (m)	CMS Calculated Invert Path Distance (m)	Error (%)
-30	4.83	-30.28	8.294	8.371	0.92
-30	4.73	-29.67	8.227	8.336	1.31
-30	4.35	-30.20	7.582	7.667	1.11
Average	**4.64**	**-30.05**	**8.034**	**8.125**	**1.11**
-40	4.07	-40.22	8.409	8.517	1.27
-40	4.00	-41.52	8.263	8.376	1.35
-40	4.58	-40.60	8.310	8.411	1.21
Average	**4.22**	**-40.78**	**8.327**	**8.435**	**1.28**
-50	4.83	-50.06	8.374	8.464	1.06
-50	3.81	-49.23	8.219	8.335	1.40
-50	3.30	-49.78	8.040	8.175	1.65
Average	**3.98**	**-49.69**	**8.211**	**8.325**	**1.37**
-60	3.22	-59.91	8.390	8.458	0.81
-60	3.01	-60.06	8.137	8.277	1.72
-60	2.80	-60.32	8.308	8.429	1.46
Average	**3.01**	**-60.10**	**8.278**	**8.388**	**1.33**
-70	1.80	-70.60	8.339	8.450	1.31
-70	2.02	-70.18	8.196	8.344	1.78
-70	1.95	-70.62	8.084	8.218	1.64
Average	**1.92**	**-70.47**	**8.206**	**8.337**	**1.58**

Table 5.7: Summary of Parallel Test Runs Inclinations –30 to –70 Degrees

Nominal Inclination of Tractor θ (deg)	Maximum Value of θ (deg)	Minimum Value of θ (deg)	Geodimeter Measured Invert Path Distance (m)	CMS Calculated Invert Path Distance (m)	Error (%)
70	70.83	13.25	8.188	8.285	1.17
60	60.49	11.17	8.141	8.218	0.93
50	50.36	13.44	8.347	8.416	0.83
40	40.52	14.01	7.954	8.005	0.64
30	30.58	12.02	8.311	8.357	0.56
20	21.42	10.53	8.089	8.125	0.45
10	12.72	7.57	8.000	8.030	0.37
0	7.20	-3.75	8.056	8.071	0.18
-10	6.68	-10.57	8.350	8.422	0.86
-20	6.42	-20.56	8.172	8.262	1.33
-30	4.64	-30.05	8.034	8.125	1.11
-40	4.22	-40.78	8.327	8.435	1.28
-50	3.98	-49.69	8.211	8.325	1.37
-60	3.01	-60.10	8.278	8.388	1.33
-70	1.92	-70.47	8.206	8.337	1.58

Table 5.8: Summary of Average Results for All Parallel Test Runs

(+70 to –70 Degrees)

From Table 5.8 the accuracy of the chainage measurement system is optimised at 0 degrees inclination as would be expected, 0.186% (relative to geodimeter measured distance). Error rises systematically for the positive inclination cases, up to 1.171% at 70 degrees inclination, with best accuracy at the small angles of inclination. Negative inclination accuracies are poor in comparison. For example –20 degrees has an accuracy of 1.328% compared with the +20 degree accuracy of 0.443%. This can be attributed to the natural left hand bias discussed in the previous section which, tends to increase the path trajectory of the tractor for –ve initial inclinations with direct consequence on the straight-line distance calculated by the system.

It should be noted that when the tractor is manually stopped, the CMS is also manually terminated. However, with a CMS sampling rate of 1 second, it is not unlikely that a tractor stop will occur between sampling points. Given that the tractor travels at approximately 0.08 m/s, the CMS will underestimate invert chainage by up to 0.08m. In practice it is likely that a trained operative will be able to place the tractor in the pipe invert (at approximately 0 degrees inclination). Considering the average result for 0 degrees inclination given in Table 5.8, the CMS calculated invert chainage could be increased in a worse case scenario from 8.071m up to 8.151. When compared with the geodimeter measured distance of 8.056m, the CMS error is increased from 0.186% to 1.179%. Current practice achieves 2% accuracy at best. Further, an ensuing prototype would employ a higher sampling rate (e.g. 0.1 seconds) dramatically improving this already useful facility.

Placing the tractor at relatively high values of initial inclination serves to mimic adverse or imperfect field situations rather than clumsy tractor emplacement practice. Even so, percentage chainage errors are clearly tolerable even with a worn tractor.

5.1.4 Skewed Chainage Runs

In order to assess the performance of the CMS under even more imperfect initialisation conditions, the tractor was placed at a skewed angle γ_s to the pipe axis as illustrated in Figure 5.7 to simulate deflection by some object such as debris.

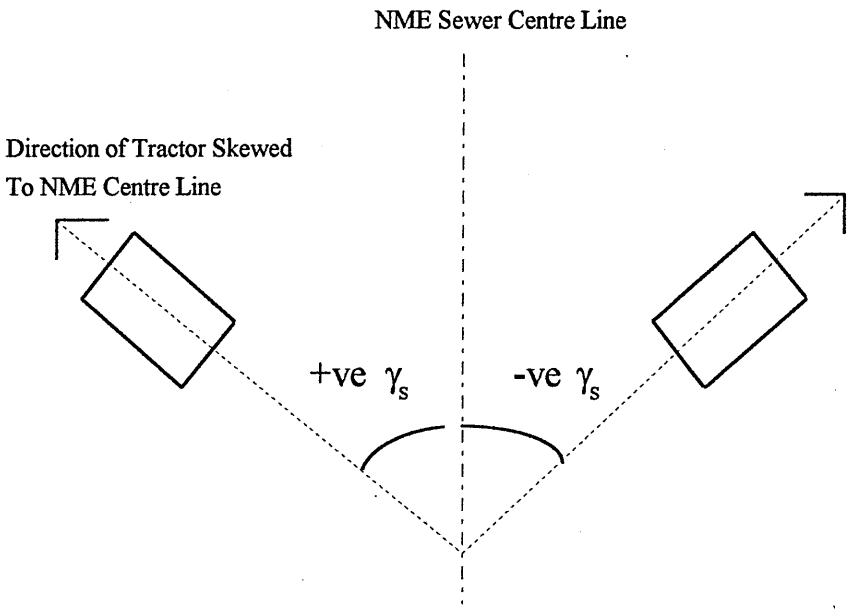

Plan on NME Sewer

Figure 5.7: Skewed Orientation About NME Axis

As shown in Figure 5.8, due to the size of the tractor relative to the ϕ_{NME} it was difficult to replicate more than a limited number of γ_s angles. Angles roughly approximating 30, 25, 20 15, -15, -20, -25 and –30 degrees were possible within the sewer and were roughly checked by determining the angular difference between the NME centreline and a point on the tractor. This was achieved by initially sighting the geodimeter along the NME centreline and recording the horizontal angle and then sighting the geodimeter at a central point on the front top plate of the tractor. Keeping the rear of the tractor roughly in the invert and by adjusting the position at the front of the tractor allowed the required

horizontal angular difference to be obtained. This was also double checked using a simple engineering instrument, i.e. a protractor.

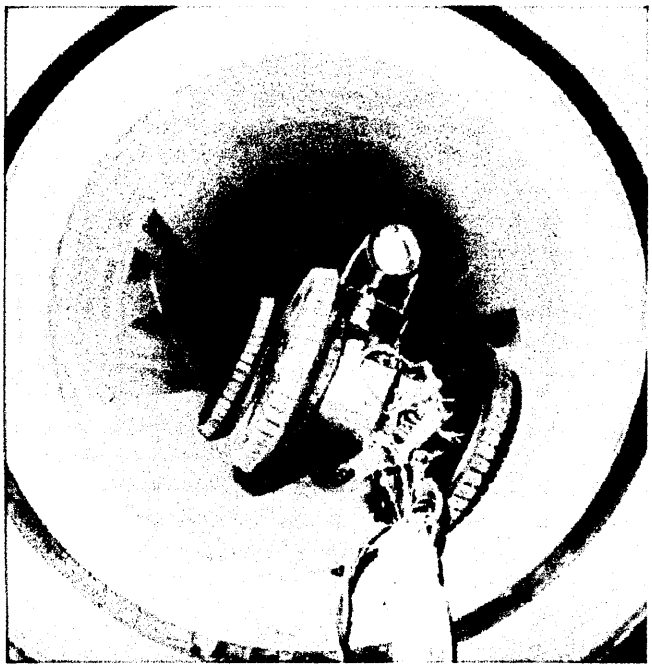

Figure 5.8: Skewed Inclination, + 30 degrees

Consider as by way of a typical example γ_s = 20 degrees. Following emplacement within the NME pipe as above, the geodimeter was again set up and employed as detailed in the preceding section to determine datum A. The CMS programme was then initiated with rotary encoder and inclinometer readings sampled at one-second intervals. With power supplied to the tractor drive motor the following was observed. The skew nature of the tractor within the pipe angles it slightly up the left hand wall. With tractor power engaged, the tractor briefly continues to climb before levelling out parallel to the NME centre line whereupon a trajectory similar to that observed for the parallel test runs is achieved. The CMS again monitored the outputs of both the inclinometer and rotary encoder at one second intervals, whilst computing culmative straight-line distance

travelled. After travelling typically 8 to 8.5m, power to the tractor drive was again manually switched off and the tractor immediately came to rest (position B). The CMS programme was then terminated and data saved. The geodimeter was again employed to measure distance to position B and the true invert path distance travelled by the tractor as measured by the geodimeter was calculated. The invert chainage calculated by the CMS was then compared to that measured by the geodimeter and the accuracy of the CMS determined.

Tables 5.9 to 5.11 provide the CMS data output for the $\gamma_s = 20$ degrees test run.

Time (s)	Culmative Distance (Rotary Encoder) (m)	Inclination (degrees)	Velocity (m/s)	Incremental Offset (m)	Culmative Invert Path Distance (m)
0	0.000	30.577	0.000	0.000	0.000
1	0.042	30.918	0.043	0.001	0.042
2	0.082	31.088	0.042	0.001	0.082
3	0.147	31.344	0.067	0.001	0.147
4	0.217	30.748	0.072	-0.002	0.217
5	0.279	31.344	0.064	0.002	0.279
6	0.339	32.877	0.061	0.005	0.338
7	0.404	32.366	0.067	-0.002	0.404
8	0.474	31.651	0.072	-0.003	0.474
9	0.552	30.833	0.079	-0.003	0.551
10	0.627	30.407	0.078	-0.001	0.627
11	0.710	29.896	0.085	-0.002	0.709
12	0.796	28.874	0.088	-0.003	0.796
13	0.880	28.448	0.087	-0.001	0.880
14	0.966	29.555	0.088	0.004	0.965
15	1.053	29.215	0.090	-0.001	1.053
16	1.139	27.937	0.088	-0.004	1.138
17	1.222	27.681	0.086	-0.001	1.222
18	1.309	26.830	0.089	-0.003	1.308
19	1.403	26.063	0.096	-0.003	1.402
20	1.487	25.552	0.087	-0.002	1.486
21	1.571	27.000	0.086	0.005	1.570
22	1.656	26.744	0.088	-0.001	1.655
23	1.745	25.893	0.091	-0.003	1.744
24	1.831	25.467	0.089	-0.002	1.830
25	1.915	24.615	0.086	-0.003	1.914
26	1.999	23.763	0.087	-0.003	1.998
27	2.086	23.167	0.089	-0.002	2.084
28	2.175	24.785	0.092	0.006	2.174
29	2.260	24.360	0.087	-0.002	2.258
30	2.341	23.508	0.083	-0.003	2.340
31	2.420	23.338	0.081	-0.001	2.419
32	2.506	22.741	0.088	-0.002	2.504
33	2.597	21.804	0.094	-0.003	2.596
34	2.684	21.464	0.089	-0.001	2.683
35	2.763	22.656	0.081	0.004	2.762
36	2.846	23.252	0.085	0.002	2.844

Table 5.9: CMS Data Output For Skewed Chainage Run, $\gamma_s = 20$ Degrees

Time Increments 0 to 36 Seconds

Time (s)	Culmative Distance (Rotary Encoder) (m)	Inclination (degrees)	Velocity (m/s)	Incremental Offset (m)	Culmative Invert Path Distance (m)
37	2.930	22.230	0.087	-0.004	2.929
38	3.020	21.549	0.092	-0.002	3.018
39	3.102	22.060	0.083	0.002	3.100
40	3.186	20.697	0.087	-0.005	3.184
41	3.269	20.356	0.085	-0.001	3.267
42	3.350	20.868	0.083	0.002	3.348
43	3.426	21.890	0.078	0.004	3.424
44	3.491	21.804	0.066	0.000	3.488
45	3.567	20.612	0.079	-0.004	3.565
46	3.636	20.016	0.070	-0.002	3.634
47	3.716	19.931	0.082	0.000	3.714
48	3.806	18.909	0.092	-0.004	3.804
49	3.893	18.568	0.089	-0.001	3.890
50	3.977	19.505	0.086	0.003	3.974
51	4.053	20.612	0.079	0.004	4.051
52	4.142	19.845	0.090	-0.003	4.139
53	4.225	18.738	0.086	-0.004	4.223
54	4.309	18.994	0.086	0.001	4.306
55	4.385	18.568	0.079	-0.002	4.383
56	4.471	18.142	0.088	-0.002	4.468
57	4.567	18.738	0.099	0.002	4.565
58	4.647	20.186	0.082	0.005	4.644
59	4.730	19.845	0.085	-0.001	4.727
60	4.807	18.738	0.079	-0.004	4.804
61	4.894	18.568	0.090	-0.001	4.891
62	4.974	16.183	0.081	-0.009	4.970
63	5.062	18.057	0.090	0.007	5.058
64	5.149	17.801	0.089	-0.001	5.145
65	5.230	19.334	0.083	0.006	5.226
66	5.303	18.994	0.075	-0.001	5.299
67	5.372	17.375	0.071	-0.006	5.368
68	5.460	18.142	0.091	0.003	5.456
69	5.540	18.227	0.081	0.000	5.535
70	5.625	17.375	0.088	-0.003	5.621
71	5.711	16.779	0.088	-0.002	5.706
72	5.799	17.461	0.090	0.003	5.794

Table 5.10: CMS Data Output For Skewed Chainage Run, $\gamma_s = 20$ Degrees

Time Increments 37 to 72 Seconds

Time (s)	Culmative Distance (Rotary Encoder) (m)	Inclination (degrees)	Velocity (m/s)	Incremental Offset (m)	Culmative Invert Path Distance (m)
73	5.877	18.653	0.081	0.004	5.873
74	5.954	18.312	0.079	-0.001	5.949
75	6.036	17.461	0.084	-0.003	6.031
76	6.118	16.864	0.084	-0.002	6.113
77	6.202	16.353	0.086	-0.002	6.197
78	6.283	15.587	0.083	-0.003	6.278
79	6.366	15.246	0.086	-0.001	6.361
80	6.443	16.609	0.079	0.005	6.438
81	6.522	17.205	0.081	0.002	6.517
82	6.606	17.035	0.086	-0.001	6.601
83	6.683	16.268	0.078	-0.003	6.677
84	6.762	16.183	0.081	0.000	6.757
85	6.841	15.416	0.081	-0.003	6.836
86	6.926	14.991	0.087	-0.002	6.921
87	7.007	14.735	0.082	-0.001	7.001
88	7.091	14.991	0.086	0.001	7.085
89	7.167	14.820	0.078	-0.001	7.162
90	7.249	14.565	0.084	-0.001	7.243
91	7.334	15.502	0.088	0.004	7.329
92	7.423	14.650	0.091	-0.003	7.417
93	7.504	14.054	0.083	-0.002	7.498
94	7.590	13.628	0.089	-0.002	7.585
95	7.673	15.161	0.085	0.006	7.667
96	7.758	15.502	0.087	0.001	7.752
97	7.837	14.820	0.082	-0.003	7.832
98	7.919	14.480	0.084	-0.001	7.913
99	8.000	14.650	0.083	0.001	7.994
100	8.082	13.713	0.085	-0.004	8.076
101	8.170	13.542	0.090	-0.001	8.164
102	8.244	13.372	0.076	0.000	8.238
103	8.288	14.394	0.045	0.004	8.282

Table 5.11: CMS Data Output For Skewed Chainage Run, $\gamma_s = 20$ Degrees

Time Increments 73 to 103 Seconds

For each initial skewed inclination case, three test runs were again conducted and the straight-line distance determined compared that again measured by the geodimeter. Test

results are provided in Tables 5.12 to 5.13 with average values summarised in Table 5.14.

Nominal Inclination of Tractor γ_s (deg)	Maximum Value of θ (deg)	Minimum Value of θ (deg)	Geodimeter Measured Invert Path Distance (m)	CMS Calculated Invert Path Distance (m)	Error (%)
30	59.31	19.97	7.911	8.134	2.74
30	60.35	17.89	8.171	8.421	2.97
30	63.84	21.32	8.069	8.351	3.38
Average	**61.17**	**19.73**	**8.050**	**8.302**	**3.03**
25	55.90	15.11	8.353	8.516	1.92
25	56.17	17.45	8.256	8.422	1.97
25	57.23	19.97	7.893	8.055	2.01
Average	**56.43**	**17.51**	**8.617**	**8.331**	**1.97**
20	31.65	13.54	8.178	8.282	1.25
20	29.83	12.31	8.350	8.435	1.01
20	30.89	12.54	7.946	8.045	1.23
Average	**30.79**	**12.80**	**8.158**	**8.254**	**1.17**
15	22.12	11.80	7.998	8.054	0.70
15	20.54	8.99	7.514	7.559	0.60
15	19.71	8.13	7.956	7.998	0.52
Average	**20.79**	**9.64**	**7.833**	**7.870**	**0.61**

Table 5.12: Summary of Results For All Skewed Test Runs

(15 to 30 Degrees)

Nominal Inclination of Tractor γ_s (deg)	Maximum Value of θ (deg)	Minimum Value of θ (deg)	Geodimeter Measured Invert Path Distance (m)	CMS Calculated Invert Path Distance (m)	Error (%)
-15	7.22	-20.39	8.537	8.640	1.19
-15	7.68	-22.31	8.406	8.522	1.36
-15	8.23	-21.73	8.363	8.465	1.21
Average	**7.71**	**-21.48**	**8.435**	**8.542**	**1.25**
-20	9.21	-35.22	8.725	8.899	1.95
-20	8.73	-34.61	8.070	8.226	1.89
-20	8.38	-35.83	8.146	8.318	2.07
Average	**8.77**	**-35.22**	**8.314**	**8.481**	**1.97**
-25	7.96	-52.17	7.982	8.198	2.63
-25	7.84	-55.61	8.232	8.476	2.88
-25	9.42	-54.16	8.067	8.297	2.78
Average	**8.41**	**-53.98**	**8.094**	**8.324**	**2.76**
-30	8.05	-63.55	8.092	8.135	2.68
-30	6.97	-61.94	8.233	8.443	2.49
-30	9.19	-65.12	7.741	7.997	3.20
Average	**8.07**	**-63.54**	**8.022**	**8.192**	**2.79**

Table 5.13: Summary of Results For All Skewed Test Runs

(-15 to –30 Degrees)

Nominal Longitudinal Orientation Of Tractor γ_s (deg)	Maximum Value of θ (deg)	Minimum Value of θ (deg)	Geodimeter Measured Invert Path Distance (m)	CMS Calculated Invert Path Distance (m)	Error (%)
30	61.17	19.73	8.050	8.302	3.03
25	56.43	17.51	8.617	8.331	1.97
20	30.79	12.80	8.158	8.254	1.17
15	20.79	9.64	7.833	7.870	0.61
-15	7.71	-21.48	8.435	8.542	1.25
-20	8.77	-35.22	8.314	8.481	1.97
-25	8.41	-53.98	8.094	8.324	2.76
-30	8.07	-63.54	8.022	8.192	2.79

Table 5.14: Summary of Average Results for All Skewed Test Runs

Whilst it is difficult to directly compare CMS accuracy values between parallel and skew cases, it is may be concluded when comparing Tables 5.9 and 5.11 that CMS accuracy for the skewed angle cases is worse that that of the parallel test runs but not excessively so. The parallel test at +30 degrees afforded an accuracy of 0.82% whilst the skewed test results with maximum inclination of 30 degrees (γ_s = 20 degrees) produced an error of 1.17%. However, whilst the tractor is skew within the pipe, so is the inclinometer. The mathematical model derived in Section 3.1.3 assumes the inclinometer to be parallel to pipe centre line. As the tractor only remains skew over the initial, and very short, length of its trajectory as shown in Table 5.9 (approximately 0.5m) the errors induced in

determining overall invert path length are not envisaged to be troublesome. It is anticipated that this problem could be overcome by provision of a second inclinometer located to monitor tractor pitch instead as to be discussed in Chapter 7.

5.1.5 Discussion

Parallel tests are not directly comparable to skewed tests because although they are both testing the chainage measurement system's suitability to determine the straight-line distance travelled accurately, they each test the system in a different way. The skewed tests by their nature ensure that the tractor must firstly climb the pipe wall as it travels along the pipe before levelling out on a course hopefully as close to the invert as possible. The degree of climb that is experienced is directly related to the skewed angle at which the tractor is initially set. The overall path length that the tractor travels is therefore longer than the equivalent parallel test run.

During the parallel test runs, the tractor body is parallel to the axis of the pipe, and the inclinometer assessment of the tractor position in the pipe is relatively accurate as is born out by the results of Table 5.8. For the skewed cases, a further inclinometer-mounted perpendicular to the first may aid assessment of the tractor position relative to the pipe axis and produce a more robust chainage measurement system.

Overall, it is considered that the data shows the CMS to work well. A higher sampling rate combined with good operative initial emplacement practice would appear to suggest that the CMS module could be put into industrial employment quite quickly.

5.2 ROBOTIC ARM SYSTEM

5.2.1 Initial Considerations

A computer program has been written in QBASIC to control the three stepper motors that drive robotic arm. Within this chapter, the performance and suitability of the arm to the task of describing the requisite lateral cut profiles for 90 and 45 degree lateral junctions are assessed. The applicability of the arm to the task of lateral reconnection as part of a NME sewer CIP lining renovation process will therefore be based upon the results produced.

It is to be noted that the arm control computer programme is based on the mathematical model derived in Section 3.2.5, and provides the facility to determine the required arm kinematic movements to move the end effector (EE) between successive points on a lateral cut profiles. However, a major assumption of the programme is that the axis of Joint 2 of the robot arm (which is the main pivot for vertical rotation) is coincident with the NME centreline.

When the arm was initially designed and constructed the pipe rig was unavailable and, as noted in Section 4.2.1, was later donated at some cost by industrial parties. Unfortunately, the diameter of NME pipe provided was smaller than anticipated resulting in the pivot of Joint 2 being some 40mm above the NME centreline. Whilst the programmed movement of joints 1 and 2 for correct positioning on a given profile were unaffected by this, joint 3 incurred problems. For lateral profiles between 9 and 3 o'clock about the lateral centre line, i.e. top half of the profile, the programme was unable to fully extend the linear actuator the determined length because of the EE grounding on the pipe wall. For positions between 3 and 9 o'clock corresponding to the

bottom half of the profile, the calculated extension was insufficient to contact the wall. Problems were also encountered with the arm counterweight grounding on the opposite pipe wall particularly when attempting lateral profiles around the 6 o'clock position with radii exceeding 80mm.

Given the time constraints and anticipated problems associated with further arm / tractor modifications, it was decided to test the arm programme based on its ability to correctly position the end effector through rotation of joints 1 and 2 only. The drill / grind path was to consist of a series of discrete points (note Table 5.15). In order to mark each point on the profile the drill computer programme was modified to allow for operator input of 'u', the translation of the linear actuator, to extend the EE until contact was made with the paper. As addressed in Chapter 4, for cost-effective research, a cotton bud attached to the linear actuator threaded bar replaced the drill based EE. This was loaded with ink prior to testing and 'topped up' as required during. Once the point was marked the operator could retract the EE to provide sufficient clearance until the next point was reached; although affording realistic cutting profiles to be produced with minimal interference, testing proved very slow, up to 90mins per test run as will now be discussed.

5.2.2 90 Degree Lateral Testing

In order to record the drill profiles produced by the arm, drawing paper was taped to the inner surface of the concrete pipe wall at approximately a 9 o'clock position. For the purposes of experimentation, it was not necessary to place the drawing paper directly over, or at, the actual lateral location, indeed, the solidity of the pipe surface behind the pliable paper aided production of the cut profile traces.

Initially the robot was placed in the sewer pipe adjacent to the drawing paper target at an assumed drilling station position. With the robotic arm initially at repose; i.e. parallel to the axis of the NME sewer, the arm control programme was then initiated requiring the input of several key parameters identified with their values in Table 5.15.

Parameter	Definition	Value
LATMAX	Maximum lateral diameter to be cut	120mm
LATMIN	Minimum cut profile diameter	40mm
RHOINPUT	Intersection angle of lateral and NME	90 degrees
LATSTEP	Increment between successive cut profiles	20mm
PHISTEP	Increment that the arm rotates about the lateral centreline between each mark placed on the paper	2 degrees

Table 5.15: Arm Control Parameters – 90 Degree Lateral

Following input of the above parameters, the arm rotates 90 degrees left from repose to on target. As the minimum lateral diameter to be 'cut' has been defined as 40mm, the EE is stepped out 20mm (through rotation of Joint 1) ready for the first mark to be made. As discussed in the previous section, the EE is manually extended and retracted to mark the first point on the drill path. The co-ordinates of the next position on the profile, corresponding to a rotation about the lateral centreline of 2 degrees (PHISTEP) are calculated, and kinematic movements employed through joints 1 and 2. Again the

EE is extended and retracted manually to mark the drawing paper. For every 2-degree circular increment, from 0 to 360 degrees around the lateral centroid, the cotton bud is therefore moved to the next co-ordinate position on the drill profile, driven in and then retracted, Figure 5.9.

MM

Figure 5.9: Drill Trace Profiles Employing Simple End Effector

Once the first full profile is produced, the program steps out the end effector by LATSTEP to produce the next drill profile trace, i.e. 20mm. The above process was repeated such that further drill profiles corresponding to radii 60mm, 80mm 100mm and 120mm were produced. Figure 5.10.

Figure 5.10: Drill Trace - Full Profile

The tests were repeated until three sets of profiles were obtained. In order to compare these robotic arm generated profiles with the idealised case, a spreadsheet was used to determine the co-ordinates lying on idealised cut profiles for each of the cut profile diameters described. Whilst the 3D profiles appear circular when viewed within the pipe, it is apparent when they are removed that the 2D profiles are elliptical; an effect of the pipe curvature. The idealised profiles were produced within AutoCAD, an example of which is provided in Figure 5.11, printed on film and then overlaid on the arm generated profiles to provide comparison. Note, the idealised profiles are doubly symmetric about X and Y axes. The three profiles produced are shown, with idealised profiles overlaid, in Figures 5.12 to 5.14.

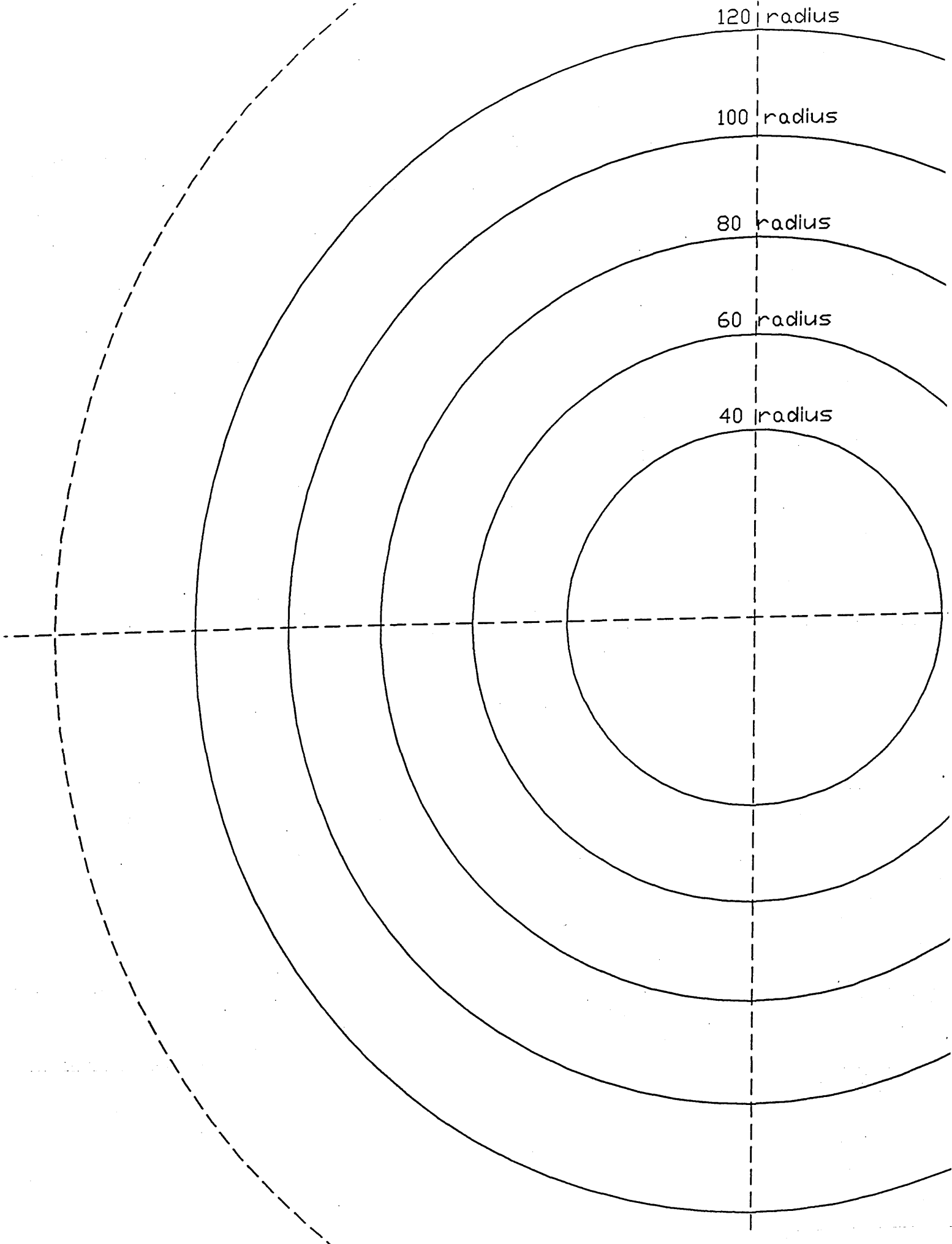

Figure 5-11 : Idealised 90 Degree Cut Prof

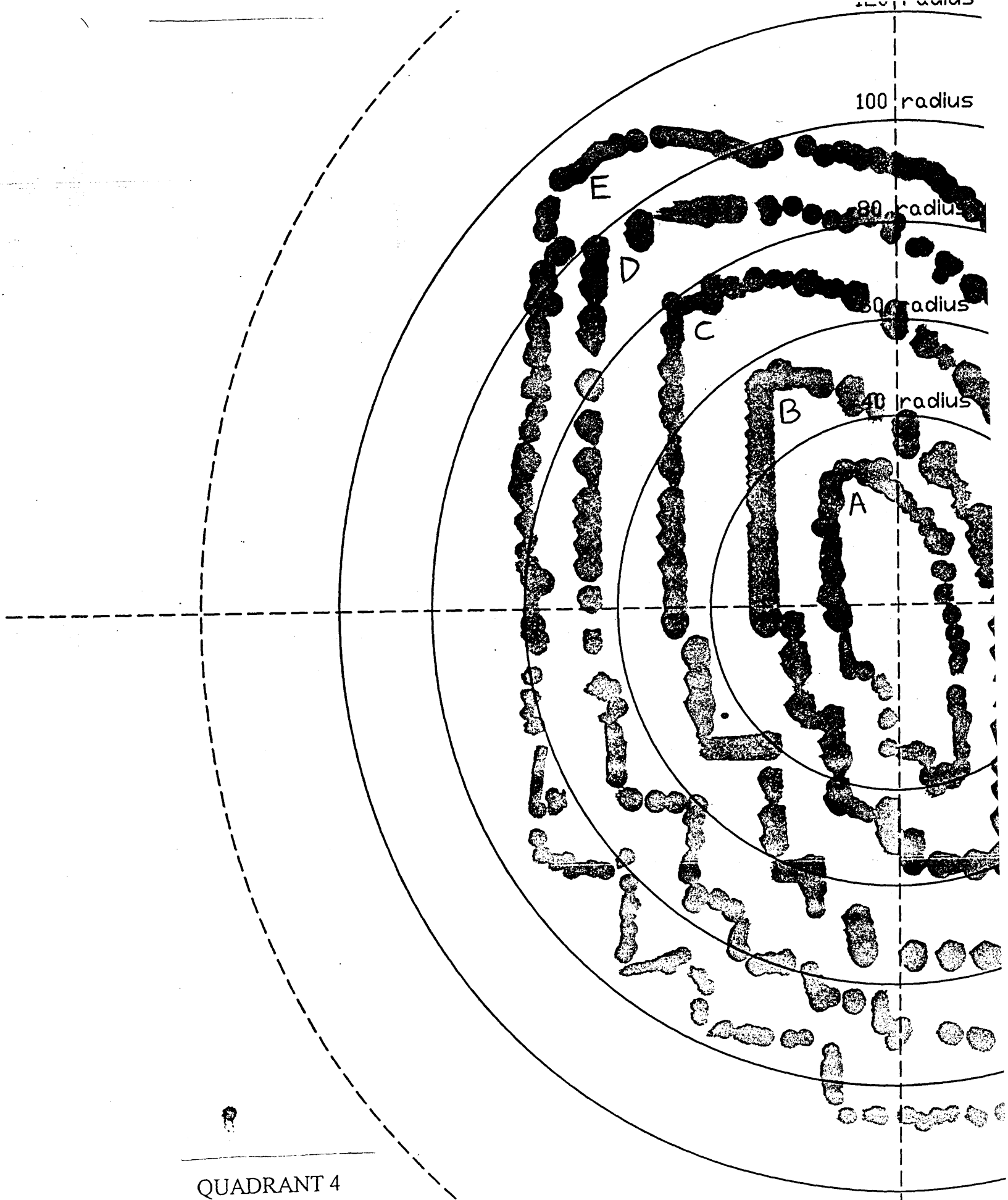

Figure 5.12: Experimental 90 Degree Cut Profiles W

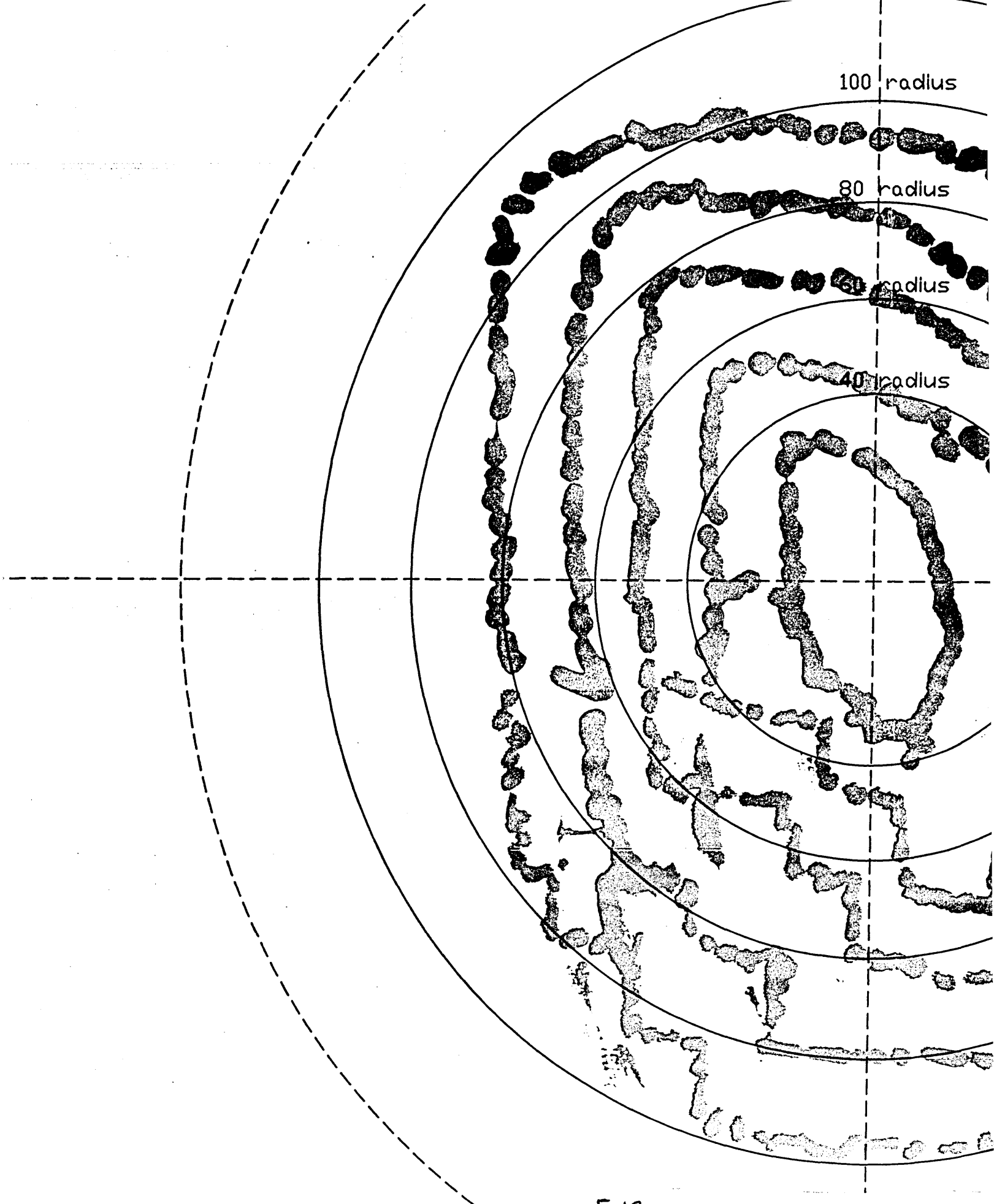

Figure 5-13: Experimental 90 Degree Cut Profiles With I

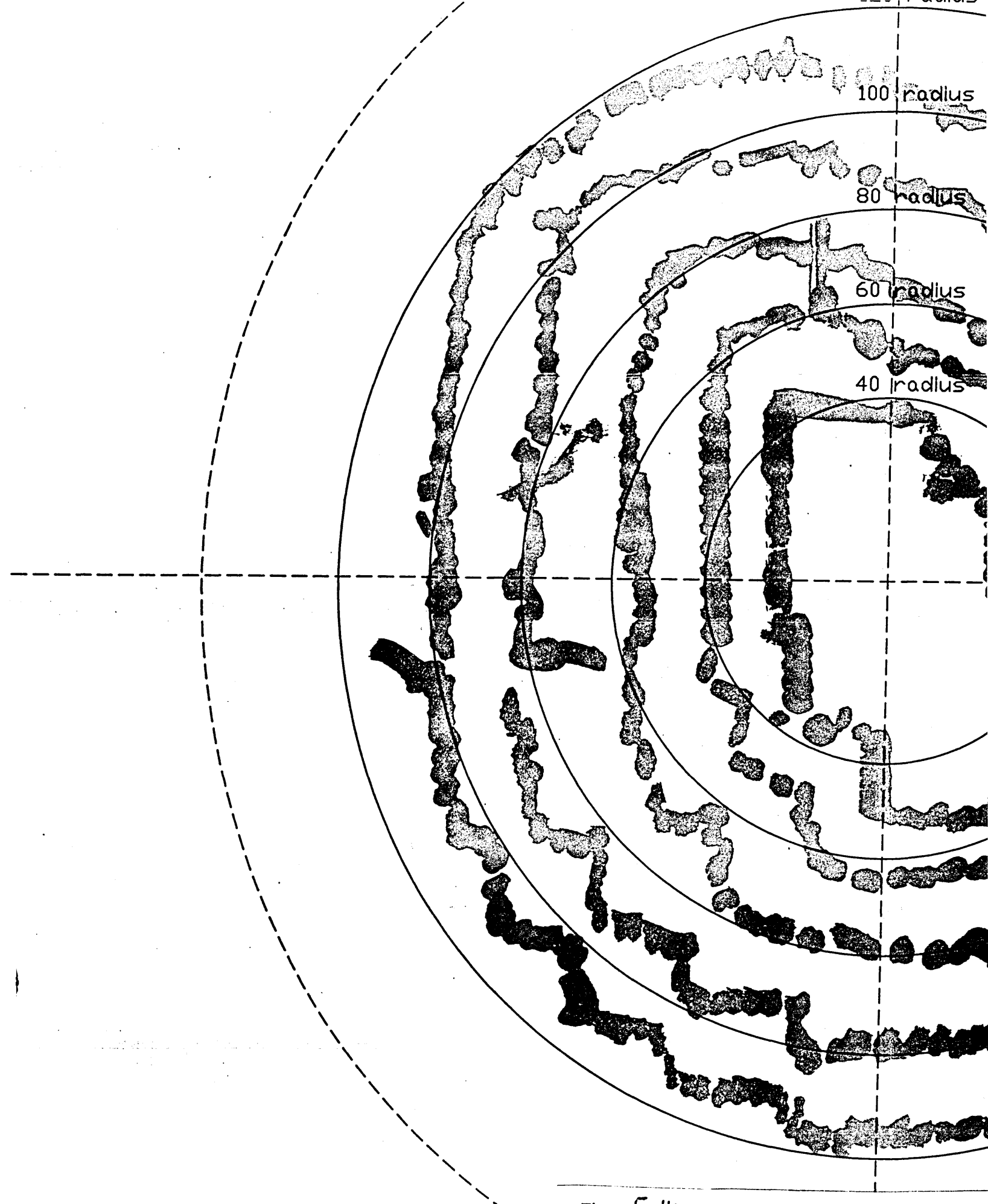

Figure 5-14: Experimental 90 Degree Cut Profiles

5.2.3 Discussion - 90 Degree Test Results

As shown in Figures 5.12 to 5.14, experimental profiles are consistent but suffer inaccuracy, particularly in horizontal dimensions. Approximately 20% undershoot is noted for vertical positioning whilst as much as 50% undershoot is observed regarding horizontal positioning; this effect is considered to be due to the poor recovery of stepper motor pulses in the absence of closed loop 'feedback' control when changing direction in this plane. Further and as noted in Section 4.3.3, the stepper motors and gearboxes used for joints 1 and 2 exhibited a certain degree of play or backlash in their drive systems.

With reference to Figure 5.12, since all arm movements stated are from centre and move horizontally left followed by a clockwise rotation, for each profile quadrant it is possible to identify change of direction (COD) of motors which may produce the backlash problems noted. In quadrant 1, the horizontal COD leads to backlash take-up producing vertical lines as is the case in quadrant 3. For quadrant 2, the vertical COD is compensated by gravity resulting in production of a good profile whilst in quadrant 4 the motors work to overcome gravity and a stepped motion for all three figures is observed. This vertical step observed at '6 o'clock' does, however, aid positioning of the overlay with respect to the arm-generated profile.

It was also noted that the step increment observed between successive profiles generally exceeded the 20mm increment selected; again motor backlash and problems encountered with joint rigidity during testing were considered responsible for this.

Despite the above noted shortcomings, it is considered that the principle of the proposed module has been proven.

5.2.4 45 Degree Lateral Testing

Adopting the same test method as that employed for the 90-degree lateral case, testing for the 45 degree lateral case was undertaken with the parameters given in Table 5.16.

Parameter	Definition	Value
LATMAX	Maximum lateral diameter to be cut	100mm
LATMIN	Minimum cut profile diameter	40mm
RHOINPUT	Intersection angle of lateral and NME	45 degrees
LATSTEP	Increment between successive cut profiles	10mm
PHISTEP	Increment that the arm rotates about the lateral centreline between each mark placed on the paper	2 degrees

Table 5.16: Arm Control Parameters – 45 Degree Lateral

To provide contrast with the 90 degree lateral experiments, a step increment of 10mm was selected for the 45 degree intersection set of trace profiles. Drill profiles corresponding to radii of 40mm, 50mm, 60mm 70mm, 80mm, 90mm and 100mm were attempted. A spreadsheet was used to generate the idealised profiles, produced on AutoCAD as shown in Figure 5.15. These profiles are singly symmetric about their X axis. Again, three experimental profiles were produced and are presented in Figures 5.16 to 5.18 with the computer generated, idealised, profiles overlaid.

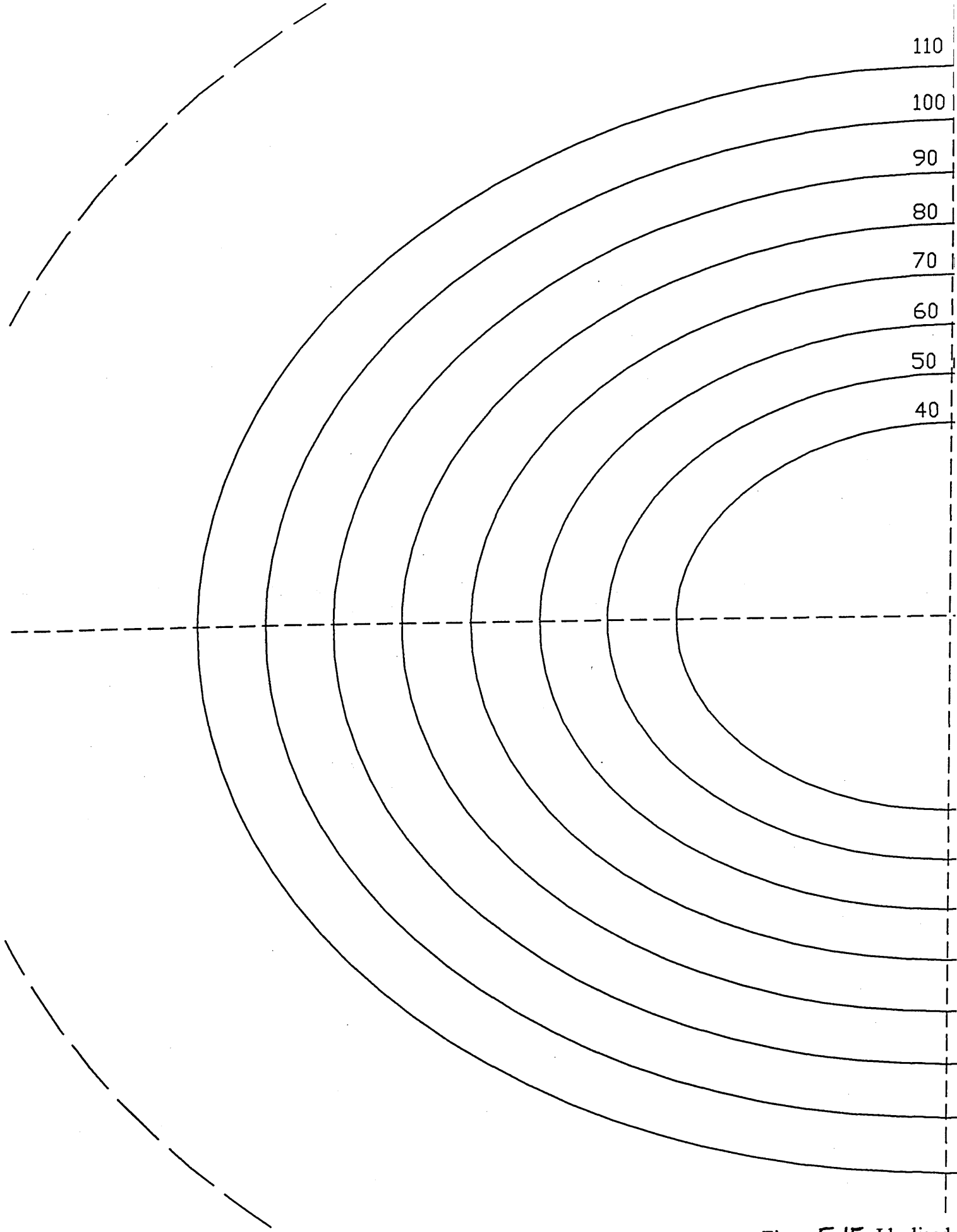

Figure 5·15: Idealised

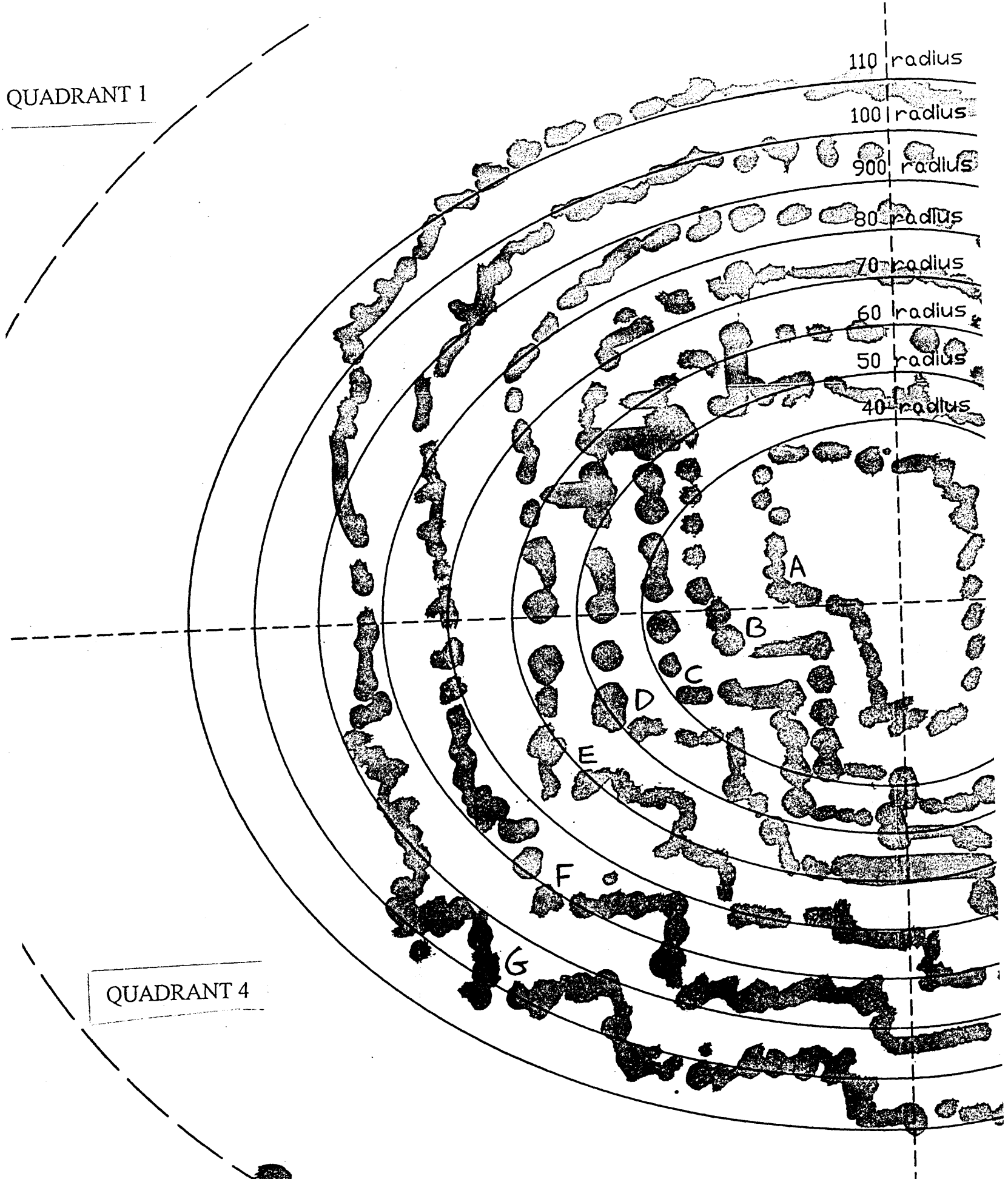

Figure 5-16: Experimental 45 Degree Cut Profiles W

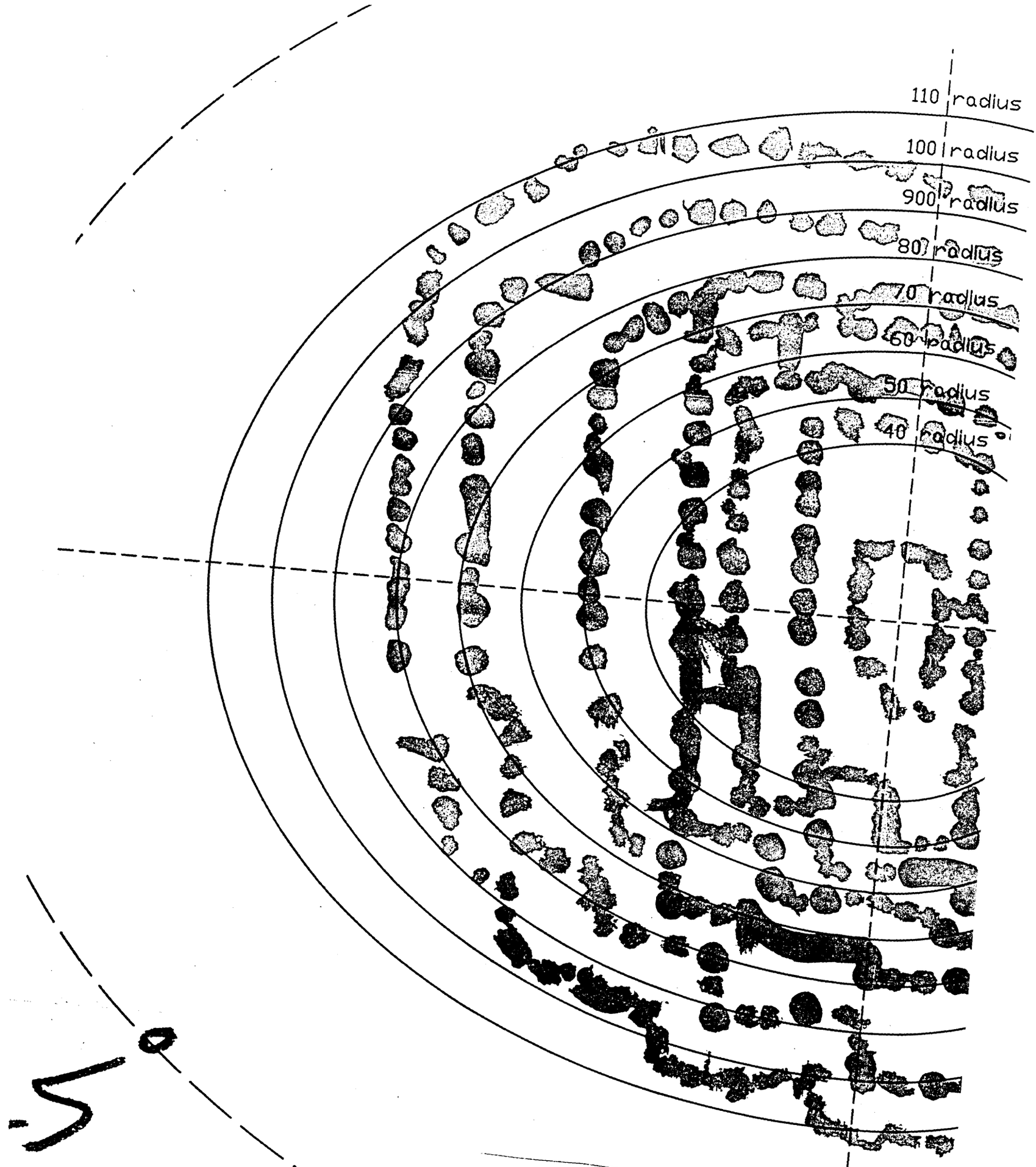

Figure 5.17 : Experimental 45 Degree Cut Profiles With Ideal

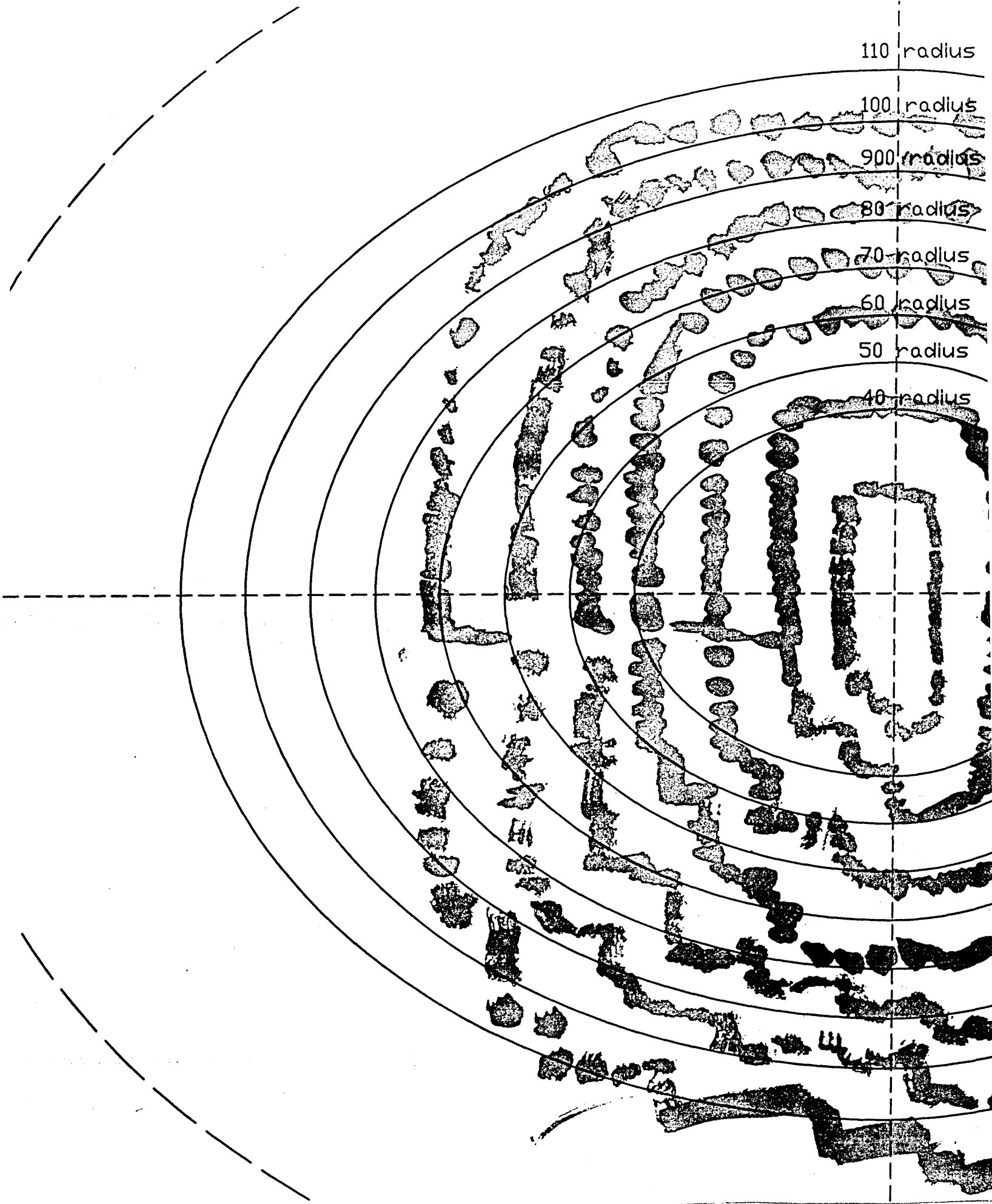

Figure 5-18: Experimental 45 Degree Cut Profiles W

5.2.5 Discussion - 45 Degree Test Results

As for the 90 degree lateral case, the experimental profiles shown in Figures 5.16 to 5.18, are consistent but relatively inaccurate; the skew nature of the 45 degree profile, however, hides this effect in horizontal dimensions more so than that observed for the 90 degree cases. Approximately 20% undershoot is noted for vertical positioning whilst as much as 50% undershoot is observed regarding horizontal positioning; this effect is again considered to be due to the poor recovery of stepper motor pulses in the absence of closed loop 'feedback' control when changing direction in this plane.

With reference to Figure 5.16, all arm movements stated are again from centre and move horizontally left followed by a clockwise rotation. For each profile quadrant it is possible to identify change of direction (COD) of motors which may produce the backlash problems noted. In quadrant 1, the horizontal COD leads to backlash take-up producing vertical lines as is the case in quadrant 3. For quadrant 2, the vertical COD is compensated by gravity resulting in production of a good profile whilst in quadrant 4 the motors work to overcome gravity and a stepped motion for all three figures is observed. This vertical step observed at '6 o'clock' again aids positioning of the overlay with respect to the arm-generated profile.

Whilst the step interval between successive drill profiles was set to 10mm for the 45 degree case, actual spacing achieved was inconsistent and generally exceeded 10mm. Profiles with radii in excess of 100mm were not attempted as more problems were being experienced with the arm set-up and the arm was subject to missing profile information. However, as the majority of laterals associated with a 450mm-diameter sewer, such as the one used here, are either 150 or 225mm, the results produced herein

are considered valid and that the principle of the proposed module has again been proven, this time with regard to the more general case of a singly symmetric lateral intersection (i.e. not an orthogonal junction as previously discussed in Sections 5.2.2. and 5.2.3).

5.3 SUMMARY

Within this chapter, the chainage measurement system and robotic arm have been evaluated within the laboratory environment.

The chainage measurement system has been shown to work well under a variety of initialisation conditions and invert chainages produced by the system compare well with geodimeter data. Noting that in practice, an accuracy of 2% is acceptable, the results produced herein significantly better those achieved in industry. The CMS module is considered suitable for immediate industrial application.

The robot arm drilling system has been shown to work in principle for both the 45 and 90 degree lateral cases though results produced are shown to exhibit significant degrees of undershoot; hardware problems and lack of feedback control are considered to be the major contributing factors producing these errors. Resolution of these problems is to be addressed in Chapter 7.

CHAPTER 6

VISION SYSTEM TESTING

6.1 LATERAL DETECTION EVALUATION

6.1.1 Preamble

As noted in Chapter 2, a lateral detection system has been implemented under the TINA Vision Research Environment. Strict numerical quantitative precision is not required for lateral detection purposes, which in effect is a qualitative procedure. The following describes the laboratory evaluation work undertaken.

6.1.2 Data Acquisition

As detailed in Section 4.2.1, a survey of the laboratory based pipe rig using a geodimeter and adapted target prism positioning system was undertaken to determine pipe rig topology; see Table 4.1. A CCTV survey, using the tractor, Watec CCD camera and twin 50W dichromatic light sources was then employed. An in-house manufactured switch box was provided to alternate which of the lights was illuminated at any one time, hence providing either direct or reflected illumination of the lateral under consideration. The iris of the camera was also carefully adjusted so as to avoid saturation of the image but maintain optimum image production. A geodimeter target prism was fixed to the rear of the tractor at a known offset of 300mm from the camera CCD element as shown in Figure 6.1.

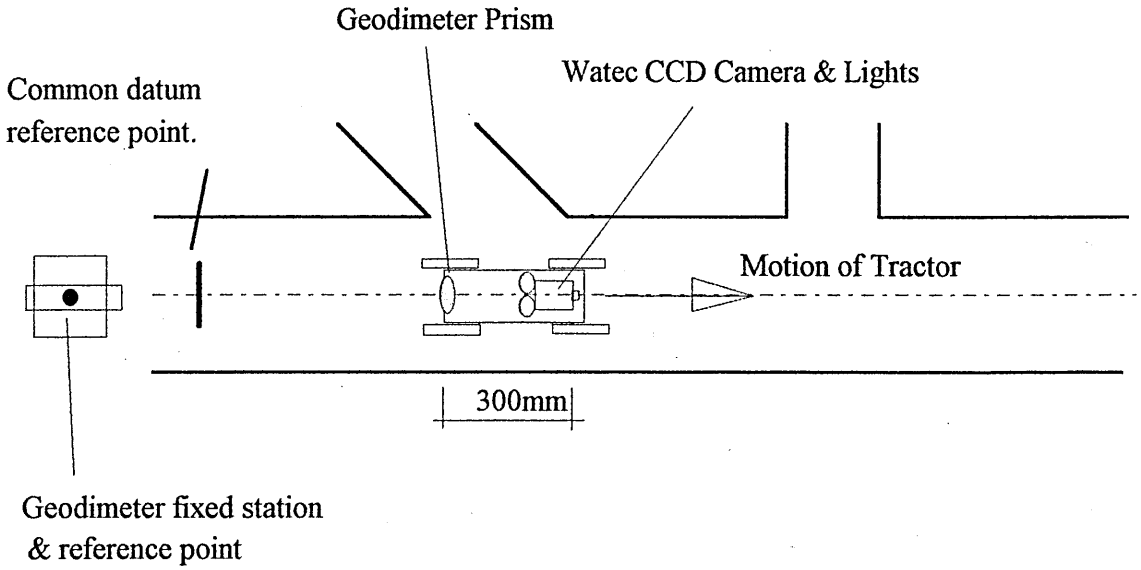

Figure 6.1: Lateral Detection Topology

Initially, consider the data acquisition process for the first image pair for the 45 degree lateral case. Using the same geodimeter set-up as that employed during the initial pipe rig survey, and noting the same datum positioning (Figure 6.1), the tractor was driven to a position within 3.5m of the lateral junction centreline intersection with the NME. Recalling Chapter 1, this distance was chosen because it is around this mark that in current practice a CCTV operator can normally visually detect the presence of a lateral. A geodimeter was used to measure the distance of the camera with respect to the datum; the geodimeter measures the distance to the rear of the tractor where the target prism is located. The offset, as noted above is known, so the distance to the camera can be resolved. By simple subtraction therefore, the distance between the camera and lateral back wall projection is determined; please recall Chapter 2, Figure 2.21 regarding distance x_{vp}.

Using a VCR linked directly to the Watec camera, images of the sewer relayed by the tractor could be viewed in real time on the monitor. Images of the lateral were recorded under both illumination conditions. The tractor was driven closer and a further geodimeter reading taken to confirm distance from the lateral. Again images were recorded under both direct and reflected light. This was repeated until five sets of images were recorded at known distance from the lateral under both direct and reflected illumination. This sequence was repeated for the 90 degree lateral. The recorded data are provided in Table 6.1

	45 Degree Lateral - *Xvp* (m)	**90 Degree Lateral - *Xvp* (m)**
Image Pair 1	3.453	3.349
Image Pair 2	3.271	3.032
Image Pair 3	2.912	2.614
Image Pair 4	2.704	2.347
Image Pair 5	2.643	2.208

Table 6.1: Image Location – Geodimeter Derived x_{vp} Distance From Lateral - for both 45 and 90° Laterals

Subsequently, the video taped images were transferred to an IT laboratory whereupon they were digitised using a frame grabber and ancillary equipment providing five image pairs per lateral. Images were then transferred to a SUN SPARC workstation for processing within the TINA computer vision environment; please refer to Section 2.1.5.

Employing the procedures outlined in Section 2.2, lateral detection was performed on each reflected image with results as follows.

6.1.3 Detection Under Optimum Illumination Conditions

Figure 6.2 illustrates the application of the proposed vision system to the image acquired at 2.614m from the 90 degree lateral junction, under reflected illumination. To conserve space, edges obtained via the Canny operator are overlaid on the original, grey level image (Figure 6.2a). Figure 6.2b shows the result of thresholding this image to identify the 'black hole'. The resulting, estimated vanishing point being shown overlaid on the grey level image, in Figure 6.2c. Figure 6.2d shows the final system output: only one edge, shown in black, meets the criteria for acceptance as a lateral junction.

It should be noted at the outset that very few edge strings are reported by the Canny operator. In a perfect concrete pipe the only visible surface discontinuities - and hence the only detected edges - should be those arising from the lateral mouth. A small number of additional edges are shown in Figure 6.2a: around half of these, however, are generated by the surface orientation discontinuity created by the intersection of far end of the pipe with the black polythene used to screen off the outside world. These edges may therefore be considered an artefact of the laboratory environment. The remaining unexpected edges are attributable to minor flaws in the pipe. The largest black region in the image of Figure 6.2b clearly corresponds to the "black hole" marking the pipe axis. Some white areas are visible inside this region; these are the result of reflections from the polythene sheet used here and so may also be considered laboratory artefacts. Accurate vanishing point detection is problematic, even in ideal concrete pipes. Examination of Figure 6.2c, however, shows that the estimated vanishing point

extracted here is sufficient to allow determination of a region of interest containing the lateral intersection. Application of the curvature signature test (Figure 6.2d) then correctly identifies the lateral mouth, the spurious edge strings being discarded on the basis of their length. Only one curvature peak is detected by the criterion used here, the remaining extrema (Figure 6.2e) being less than 90% of the height of the largest.

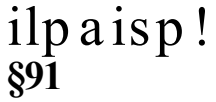

e.

Figure 6.2: Lateral Detection, Reflected Illumination, 90 Degree Junction at 2.614m

(Optimum Illumination Conditions)

Figure 6.3 shows the result of applying the proposed system to an image of the same lateral intersection from the same viewpoint but captured under direct illumination. Edges overlaid on the grey level image, the thresholded image, estimated vanishing point and grey-coded edge strings are shown in Figure 6.3a-d respectively.

c. d.

Figure 6.3: Lateral Detection, Direct Illumination, 90 Degree Junction at 2.614m

(Optimum Illumination Conditions)

While the estimated vanishing point again provides a useful region of interest, many more edge strings now lie within that region. Several strings arising from the lateral mouth display one curvature peak (shown mid-grey in Figure 6.3d) and would therefore be accepted as marking the intersection. Some additional method of recovering the lateral from these strings would however be required as none of them provides a clear representation of the shape of the mouth. One string (shown black in Figure 6.3d) has two discernible peaks and would, under the proposed scheme, be given preference. Unfortunately this data arises, not from the lateral junction, but from a connection between two segments of the main pipe. Under reflected illumination this feature did not generate any edge strings. Even in a new pipe direct illumination introduces spurious edges which can seriously disrupt the lateral identification process.

6.1.4 Detection Under Imperfect Illumination Conditions

Attention is now turned to evaluation of the vision system under more realistic conditions. Imperfections arise from poor illumination, pipe wall encrustation and damage together with irregular sled/tractor movement; these are interactive factors and the first is now replicated.

Figure 6.4 shows edges overlaid on an image acquired under reflected illumination from the same viewpoint as Figures 6.2 and 6.3, but with the camera iris closed slightly. This simulates image capture under poor illumination and so checks the robustness of the vision system. As can be seen, the top of the lateral profile is well represented. Low light levels, however, prevent detection of the lower section of the junction. The Canny operator has been applied to a variety of images captured within the laboratory pipe. It was found that although reflected illumination consistently eased the task of identifying lateral intersections, under low intensity light it was common for only part of the profile to be represented by an edge string. As variations in the reflectivity of the sewer walls may at any time lead to only a small proportion of the original light being reflected onto a (potential) lateral junction, any proposed vision system must be able to detect poorly lit intersections. One solution to this problem is to increase the power of the light source included in the survey rig. This, however, is likely to introduce image noise and glare when the sewer pipe is light in colour or wet. The alternative is to enhance the captured images to support more robust edge detection under low intensity light. A wide variety of image enhancement techniques exist, with Median Filtering and Histogram Equalisation being particularly suited to the task at hand; please refer to Section 2.1.4

e.

Figure 6.4: Lateral Detection, Reflected Illumination, 90 Degree Junction at 2.614m

(Imperfect Illumination Conditions)

Median filtering is particularly effective for images where noise patterns consist of strong, spike like components, and where the characteristic to be preserved is edge sharpness. The filter replaces the grey level of each pixel by the median of the neighbouring grey levels. To determine the median value, the neighbourhood or window size must be chosen; a window size of 3, for example, calculates the median value from a 3 x 3 area centred on the pixel under consideration. It was determined empirically that a window size of 9 pixels consistently produced the required degree of enhancement. Figure 6.4b shows the result of median filtering the image of Figure 6.4a. The lateral profile definition is clearly better, though the image is still rather low in contrast and, therefore, overall definition. Histogram equalisation is now applied to rectify this.

A histogram of grey levels provides a global description of the appearance of an image. Image enhancement may be achieved by modifying the histogram of a given image. Histogram equalisation modifies the appearance of image by controlling the probability density function of its grey levels via a transformation function. Again, when applying such a technique, a window size is assigned. Again empirically, it was determined that a window size of 55 was appropriate for this application. Equalisation of the filtered image of Figure 6.4b produces the image underlying Figure 6.4c upon which edges obtained via the Canny operator have been overlaid. It should be noted that the dynamic range of the pixel distribution has been increased, considerably altering the appearance of the image. As a result the lateral profile is well represented by the edge strings supplied by the Canny operator.

The outcome of applying the proposed lateral detection criteria to the edges shown in Figure 6.4c is given in Figure 6.4d. Only the true lateral profile (shown in black) has been identified as possessing 2 curvature peaks (Figure 6.4e). The system has therefore successfully detected the lateral under imperfect conditions.

Figure 6.5a shows edge data overlaid on an image, similar to Figure 6.4a, but captured under direct illumination. More of the lateral profile is represented than in Figure 6.4a, though the additional edges arising within the lateral opening present problems. The outcome of median filtering is shown in Figure 6.5b while Figure 6.5c shows the result of applying histogram equalisation and edge detection. As Figure 6.5d shows, the lateral profile this time is more fragmented and the lower edge data is misleading. Image enhancement makes the overall system more robust but cannot always compensate for problems introduced by direct lighting.

c. d.

Figure 6.5: Lateral Detection, Direct Illumination, 90 Degree Junction at 2.614m

(Imperfect Illumination Conditions)

6.1.5 Summary

As has been shown in the preceding sections, the qualitative lateral detection system proposed in Chapter 2 performs well on images obtained from the laboratory based pipe rig under both optimum and less perfect illumination conditions. The applicability of the detection procedure to the detection of lateral intersections from field data has already been shown in Section 2.2.2.

According to the system strategy proposed in Section 2.3.1, once a lateral junction is detected, alternating direct and reflected light is employed regarding lateral classification (x_{vp}, ρ and φ_{LAT}), the investigation of which will now be addressed in the following section.

6.2 LATERAL CLASSIFICATION

6.2.1 Preamble

Referring to Figure 6.6, the lateral classification system proposed provides estimation of distance from the camera to the lateral, x_{vp}, and the angle of intersection of the lateral and NME sewer, ρ.

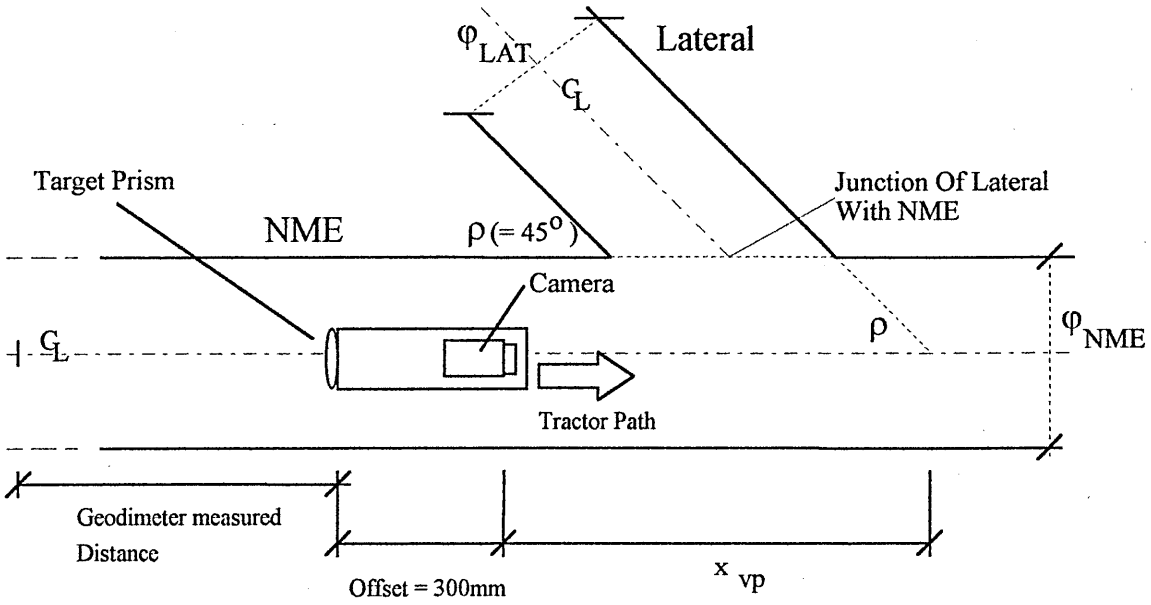

Figure 6.6: Classification Topology

Initially, evaluation of the system employing images obtained from the laboratory pipe rig is now considered for determining x_{vp} and ρ, noting that estimates of ρ are to be only to be compared to the set of likely values (45 or 90 degrees). Investigation of the procedure for determining φ_{LAT} as outlined in Section 2.3.4 is then made.

(As discussed in Section 2.4, a computer vision specialist has been responsible for the provision of the mathematical basis of the lateral classification system regarding x_{vp} and ρ. Full system implementation and associated issues are included in Appendix C. The original specification regarding requirements of the system was provided, and all testing undertaken, by the author).

6.2.2 Image Data Acquisition

Images were acquired as noted in Section 6.1.1. As described in Chapter 2, the basis of lateral classification requires the correspondence between image intensities and those determined from the reflective photometric stereo equations describing direct and reflected illumination, to be determined for a particular image feature – i.e. lateral edge. Using TINA, the computer vision development environment, components required for lateral classification have been provided by the aforementioned specialist and comprise several task specific vision 'Tools' modelled within the TINA vision environment, the first of which is the 'Data Acquisition Tool' (DAT).

The DAT provides the ability to locate the vanishing point of the sewer pipe in both the direct and reflected illumination image and to provide a mean estimate; the mean vanishing point as will be seen later is generally more centrally placed within the image as would be expected. The mean is then used to acquire an image intensity profile across the lateral mouth. Image intensities may then be acquired as necessary, from these profiles, for input into the 'Reflective Photometric Stereo Tool' (RPST) considered in Section 6.2.4. The image pair shown in Figure 6.7 is used as an example to aid understanding of the data acquisition process.

Direct Illumination Reflected Illumination

Figure 6.7: RPS Image Pair

Initially, a pair of direct and reflected illumination images is loaded into the system using the existing TINA Stereo Tool. Vanishing points are then extracted from each image as described in Sub-Section 2.1.6. A threshold value of 100, a grey-scale in the range of 0 to 255 where a 0 represents black and 255 white, is first employed (Figure 6.8) and, using the DAT, vanishing points are determined as shown in Figure 6.9.

Direct Illumination Reflected Illumination

Figure 6.8: Thresholded Images

Direct Illumination Reflected Illumination

Figure 6.9: Vanishing points computed independently from each image

In both cases the vanishing points estimated are in the region we would expect the vanishing point to lie, but are offset slightly. In the direct case the vanishing point is estimate slightly to the right of the sewer centre line, for the reflected case it is slightly to the left; these offsets are indicative of the asymmetric illumination used. However, if the mean of these two vanishing point estimates is used, a much better estimation of the vanishing point is obtained, Figure 6.10. This is because the tractor lies approximately along the axis, the lights are symmetric about the tractor, so the error in each vanishing point should be approximately equal but in opposite directions.

Direct Illumination Reflected Illumination

Figure 6.10: The mean vanishing point

Now that the vanishing points for the images have been estimated, the next step is to find the edge string corresponding to the lateral mouth. The Canny algorithm is next applied involving the removal of image noise by Gaussian smoothing, factor a, followed by differentiation and a search for significant edge heights or peaks. Two thresholds assess the height, and therefore significance, of peaks in the first derivative of intensity whilst a single threshold places a lower limit on acceptable edge length. A low a value provides for minimal smoothing whilst a high a value gives greater noise reduction but may lose significant structures. Thresholding anticipates targeted edge length. The operator is applied employing parameters; *cr*= 1.0, lower threshold = 1.0, upper threshold = 3.0 and line length threshold = 25 pixels determined empirically. The resulting edge detail extracted from the reflected illumination image is shown in Figure 6.11.

Figure 6.11: Edge strings extracted from the reflected illumination image.

The DAT is then used to determine image intensity across the lateral mouth. Assuming the image vanishing point to have been estimated a line is projected horizontally through the vanishing point.

For each edge on the string, a line is projected from the edge to the vanishing point. The angle is calculated between this line and that of the horizontal. When this has been completed for all edges on the string, the two edges with the maximum (+ve) and minimum (-ve) value about the horizontal are marked as being the top and bottom edges of the profile. A line is then drawn to connect these two points. A second line is then projected from the vanishing point through a point which bisects the maxima / minima connecting line. This line is set a small amount longer than the distance of the furthest point on the string from the vanishing point, ensuring the line crosses both sides of the lateral mouth. Once the line of interest has been selected, The DAT superimposes it on both the direct and reflected images and by 'walking' along the line, extracts the intensity data from each image.

The intensity profile and data for the whole line can then be displayed. For the image pair of Figure 6.7, results are shown in figure 6.12.

Direct Illumination Reflected Illumination

Figure 6.12: Line of interest & intensity profile acquired from the images of Figure 6.7.

For Reflective Photometric Stereo, image intensity need only to be measured within the lateral mouth, this may be obtained using the 'Find Mouth' option of the DAT. The Find Mouth option causes the system to walk along the line of interest and mark the locations where the line crosses the lateral edge string. If only one or more than 2 crossing points are found, a system error is reported. Otherwise, the line of interest is replaced by the section which connects the two pixels lying on the front and back lateral edges. The intensity profile across the mouth can then be displayed, and the actual data

output to a text file. Applying this to our images produces the result shown in Figure 6.13.

Direct Illumination Reflected Illumination

Figure 6.13: Intensity profile across the lateral mouth

The area of lateral pipe wall of prime interest is that which is visible and closest to the intersection of the NME and lateral pipe; the rightmost end of the profile shown in Figure 6.13. The average intensity of the three pixels at the “far” end of each of the pixel tracks shown in Figure 6.13 is therefore recorded for use in the lateral classification system; the local average of these is taken to reduce the effects of noise. The intensity values therefore acquired for both the 45 and 90 degree lateral junctions

corresponding to the image pairs of Table 6.1 are given in Tables 6.2 and 6.3 respectively.

Lateral (degrees)	Xvp (m)	Image Intensity Direct Illumination (grey scale)	Image Intensity Reflected Illumination (grey scale)
45	3.453	146.67	73.33
	3.271	163.00	75.33
	2.912	182	79.67
	2.704	198	78.67
	2.643	204	80.33

Table 6.2: Experimental Image Intensity Values E_d - 45° Lateral

Lateral (degrees)	Xvp (m)	Image Intensity Direct Illumination (grey scale)	Image Intensity Reflected Illumination (grey scale)
90	3.349	125.00	64.67
	3.032	117	67.67
	2.614	153.67	86.67
	2.347	183.33	87.33
	2.208	200.333	99.33

Table 6.3: Experimental Image Intensity Values E_r - 90° Lateral

From Tables 6.2 and 6.3 it can be observed that image intensity generally increases with decreasing as is to be anticipated. Further, it can be noted that there is greater variation in image intensity under direct illumination than under reflected illumination; reflected illumination provides an elongated light source which is much less directional that the source of direct illumination thereby producing the noted effect.

Having obtained the image data to which the mathematical models derived in Chapter 2 are to be compared, consideration is now turned to their determination.

6.2.3 Mathematical Model Prediction - Reflectance Maps

Pairs of reasonable values (xvp = 4 to 2.4m, p = 0 to 90 degrees) were substituted into Equations 2.6 and 2.14 to produce paired values for Ed/Ik and Er/lk2 and these were produced using TINA as reflectance maps as shown in Figures 6.14 and 6.15 respectively. Note that the values of Ej/Ik and Er/lk2 are recording degrees of greyness (0 (black) to 255 (white)).

Typical

Ik

V

x vp

Figure 6.14. Surface Luminance Values Predicted by Direct Illumination Model

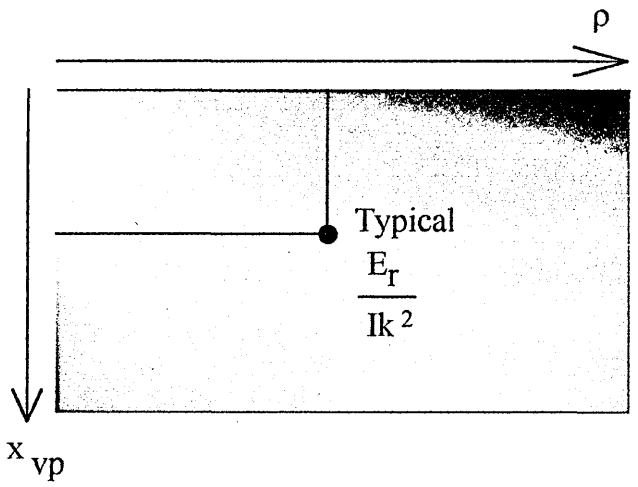

Figure 6.15. Surface Luminance Values Predicted by Reflected Illumination Model

Tables 6.4 and 6.5 provide a summary of the specific intensity values predicted by Equations 2.6 and 2.14 corresponding to the experimental data given in tables 6.2 and 6.3 respectively. The theoretical data given relates to the respective left hand sides of Equations 2.6 and 2.14.

Lateral (degrees)	Xvp (Geodimeter) (m)	Predicted Surface Luminance Factor under Direct Illumination E_d/Ik	Predicted Surface Luminance Factor under Reflected Illumination E_r/Ik^2
45	3.453	0.072	3.087
	3.271	0.081	3.191
	2.912	0.105	3.389
	2.704	0.124	3.469
	2.643	0.130	3.471

Table 6.4: Theoretical Surface Radiance Values - 45° Lateral,.

Lateral (degrees)	Xvp (Geodimeter) (m)	Predicted Surface Luminance Factor under Direct Illumination E_d/Ik	Predicted Surface Luminance Factor under Reflected Illumination E_r/Ik^2
90	3.349	0.089	3.183
	3.032	0.108	3.026
	2.614	0.145	2.289
	2.347	0.179	(0.947)
	2.208	0.202	(-0.089)

Table 6.5: Theoretical Surface Radiance Values - 90° Lateral.

It is to be noted that in Table 6.5, the theoretical reflected values corresponding to x_{vp} = 2.347 and 2.208m shown bracketed do not correlate with the preceding values. An explanation for this is that the midpoint of the linear light source model presented in Section 2.3.2 lies approximately 2.4m from the camera; please refer to Appendix C. For these two cases the midpoint of the light source lies beyond the lateral mouth and the theoretical data are therefore not reliable.

6.2.4 Experimental / Theoretical Correlation

Direct correspondence between experimental and theoretical data as given in Tables 6.2 and 6.4 (45 degree lateral) and Tables 6.3 and 6.5 (90 degree lateral) is unavailable due to the lack of knowledge of the actual I (bulb intensity) and k (reflectivity factor of the pipes) employed. Failure to acquire a priori values for k and I was due to the lack of

appropriate and expensive specialist equipment. A method of dealing with this problem is now proposed.

A parameter λ is now introduced where

$$\lambda = \frac{\text{Experimental Data}}{\text{Corresponding Theoretical Data}} \qquad \text{(Equation 6.1)}$$

For use with both direct (λ_d) and reflected (λ_r) light cases. Tables 6.6 and 6.7 show approximate data for each x_{vp} case employing the data from Tables 6.2 and 6.4, and Table 6.3 and 6.5 respectively. For example, $\lambda_d = 2037$ in Table 6.6 arises from the use of 146.67 (Table 6.2) and 0.072 (Table 6.3).

Xvp (m)	λ_d Direct Illumination	λ_r Reflected Illumination
3.453	2037	23.75
3.271	2012	23.61
2.912	1733	23.51
2.704	1597	22.68
2.643	1569	23.14

Table 6.6: λ For 45° Lateral Intersection

Xvp (m)	λ_d Direct Illumination	λ_r Reflected Illumination
3.349	1404	20.32
3.032	1083	22.36
2.614	1059	37.86
2.347	1024	(89.66)
2.208	992	(-1116)

Table 6.7: λ For 90° Lateral Intersection

Using TINA and employing a Reflective Photometric Stereo Tool and extrapolation function provided by the computer vision specialist, λ_d and λ_r covering distances in the range 4 to 2.4m to encompass test cases were determined. The intensity values within the theoretical reflectance maps corresponding to direct and reflected illumination were then scaled to by these extrapolated values to produce suitably modified reflectance maps similar to Figures 6.14 and 6.15.

Recalling the procedure employing the intersection of isoluminance contours as presented in Section 2.3.3, with theoretical estimates for x_{vp} and ρ are obtained from the modified reflectance maps. These are compared with the experimental x_{vp} and ρ data pairs of Tables 6.2 and 6.3. For example if the respective E_d and E_r corresponding to ρ = 45, x_{vp} = 3.453 from Table 6.2 are identified in the modified reflectance maps, isoluminance contours are produced as shown in Figures 6.16a and b respectively; the

resulting intersection of these two contours, and theoretical estimates of Xvp and p are provided in Figure 6.16c.

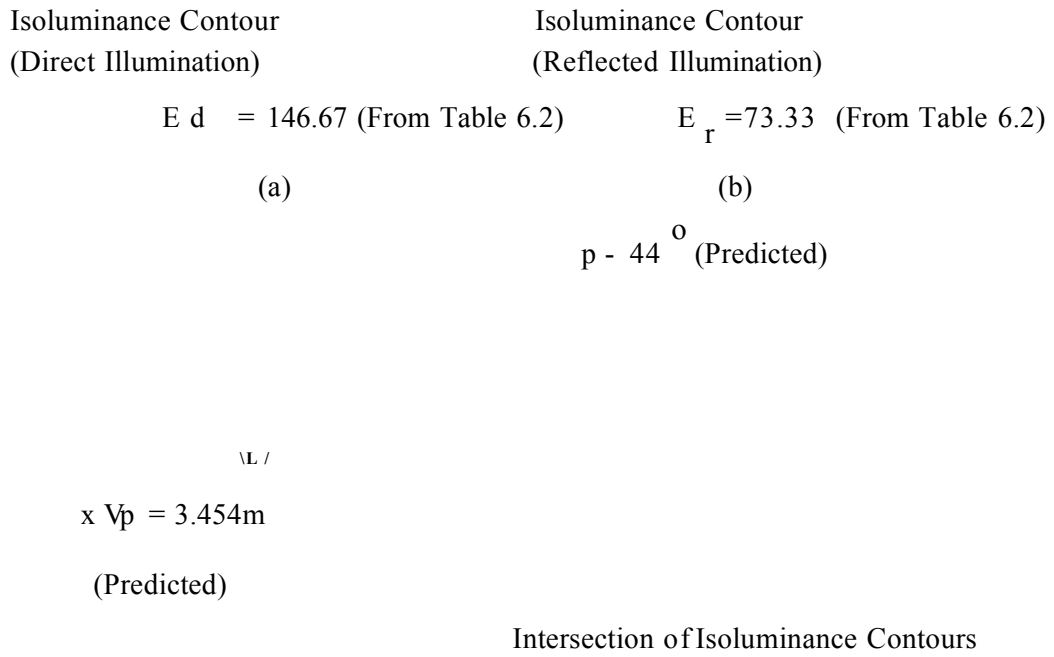

Figure 6.16: Isoluminance contours on the direct and reflected illumination reflectance maps and their intersection, p = 45, x vp = 3.453 (nb Table 6.2)

Five data pairs are used for the 45 degree case whilst, as noted above, only the first three data pairs are used for the 90 degree case; comparisons are presented in Tables 6.8 and 6.9 with corresponding remaining isolummance contours and intersections provided in Appendix C.

Experimental Xvp (m)	Experimental ρ (degrees)	Theoretical Xvp (m)	Theoretical ρ (degrees)
3.453	45	3.454	44.00
3.271	45	3.085	38.50
2.912	45	2.560	19.00
		2.610	28.50
		3.060	50.00
		3.350	77.50
2.704	45	2.540	14.00
		2.720	45.00
		3.090	76.50
		3.120	77.00
2.643	45	2.640	43.00
		2.875	61.00

Table 6.8: Comparison of Experimental & Theoretical x_{vp} and ρ for the 45 Degree Lateral Case Employing Modified Reflectance Maps

Experimental Xvp (m)	Experimental ρ (degrees)	Theoretical Xvp (m)	Theoretical ρ (degrees)
3.349	90	3.375	87.00
		3.410	85.00
		3.444	87.00
3.032	90	3.030	88.00
		3.060	88.00
		3.350	53.00
2.614	90	2.75	9.00
		2.610	88.00

Table 6.9: Comparison of Experimental & Theoretical x_{vp} and ρ for the 90 Degree Lateral Case Employing Modified Reflectance Maps

Recalling Figure 6.16, the isoluminance contours produced were open and when intersected produced a single intersection point and therefore a unique solution. As can be observed in Tables 6.8 and 6.9, for the majority of the data values multiple intersections between isoluminance contours arise indicating the presence of closed contours. This in turn generates multiple possible solutions for x_{vp} and ρ. As the set of possible ρ values is known a priori, the simple strategy of selecting the intersection falling closest to one of these possible orientations is effective in most cases. Tables 6.10 and 6.11 show the solutions selected from Tables 6.8 and 6.9 respectively by this method.

Experimental Xvp (m)	Experimental ρ (degrees)	Theoretical Xvp (m)	Theoretical ρ (degrees)
3.453	45	3.454	44.00
3.271	45	3.085	38.50
2.912	45	3.060	50.00
2.704	45	2.720	45.00
2.643	45	2.640	43.00

Table 6.10: Solutions Falling Closest To One of The Expected Lateral Orientations, 45 Degree Lateral

Experimental Xvp (m)	Experimental ρ (degrees)	Theoretical Xvp (m)	Theoretical ρ (degrees)
3.349	90	3.375	87.00
		3.410	85.00
		3.444	87.00
3.032	90	3.030	88.00
		3.060	88.00
2.614	90	2.610	88.00

Table 6.11: Solutions Falling Closest To One of The Expected Lateral Orientations, 90 Degree Lateral

As shown in Table 6.10, based on theoretical ρ the lateral would be correctly identified as a 45 degree junction for all cases. Estimation for x_{vp} requires more accuracy; at best, for experimental x_{vp} = 3.453m the theoretical estimate of 3.454m was 99.97% accurate, whilst at worst, experimental x_{vp} = 3.271m compared with theoretical x_{vp} = 3.085m gave 94.31% accuracy. For the 90 degree lateral, Table 6.11 provided similar results; again based on theoretical ρ the lateral would be correctly identified with best and worst accuracies being 99.93% and 99.22% respectively.

6.2.5 Adjunct Interpretation For k and I

Failure to acquire values for k and I has been problematic as noted in Section 6.2.4. The following procedure provides a method for their estimation.

As noted in Section 6.2.2, for any given I value E_d and E_r vary inversely with distance. Accordingly, values for λ similarly vary with x_{vp}.

Using,

$$\frac{\lambda_r}{\lambda_d} = \frac{Ik^2}{Ik} \qquad \text{(Equation 6.2)}$$

enables evaluation of k with back substitution yielding values for I. Table 6.12 shows approximate data for the 45 degree case.

Xvp (m)	k	I (lux)
3.453	0.0117	174701
3.271	0.0117	171966
2.912	0.0136	127745
2.704	0.0142	112452
2.643	0.0148	10639

Table 6.12: Approximated k and I Values for 45° Lateral Intersection

For the 45 degree lateral case the average k and I values are 0.0132 and 119501 lux respectively, noting k is in the acceptable range of 0 to 1. Applying the above method to the λ values of Table 6.7 for the 90 degree lateral case approximations for k and I are similarly determined; average k and I values are 0.0238 and 59635 lux respectively. These averages are, however, only based on the first three data points of Table 6.7 due to the unreliability of values for to X_{vp} = 2.347 and 2.208m; please refer to Section 6.2.3.

The above serves only to provide an initial estimation of potential k and I values. Further investigation currently considered beyond the scope of this research programme may afford better estimates.

Consideration is now turned to determination of $\varphi_{LAT.}$

6.2.6 Determination of Lateral Diameter (PLAT

A method has been proposed by the author in Section 2.3.4 to provide an estimate for the lateral diameter from an image obtained under direct illumination with known vanishing point determined employing the procedure discussed in Section 6.2.2. With reference to Figure 6.17 showing an image of a lateral obtained from the pipe rig under direct illumination, 'a' and 'b' are scaled lengths in the image corresponding to straight lines connecting the top and bottom of the lateral profile and the vanishing point to the top of the lateral profile respectively.

Figure 6.17: Estimation of lateral diameter

In the figure provided, φ_{NME} = 450mm. If the line lengths are now measured then by inspection a = 40mm and b = 58. From Equation 2.16, φ_{LAT} is approximately 310mm which is close enough in terms of tolerance value to classify the lateral as being of 300mm as opposed to 150 or 225mm. Further examples are provided in Appendix C.

6.3 SUMMARY

It is considered that this Chapter has shown the viability of several new procedures relating to the use of computer vision in the Construction Industry, in particular the renovation of sewers.

Detection is qualitative and the findings most encouraging in that laterals are detected under imperfect conditions. In particular the justification for the somewhat counter intuitive practice of inverting the interrogating light source away from the target is considered particularly successful.

Regarding the quantitative study relating to classification the findings are admittedly less satisfactory, however, this is a far more complex matter. Whilst approximation of φ_{LAT} affords a robust and straightforward procedure giving good results, determination of ρ and x_{vp} is more problematic; furthermore and as discussed in Chapter 8, there is a more fundamental problem associated with the use of Lambertian modelling.

It is considered that the means of dealing with the issue of k and I is satisfactory in terms of the current research study. It is hoped that given the highly innovative nature of the study that should a prototype be developed it is assumed that suitable funding will be made available to afford their solution.

CHAPTER 7

PROTOTYPE DEVELOPMENT

7.1 INTRODUCTION

As presented in the preceding chapters, a research study has been undertaken on a restricted budget to investigate the modular kinematic and computer vision components comprising a pre-prototype robotic system. The study has involved significant Multi Disciplinary studies undertaken by the candidate, and has subsequently incorporated the key aspects within the components. It is considered that a working prototype would require considerable input of both expertise and finance from industrial partners.

Recalling the Engineering Task Specification proposed in Section 1.15, the following section now proposes a more detailed three pass strategy to be employed by a working prototype, with particular attention paid to the initial survey pass.

7.2 STRATEGY RESUME

It is assumed that a NME sewer length has been selected for renovation employing CIP lining. The following strategy identifies the operational steps that would be associated with the initial survey pass undertaken by the envisaged working prototype robotic system incorporating tractor unit, fully integrated on-board control and modular kinematic and computer vision modular components.

1) The robot is brought to site and lowered into the upstream manhole of the sewer length to be lined and manually positioned by an operative in the invert of the pipe length to be surveyed, pointed in the downstream direction. From a fixed invert reference point in the manhole, the datum chainage position for the tractor is measured by the operative to enable tractor re-emplacement at the same datum position for the task and monitoring passes following sewer lining.

2) A stand-alone power pack / generator is placed in the manhole and connected to the tractor by an umbilical cable of suitable length for the survey to be undertaken. With the robot in position, the power pack is switched on and the on board, fully integrated, control system initialises all system parameters before directing power to the tractor drive at which time the following operations automatically and concurrently ensue;

a) With tractor drive engaged, the tractor commences the survey pass at a pre set speed of 0.08m/s, monitored by the control system employing the rotary encoder.

b) The chainage measurement system samples the outputs of the rotary encoder and the two inclinometers every 0.5 seconds to determine invert path distance travelled; the first inclinometer measures tractor roll relative to the NME centreline whilst the second inclinometer measures tractor pitch. (Note, sampling rate has been increased from 1 second to 0.5 seconds to provide for improved CMS accuracy)

c) The computer vision system (CVS) is placed in detection mode and automatically alternates which of the twin, fixed lights is switched on such that only one light is illuminated at any one time with alternation between them

taking place at 0.5 seconds intervals. As discussed in Section 2.3.1, the lights are directed to provide direct and reflected illumination of the sewer walls. A linear array (camera) is provided to sample sewer images for each alternation of the lights. On board processing enables the images to be digitised and then processed in real time. By employing the detection criteria provided in Section 2.2.1, the CVS searches for potential lateral junctions employing reflected illumination; i.e. when the left light is switched on laterals are searched for on the right hand side of the pipe and vice versa.

3) When a lateral junction is detected, typically at a distance of 3.5 to 2.0m away, a signal is sent from the control system to stop the tractor motor and CMS. Total invert distance travelled to this position is stored for later recall. The CVS switches from detection mode to classification mode.

4) Noting that an image of the junction has already been taken under reflected illumination, an image is taken under direct illumination. Employing the classification procedure described in Section 2.3.1, estimates are obtained for both the lateral intersection angle ρ (which is confined to the data set of 45 and 90 degrees), and for the closure to target distance x_{vp} for which a more accurate estimate is required. From the directly illuminated image, using the lateral diameter estimation procedure outlined in Section 2.3.4, an estimate of φ_{LAT} is obtained (also of restricted data set, 150, 225 or 300mm diameter). Recalling the mathematical model underlying the CMS presented in Section 3.13, based on the lateral classification data ρ, x_{vp} and φ_{LAT}, invert chainage distance to drilling station x_L is afforded. As noted in Section 6.2.4, classification results indicate that with the camera / linear array approximately 2.6m from the lateral, good

estimations for ρ, x_{vp} are obtained. It is therefore anticipated that following initial classification the tractor drive will be re-engaged concurrently with the CMS and moved closer to within 2.6m from that lateral whereupon the tractor / CMS is stopped and classification repeated.

5) The following classification parameters are then stored for each lateral in the onboard memory for later recall during the task / drilling and monitoring passes.

   a) Lateral intersection angle ρ,

   b) Lateral diameter φ_{LAT}, and

   c) Closure to target distance x_{vp}, and hence distance from datum to drilling station x_L.

6) Following lateral classification, CMS and tractor power is re-initiated, and the CVS reverts to detection mode until the next lateral is detected whereupon the classification procedure is repeated

7) This process is repeated until the survey pass has been completed. Modifications to the CVS not available to the pre-prototype would include provision of an on-board pattern recognition routine programmed to recognise an image of a triangle centrally placed within the pipe, please refer to Chapter 8. The intention is that a triangular shaped marker is to be positioned in the downstream manhole invert of the sewer length being surveyed. So that the robot does not continue to survey past this point, the pattern recognition routine is programmed to send a control signal to cut power to the tractor drive should the triangle be observed. A radio signal is then broadcast to alert the operative(s) above ground and the tractor automatically powers down awaiting removal from the sewer system; see Chapter 8.

8) Following removal from the sewer, the on board memory will be interrogated. Should during a survey no laterals be detected, the onboard memory will report that no laterals have been found and provide the total invert chainage measured within the sewer; the drill / task and monitoring passes will not be required for such sewer lengths.

9) Please note, if for any reason (mechanical or otherwise) the tractor stops and progresses no further, after a pre-determined duration, say 5 minutes, a radio signal is again broadcast to alert the operative(s) above ground. The tractor can be pulled out using the umbilical cable if required.

The procedure employed above assumes the general case of laterals intersecting the NME at either 3 or 9'oclock. Whilst this is the typical case, situations do arise when laterals intersect at other angles. As is discussed in Chapter 8, an enhanced computer vision classification system may provide an assessment of this.

Following lining of the NME sewer, if laterals have been detected then the robot is again placed in the invert of the upstream manhole at the same datum position as noted in 1) above and equipment installed in the launching manhole as discussed in 2). Noting that the drill pass is a purely kinematic procedure, laterals reconnection is now discussed;

1) Before emplacement within the pipe, the vertical height of the robotic arm is adjusted to ensure that the axis of revolute arm joint 2 is approximately coincident with the NME centreline.

2) With the robot positioned at datum, the power pack is switched on and the on board, fully integrated, control system initialises all system parameters before directing power to the tractor drive at the same time the following operations concurrently ensue;

a) The classification parameters for the first lateral to be reconnected are recalled, i.e. lateral intersection angle ρ, lateral diameter φ_{LAT}, and chainage to drilling station x_L from datum. Whilst the chainage to drilling station has been determined, the axis of revolute joint 1 must be located at the drilling station during lateral reconnection. A geometrical offset is therefore determined to correctly position the arm at the required position and allowed for in x_L.

b) With tractor drive engaged, the tractor commences the drill pass at a pre set speed of 0.08m/s, monitored by the control system employing the rotary encoder (CMS)

c) The CMS samples the again outputs of the rotary encoder and the two inclinometers every 0.5 seconds to determine invert path distance travelled until x_L is reached with the arm located at the drilling station, whereupon the control system stops the tractor motor and CMS.

3) Recalling lateral intersection angle ρ and lateral diameter φ_{LAT}, the arm control programme is automatically initiated to deploy the drill / end effector from park position (i.e. parallel to tractor body) to on target; first position at centre of obscured lateral target. The end effector is stepped horizontally left through a distance equal to the radius of the drill (r_d) and drill twist initiated to grind the liner. The end effector then follows its first drilling / grinding curve of interpenetration until returning to the first point on the curve. The arm again steps

out r_d horizontally left before grinding out the next curve of interpenetration. Based on the known value of φ_{LAT}, this process is repeated until the penultimate drill profile has been ground out (i.e. $\varphi_{LAT} - r_d$). The final curve is then ground out at a slower drill speed to prevent damage to the existing lateral. The arm is then automatically returned to park before power to the tractor and CMS are reactivated and tractor continues to next drilling station whereupon the process is repeated.

4) At the end of the drill pass, the pattern recognition system detects the triangle as mentioned above and the robot automatically powers down awaiting retrieval.

It is anticipated that the monitor pass will mimic the key operations of 1) 2) and 4) of the above drill pass, however operation 3) will be replaced effectively by a computer vision system operation involving taking images of the reconnected lateral junctions. These will be used to assess quality of cut and provide proof to the client that all laterals have been reopened; please refer to Chapter 8.

The following sections discuss the improvements considered necessary towards production of an industrial working prototype.

7.3 SYSTEMS INTEGRATION AND CONTROL

For cost effective research, the robotic system developed herein comprises three main retrofit components. Whilst control issues have been addressed, the control provided has been specific to each individual system component; i.e. application specific software was written for the chainage measurement system, for the drill task arm and for the lateral detection and classification system. The inability to provide system integration necessitated isolated testing of each component. Whilst a remote PC of limited specification, i.e. IBM compatible 386 with 8M RAM, provided the necessary computing power for the control of the chainage and arm systems with programs written in QBASIC, more powerful and again remote computing power and dedicated software was required for the image processing work.

Although beyond the scope of the research programme reported herein, integration of the components is a fundamental pre-requisite of a working prototype as can be concluded from the strategy resume of Section 7.2.

For the prototype system it is considered that an on-board CPU married with a suitable programme compiler would provide sufficient processing power to achieve the system integration required and control the CVS, CMS and arm components. The on-board system will incorporate frame grabber for digitising images and simplified software to achieve the lateral detection and classification; the TINA environment used to produce the vision system of Chapter 2 worked well but incorporated many functions not used by the detection and classification systems. The system to be employed, given suitable development by an experienced programmer would be vastly simplified. All the

necessary digital / analogue input / output device drivers to sample the rotary encoder and inclinometers used for the chainage measurement system will also be on board. The CPU will also be capable of driving the task arm motors and monitoring the feedback generated. Typical integration / control aspects offering significant improvement over the current system would include;

1) Automatic activation / deactivation of CMS when tractor power engaged / disengaged.
2) Automatic activation of lateral detection system when tractor power engaged and including automatic alternation of light sources.
3) Once lateral detected, automatic classification of lateral junction and storage of data for later retrieval.
4) Automatic activation of drill arm at drilling station recalling lateral classification parameters.
5) Closed loop feedback control over arm movement during drilling and automatic activation of drill.
6) Automatic return to park after drilling.
7) Automatic tractor stop and power down at end of survey (note use of pattern recognition system).
8) Automatic activation of a radio beacon should a problem arise.

7.4 UMBILICAL SUPPORT

During testing, the tractor unit 'trailed' a number of umbilical cables providing power to the on board systems including tractor drive, and feedback from the camera, inclinometer, rotary encoder.

With the proposed on board integration of the individual system control components, the number of umbilicals required will be vastly reduced to those supplying tractor power and feedback to a remote operator, if required, which is considered an improvement over the current system.

Nautical cables which are currently used in practice would again be specified as their inherent strength provides the ability to drag the tractor back out of a sewer length should it get stuck or a problem arise. Such a problem would be reported to A remote operator as noted in Section 7.2

7.5 CHAINAGE MEASUREMENT

The chainage measurement system tested in Section 5.1 has performed well during testing with accuracies obtained better than those of 2% currently accepted in industry. The provision of a second inclinometer to determine tractor pitch within the pipe would improve the system's ability to better assess invert distance travelled when encountering deflection away from the pipe invert – note Section 5.1.4; which may be due to debris. The second inclinometer would therefore provide for a more robust CMS. As noted in Section 5.1.5, improving the sampling rate from 1 second to 0.5 seconds is also considered to offer clear improvement.

7.6 ROBOTIC DRILL TASK ARM

The robotic arm developed during this research study operated in the absence of feedback control and the problems associated with this are clearly evident in the drill profile results presented in Section 5.2.

Whilst the McLennan stepper motors and gearboxes used to drive rotational joints 1 and 2 provided positive results in one direction, the lag and backlash present in the motor and gearboxes produced poor results when encountering changes in direction. Even though the arm control programme was providing drive pulses, the slack in the system resulted in their 'loss' together with the positional accuracy of the arm. Closed loop feedback motor control, monitoring arm / joint movement rather than the digital pulses employed to drive them is clearly advantageous. It is therefore considered that the robotic arm design would benefit in terms of overall operation, accuracy of drilling and task suitability from incorporating feedback control for each motor including the linear actuator. The proposed specification therefore comprises replacing stepper motors to joints 1 and 2 with Absolute Contacting Encoder (ACE) 50W DC control motors

Consideration must also be given to the provision of a fourth motor to provide the necessary drill twist action of the drilling tool replaced here for experimental purposes by the cotton bud marking system. It is envisaged that a simple conical grinding tool will be used as per current practice. A stepper motor is to be specified to provide the necessary drill rotation to achieve liner penetration and profile cutting, as positional feedback is not required of this system component.

Noting the problems encountered during testing with regard to the position of the arm (in particular revolute joint 2) with respect to NME centreline, for the prototype model a vertically adjustable arm base would be advantageous. The ability to adjust the arm height with respect to the NME diameter within which the robot will be deployed would be a simple yet effective improvement.

7.7 LATERAL DETECTION & CLASSIFICATION SYSTEM

The vision system employed incorporated fixed twin 50W dichromatic lights and fixed lens CCD camera, which were found to be adequate for the task of producing image data for later post processing; i.e. recorded image data was digitised and manipulated at a later stage remote from the pipe rig. The computer vision system used comprised several key components including a frame grabber accessed on a stand alone PC with digitised images then transferred to a dedicated SUN SPARC workstation which provides the necessary hardware and software to run the image processing environment TINA.

For the prototype all computing is to be on board. The miniaturisation and simplification of the system employed and resulting software will again be a major issue with regard to both cost and time required for implementing such a programme of work. As discussed in Section 7.3, the specification of onboard CPU to be used must be of sufficient processing power to handle the image quality and quantity provided to achieve both detection and classification in real time.

Although all testing has been carried out in the dry laboratory environment, problems of surface glare in a wet pipes is not anticipated to be problematic for detection under reflected illumination, recall Section 2.2.2. The ability to vary the wattage of the light produced may prove beneficial during detection if image saturation or exceptional glare occurs, but must remain constant for both illumination conditions during lateral classification operations.

For the prototype model, twin 50W dichromatic light sources are again specified whilst a linear array may provide benefits over the CCD camera employed herein. It should be noted that all electrical equipment employed on the prototype must be intrinsically safe; i.e. all electrical components sealed so as to prevent contact with potentially dangerous atmospheres / substances; i.e. methane may be present in the sewer being renovated leading to risk of explosion.

Whilst intrinsically safe lights and linear arrays / cameras are commercially available, they are expensive.

7.8 OVERVIEW OF PROTOTYPE MODEL PROPOSALS

Figure 7.1 illustrates the proposed tractor based prototype robotic system. The significant differences between the above figure and that of Figure 1.9 detailing the research programme proposals in Chapter 1, is the provision of onboard CPU and ancillary control, and of power supply / transformer for all on board components.

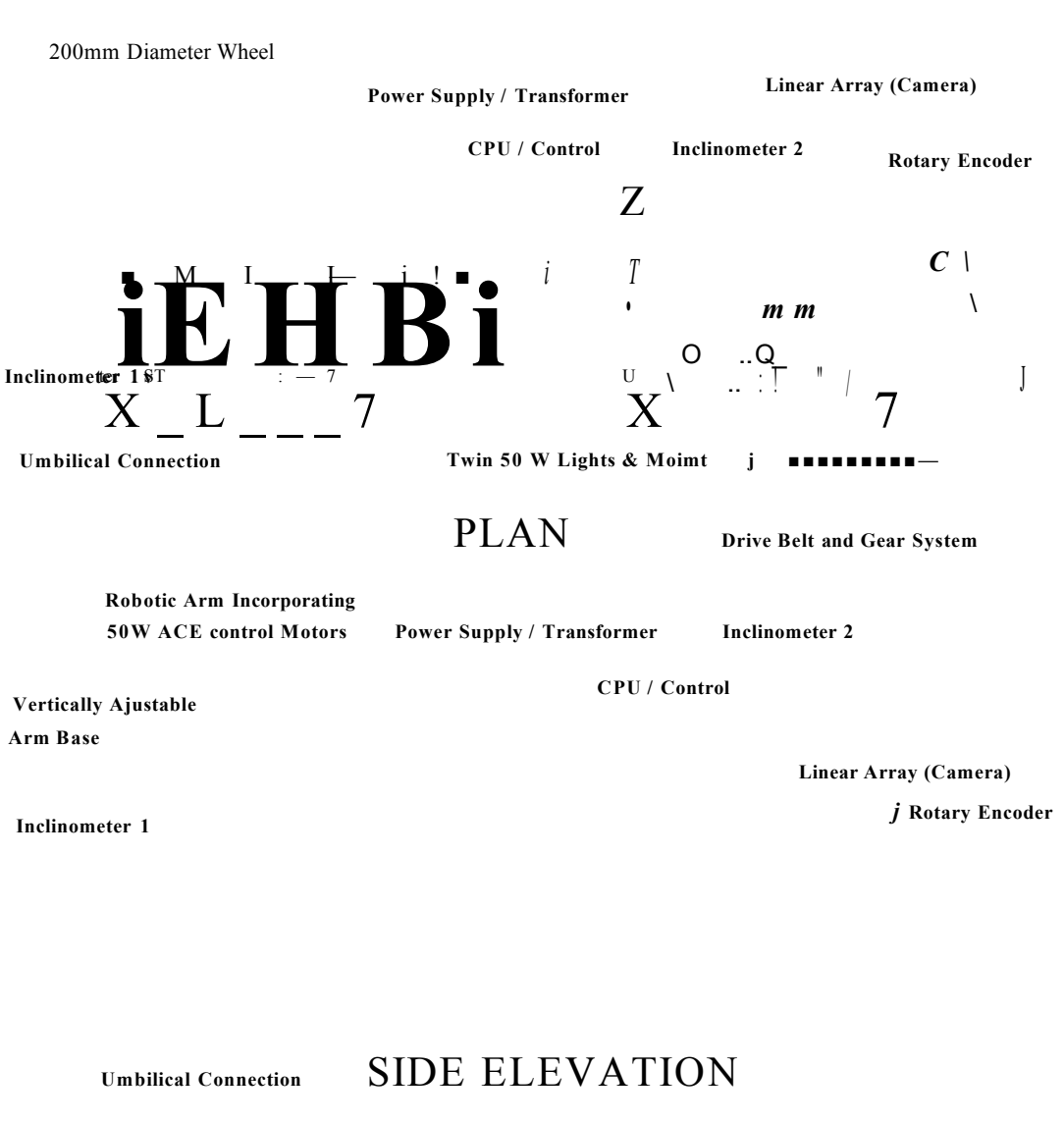

Figure 7.1: Diagrammatic Sketch Of Proposed Prototype

It should be noted that in order for the prototype to meet current industrial needs the tractor and all on board components must be capable of safely working within the NME sewer environment, that is all components must be intrinsically safe as noted in Section 7.7. The prototype must be capable of withstanding typical cleansing measures following a survey, task or monitoring activity, in effect surviving the effect of a high-pressure water hose. In effect the prototype needs to be mechanically robust.

All the improvements and considerations discussed in the previous sections have significant effects on cost. The following section seeks to briefly summarise the anticipated costs of the key components comprising such a system and provide comparison with pre-prototype considered within this programme of research.

7.9 COST COMPARISON OF PRE-PROTOTYPE AND PROTOTYPE SYSTEMS

Table 7.1 provides an overview of the pre-prototype component specification and approximate system costs.

Equipment Item	**Specification**	**Approx' Cost (£)**
Remote PC for control & Ancillaries	386 IBM Compatible, DEVA 3 Axis rotary encoder sampling card, Digital Output Card, Analogue sampling card.	1000
Robotic Arm	2 No McLennan IDE Stepper Motors & 50:1 Gearboxes, control cards and buffers.	150
	1 No RS Linear Actuator, control card and power supply	170
Chainage Measurement System	British Instruments Rotary Encoder	20
	Inclinometer	50
Vision System	Twin dichromatic lamps, transformer and fittings	30
	Switch box	10
	Watec CCD Camera & lens	350
	TOTAL	£1780

Table 7.1: Cost Estimate of Physical Pre-Prototype System

Table 7.2 provides an overview of the anticipated prototype component specification and approximate system costs.

Equipment Item	**Specification (Noting all components to be intrinsically safe)**	**Approx' Cost (£)**
Onboard PC for control & sampling Ancillaries	Pentium IBM Compatible processor and incorporated sampling add on components for rotary encoder and inclinometer and power supplies.	2000
Robotic Arm	3 No RS Absolute Contacting Encoder 50W DC control motors and anti-backlash gearboxes, control cards and buffers.	600
	1 No RS Linear Actuator, control card and power supply	170
Chainage Measurement System	British Instruments Rotary Encoder	20
	2 No Inclinometer	100
Vision System	Twin Lights or Single Motorised (Intrinsically safe)	200
	Linear Array	1000
	TOTAL	£4090

Table 7.2: Cost Estimate of Physical Prototype System

Comparing the cost estimates provided in Tables 7.1 and 7.2, it is evident that based on the revised modular components comprising the prototype system, industrial collaboration / financial support is a prerequisite. Whilst Tables 7.1 and 7.2 address mechanical and hardware issues, the integration aspects discussed herein would require significant software development, the cost of which is anticipated to be significant and hard to quantify.

7.10 SUMMARY

Within this chapter a revised strategy for the prototype has been proposed, with due regard to the surveying, drilling and monitoring passes described in Section 1.15, and a revised specification for a working robot prototype has been discussed.

It has been concluded that system integration of the key components comprising the robotic system, i.e. that of the computer vision system, chainage measurement system and robotic task arm is a fundamental pre-requisite for a working prototype. The ability to provide closed loop control offers clear advantage over the pre-prototype system; for the robotic task arm, the provision of arm motors with feedback is expected to offer significant improvement.

The cost comparison presented in Section 7.9 highlights the need for industrial collaboration in order to introduce such a prototype to the sewer renovation industry.

Chapter 8 now draws conclusions and makes suggestions for further work based on the findings herein.

CHAPTER 8

CONCLUSIONS

8.1 INTRODUCTION

To date, the vast proportion of commercial robotic/autonomous devices have been employed within the context of industrial manufacturing situations. These are largely static based and function in a structured environment. Present industrial robots are actually mechanical handling devices manipulated under computer control. Consequently, products using standardised components and manufactured in bulk are prime candidates for robotization, and this is one reason for the widespread integration of them into the world's automotive industry. Component design has therefore become substantially controlled by, and tailored to, robotic assembly and finishing operations.

Of late, a restricted number of robotic applications has outgrown the confines of structured manufacturing to be employed within more hostile environments. One example is that of the nuclear industry. Disasters at Three Mile Island and at Chernobyl highlighted the desperate need for remote / telerobotic machines to explore contaminated areas of nuclear plants. Teleoperated drones have also been used for the inspection and repair of deep sea gas pipelines and oil rig support legs.

The construction industry is one of the latest industries to which automation has been applied, in particular Japanese innovation has led to the development of telerobots for application to material handling and finishing operations. Contemporary research projects in the UK have been undertaken concerned with the provision of climbing robots capable of undertaking simple building maintenance tasks such as exterior crack

identification surveys, and investigations relating to the provision of automated mechanical excavation plant. The research programme studied here is primarily centred on one key aspect of the construction industry, i.e. non-man-entry sewer (NME) renovation, and it is hoped that this study has provided some contribution to this field of opportunity.

8.2 PRIMARY FINDINGS

Throughout this research study the benefit / usefulness of Multi-Disciplinary engineering, in particular the application of Information Technology driven systems such as computer vision and robotics, have been found to be suited to the sewer inspection task and lateral reconnection tasks respectively. The application of such systems to such inaccessible and hazardous environments as that of the NME sewer is of prime import.

An important aspect of this research programme has been the investigation of modular components which can be retrofitted to existing industrial available hardware; i.e. existing sewer inspection tractors. The ability to retrofit not only provides the facility to upgrade / test individual components without the need for total re-designs, but for eventual application within the sewer inspection sector, industrialists are more likely to welcome systems that can be added to their existing expensive plant.

Through the experimental testing carried out on the mechanically based modules, i.e. that of chainage and robotic task arm, the chainage test appears particularly successful given the use of equipment exhibiting wear and tear. A number of initialization conditions were employed to determine the robustness of the chainage measurement

system. Tests simulating non-idealized invert lie were undertaken with the tractor placed parallel to NME center line, but at various inclinations about it. Others tests were conducted with the tractor skewed to it to mimic effects of possible deflection due to debris within the pipe. The accuracies obtained from the chainage measurement system were very good. For parallel tests with the tractor located at or close to the invert, the chainage measurement system reported invert path distance to within 0.18% of that measured by geodimeter methods. Noting that current practice is satisfied on 2% accuracy the system provided here offers significant improvement.

The use of GRASP to enable design of the pre-prototype without the need for constructing expensive physical prototypes has worked well and the task of automated drilling has been proven in GRASP.

A mathematical model has been proposed in Chapter 3 providing the ability to determine the arm kinematics required for each arm joint to describe the curves of interpenetration that form a series of lateral drill profiles. The equations have been employed within a computer programme to generate a series of 3D polylines, representing curves of interpenetration cut profiles, for simulation within GRASP. The cut profiles produced and the resulting simulation served to validate the suitability of the equations for incorporation within the robotic arm control programme, and showed GRASP's applicability to simulations of robots in environments other than typical factory bin picking operations.

The performance of the robotic drill arm seems adequate although quantification of data i.e. hole drill to hole target is admittedly loose with problems of undershoot

reported. This is largely due to the quality (and expense) of equipment required to undertake the task. The lack of closed loop feedback control was considered a major drawback and it is considered that had there been suitable equipment and time to incorporate such within the controlling software routines, then better results would have been expected. The principal of automated drilling has, however, been proven.

The qualitative detection of lateral junctions using computer vision techniques and use of Knowledge Based Engineering (KBE) has proven most effective noting the crucial difference between direct and reflected illumination. Validation of the practical counter intuitive notion of directing the light source away from the feature under consideration to avert such problems as those of glare has been most useful. The detection system based around a number of criteria / rules has been shown to detect lateral junctions employing reflected illumination for images captured in the laboratory, under both good and imperfect illumination conditions, and from field images.

A computer vision lateral classification system has been developed and, given that 2 of the parameters, ρ and φ_{LAT}, are of discrete form, the work would appear to be quite acceptable. Clear difficulties however are apparent when more specific tolerances had to be met, i.e. closure to target distance x_{vp}. Key problems are considered to lie with the lambertian modeling assumption which underlies the derived illumination models, which is that where matte surfaces are preferred. Whilst this was made available in the laboratory environment, due to the very nature of the sewer environment, it can hardly be expected in field studies. Whilst laboratory testing was satisfactorily employed, field tests were prohibitive in terms of the hazardous and restrictive nature of the NME sewer. Again testing was influenced by limits on expenditure.

Whilst the usefulness of retrofit modular component has been a key finding of this study, the inability to provide digital integration between them of any kind is disappointing. However, the prototype specification proposed in Chapter 7 goes some way towards addressing this matter.

Whilst the first point above offers an abundant field of future research study, at the same time the construction industry must be convinced to provide support.

8.3 FURTHER CONSIDERATIONS

It has been proven during the course of this research programme, that it is essential that research teams be developed when entering into Multi-Disciplinary engineering studies, particularly when considering the application of Information Technology to provide solutions for general engineering problems. Not only should provision of suitable equipment be of import, but also the facility to provide a pool of research staff to share the invariably onerous work load associated with such a programme of research.

Considering the work detailed herein, the provision of a computer vision specialist to produce the computer vision detection and classification systems to be incorporated by the candidate may have been better served by a team of research staff each concerned with a investigation of one particular modular component. It is envisaged that provision of such of a team would have allowed control integration aspects to be investigated whilst completing this programme of research much sooner.

8.4 SUGGESTIONS FOR FURTHER WORK

In Chapter 7 a specification for development of a prototype system has been outlined, however, financial implications suggest substantial industrial support to be of necessity. With industrial development of linear arrays perhaps some integration of these mechanical components discussed herein offers the best route forward.

This is not to suggest that the computer vision work included herein is to be ignored, rather, that the techniques involved be incorporated within the use of linear arrays particularly with respect to the detection KBE procedure established in Chapters 2 and 6. The lateral classification system requires some work to overcome the difficulties associated with the lambertian modeling employed. And it would be hoped that whilst estimation of lateral intersection angle ρ proved satisfactory, a better illumination model would provide more robust estimation of closure to target distance x_{vp}. The procedure for estimating φ_{LAT} remains acceptable.

A discussed in Chapter 7, further systems required to enable such a robotic solution to the sewer renovation survey and drilling task include investigation into providing a method of stopping the tractor once the end of a sewer run has been reached. It is suggested that the provision of triangular target centrally placed in the invert of the downstream manhole and on board pattern recognition software to recognize it would be a future project. The ability to be aware of a problem should it occur, such as encountering a blockage would be advantageous; a radio beacon could be activated automatically should the tractor stop for more than a pre defined duration. Should such a situation occur the umbilical cable is sufficiently strong to allow it to be pulled out.

It is considered that the mechanical chainage systems developed here may have application within the petrochemical industry, again employed within pipeline inspection tasks, as may aspects of the computer vision work.

The Mathematical model derived in Chapter 3 relating to interpenetration curve arm kinematics has performed well with respect to laterals nominally intersecting the NME at either 3 or 9 o'clock. The mathematics to provide solution for lateral lies other than these is already in place and further work may be employed to develop this. A computer vision approach to determining the angle of lateral intersection may be feasible and addressed appropriately within further developments of the lateral classification work as may a method for confirming accuracy of cut during the monitoring pass; perhaps again employing edge detection.

Investigation of a robotic arm with vertically adjustable base plate may overcome the difficulties encountered during the reported testing of this module. The facility to fine tune arm positioning not only provides for employment within a wider range of NME diameters but would also enhance its appeal for industrial application.

As reported in the introductory section of this chapter, automation in the construction industry is already in place and given the hazardous, dirty environment encountered on many construction sites, investigations into producing automated solutions seem likely to continue. It is hoped that this study forms part of that development.

CHAPTER 9

REFERENCES

[1] WARING G E JR, *Sewerage And Land Drainage*, 3rd Edition, E & F N Spon, London, 1891.

[2] WHITE J B, *Wastewater Engineering*, 3rd Edition, Edward Arnold, 1987.

[3] REED E C, The assessment of the problem in the UK, *Restoration Of Sewerage Systems*, ICE, Thomas Telford Ltd, London, 1982, 3-8.

[4] SKEAL W O, Editor, *Manual Of British Water Engineering Practice*, 4th Edition, The Institution Of Water Engineers, London, 1969.

[5] *Sewerage Rehabilitation Manual*, Water Research Centre, Swindon, 1983.

[6] ARTHUR R A J, Whatever happened to the sewer crisis, *Waste And Water Treatment*, September 1989, 54-57,63,78.

[7] READ G F, Sewer renovation and reconstruction in Manchester, *Municipal Engineer*, June 1984, 27-38.

[8] NATIONAL WATER COUNCIL, *Manual Of Sewer Condition Classification*, London, May 1980.

[9] NATIONAL WATER COUNCIL, *Sewers And Water Mains - A National Assessment*, London, June 1977.

[10] COX G C, Background notes in developments in sewer renovation technology, *Internal Memo*, Sheffield City Polytechnic, (19th June 1985).

[11] HEALTH AND SAFETY EXECUTIVE, *Injuries In Sewers*, Requested Statistical Data, 9th March 1993.

[12] ANDREWS W, SEWERS - Replace or renovate, *Tunnels And Tunnelling*, March 1982, 45-48.

[13] GREEN D J, KA-TE goes underground, *Water Services*, September 1993, 60-62.

[14] ANON, Trenchless sewer reline conquers laterals limit, *New Civil Engineer*, 27th May 1993, 6.

[15] EVANS B, Robotics in construction - brains beating the brawn, *A J Supplement*, 21st December 1988, 38-41.

[16] COIFFET P, *Robot Technology Volume 1 - Modelling And Control*, Kogan Page, London, 1983.

[17] BRADY M, Artificial intelligence and robotics, *Artificial Intelligence*, **26**, 1985, 79-121.

[18] WING R D, Robots in the construction industry - a state of the art review, *Proceedings Of The Institution Of Civil Engineers Part 1*, **86**, October 1989, 937-952.

[19] FILLNOW R H et al, development of remotely controlled devices for three mile island unit 2, *Nuclear Technology*, **87**, November 1989, 624-630.

[20] HISATOMI YO, Introduction of construction robotics In Japan, *IABSE Journal*, **40**, 1990, 1-12.

[21] WARSZAWSKI A, Robots in the construction industry, *Robotica*, **4**, 1986, 181-188.

[22] HEALTH AND SAFETY EXECUTIVE, *Blackspot Construction*, Her Majesty's Stationary Office, 1988.

[23] SKIBNIEWSKI M J, *Robotics In Civil Engineering*, Van Nostrand Rheinhold, 1988.

[24] ATKIN B L et al, On automation in the construction industry, *University Of Technology Sydney*, **6**, 1990, 34-45.

[25] MUSPRATT M A, Robot ensembles for building construction, *Robotica*, **6**, 1988, 275-284.

[26] KANGARI R et al, identification of factors influencing implementation of construction robotics, *Construction Management And Economics*, **8**, 1990, 89-104.

[27] BYLES R, Rooting for robots, *New Civil Engineer*, 18th June !992, 24.

[28] BRADLEY D et al, Knowledge acquisition for a robotic excavator, *Proceedings Of The 7th ISARC*, DTI, **2**, 1990, 351-357.

[29] COLLIE A A et al, Design and performance of the Portsmouth climbing robot, *Proceedings Of The 7th ISARC*, DTI, **1**, 1990, 16-23.

[30] CHAMBERLAIN D, A Masonry tasking robot, *Proceedings Of The 7th ISARC*, DTI, **1**, 1990, 1-8.

[31] BALLARD D H, BROWN C M, *Computer Vision*, Prentice-Hall Inc, New Jersey, 1982.

[32] WALLACE A M, Industrial applications of computer vision since 1982, IEE Proceedings, **135**, Part E, 3, May 1988, 117-135.

[33] LOWE, D. G., The viewpoint consistency constraint, *International Journal Of Computer Vision*, Kluwer, Boston, 1, **1**, 1987, 57-72.

[34] PORRILL, J., POLLARD, S. B., PRIDMORE, T., BOWEN J., MAYHEW, J. E. W., FRISBY, J. P., TINA: a 3D vision system for pick and place, *Image and Vision Computing*, 1988, **6**, 2, 91-99.

[35] POLLARD, S. B., PRIDMORE, T., PORRILL, J., MAYHEW, J. E. W., FRISBY, J. P., Geometrical modelling from multiple stereo views, *The International Journal Of Robotics Research*, **8**, 4, August 1989, 3-32.

[36] HENRY R, LUXMOORE A R, A pipe profiling adapter for CCTV inspection cameras: development of a pipe profiling instrument. *Measurement Science and Technology*, 1996, **7**, 495-504.

[37] JARVIS R, A perspective on range finding techniques for computer vision, *IEEE Transactions on Pattern Analysis and Machine Intelligence*, 1983, **5**, 2, 122-139.

[38] PATERSON, A. M., DOWLING, G. R., CHAMBERLAIN, D. A., Identifying key features in building using a single uncalibrated camera, *Proceedings 11th International Symposium On Automation And Robotics In Construction, Brighton*, May 1994, 657-664.

[39] TAYLOR, N., DRAPER, R., BROADHURST, S. J., MALLINDER, P. A., Static and kinematic limit states of masonry vaults, *The Centenary Year Bridge Conference Proceedings,* University Of Wales College Of Cardiff, Elesvier, 1994, 181-186.

[40] DRAPER, R., SOAR, K., TAYLOR, N., PRIDMORE, T., Computer vision for masonry vault testing, *Proceedings 1st International Arch Bridge Conference*, Bolton, Telford, September 1995, 257-266.

[41] ABE, Y., TANAKA, K., FUKUDA, T., ARAI, F., ITO, S., development of air conditioning equipment inspection robot with vision based navigation system, *Proceedings 12th International Symposium On Automation And Robotics In Construction, Warsaw*, May 1995, 665-674.

[42] J CANNY, A computational approach to edge detection, *IEEE Transactions on Pattern Analysis And Machine Intelligence*, **8**, 6, 1986, 679-698.

[43] CHANTLER, M.J., Why illuminant direction is fundamental to texture analysis, *IEE proceedings on Vision, Image and Signal Processing*, 1995, **142**, 4, 199-206.

[44] BOVIK, A.C., HUANG, T.S. and MUNSON, D.C., The effect of median filtering on edge estimation and detection, *IEEE Transactions On Pattern Analysis And Machine Intelligence*, 1987, **9**, 2, 181-194.

[45] PRIDMORE, T.P., COOPER, D., and TAYLOR, N, Estimating camera orientation from vanishing point location during sewer surveys, *Automation in Construction*, 1997, 5, 407-419.

[46] WOODHAM, R J, Photometric method for determining surface orientation from multiple images, *Optical Engineering*, January / February 1980, **19**, 1, 301 – 306

[47] WOODHAM, R. J., Analysing images of curved surfaces, *Artificial Intelligence*, **17**, 1981, 117-140.

[48] HORN B K P, *Robot Vision, MIT Press*, 1986

[49] KEITZ H A E, *Light Calculations and Measurements*, 2nd Ed, Philips Technical Library, 1971.

[50] TAGARE H D et al, A theory of photometric stereo for a class of diffuse non-lambertian surfaces, *IEEE Trans On Pattern Analysis And Machine Intelligence*, **13**, 2, Feb 1991, 133-151.

[51] ROBOT DESIGN HANDBOOK, SRI International, McGraw-Hill , 1988.

[52] COIFFET P, *Robot Technology Volume 1 - Modelling And Control*, Kogan Page, London, (1983).

[53] BYG SYSTEMS LTD, *GRASP - Reference Manual (Version 8)*, 1990.

[54] NAGHDY F., BALDWIN S. D., Simulation Of Locomotion On GRASP, *Automation In Construction*, **1**, 1, May 1992, 83-96.

APPENDICES

APPENDIX A

PUBLICATIONS LISTING

1) BROADHURST, S. J., PRIDMORE, T. P., TAYLOR, N., Sensing for feature identification in sewers, *Proceedings 11th International Symposium On Automation And Robotics In Construction*, Brighton, May 1994, 675-682.

2) TAYLOR, N., DRAPER, R., BROADHURST, S. J., MALLINDER, P. A., Static and kinematic limit states of masonry vaults, *The Centenary Year Bridge Conference Proceedings*, University Of Wales College Of Cardiff, Elesvier, 1994, 181-186.

3) BROADHURST, S. J., PRIDMORE, T. P., TAYLOR, N., COCKERHAM, G., Three-dimensional description of sewer laterals via reflective photometric stereo, *Proceedings 12th International Symposium On Automation And Robotics In Construction*, Warsaw, May 1995, 547-556.

4) BROADHURST, S. J., COCKERHAM, G., TAYLOR, N., PRIDMORE, T. P., Robotic kinematic simulation for sewer renovation, *12th International Symposium On Automation And Robotics In Construction, Warsaw*, May 1995, 321-328.

5) BROADHURST, S. J., COCKERHAM, G., TAYLOR, N. AND PRIDMORE, T. P., Automatic task modelling for sewer studies, *Automation in Construction*, 1996, vol. 5, 61-71.

APPENDIX B

COMPUTER SOFTWARE

The following programmes were written in QBASIC by the author, unless where stated otherwise.

1) Chainage Measurement System (written by K Soar Esq. with portions by the author); please refer to page 261.

2) Robotic Arm Control System; please refer to page 268.

1) Chainage Measurement System

```
DECLARE FUNCTION GETSTRLNDIST! (dist!, offsetdist!)
DECLARE FUNCTION GETINCLINATION! ()
DECLARE FUNCTION GETOFFSET! (angle!)
DECLARE SUB SHOWSTARTSCREEN ()
DECLARE SUB FINISH ()
DECLARE SUB SHOWDATASCREEN ()
DECLARE SUB ECHODATA (timeslot AS INTEGER)
DECLARE FUNCTION GETDIST! ()
DECLARE SUB PRINTDATA ()
DECLARE FUNCTION GETTIME! ()

'############################################################
' PROGRAM FILE NAME : chainage.bas
' Program Last Revised 7th October 1997
' Program by Karl Soar, School of Construction
' Portions by Simon J Broadhurst
' This program counts the pulses given by the tractor mounted
' Rotary Encoder, and resolves the angular roll of the tractor
' measured by the on-board inclinometer, to determine the overall
' straight line distance travelled by the tractor
' Resolution of the encoder = 1800 pulses per revolution
'############################################################

'====Inititialise Encoder
OUT &H32B, &H89

'====Zero Ports A, B
OUT &H328, &H0
OUT &H329, &H0

'====Reset THCT12316
OUT &H32B, &H89

'====Set Chan x to Mode 1
OUT &H328, &H1

'====Clear X chan count
OUT &H327, &H0
OUT &H326, &H0

'====Init ADC For Inclinometer
OUT &H309, 0
OUT &H706, 0
OUT &H30B, 0

'#### Declare Constants
resolution = 1800
```

```
pi = 3.141592654#
piperad = .45 / 2
wheelradius = .1
circumference = 2 * pi * wheelradius
pulsecount = 0
distfmt$ = "##.###"
velfmt$ = "#.###"
inclfmt$ = "+##.###"
strlinefmt$ = "##.###"
offfmt$ = "+##.###"

'#### Initialise program Variables
startdist = 0: totaldist = 0: starttime = 0: strlndist = 0
t1 = 0: t2 = 0: d1 = 0: d2 = 0: i1 = 0: i2 = 0
sd1 = 0: sd2 = 0: currvel = 0

MAINPROGRAM:
SHOWSTARTSCREEN

'##### Get a file handle
CLS
LOCATE 10, 5, 0
PRINT "Please enter a valid test "
LOCATE 11, 5, 0
PRINT "(Comma Separated Values)"
LOCATE 12, 5, 0
INPUT "Logfile name (eg chain1.csv) :", filename$
IF filename$ = "" THEN filename$ = "chain1.csv"   'use default name

'#####   Open the file for writing
OPEN filename$ FOR OUTPUT AS #1

WRITE #1, "Logfile name    : ", filename$
WRITE #1, "Test Started on : ", DATE$
WRITE #1, "                at : ", TIME$
WRITE #1, "Time (s)", "Dist (m)", "Inclination (degs)", "Offset (m)", "StrLine Dist
(m)", "Velocity (m/s)"

'#### TAKE INITIAL MEASUREMENTS.....

'#### Rotary Encoder Sampling
startdist = 0
starttime = GETTIME
startinclination = GETINCLINATION
startoffset = GETOFFSET(theta)
startstrlndist = GETSTRLNDIST(startdist, startoffset)

CLS
SHOWDATASCREEN
```

```
'#### Loop to read & Display All Data
'#### ========Main loop=================

ts = GETTIME
DO
  t2 = GETTIME
  'd2 = GETDIST
LOOP UNTIL t2 = (ts + 1)  'Loops until next whole second starts
d2 = 0
inclination2 = GETINCLINATION
offset2 = GETOFFSET(inclination2)
sd2 = GETSTRLNDIST(d2, offset2)
currvel = 0
WRITE #1, t2, d2, inclination2, offset2, sd2, currvel

WHILE 1 AND INKEY$ <> CHR$(27)
   'While 'not Break' and 'not key pressed' do.....

   DO  'Get T1 values
       t1 = GETTIME
       d1 = GETDIST
       inclination1 = GETINCLINATION
       offset1 = GETOFFSET(inclination1)
       sd1 = GETSTRLNDIST(d1, offset1)
   LOOP UNTIL (t1 = t2 + 1)    'Loops until next whole second starts

   currvel = (d1 - d2)
   WRITE #1, t1, d1, inclination1, offset1, sd1, currvel
   ECHODATA (1)

   DO  'Get T2 values
       t2 = GETTIME
       d2 = GETDIST
       inclination2 = GETINCLINATION
       offset2 = GETOFFSET(inclination2)
       sd2 = GETSTRLNDIST(d2, offset2)
   LOOP UNTIL t2 = (t1 + 1)    'Loops until next whole second starts

   currvel = (d2 - d1)
   WRITE #1, t2, d2, inclination2, offset2, sd2, currvel

   ECHODATA (2)

WEND   'End of Main Loop....
WRITE #1, "Test Ended on : ", DATE$
WRITE #1, "          at : ", TIME$

CLOSE #1  'Close open file

CLS
```

```
starttime = 0
GOTO MAINPROGRAM

END

SUB ECHODATA (timeslot AS INTEGER)
SHARED currvel
SHARED t1
SHARED t2
SHARED d1
SHARED d2
SHARED inclination1
SHARED inclination2
SHARED offset1
SHARED offset2
SHARED sd1
SHARED sd2
SHARED distfmt$
SHARED velfmt$
SHARED strlinefmt$
SHARED inclfmt$
SHARED offfmt$

IF timeslot = 1 THEN

   LOCATE 9, 27, 0
   PRINT t1
   LOCATE 10, 27, 0
   PRINT USING distfmt$; d1
   LOCATE 11, 27, 0
   PRINT USING inclfmt$; inclination1
   LOCATE 12, 27, 0
   PRINT USING offfmt$; offset1
   LOCATE 16, 43, 0
   PRINT USING strlinefmt$; sd1

ELSE
   LOCATE 9, 45, 0
   PRINT t2
   LOCATE 10, 45, 0
   PRINT USING distfmt$; d2
   LOCATE 11, 45, 0
   PRINT USING inclfmt$; inclination2
   LOCATE 12, 45, 0
   PRINT USING offfmt$; offset2
   LOCATE 16, 43, 0
   PRINT USING strlinefmt$; sd2
END IF

 'Always print common data.....
```

```
  LOCATE 18, 44, 0
  PRINT USING velfmt$; currvel

 END SUB

 SUB FINISH
 CLS
 END

 END SUB

 FUNCTION GETDIST

  SHARED resolution
  SHARED circumference

  encolobyte = INP(&H327)
  encohibyte = INP(&H326)
  pulsecount = (256 * encohibyte) + encolobyte
  rotations = pulsecount / resolution
  distmt = rotations * circumference

GETDIST! = distmt
END FUNCTION

FUNCTION GETINCLINATION

  '#### Inclinometer Sampling
   OUT &H302, 0                    'Select chan
   OUT &H300, 0                    'Request conversion

   WHILE (INP(&H308) AND &H80) = &H80     'Wait for conversion complete
   WEND

   inchighb = INP(&H301)
   inclowb = INP(&H300)
   vout = ((inchighb * 16 + (inclowb AND &HF0) / 16) - 2048) / 100
   sintheta = (vout * .707) / 5
   theta = (vout / 4.755) * 45

GETINCLINATION! = theta
END FUNCTION

FUNCTION GETOFFSET (angle)

SHARED piperad
SHARED pi

  offset = piperad * SIN((angle * pi) / 180)
```

```
GETOFFSET! = offset
END FUNCTION
FUNCTION GETSTRLNDIST (dist, offsetdist)

    strlndist = SQR(ABS((dist ^ 2) - (offsetdist ^ 2)))
GETSTRLNDIST! = strlndist
END FUNCTION

FUNCTION GETTIME

 SHARED starttime
 TIMESTR$ = TIME$

 LOCATE 21, 18, 0
 PRINT TIMESTR$

 MIN$ = MID$(TIMESTR$, 4, 2)
 SEC$ = MID$(TIMESTR$, 7, 2)

 MINS = VAL(MIN$)
 SECS = VAL(SEC$)

 NOW = ((MINS * 60) + SECS)

 GETTIME! = (NOW - starttime)
END FUNCTION

SUB SHOWDATASCREEN

 CLS
 LOCATE 4, 1, 0

 PRINT "     É͸͸͸͸͸͸͸͸͸͸͸͸͸͸͸͸͸͸͸͸͸͸͸͸͸͸͸͸͸͸͸͸͸͸͸͸͸͸͸͸͸͸͸͸͸͸»"
 PRINT "     º                                                                  º"
 PRINT "     º  Chainage Measurement - Encoder & Inclinometer                   º"
 PRINT "     º
ÚÄÄÄÄÄÄÄÄÄÄÄÄÄÄÄÄÄÄÄÄÄÄÄÄÄÄÄÄÄÄÄÄÄÄÄÄÄÄÄÄÄÄÄÄÄÄÄÄÄÄÄÄÄÄÄÄÄÄÄÄÄÄÄÄÄÄÄÄÄÄÄÄÄÄÄ¿     º"
 PRINT "     º  ³                                                          ³     º"
 PRINT "     º  ³  Time 1:          Time 2:                                 ³     º"
 PRINT "     º  ³  Dist 1:          Dist 2:                                 ³     º"
 PRINT "     º  ³  Incl 1:          Incl 2:                                 ³     º"
 PRINT "     º  ³  Offs 1:          Offs 2:                                 ³     º"
 PRINT "     º  ³                                                          ³     º"
 PRINT "     º  ³  Calculated Data:                                        ³     º"
 PRINT "     º  ³                                                          ³     º"
 PRINT "     º  ³  Str' Line Distance (m) =                                ³     º"
 PRINT "     º  ³                                                          ³     º"
 PRINT "     º  ³  Average Velocity (m/s) =                                ³     º"
```

```
 PRINT "      º
ÀÄÄÄÄÄÄÄÄÄÄÄÄÄÄÄÄÄÄÄÄÄÄÄÄÄÄÄÄÄÄÄÄÄÄÄÄÄÄÄÄÄÄÙ      º"
 PRINT "      º                                º"
 PRINT "      º Time:          Press 'Esc' to Quit....   º"
 PRINT "      ÈÍÍÍÍÍÍÍÍÍÍÍÍÍÍÍÍÍÍÍÍÍÍÍÍÍÍÍÍÍÍÍÍÍÍÍÍÍÍÍÍÍÍÍÍÍÍÍ¼"
END SUB
SUB SHOWSTARTSCREEN

 CLS

 LOCATE 3, 1, 0

 PRINT "   ÉÍÍÍÍÍÍÍÍÍÍÍÍÍÍÍÍÍÍÍÍÍÍÍÍÍÍÍÍÍÍÍÍÍÍÍÍÍÍÍÍÍÍÍÍÍÍÍÍÍÍÍÍÍÍÍÍÍÍ»"
 PRINT "   º                                   º"
 PRINT "   º                                   º"
 PRINT "   º     Sewer Tractor Chainage Measurement System      º"
 PRINT "   º
ÄÄÄÄÄÄÄÄÄÄÄÄÄÄÄÄÄÄÄÄÄÄÄÄÄÄÄÄÄÄÄÄÄÄÄÄÄÄÄÄÄÄÄÄÄÄÄÄÄÄÄÄÄÄ
ÄÄÄÄ   º"
 PRINT "   º                                   º"
 PRINT "   º     (c) K Soar /S Broadhurst,            º"
 PRINT "   º       School of Construction             º"
 PRINT "   º       Sheffield Hallam University, 1997        º"
 PRINT "   º                                   º"
 PRINT "   º                                   º"
 PRINT "   º     Press the Space Bar to start measurement        º"
 PRINT "   º                                   º"
 PRINT "   º         or  press 'Esc' to Quit....          º"
 PRINT "   º                                   º"
 PRINT "   º                                   º"
 PRINT "   ÈÍÍÍÍÍÍÍÍÍÍÍÍÍÍÍÍÍÍÍÍÍÍÍÍÍÍÍÍÍÍÍÍÍÍÍÍÍÍÍÍÍÍÍÍÍÍÍÍÍÍÍÍÍÍÍÍÍÍ¼"

DO
KEYPRESS$ = INKEY$
LOOP UNTIL (KEYPRESS$ = CHR$(32)) OR (KEYPRESS$ = CHR$(27))
IF KEYPRESS$ = CHR$(27) THEN FINISH

END SUB
```

2) Robotic Arm Control System

```
DECLARE SUB extendprog1 ()
REM    Robot Arm Movement - Motors 1 and 2 and 3!!
REM    Revised on Tues 28th September 99 - Correct Linear Stepper mem addresses
added
REM    Written by S J Broadhurst
REM    Last Revision Date 13th August 1999
REM    Motor3 Output Address statements added
REM    The programme calculates motor steps for the four quadrants of the
REM    lateral , ie phi 0 to 90, 90 to 180, 180 to 270, 270 to 360 degrees
REM    THIS PROG WORKS FOR THETA 0 to 360 !!! FOR ALL MOTORS
REM    ALSO INCLUDES ONTO TARGET
REM     FOR ANY LATERAL INTERSECTION ANGLE.
REM    1 step of motor = 7.5 degrees
REM    Gearbox ratio 250 : 1
REM    For Motor Only, 48 Steps = 360 degrees
REM    For Motor & Gearbox - 12,000 Steps = 360 degrees
REM    Therefore 1 step = 0.03 degrees
REM    Linear Actuator, 1 step = 0.025mm

REM ************************************************
REM    Set Varaibles & Initialise
REM ************************************************

CLS

pi = 3.141592654#
phi = 0
theta = 0                    'initialise theta - motor 2 rotation
thetan = 0
thetao = 0
omega = 0
omegao = 0
omegan = 0

REM ************************************************
REM    To Keep pen in free space - assume longer arm 's'
REM ************************************************

s = 200      'arm body length from pivot to end of linear body'
t = 25       'Pen body length from base to tip'
ext = 0      'extension of motor screw - this can be the datum position!!'

REM ************************************************
REM    Create a text output file
REM ************************************************

INPUT "Enter a test logfile name (eg TEST1.csv) :", filename$
```

```
REM ***********************************************
REM     Open the file for writing to
REM ***********************************************

OPEN filename$ FOR OUTPUT AS #1

WRITE #1, "Test Started on : ", DATE$
WRITE #1, "          at : ", TIME$
loops = 0

WHILE 1 AND loops = 0 AND INKEY$ <> CHR$(27)

  loops = 1

REM ***********************************************
REM     INPUT VALUES
REM ***********************************************

INPUT "Enter MAXIMUM lateral diameter:", latmax
INPUT "Enter MINIMUM lateral radius for drill (mm):", latmin
INPUT "Step increment between profiles (mm) :", latstep
INPUT "Enter intersection angle (degrees):", rhoinput
INPUT "Enter PHI to be incremented by (degrees):", phistep

rho = rhoinput * (pi / 180)                'angle of lateral intersection
pulsewait = 10

WRITE #1, "Time between pulses : ", pulsewait
WRITE #1, "PHI to be incremented by (degrees) : ", phistep
WRITE #1, "MIN lateral radius : ", latmin
WRITE #1, "MAX lateral radius : ", latmax
WRITE #1, "drill INCREMENT : ", latstep
WRITE #1, "Rho : ", rhoinput
WRITE #1,

REM ***********************************************
REM     FROM PARK TO ON TARGET
REM ***********************************************

parkanglerad = (ATN(latmin / 225))
parkangledeg = parkanglerad * (180 / pi)

parktodatumsteps = INT(((ABS(parkangledeg / .03))) + .5)

yinit = 1 * (SQR((50625) + (latmin * latmin)))
initialext = yinit - (s + t)
initextstep = INT(((initialext / .025)) + .5)

OUT &H280, 4                    'decrement'
```

```
FOR i = 0 TO parktodatumsteps STEP 1
OUT &H280, 12
FOR n = 0 TO pulsewait: NEXT n  'delay
OUT &H280, 4          'clear port
FOR n = 0 TO pulsewait: NEXT n  'delay
NEXT i

OUT &H281, 1                    'increment'
FOR i = 0 TO initextstep STEP 1
OUT &H281, 3
FOR n = 0 TO pulsewait: NEXT n  'delay
OUT &H281, 1          'clear port
FOR n = 0 TO pulsewait: NEXT n  'delay
NEXT i

REM ************************************************
REM    Arm should now be at correct position, on profile
REM    for lateral minimum radius 'latmin'
REM ************************************************

WRITE #1, "omegao was = ", omegao
WRITE #1, "parkanglerad = ", parkanglerad
WRITE #1, "parkangledeg = ", parkangledeg
WRITE #1, "parktodatumsteps = ", parktodatumsteps
WRITE #1,
WRITE #1, "initial ext steps = ", initextstep
WRITE #1,

extendprog1

REM ************************************************
REM    Set Up Loop for LATERAL - LAT
REM ************************************************


FOR lat = latmin TO latmax STEP latstep    'for drilling lateral profile radius between
                                           '10mm at centre to 150mm at outer profile

WRITE #1, "LATERAL RADIUS : ", lat
PRINT "lateral radius = ", lat

WRITE #1,
WRITE #1, "phi", "x", "y", "z", "Theta", "Omega", "Linear Ext (mm)", "Theta Pulse",
"Omega Pulse", "Linear Pulse"

phi = 0

z = lat * SIN(phi)
a = lat * COS(phi) * SIN(rho)
b = (1 + (2 / ((TAN(rho)) * (TAN(rho)))))
```

```
c = (SQR((50625) - (z * z))) / (TAN(rho))
x = (a * b) + c
y = 1 * (SQR((50625) + (z * z)))

REM    NOW WORK IN DEGREES!!

thetao = ATN(z / y) * (180 / pi)        'to initialise position'
omegao = ATN(x / y) * (180 / pi)        'to initialise position'
exto = y - (s + t)                      'to initialise position'
REM exto = initialext

REM ************************************************
REM    PHI 0 TO 90 DEGREES ##############################
REM ************************************************

FOR phi = .00001 TO (90.00001 * pi / 180) STEP (phistep * pi / 180)
phideg = (phi * 180 / pi)
PRINT "phi = ", phideg

z = lat * SIN(phi)
a = lat * COS(phi) * SIN(rho)
b = (1 + (2 / ((TAN(rho)) * (TAN(rho)))))
c = (SQR((50625) - (z * z))) / (TAN(rho))
x = (a * b) + c
y = 1 * (SQR((50625) + (z * z)))

REM    NOW WORK IN DEGREES!!

theta = ATN(z / y) * (180 / pi)        'in degrees'
omega = ATN(x / y) * (180 / pi)        'in degrees'
ext = y - (s + t)

thetan = theta - thetao
omegan = omega - omegao
extn = ext - exto

thetastep = INT((ABS(thetan / .03)) + .5)
omegastep = INT((ABS(omegan / .03)) + .5)
extstep = INT(((extn / .025)) + .5)

WRITE #1, phideg, x, y, z, theta, omega, ext, thetastep, omegastep, extstep

OUT &H282, 0                    'increment'
FOR i = 0 TO thetastep STEP 1
OUT &H282, 2
FOR w = 1 TO pulsewait: NEXT w
OUT &H282, 0
FOR w = 1 TO pulsewait: NEXT w
NEXT i
```

```
OUT &H280, 0                    'increment'
FOR i = 0 TO omegastep STEP 1
OUT &H280, 8
FOR n = 0 TO pulsewait: NEXT n  'delay
OUT &H280, 0            'clear port
FOR n = 0 TO pulsewait: NEXT n  'delay
NEXT i

OUT &H281, 0                    'decrement'
FOR i = 0 TO exstep STEP 1
OUT &H281, 2
FOR n = 0 TO pulsewait: NEXT n  'delay
OUT &H281, 0            'clear port
FOR n = 0 TO pulsewait: NEXT n  'delay
NEXT i

extendprog1

thetao = theta
omegao = omega
exto = ext

NEXT phi

WRITE #1,

REM ************************************************
REM    PHI 90 TO 180 DEGREES ############################
REM ************************************************

FOR phi = (90.00001 * pi / 180) TO (180.00001# * pi / 180) STEP (phistep * pi / 180)
phideg = (phi * 180 / pi)
PRINT "phi = ", phideg

z = lat * SIN(phi)
a = lat * COS(phi) * SIN(rho)
b = (1 + (2 / ((TAN(rho)) * (TAN(rho)))))
c = (SQR((50625) - (z * z))) / (TAN(rho))
x = (a * b) + c
y = 1 * (SQR((50625) + (z * z)))

REM    NOW WORK IN DEGREES!!

theta = ATN(z / y) * (180 / pi)       'in degrees'
omega = ATN(x / y) * (180 / pi)       'in degrees'
ext = y - (s + t)

thetan = theta - thetao
omegan = omega - omegao
extn = ext - exto
```

```
thetastep = INT((ABS(thetan / .03)) + .5)
omegastep = INT((ABS(omegan / .03)) + .5)
extstep = INT(((extn / .025)) + .5)

WRITE #1, phideg, x, y, z, theta, omega, ext, thetastep, omegastep, extstep

OUT &H282, 1                'decrement'
FOR i = 0 TO thetastep STEP 1
OUT &H282, 3
FOR w = 1 TO pulsewait: NEXT w
OUT &H282, 1
FOR w = 1 TO pulsewait: NEXT w
NEXT i

OUT &H280, 0                'increment'
FOR i = 0 TO omegastep STEP 1
OUT &H280, 8
FOR n = 0 TO pulsewait: NEXT n  'delay
OUT &H280, 0          'clear port
FOR n = 0 TO pulsewait: NEXT n  'delay
NEXT i

OUT &H281, 1                'increment'
FOR i = 0 TO exstep STEP 1
OUT &H281, 3
FOR n = 0 TO pulsewait: NEXT n  'delay
OUT &H281, 1          'clear port
FOR n = 0 TO pulsewait: NEXT n  'delay
NEXT i

extendprog1

thetao = theta
omegao = omega
exto = ext

NEXT phi

WRITE #1,

REM ************************************************
REM    PHI 180 TO 270 DEGREES ##############################
REM ************************************************

FOR phi = (180.00001# * pi / 180) TO (270.00001# * pi / 180) STEP (phistep * pi /
180)
phideg = (phi * 180 / pi)
PRINT "phi = ", phideg
```

```
z = lat * SIN(phi)
a = lat * COS(phi) * SIN(rho)
b = (1 + (2 / ((TAN(rho)) * (TAN(rho)))))
c = (SQR((50625) - (z * z))) / (TAN(rho))
x = (a * b) + c
y = 1 * (SQR((50625) + (z * z)))
REM    NOW WORK IN DEGREES!!

theta = ATN(z / y) * (180 / pi)        'in degrees'
omega = ATN(x / y) * (180 / pi)        'in degrees'
ext = y - (s + t)

thetan = theta - thetao
omegan = omega - omegao
extn = ext - exto

thetastep = INT((ABS(thetan / .03)) + .5)
omegastep = INT((ABS(omegan / .03)) + .5)
extstep = INT(((extn / .025)) + .5)

WRITE #1, phideg, x, y, z, theta, omega, ext, thetastep, omegastep, extstep

OUT &H282, 1                    'decrement'
FOR i = 0 TO thetastep STEP 1
OUT &H282, 3
FOR w = 1 TO pulsewait: NEXT w
OUT &H282, 1
FOR w = 1 TO pulsewait: NEXT w
NEXT i

OUT &H280, 4                        'decrement'
FOR i = 0 TO omegastep STEP 1
OUT &H280, 12
FOR n = 0 TO pulsewait: NEXT n  'delay
OUT &H280, 4            'clear port
FOR n = 0 TO pulsewait: NEXT n  'delay
NEXT i

OUT &H281, 0                        'decrement'
FOR i = 0 TO exstep STEP 1
OUT &H281, 2
FOR n = 0 TO pulsewait: NEXT n  'delay
OUT &H281, 0            'clear port
FOR n = 0 TO pulsewait: NEXT n  'delay
NEXT i

extendprog1

thetao = theta
omegao = omega
```

```
exto = ext

NEXT phi

WRITE #1,

REM ************************************************
REM     PHI 270 TO 360 DEGREES ##########################
REM ************************************************

FOR phi = (270.00001# * pi / 180) TO (360.00001# * pi / 180) STEP (phistep * pi /
180)
phideg = (phi * 180 / pi)
PRINT "phi = ", phideg

z = lat * SIN(phi)
a = lat * COS(phi) * SIN(rho)
b = (1 + (2 / ((TAN(rho)) * (TAN(rho)))))
c = (SQR((50625) - (z * z))) / (TAN(rho))
x = (a * b) + c
y = 1 * (SQR((50625) + (z * z)))

REM     NOW WORK IN DEGREES!!

theta = ATN(z / y) * (180 / pi)        'in degrees'
omega = ATN(x / y) * (180 / pi)        'in degrees'
ext = y - (s + t)

thetan = theta - thetao
omegan = omega - omegao
extn = ext - exto

thetastep = INT((ABS(thetan / .03)) + .5)
omegastep = INT((ABS(omegan / .03)) + .5)
extstep = INT(((extn / .025)) + .5)

WRITE #1, phideg, x, y, z, theta, omega, ext, thetastep, omegastep, extstep

OUT &H282, 0                'increment'
FOR i = 0 TO thetastep STEP 1
OUT &H282, 2
FOR w = 1 TO pulsewait: NEXT w
OUT &H282, 0
FOR w = 1 TO pulsewait: NEXT w
NEXT i

OUT &H280, 4                        'decrement'
FOR i = 0 TO omegastep STEP 1
OUT &H280, 12
FOR n = 0 TO pulsewait: NEXT n  'delay
```

```
OUT &H280, 4          'clear port
FOR n = 0 TO pulsewait: NEXT n  'delay
NEXT i

OUT &H281, 1                    'increment'
FOR i = 0 TO exstep STEP 1
OUT &H281, 3
FOR n = 0 TO pulsewait: NEXT n  'delay
OUT &H281, 1          'clear port
FOR n = 0 TO pulsewait: NEXT n  'delay
NEXT i

extendprog1

thetao = theta
omegao = omega
exto = ext

NEXT phi

WRITE #1,

REM ************************************************
REM    MOVE ARM TO NEXT DATUM POSITION ####################
REM ************************************************

REM    Assuming lateral increment to be 20 degrees

latshiftdeg = (ATN(latstep / 225)) * (180 / pi)
latshiftstep = INT((ABS(latshiftdeg / .03)) + .5)

OUT &H280, 4                    'decrement'
FOR i = 0 TO latshiftstep STEP 1
OUT &H280, 12
FOR n = 0 TO pulsewait: NEXT n  'delay
OUT &H280, 4          'clear port
FOR n = 0 TO pulsewait: NEXT n  'delay
NEXT i

WRITE #1, "latshiftdeg (degs) = ", latshiftdeg
WRITE #1, "latshiftsteps (steps) = ", latshiftstep

WRITE #1,

NEXT lat

WEND

CLOSE  'Close all open files and devices
END
```

```
SUB extendprog1
REM
**********************************************************************
REM     This sub routine extends pen by user defined increment then retracts to put dot
on paper
REM
**********************************************************************

jog

INPUT "Extension in mm :", extension
WRITE #1,
WRITE #1, "Extension to be (mm) = ", extension
extend = INT(((extension / .025)) + .5)

OUT &H281, 1                    'increment arm'
FOR i = 0 TO extend STEP 1
OUT &H281, 3
FOR n = 0 TO 10: NEXT n  'delay
OUT &H281, 1            'clear port
FOR n = 0 TO 10: NEXT n  'delay
NEXT i

WRITE #1, "DOT PLACED ON PAPER "

INPUT "Retraction in mm :", retraction
WRITE #1,
WRITE #1, "retraction to be (mm) = ", retraction
retract = INT(((retraction / .025)) + .5)

OUT &H281, 0                    'decrement arm'
FOR i = 0 TO retract STEP 1
OUT &H281, 2
FOR n = 0 TO 10: NEXT n  'delay
OUT &H281, 0            'clear port
FOR n = 0 TO 10: NEXT n  'delay
NEXT i

WRITE #1, "ARM RETRACTED"

WRITE #1,

END SUB
```

APPENDIX C

COMPUTER VISION STUDIES

1) Dr T Pridmore provided edge detection routines to a specification drawn up by the candidate.

2) Derivation of Computer Vision Illumination Models for Lateral Classification provided by Dr T Pridmore to a specification drawn up by the candidate. Please refer to page 279.

3) Lateral Classification Experimental Evaluation – Isoluminance Contour and Intersection data. Please refer to page 290.

4) Estimation of Lateral Diameter φ_{LAT}, Further Examples (Images From Laboratory Pipe Rig). Please refer to page 295.

2) Derivation of Computer Vision Illumination Models for Lateral Classification provided by Dr T Pridmore to a specification drawn up by the candidate

Assumptions, Geometry and Notation

Assumed that both the reflecting and target surfaces are lambertian Figure C.1.

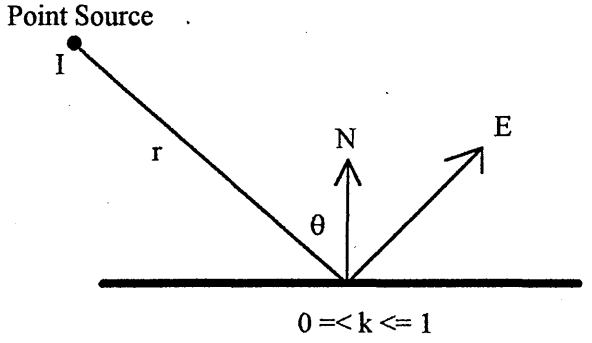

Figure C.1: Lambertian Reflectance

The lambertian reflectance function

$$E = \frac{kI\cos\theta}{r^2}$$

is the building block for all following derivations. Here,

E = surface luminance

k = surface reflectivity ($0 =< k <= 1$)

I = intensity of the light source

θ = angle between the incident light ray and the surface normal N

r = distance the ray travels between light source and surface

Figures C.2 and C.3 show the illumination and surface geometry employed. A two-dimensional arrangement is considered, obtained by taking a horizontal slice through the 3D environment. The origin O of a polar co-ordinate system lies a distance w along a perpendicular to the (effectively infinite) reflecting surface (the wall of the main pipe); the $\phi = 0$ axis of that system being parallel to the reflecting surface. A notionally infinite target surface (the lateral wall) with normal N lies at an angle ρ to $\phi = 0$. Figure C.2 gives the geometry of direct illumination. A light source positioned at O emits a light ray towards a point P, (ϕ, r), on the target surface. This ray arrives with angle of incidence θ and is reflected proportional to $\cos(\theta)$.

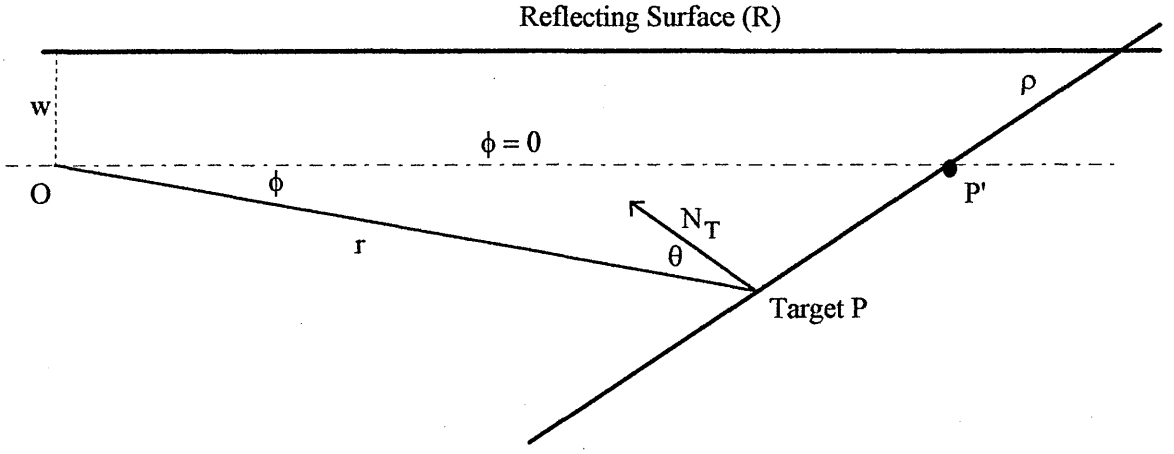

Figure C.2: The Geometry Of Direct Illumination

Figure C.3 shows the geometry of reflected illumination. Here the light source at O emits a light ray towards a point R, (α, r_1), on the reflecting surface. This ray makes an angle of incidence θ_1 with the reflecting surface normal N_r. As this surface is lambertian, light from R is reflected equally in all directions. One reflected ray, making an angle θ_2 with N_r, exits R and travels a distance r_2 to P, where it has an angle of

incidence ϕ_2 and is again reflected, according to the lambertian reflectance function, from the target surface.

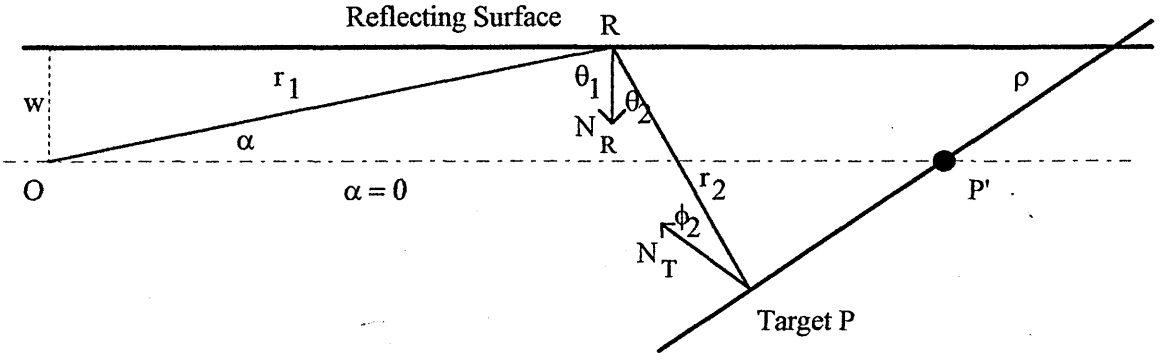

Figure C.20: The Geometry of Reflected Illumination

In is assumed that the relative position and orientation of the light source and reflecting surface are known or computable, i.e. that w, ϕ and α are available, and that the goal is to recover the distance d and orientation ρ of the target surface. For our purposes d = OP', the distance from the origin to the intersection of lateral wall with the axis of the pipe.

Direct Illumination

Direct illumination of P will be considered first, assuming the situation shown in Figure C.4.

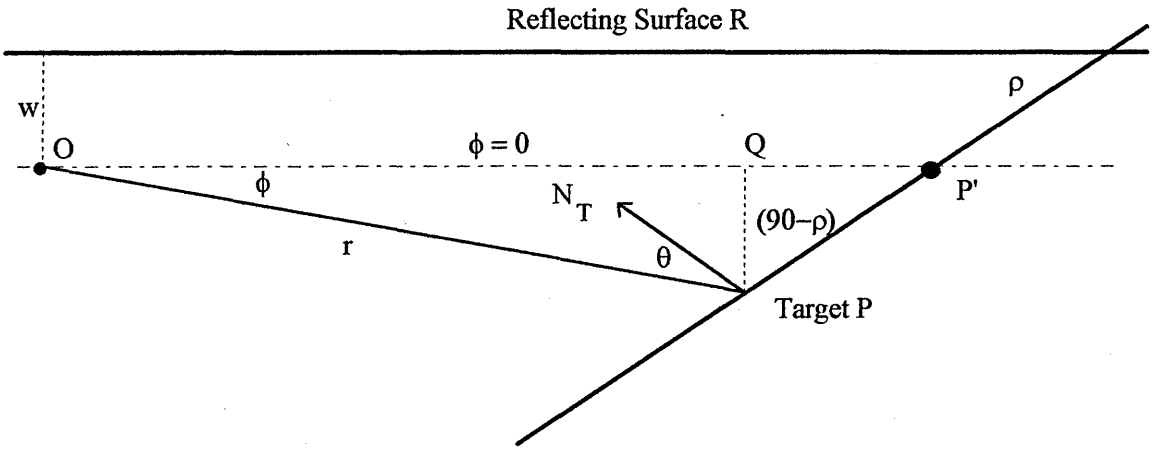

Figure C.4: Surface luminance under direct illumination

Assuming the lateral wall to be a lambertian target, the luminance E_d of P due to direct illumination from O is given by Equation C.1

$$E_d = \frac{kI\cos\theta}{r^2} \qquad \text{(Equation C.1)}$$

k and I are assumed known *a priori*; the aim here is to estimate values for ρ and d. It is therefore necessary to introduce these into Equation C.1. From triangle OQP in Figure C.4 it can be seen that $\theta = 90 - (\phi + \rho)$, hence

$$E_d = \frac{kI\sin(\phi+\rho)}{r^2} \qquad \text{(Equation C.2)}$$

$$r = \frac{1}{\cos\phi}\left(d - \frac{w}{\tan\rho}\right) \qquad \text{(Equation C.3)}$$

$$\tan\phi = \frac{w}{\left(d - \frac{w}{\tan\rho}\right)} \qquad \text{(Equation C.4)}$$

$$E_d = \frac{kI\sin(\phi+\rho)}{\left(\frac{1}{\cos\phi}\left(d-\frac{w}{\tan\rho}\right)\right)^2} \qquad \text{(Equation C.5)}$$

where

$$\phi = \arctan\left(\frac{w}{\left(d-\frac{w}{\tan\rho}\right)}\right)$$

Reflected Illumination

Reflected illumination of P is now considered. Illumination is now directed towards the wall opposite the lateral mouth and light from this wall reflected towards the target surface (Figure C.5). The luminance E_r of point P due to this reflected light is given by

$$E_r = \frac{kI_1\cos\theta_2}{r_2^2} \qquad \text{(Equation C.6)}$$

where I_1 represents the intensity of light reflected off the main sewer wall.

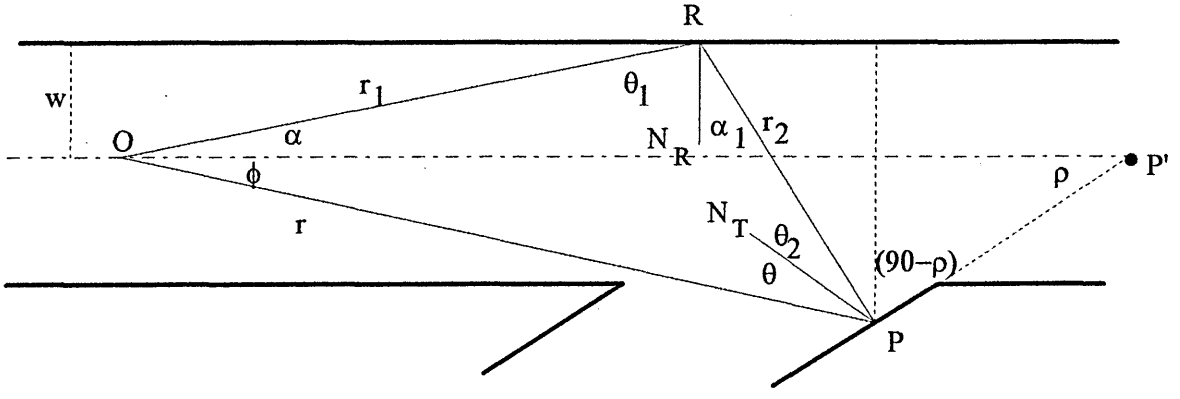

Figure C.25: Surface luminance under reflected illumination

I_1 may be derived as before: from point source to wall the light is travelling directly,

Equation C.7.

$$I_1 = \frac{kI\cos\theta_1}{r_1^2} \qquad \text{(Equation C.7)}$$

By inspection of Figure C.5 we have,

$$r_1 = \frac{w}{\sin\alpha}$$

$$\theta_1 = 90 - \alpha$$

and so

$$I_1 = \frac{kI\sin^3\alpha}{w^2} \qquad \text{(Equation C.8)}$$

Now consider r_2 and Figure C.6

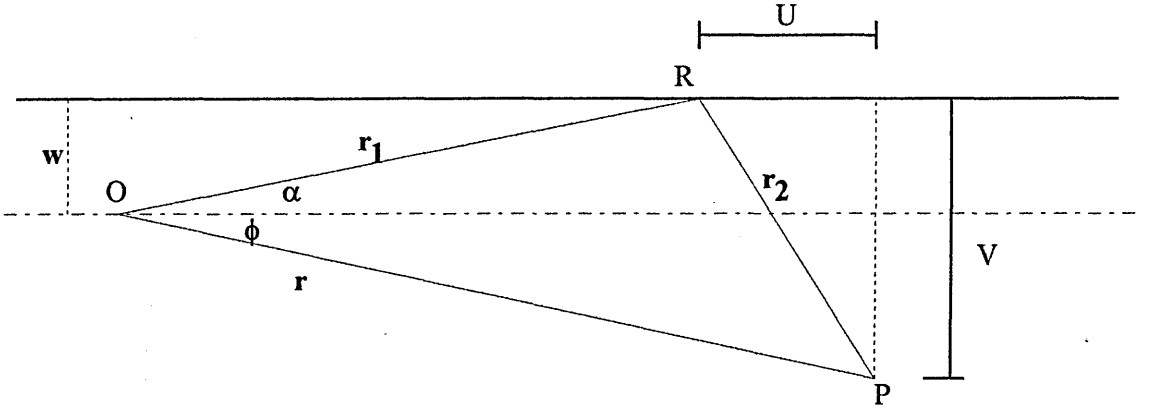

Figure C.6

$$r_2^2 = U^2 + V^2 \qquad \text{(Equation C.9)}$$

where

$$U = d - \frac{w}{\tan\rho} - \frac{w}{\tan\alpha} \qquad \text{(Equation C.10)}$$

and

$$V = 2w \qquad \text{(Equation C.11)}$$

Hence, substituting Equations C.10 and C.11 into Equation C.9 produces;

$$r_2^2 = 4w^2 + \left(d - w\left(\frac{1}{\tan\rho} + \frac{1}{\tan\alpha} \right) \right)^2 \qquad \text{(Equation C.12)}$$

Finally we require an expression for θ_2. Recalling Figure C.5;

$$\theta_2 = \rho - \alpha_1 \qquad \text{(Equation C.13)}$$

α_1 may now be expressed in terms of r_2. We have

$$r_2 \cos\alpha_1 = 2w$$

$$\alpha_1 = \cos^{-1}\left(\frac{2w}{r_2} \right)$$

so

$$\theta_2 = \rho - \cos^{-1}\left(\frac{2w}{r_2} \right) \qquad \text{(Equation C.14)}$$

Recalling the initial expression for reflected illumination given by Equation C.6, Equation C.15 is now obtained by substitution

$$E_r = \frac{k^2 I \sin^3\alpha . \cos(\rho - \cos^{-1}\left(\frac{2w}{r_2} \right))}{w^2 {r_2}^2} \qquad \text{(Equation C.15)}$$

where

$$r_2 = \sqrt{4w^2 + \left(d - w\left(\frac{1}{\tan\rho} + \frac{1}{\tan\alpha} \right) \right)^2}$$

Reflected Illumination as a Linear Light Source

Non-point sources and their properties are considered in some detail by Keitz (1971), who gives equations describing the illumination provided by a simple linear source which emits light uniformly along its length. This is a more accurate description of reflected illumination in the present circumstances than the model derived above.

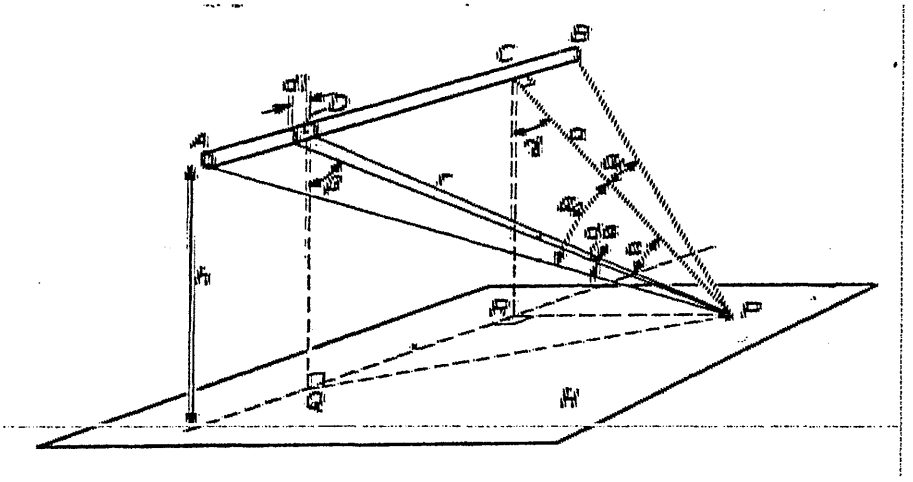

Figure C.7. Scanned in from Keitz page 137.

Figure C.24 shows the arrangement modelled by Keitz. A linear light source AB is suspended parallel to a plane H and the illumination at point P on H is sought. The derivation proceeds by first calculating the contribution dE_α of a cylindrical surface element of AB, *dl* in length. Integration of dE_α between the angles $\alpha 1$ and $\alpha 2$ then provides an estimate of total illumination. If AB is uniformly diffuse, the total illumination E at P is given by

$$E = \mathrm{I}_1 \frac{h}{a^2} \frac{1}{4} \left[2(\alpha_2 - \alpha_1) + \sin 2\alpha_2 - \sin 2\alpha_1 \right] \qquad \text{(Equation C.16)}$$

where

I is the maximum luminous intensity of a part of AB one unit in length

h is the height of the source above H

a is the perpendicular distance from P to AB

$\alpha 1$ and $\alpha 2$ are the angles subtended by the parts of AB on each side of the perpendicular from P to AB

In the current application, the point of interest P is coplanar with the light source and so a = h = 2w. Hence

$$E = I_1 \frac{1}{8w}\left[2(\alpha_2 - \alpha_1) + \sin 2\alpha_2 - \sin 2\alpha_1\right] \qquad \text{(Equation C.17)}$$

Derivation of expressions for α_1 and α_2 requires knowledge of the position and extent of the linear light source. To achieve this we assume that the true light source lying at O is directional, with its principle axis oriented α degrees from the pipe axis. We further assume that this lamp emits light only in directions lying within +/-β degrees of its principle axis. Both the position and length of the linear source are then functions of α, β and w (see Figure C.8).

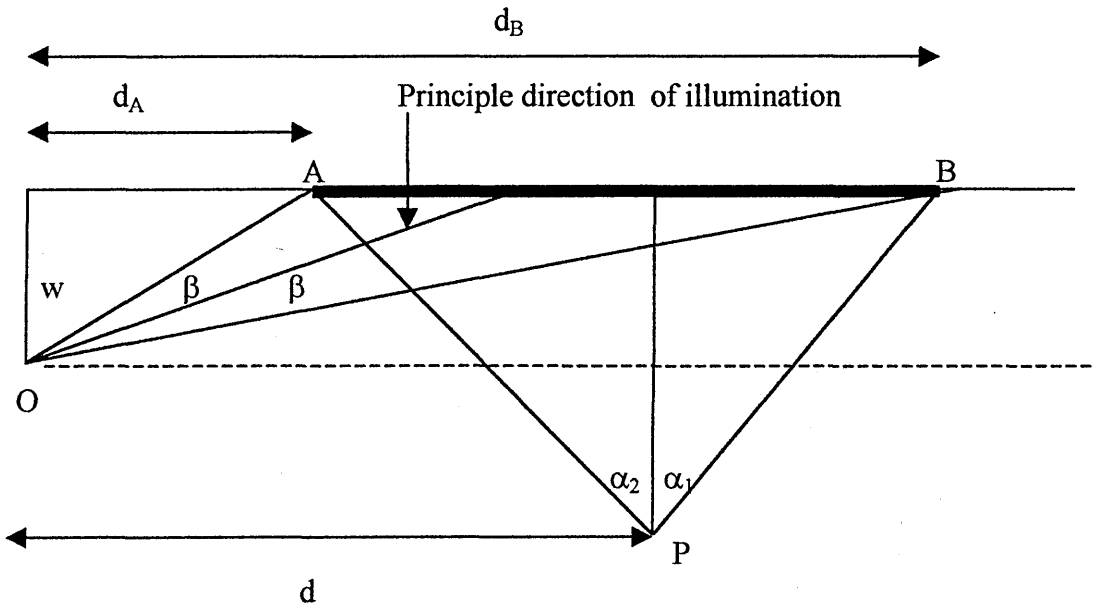

Figure C.8. The notional linear light source (shown bold) introduced on the reflecting wall during indirect illumination of P by a directional light source at O

If points A and B mark the endpoints of the linear source and d_A and d_B are the distances, measured in the direction of the pipe axis, from O to A and B respectively, then we have:

$d_A = w.\tan(90 - (\alpha + \beta))$ (Equations C.18)

$d_B = w.\tan(90 - (\alpha - \beta))$

Since

$\tan \alpha_1 = (d_B - d)/2w$

and (Equations C.19)

$\tan \alpha_2 = (d - d_A)/2w$

where d is the distance in the direction of the pipe axis to P from O as before, substituting Equations C.18 into Equations C.19 and rearranging gives

$\alpha_1 = \tan^{-1}(w.\tan(90 - (\alpha - \beta)) - d)/2w$ (Equations C.20)

$\alpha_2 = \tan^{-1}(d - d_A = w.\tan(90 - (\alpha + \beta)))/2w$

Further substitution of Equations C.20 into Equation C.17 provides an expression for the total illumination at P.

It remains to produce an expression for surface radiance at P. To achieve this, the standard assumption that the pipe wall is lambertian is made and the principle direction of illumination is taken to be along a line to P from the midpoint of our notional linear light source. Then;

$Er = E.k.\cos\theta$

where

$\theta = \rho - \theta_1$

and

$\theta_1 = \tan^{-1}((d- (d_A + (d_B - d_A)/2)) /2w)$

The candidate has been made aware by Dr Tony Pridmore that the midpoint of the notional linear light source lies some 2.4m from the camera; for all values of d less than 2.4 m the principal direction of illumination is from a point behind the lateral mouth. In these circumstances the model values are not reliable.

3) Lateral Classification Experimental Evaluation - Isoluminance Contour and Intersection data

Isoluminance contours are provided in their 'raw' screened dumped form. Please note, for each figure, top left contour represents isoluminance contour corresponding to Ed whilst top right contour corresponds to Er, with their intersection (s) provided as shown. Axis for Xyp and p are as noted in Section 2.3.3

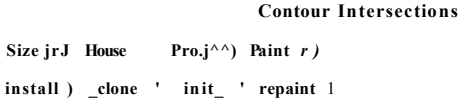

a. Isoluminance contours on the direct and reflected illumination reflectance maps and their intersection, p = 45, d = 3.453

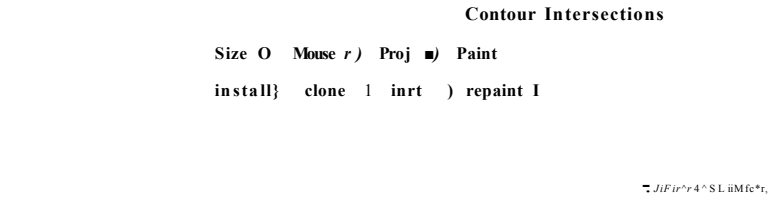

b. Isoluminance contours on the direct and reflected illumination reflectance maps and their intersection, p = 45,d = 3.271

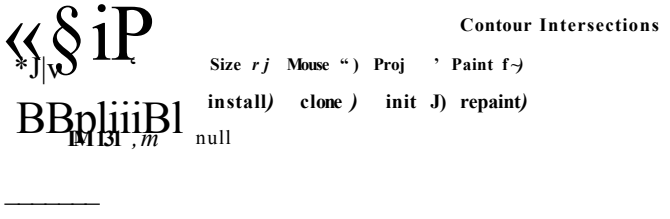

c. Isoluminance contours on the direct and reflected illumination reflectance maps and their intersection, p = 45,d = 2.912

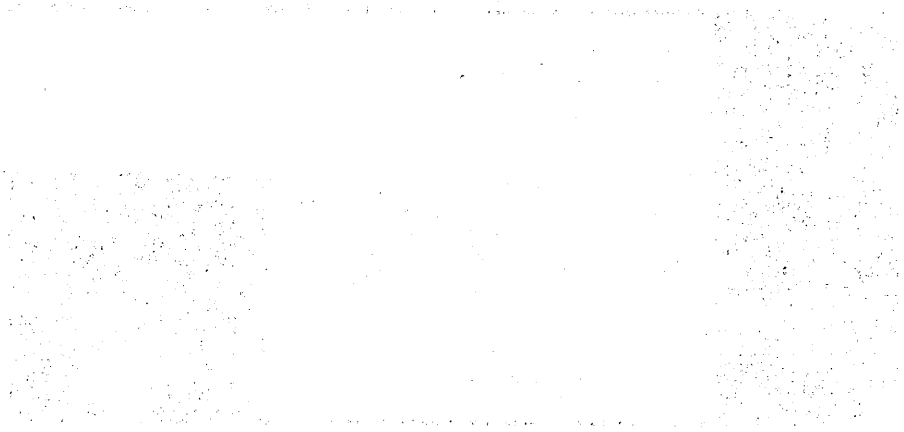

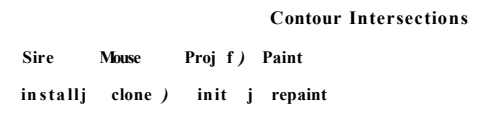

d. Isolurainance contours on the direct and reflected illumination reflectance maps and their intersection, p = 45, d = 2.704

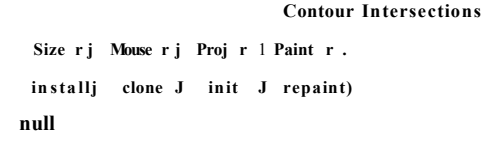

e. Isoluminance contours on the direct and reflected illumination reflectance maps and their intersection, p = 45, d = 2.643

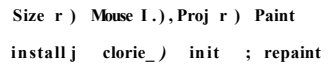

f. Isoluminance contours on the direct and reflected illumination reflectance maps and their intersection, p = 90, d = 3.349

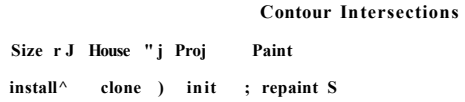

g. Isoluminance contours on the direct and reflected illumination reflectance maps and their intersection, p = 90, d = 3.032

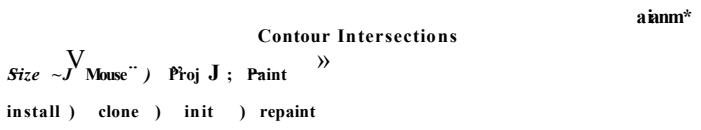

h. Isoluminance contours on the direct and reflected illumination reflectance maps and their intersection, p = 90, d = 2.614

4) Estimation of Lateral Diameter (PLAT? Further Examples

EXAMPLE 1

Figure C.9: Estimation of lateral diameter - Example 1

In the above figure provided, (pNME = 450mm. If the line lengths are now measured then by inspection a = 29mm and b = 40mm. From Equation 2.16, (Plat is approximately 310mm which is close enough in terms of tolerance value to classify the lateral as being of 300mm as opposed to 150 or 225mm.

Figure C. 10: Estimation of lateral diameter - Example 2

In the above figure provided, ϕ_{NME} = 450mm. If the line lengths are now measured then by inspection a = 40mm and b = 56mm. From Equation 2.16, C_{pLAT} is approximately 315mm which is close enough in terms of tolerance value to classify the lateral as being of 300mm as opposed to 150 or 225mm.

APPENDIX D

CMS OUTPUT – TYPICAL CASES

1) CMS Data Output For Parallel Chainage Run, Nominal Tractor Inclination of 0 Degrees; please refer to page 298

2) CMS Data Output For Parallel Chainage Run, Nominal Tractor Inclination of -30 Degrees; please refer to page 301

3) CMS Data Output For Skewed Chainage Run, γ_s = -20 Degrees; please refer to page 304

CMS Data Output For Parallel Chainage Run, Nominal Tractor

Inclination of 0 Degrees

Time (s)	Culmative Distance (Rotary Encoder) (m)	Inclination (degrees)	Velocity (m/s)	Incremental Offset (m)	Culmative Invert Path Distance (m)
0	0.000	0.189	0.000	0.000	0.000
1	0.052	-0.095	0.053	-0.001	0.052
2	0.126	-0.852	0.076	-0.003	0.126
3	0.205	-0.946	0.081	0.000	0.204
4	0.275	-0.946	0.072	0.000	0.275
5	0.348	-1.420	0.075	-0.002	0.348
6	0.424	-1.609	0.078	-0.001	0.424
7	0.501	-0.189	0.079	0.006	0.501
8	0.580	1.325	0.081	0.006	0.580
9	0.657	1.325	0.079	0.000	0.657
10	0.741	0.568	0.086	-0.003	0.740
11	0.818	0.379	0.079	-0.001	0.818
12	0.897	-0.189	0.081	-0.002	0.896
13	0.955	-0.473	0.059	-0.001	0.954
14	0.957	-0.568	0.003	0.000	0.957
15	0.956	-0.568	-0.001	0.000	0.958
16	0.955	-0.473	-0.001	0.000	0.959
17	0.971	-0.568	0.016	0.000	0.975
18	1.052	-0.946	0.083	-0.001	1.055
19	1.130	0.852	0.080	0.007	1.133
20	1.208	2.082	0.079	0.005	1.210
21	1.284	1.987	0.079	0.000	1.287
22	1.367	1.325	0.085	-0.003	1.370
23	1.452	1.230	0.087	0.000	1.455
24	1.532	0.284	0.081	-0.004	1.534
25	1.613	-0.473	0.083	-0.003	1.616
26	1.696	0.000	0.086	0.002	1.699
27	1.780	2.271	0.086	0.009	1.782
28	1.861	2.744	0.083	0.002	1.863
29	1.939	1.798	0.080	-0.004	1.941
30	2.017	2.744	0.080	0.004	2.019
31	2.093	2.366	0.078	-0.001	2.095
32	2.182	0.946	0.091	-0.006	2.184
33	2.269	0.568	0.089	-0.001	2.270
34	2.344	1.420	0.077	0.003	2.346
35	2.422	3.596	0.080	0.009	2.423
36	2.496	3.123	0.075	-0.002	2.497
37	2.584	2.271	0.090	-0.003	2.585
38	2.661	2.366	0.080	0.000	2.663

39	2.741	1.987	0.082	-0.001	2.743
40	2.823	1.514	0.084	-0.002	2.824
41	2.902	0.757	0.081	-0.003	2.903
42	2.984	2.934	0.084	0.009	2.985
43	3.061	3.407	0.079	0.002	3.062
44	3.141	3.218	0.081	-0.001	3.141
45	3.213	3.123	0.075	0.000	3.214
46	3.293	2.744	0.082	-0.001	3.294
47	3.377	2.271	0.086	-0.002	3.377
48	3.455	1.798	0.080	-0.002	3.456
49	3.535	2.082	0.082	0.001	3.535
50	3.607	3.691	0.074	0.006	3.607
51	3.683	3.975	0.078	0.001	3.683
52	3.766	3.502	0.085	-0.002	3.766
53	3.840	3.407	0.076	0.000	3.841
54	3.918	3.123	0.080	-0.001	3.919
55	3.996	2.555	0.080	-0.002	3.996
56	4.075	2.271	0.080	-0.001	4.075
57	4.156	3.028	0.083	0.003	4.156
58	4.229	4.448	0.075	0.006	4.229
59	4.297	4.921	0.070	0.002	4.297
60	4.370	4.637	0.075	-0.001	4.370
61	4.443	4.637	0.075	0.000	4.443
62	4.514	4.732	0.073	0.000	4.514
63	4.596	4.259	0.084	-0.002	4.596
64	4.671	3.785	0.077	-0.002	4.671
65	4.750	3.502	0.081	-0.001	4.750
66	4.819	5.394	0.071	0.007	4.819
67	4.893	5.773	0.076	0.001	4.893
68	4.979	5.489	0.088	-0.001	4.979
69	5.055	5.394	0.078	0.000	5.055
70	5.131	5.394	0.077	0.000	5.130
71	5.211	4.637	0.082	-0.003	5.211
72	5.288	4.164	0.078	-0.002	5.287
73	5.365	4.164	0.080	0.000	5.365
74	5.437	6.057	0.074	0.007	5.436
75	5.511	6.625	0.075	0.002	5.510
76	5.590	6.530	0.081	0.000	5.589
77	5.662	5.962	0.074	-0.002	5.660
78	5.737	5.868	0.077	0.000	5.736
79	5.802	3.596	0.067	-0.009	5.800
80	5.882	4.448	0.082	0.003	5.880
81	5.963	4.353	0.083	0.000	5.961
82	6.031	6.246	0.071	0.007	6.029
83	6.103	7.003	0.073	0.003	6.100
84	6.176	7.003	0.076	0.000	6.174
85	6.240	4.164	0.065	-0.011	6.237
86	6.320	5.205	0.082	0.004	6.316
87	6.392	4.921	0.074	-0.001	6.388

88	6.466	4.164	0.076	-0.003	6.462
89	6.539	3.975	0.075	-0.001	6.535
90	6.615	4.448	0.078	0.002	6.612
91	6.682	6.341	0.068	0.007	6.678
92	6.749	6.435	0.069	0.000	6.745
93	6.823	5.962	0.076	-0.002	6.820
94	6.896	5.678	0.074	-0.001	6.892
95	6.965	5.584	0.071	0.000	6.961
96	7.039	5.394	0.076	-0.001	7.035
97	7.110	2.650	0.073	-0.011	7.105
98	7.183	2.650	0.075	0.000	7.178
99	7.254	4.637	0.072	0.008	7.248
100	7.326	6.246	0.074	0.006	7.321
101	7.395	7.098	0.071	0.003	7.389
102	7.475	5.394	0.082	-0.007	7.469
103	7.551	5.868	0.078	0.002	7.545
104	7.622	5.584	0.072	-0.001	7.616
105	7.702	4.637	0.083	-0.004	7.696
106	7.779	4.826	0.079	0.001	7.773
107	7.848	6.489	0.071	0.003	7.842
108	7.916	6.719	0.070	0.005	7.910
109	7.988	7.192	0.074	0.002	7.982
110	8.063	8.194	0.077	0.003	8.057
111	8.140	6.341	0.079	-0.006	8.133
112	8.215	6.057	0.077	-0.001	8.209
113	8.290	5.016	0.077	-0.004	8.284
114	8.361	4.732	0.073	-0.001	8.355
115	8.430	4.826	0.071	0.000	8.424
116	8.484	6.341	0.055	0.006	8.477
117	8.482	6.341	-0.002	0.000	8.479

CMS Data Output For Parallel Chainage Run, Nominal Tractor

Inclination of -30 Degrees

Time (s)	Culmative Distance (Rotary Encoder) (m)	Inclination (degrees)	Velocity (m/s)	Incremental Offset (m)	Culmative Invert Path Distance (m)
0	0.000	-30.000	0.000	0.000	0.000
1	0.035	-30.284	0.036	-0.001	0.035
2	0.117	-30.000	0.084	0.001	0.117
3	0.195	-29.148	0.080	0.003	0.195
4	0.267	-26.688	0.073	0.009	0.266
5	0.333	-25.647	0.068	0.004	0.333
6	0.416	-24.890	0.085	0.003	0.416
7	0.498	-24.322	0.084	0.002	0.497
8	0.581	-23.849	0.085	0.002	0.580
9	0.659	-24.322	0.080	-0.002	0.658
10	0.744	-24.132	0.088	0.001	0.744
11	0.828	-22.997	0.086	0.004	0.827
12	0.906	-20.631	0.080	0.009	0.904
13	0.988	-20.063	0.084	0.002	0.987
14	1.069	-19.968	0.083	0.000	1.067
15	1.149	-19.779	0.082	0.001	1.148
16	1.231	-19.306	0.084	0.002	1.229
17	1.308	-20.442	0.080	-0.004	1.307
18	1.400	-19.306	0.094	0.004	1.399
19	1.479	-17.129	0.081	0.008	1.477
20	1.554	-16.183	0.077	0.004	1.552
21	1.639	-15.899	0.088	0.001	1.637
22	1.718	-15.899	0.081	0.000	1.716
23	1.805	-15.521	0.089	0.001	1.803
24	1.882	-15.710	0.080	-0.001	1.880
25	1.968	-15.615	0.088	0.000	1.966
26	2.037	-14.006	0.070	0.006	2.034
27	2.119	-12.114	0.084	0.007	2.116
28	2.201	-11.451	0.085	0.003	2.199
29	2.285	-11.830	0.086	-0.001	2.282
30	2.362	-12.208	0.079	-0.001	2.359
31	2.432	-11.356	0.072	0.003	2.430
32	2.516	-11.735	0.086	-0.001	2.514
33	2.601	-11.924	0.087	-0.001	2.598
34	2.681	-10.505	0.082	0.005	2.678
35	2.756	-8.801	0.076	0.007	2.752
36	2.832	-8.423	0.078	0.001	2.828
37	2.915	-8.517	0.086	0.000	2.912
38	2.990	-8.707	0.076	-0.001	2.986

39	3.065	-8.707	0.077	0.000	3.061
40	3.146	-9.085	0.083	-0.001	3.142
41	3.222	-8.707	0.079	0.001	3.219
42	3.304	-7.192	0.084	0.006	3.300
43	3.382	-5.584	0.080	0.006	3.378
44	3.457	-5.678	0.077	0.000	3.453
45	3.530	-5.678	0.075	0.000	3.526
46	3.604	-6.151	0.075	-0.002	3.600
47	3.685	-5.773	0.083	0.001	3.681
48	3.760	-6.341	0.077	-0.002	3.756
49	3.840	-6.814	0.081	-0.002	3.836
50	3.910	-5.489	0.073	0.005	3.906
51	3.988	-3.785	0.079	0.007	3.983
52	4.069	-3.407	0.083	0.001	4.065
53	4.143	-3.596	0.075	-0.001	4.138
54	4.217	-3.691	0.076	0.000	4.213
55	4.288	-3.596	0.073	0.000	4.284
56	4.367	-4.069	0.080	-0.002	4.362
57	4.445	-4.164	0.080	0.000	4.440
58	4.516	-3.028	0.073	0.004	4.512
59	4.598	-0.852	0.083	0.009	4.593
60	4.676	-0.757	0.080	0.000	4.671
61	4.756	-1.041	0.082	-0.001	4.751
62	4.828	-1.325	0.074	-0.001	4.823
63	4.898	-1.325	0.072	0.000	4.893
64	4.992	-1.893	0.096	-0.002	4.987
65	5.068	-2.271	0.079	-0.001	5.063
66	5.146	-0.473	0.080	0.007	5.141
67	5.220	0.757	0.076	0.005	5.214
68	5.295	0.662	0.076	0.000	5.289
69	5.368	0.189	0.075	-0.002	5.363
70	5.442	0.189	0.076	0.000	5.436
71	5.521	0.189	0.081	0.000	5.515
72	5.599	-0.189	0.080	-0.001	5.593
73	5.673	-1.703	0.076	-0.006	5.667
74	5.749	0.568	0.078	0.009	5.743
75	5.819	1.987	0.072	0.006	5.812
76	5.897	2.271	0.080	0.001	5.890
77	5.971	1.798	0.076	-0.002	5.964
78	6.042	1.798	0.073	0.000	6.036
79	6.115	1.514	0.074	-0.001	6.108
80	6.190	1.136	0.077	-0.001	6.183
81	6.268	0.000	0.080	-0.004	6.261
82	6.337	0.757	0.071	0.003	6.330
83	6.405	2.271	0.069	0.006	6.398
84	6.474	2.744	0.071	0.002	6.466
85	6.545	2.555	0.073	-0.001	6.538
86	6.620	2.555	0.077	0.000	6.613
87	6.689	2.461	0.071	0.000	6.681

88	6.760	2.271	0.074	-0.001	6.753
89	6.831	1.798	0.073	-0.002	6.824
90	6.902	0.757	0.073	-0.004	6.895
91	6.973	2.082	0.072	0.005	6.965
92	7.031	3.218	0.059	0.004	7.023
93	7.111	0.095	0.083	-0.012	7.103
94	7.181	1.136	0.072	0.004	7.173
95	7.254	1.609	0.075	0.002	7.246
96	7.327	1.893	0.074	0.001	7.318
97	7.400	2.366	0.075	0.002	7.391
98	7.478	3.312	0.080	0.004	7.469
99	7.545	1.420	0.069	-0.007	7.536
100	7.622	3.502	0.079	0.008	7.612
101	7.697	3.596	0.077	0.000	7.687
102	7.770	3.312	0.075	-0.001	7.760
103	7.843	3.312	0.075	0.000	7.833
104	7.911	3.312	0.070	0.000	7.901
105	7.989	2.934	0.080	-0.001	7.980
106	8.067	2.461	0.080	-0.002	8.057
107	8.141	2.461	0.076	0.000	8.131
108	8.210	3.596	0.071	0.004	8.200
109	8.277	4.832	0.069	0.003	8.267
110	8.353	3.785	0.077	-0.002	8.343
111	8.381	3.596	0.029	-0.001	8.371

CMS Data Output For Skewed Chainage Run, γ_s = -20 Degrees

Time (s)	Culmative Distance (Rotary Encoder) (m)	Inclination (degrees)	Velocity (m/s)	Incremental Offset (m)	Culmative Invert Path Distance (m)
0	0.000	-30.230	0.000	0.000	0.000
1	0.000	-30.230	0.000	0.000	0.000
2	0.001	-30.230	0.000	0.000	0.001
3	0.020	-31.271	0.020	-0.004	0.020
4	0.085	-33.259	0.066	-0.007	0.084
5	0.137	-33.069	0.054	0.001	0.137
6	0.187	-32.880	0.050	0.001	0.186
7	0.248	-33.069	0.063	-0.001	0.247
8	0.316	-35.218	0.070	-0.005	0.315
9	0.385	-33.637	0.071	0.003	0.384
10	0.397	-32.407	0.012	0.004	0.395
11	0.452	-31.366	0.057	0.003	0.450
12	0.521	-31.177	0.071	0.001	0.520
13	0.589	-31.271	0.070	0.000	0.588
14	0.654	-30.420	0.066	0.003	0.652
15	0.719	-28.905	0.067	0.005	0.717
16	0.779	-27.486	0.061	0.005	0.776
17	0.845	-26.539	0.068	0.003	0.843
18	0.907	-26.066	0.064	0.002	0.905
19	0.957	-26.066	0.051	0.000	0.955
20	0.964	-26.161	0.007	0.000	0.961
21	1.001	-25.782	0.038	0.001	0.999
22	1.067	-25.404	0.068	0.001	1.065
23	1.133	-25.688	0.067	-0.001	1.130
24	1.198	-25.404	0.067	0.001	1.195
25	1.265	-24.836	0.069	0.002	1.263
26	1.329	-23.322	0.065	0.005	1.326
27	1.389	-21.618	0.062	0.006	1.386
28	1.453	-20.861	0.065	0.003	1.450
29	1.517	-20.672	0.066	0.001	1.514
30	1.580	-20.483	0.064	0.001	1.576
31	1.646	-20.293	0.068	0.001	1.643
32	1.715	-19.820	0.071	0.002	1.712
33	1.781	-20.104	0.068	-0.001	1.778
34	1.849	-19.915	0.069	0.001	1.846
35	1.912	-19.536	0.065	0.001	1.909
36	1.972	-17.076	0.062	0.009	1.968
37	2.026	-15.467	0.056	0.006	2.022
38	2.089	-14.615	0.064	0.003	2.084
39	2.155	-14.710	0.068	0.000	2.151

40	2.221	-14.994	0.067	-0.001	2.216
41	2.290	-15.278	0.071	-0.001	2.286
42	2.351	-15.656	0.063	-0.001	2.346
43	2.412	-15.183	0.063	0.002	2.408
44	2.473	-14.804	0.063	0.001	2.469
45	2.536	-14.047	0.064	0.003	2.531
46	2.600	-12.249	0.066	0.007	2.595
47	2.661	-11.208	0.062	0.004	2.656
48	2.727	-10.735	0.068	0.002	2.722
49	2.794	-10.451	0.068	0.001	2.789
50	2.858	-10.451	0.066	0.000	2.853
51	2.926	-10.640	0.070	-0.001	2.921
52	2.990	-10.924	0.066	-0.001	2.985
53	3.057	-11.208	0.069	-0.001	3.052
54	3.118	-10.735	0.062	0.002	3.113
55	3.178	-9.126	0.062	0.006	3.173
56	3.238	-7.423	0.061	0.007	3.232
57	3.299	-7.328	0.063	0.000	3.293
58	3.358	-7.044	0.061	0.001	3.352
59	3.418	-7.707	0.062	-0.003	3.413
60	3.481	-7.139	0.064	0.002	3.475
61	3.544	-7.328	0.065	-0.001	3.538
62	3.602	-7.612	0.060	-0.001	3.596
63	3.666	-7.707	0.066	0.000	3.661
64	3.728	-7.612	0.063	0.000	3.722
65	3.785	-6.382	0.059	0.005	3.779
66	3.845	-4.962	0.061	0.006	3.839
67	3.901	-4.489	0.058	0.002	3.895
68	3.963	-4.300	0.063	0.001	3.957
69	4.022	-4.489	0.060	-0.001	4.016
70	4.084	-4.300	0.064	0.001	4.078
71	4.148	-4.110	0.066	0.001	4.142
72	4.207	-4.394	0.060	-0.001	4.201
73	4.270	-4.678	0.065	-0.001	4.264
74	4.332	-4.489	0.064	0.001	4.326
75	4.392	-3.259	0.061	0.005	4.385
76	4.441	-1.934	0.051	0.005	4.435
77	4.497	-0.987	0.057	0.004	4.490
78	4.568	-0.798	0.073	0.001	4.561
79	4.627	-1.082	0.061	-0.001	4.620
80	4.693	-0.987	0.068	0.000	4.686
81	4.750	-0.798	0.058	0.001	4.743
82	4.807	-1.177	0.059	-0.001	4.800
83	4.865	-1.650	0.059	-0.002	4.858
84	4.932	-1.650	0.069	0.000	4.925
85	5.003	-0.703	0.073	0.004	4.996
86	5.058	0.905	0.057	0.006	5.051
87	5.118	1.379	0.061	0.002	5.111
88	5.179	1.662	0.063	0.001	5.172

89	5.238	1.189	0.060	-0.002	5.230
90	5.302	1.284	0.066	0.000	5.295
91	5.361	1.189	0.060	0.000	5.354
92	5.418	1.095	0.059	0.000	5.411
93	5.477	0.811	0.060	-0.001	5.470
94	5.539	0.621	0.063	-0.001	5.531
95	5.601	1.189	0.064	0.002	5.593
96	5.654	2.703	0.055	0.006	5.647
97	5.712	4.028	0.059	0.005	5.703
98	5.769	3.839	0.059	-0.001	5.761
99	5.827	3.366	0.060	-0.002	5.819
100	5.889	3.271	0.063	0.000	5.880
101	5.946	3.461	0.059	0.001	5.938
102	6.002	2.987	0.057	-0.002	5.994
103	6.058	2.703	0.057	-0.001	6.049
104	6.121	2.230	0.065	-0.002	6.113
105	6.178	2.325	0.058	0.000	6.170
106	6.233	3.271	0.057	0.004	6.225
107	6.284	4.596	0.053	0.005	6.276
108	6.338	4.880	0.056	0.001	6.330
109	6.396	4.975	0.059	0.000	6.388
110	6.449	4.691	0.055	-0.001	6.441
111	6.506	4.691	0.058	0.000	6.498
112	6.564	4.596	0.059	0.000	6.555
113	6.615	4.407	0.053	-0.001	6.607
114	6.672	4.218	0.058	-0.001	6.663
115	6.729	3.839	0.059	-0.001	6.720
116	6.785	3.934	0.057	0.000	6.776
117	6.840	4.596	0.057	0.003	6.831
118	6.888	5.826	0.050	0.005	6.879
119	6.945	6.394	0.058	0.002	6.936
120	7.003	6.962	0.060	0.002	6.994
121	7.065	3.744	0.064	-0.013	7.055
122	7.127	4.218	0.063	0.002	7.116
123	7.184	4.218	0.059	0.000	7.174
124	7.243	4.218	0.061	0.000	7.233
125	7.302	4.312	0.061	0.000	7.292
126	7.362	5.069	0.061	0.003	7.351
127	7.422	6.016	0.062	0.004	7.411
128	7.480	6.678	0.060	0.003	7.469
129	7.538	7.625	0.059	0.004	7.527
130	7.596	7.435	0.060	-0.001	7.585
131	7.658	7.246	0.064	-0.001	7.648
132	7.716	6.962	0.059	-0.001	7.705
133	7.780	6.962	0.065	0.000	7.769
134	7.838	6.584	0.060	-0.001	7.828
135	7.898	6.110	0.061	-0.002	7.887
136	7.959	6.110	0.063	0.000	7.948
137	8.019	6.016	0.062	0.000	8.009

138	8.079	7.530	0.061	0.006	8.068
139	8.134	8.382	0.056	0.003	8.123
140	8.191	8.287	0.059	0.000	8.180
141	8.248	8.192	0.059	0.000	8.237
142	8.301	7.625	0.054	-0.002	8.289
143	8.359	7.530	0.060	0.000	8.348
144	8.413	7.435	0.055	0.000	8.402
145	8.467	7.246	0.056	-0.001	8.456
146	8.528	6.773	0.062	-0.002	8.516
147	8.584	6.394	0.058	-0.001	8.573
148	8.642	6.394	0.059	0.000	8.630
149	8.692	7.719	0.052	0.005	8.681
150	8.742	8.760	0.051	0.004	8.730
151	8.793	9.328	0.053	0.002	8.782
152	8.845	9.044	0.053	-0.001	8.834
153	8.901	8.476	0.057	-0.002	8.889
154	8.921	8.571	0.010	0.000	8.899

APPENDIX E

NOMENCLATURE

E_d	Reflected light intensity (lux) at target surface (direct illumination).
E_r	Reflected light intensity (lux) at target surface (direct illumination).
I	Intensity of point light source (lux).
I_l	Intensity of light off reflecting surface (lux).
N	Surface normal.
O_i	Horizontal offset of tractor from invert at increment i.
O_j	Horizontal offset of tractor from invert at increment j.
O_k	Horizontal offset of tractor from invert at increment k.
R	Radii of NME sewer pipe.
R_l	Radii of the lateral pipe.
R_m	Radii of the NME sewer.
X, Y, Z	Co-ordinate frame of reference specifying position of arbitrary point on lateral intersection profile with origin located at the intersection of lateral and NME centre lines; X axis extending to the right along NME centre line and Z axis extending upwards.
a	Length of straight line projected from vanishing point to top of lateral profile.
b	Length of straight line projected from top to bottom of lateral profile.
d	Invert distance from camera to target edge.
d_A	Invert distance from camera to start of linear light source.
d_B	Invert distance from camera to end of linear light source.

dI_l	Reflected intensity of elemental unit of linear light source.
dl	Elemental length of linear light source.
d_{proj}	Chainage distance from datum to lateral back wall projection with NME centre line.
k	Surface reflectivity function ($0 \leq k \leq 1$).
l	Length of linear light source.
l_d	Distance from EE to axis of revolute joint 1.
n	Number of samples.
r	Distance light ray travels between light source and target surface.
r_1	Distance light ray travels between light source and reflecting surface.
r_2	Distance light ray travels between reflecting surface and target surface.
r_d	Radius of conical drill.
u	Robot arm kinematic translation (joint 3).
u_0	Reposed arm length.
x	General invert chainage.
x_ρ	Geometrical offset from lateral wall.
x_i	Invert line distance travelled by tractor between increments i and j.
x_{i+1}	Invert line distance travelled by tractor between increments j and k.
x_L	Chainage to drilling station position.
x_o	Geometrical offset for drilling station.
x_t	Camera CCD chip offset from rear of tractor.
x_{vp}	Close-to-target distance chainage increment.

Δ_i	Distance measured by Rotary Encoder at between increments i and j.
Δ_{i+1}	Distance measured by Rotary Encoder at between increments j and k.
α_1	Angle subtended from target surface normal to end of linear light source.
α_2	Angle subtended from target surface normal to start of linear light source.
α_d	Emittance angle with respect to NME centre line (direct illumination).
α_i	Angle of Δ_i vector relative to pipe centre line at increment i.
α_{i+1}	Angle of Δ_{i+1} vector relative to pipe centre line at increment j.
α_r	Emittance angle with respect to NME centre line (reflected illumination).
β	Spread about α_r which defines length of linear light source.
ϕ	Angle about lateral centre line incremented from 0 to 360^o in 1^o steps.
ϕ_{LAT}	Diameter of lateral connection to NME sewer.
ϕ_{NME}	Diameter of NME sewer.
λ_d	Reflectance map scaling factor – direct illumination
λ_r	Reflectance map scaling factor – reflected illumination
γ	Angle of lateral fall away from the 3 or 9 o'clock horizontal.
γ_s	Angle of tractor skew with respect to NME centre line.
θ	Angle between incident light ray and surface normal, Chapter 2.
θ	Robot arm kinematic rotation (joint 2), Chapter 3.
θ_1	Angle between the incident light ray and the surface normal (reflected illumination, reflecting wall).

θ_2 Angle between the E_ρ and the surface normal (reflected illumination, target surface).

θ_i Inclinometer reading at increment i.

θ_j Inclinometer reading at increment j.

ρ Angle of lateral intersection with NME sewer.

ω Robot arm kinematic rotation (joint 1).

APPENDIX F

BIBLIOGRAPHY

1. AKEN L V et al, Robot programming languages: the statement of a problem Robotica, **6**, 1988, 141-148.
2. ALLEN P et al, Object recognition using vision and touch , *Proceedings of the Ninth International Joint Conference on Artificial Intelligence, Los Angeles California* , 18th-23rd August, 1985, 1131-1136.
3. ANDERSON G C, Soviet official admits that robots couldn't handle Chernobyl cleanup, *The Scientist*, January 22, 1990, 2-3.
4. ANDREWS W, Sewers - replace or renovate, *Tunnels and Tunnelling*, March 1982, 45-48.
5. ANON, Analysis of defects in 180km of pipe sewers in southern water authority, TRRL, **172**, 1989.
6. ANON, Cracking Pace, *Water Services*, January 1992, 28
7. ANON, How the sarcophagus was built, *Nuclear Engineering International*, March 1989, 34-37.
8. ANON, Inside Chernobyl sarcophagus, *transcript*, Horizon, BBC, 22nd April 1991.
9. ANON, Insituform breaks through with sewer lateral renovation, *Pipes & Pipelines International*, July - August 1993, 23-25.
10. ANON, *International Public Health Engineering*, Kean Publications Ltd, 1991.
11. ANON, Mole clears up bodgers job, *New Civil Engineer*, 7th February 1985, 2-3
12. ANON, Operation, replacement and maintenance of sewers, *Tunnels & Tunnelling*, May 1977, 59-64

13. ANON, Proceedings of Symposium on Deterioration of Underground Assets, *The Institution of Water Engineers and Scientists*, 7th & 8th December 1983.

14. ANON, Remote - controlled equipment for decommissioning, *IAEA Bulletin*, Winter 1985, 35-39.

15. ANON, Robotic characterisation of the 86.1m elevation of the three mile island unit 2 reactor building, *Nuclear Technology*, **87**, November 1989, 443-449.

16. ANON, Setting the seal on sewers' future, *Contract Journal*, 18th January 1979, 38-41

17. ANON, Trenchless Sewer Reline Conquers Laterals Limit, *New Civil Engineer*, 27th May 1993, 6.

18. ANON, Underground Pipe Repairs by Remote Control, *Surveyor*, 12th July 1984, 34

19. ARTHUR, R. A. J., Whatever happened to the sewer crisis, *Waste and Water Treatment*, September 1989, 54-57, 63, 78.

20. ATKIN B L et al, On automation in the construction industry, *University of Technology Sydney*, **6**, 1990, 34-45.

21. BALLARD D H et al, *Computer Vision*, Prentice-Hall Inc, New Jersey, 1982.

22. BEREZNAYA I Y et al, Robot vision as a problem of picture analysis optimisation, *Robotica*, **4**, 1986, 189- 192.

23. BERNOLD L E et al, Teaching construction automation to tomorrow's engineers, *International Journal of Applied Engineering*, 6, **2**, 1990, 91-199.

24. BICKNELL D A, A local authority viewpoint, *The Public Health Engineer*, 14, **4**, October 1986, 14-23.

25. BLACK P, Water supply and sewerage services: present and future, *The Public Health Engineer*, 6, **4**, October 1978, 250-255.

26. BLOCKLEY D I, *The Nature of Structural Design and Safety*, Ellis Horwood Limited, 1980.

27. BONE G M et al, Robotic force control for deburring using an active end effector, *Robotica*, 7, 1989, 303-308.

28. BOVIK A C, HUANG T S and MUNSON D C, The effect of median filtering on edge estimation and detection, *IEEE Transactions On Pattern Analysis and Machine Intelligence*, 1987, 2, **9**, 181-194.

29. BOYLE T, *Computer Vision: A First Course*, Blackwell, 1988.

30. BRADLEY D et al, Knowledge acquisition for a robotic excavator, *Proceedings of The 7th ISARC*, DTI, **2**, 1990, 351-357.

31. BRADY M, Artificial intelligence and robotics, *Artificial Intelligence*, **26**, 1985, 79-121.

32. BROADHURST S J, COCKERHAM G, TAYLOR N, PRIDMORE T P, Automatic task modelling for sewer studies, *Automation in Construction*, **5**, 1996, 61-71.

33. BROADHURST S J, COCKERHAM G, TAYLOR N, PRIDMORE T P, Robotic kinematic simulation for sewer renovation, *Proceedings of the 12th International Symposium on Automation and Robotics in Construction,* Warsaw, May 1995, 321-328.

34. BROADHURST S J, PRIDMORE T P, TAYLOR N, COCKERHAM G, Three-dimensional description of sewer laterals via reflective photometric stereo, *Proceedings of the 12th International Symposium on Automation and Robotics in Construction,* Warsaw, May 1995, 547-546.

35. BROADHURST S J, PRIDMORE T P, TAYLOR N, Sensing for feature identification in sewers, *Proceedings 11th International Symposium on Automation and Robotics in Construction*, Brighton, May 1994, 675-682.

36. BROWN M, Robotics: too late again?, *National Builder*, July / August, 1989, 16.

37. BS 8005 Part 5 - Sewerage: Guide To Rehabilitation of Sewers, 1983.

38. BUCKLEY C e et al, A proximity metric for continuum path planning, *Proceedings of the 9th International Joint Conference on Artificial Intelligence*, Los Angeles California, 18th - 23rd August 1985, **2**, 1096- 1102.

39. BYG SYSTEMS LTD - *GRASP - Reference Manual (Version 8)*, 1990.

40. BYG SYSTEMS LTD - *GRASP - Training Manual (Version 8.2)*, 1991.

41. BYLES R, Rooting for robots, *New Civil Engineer*, 18th June 1992, 24.

42. CANNY J, A computational approach to edge detection, *IEEE Transactions on Pattern Analysis and Machine Intelligence*, 6, **8**, 1986, 679-698.

43. CHAMBERLAIN D, A masonry tasking robot, *Proceedings of the 7th ISARC*, DTI, **1**, 1990, 1-8.

44. CHAMPENY L E et al, Conception and development of two mobile teleoperated systems for three mile island unit 2, *Nuclear Technology*, 87, November 1989, 631-640.

45. CHANTLER M J, Why illuminant direction is fundamental to texture analysis, *IEE Proceedings on Vision, Image and Signal Processing*, 1995, **142,** 4, 199-206.

46. CHMIDBERGER E J et al, Quality control with a robot guided electro-optical sensor, *Proceedings of 4th International Conference on Robot Vision and Sensory Controls*, London, 1984, 27-36.

47. CLOSSON Y, Robotics before its time, *Revue de L'energie*, 385, August/September 1986, 610-615.

48. COIFFET P, *Robot Technology Volume 1 - Modelling and Control*, Kogan Page, London, 1983.

49. COLLIE A A et al, Design and performance of the Portsmouth climbing robot, *Proceedings of the 7th ISARC*, DTI, **1**, 1990, 16-23.

50. COX G C, Background notes in developments in sewer renovation technology, *Internal Memo*, Sheffield City Polytechnic, 19th June 1985.

51. COX G C, Survey of the renovation of sewers, *Proceedings of Symposium on Deterioration of Underground Assets, The Institution of Water Engineers and Scientists*, 7th and 8th December 1983, chameleon press, 5.1-5.15

52. COX G C, Underground heritage: new techniques for sewer renovation, *The Public Health Engineer*, **9**, 3, July 1981, 145-153.

53. CULLEN N, CCTV sewer surveys - computerisation, *Water Research Centre*, 1982

54. CULLEN N, Performance and utilisation of sewer jetting plant, *The Public Health Engineer*, **9**, 1, January 1981, 18- 23.

55. DALEY S et al, A design study of a self-organising fuzzy logic controller, *Proceedings Institution of Mechanical Engineers*, 200, c1, 1986, 59-69.

56. DANGERFIELD B J, Water practice manuals: the structure and management of the British water industry, *The Institution of Water Engineers and Scientists*, London, 1979.

57. DAVIES P, *Introduction to C Programming For Embedded Systems: An Industrial Short Course*, Sheffield City Polytechnic (School of Engineering Information Technology.

58. DELGADO M et al, A procedure for ranking fuzzy numbers using fuzzy relations, *Fuzzy Sets and Systems*, **26**, (1), April, 1988, 49-62.

59. DEPARTMENT OF TRADE AND INDUSTRY, *The 7th International Symposium on Automation and Robotics in Construction*, Bristol, 5th-7th June 1990.

60. DRAPER R, SOAR K, TAYLOR N, PRIDMORE T, Computer vision for masonry vault testing, *Proceedings 1st International Arch Bridge Conference*, Bolton, Telford, September 1995, 257-266.

61. DUELEN G et al, Control systems for robots - development trends, *Schweissen Und Schneiden*, 42, (7), 1990, 323-327.

62. DUTTON K, *Introduction to Modern Control Engineering - A Short Course*, Sheffield Hallam University.

63. ECHIGO T et al, A fast method for extraction of 3-d information using multiple stripes and two cameras, *Proceedings of the 9th International Joint Conference on Artificial Intelligence*, Los Angeles California, 18th-23rd August 1985, 1127-1130.

64. EFSTATHIOU J, Expert systems fuzzy logic and rule-based control explained at last, *Transactions Institution of Mechanical Engineers*, **10**, 4, July-September 1988, 198-206.

65. EL KHAFIF M, Reconnection of laterals after HDPE relining by a new trenchless technology, *Proceedings 12th International Symposium on Automation and Robotics in Construction,* Warsaw, May 1995.

66. EVANS B, Robotics in construction - brains beating the brawn, *A J Supplement*, 21st December 1988, 38-41.

67. FAIRCLOUGH J & R MALPAS REVIEW'S, SERC

68. FIDDES D et al, Infiltration - do we have to live with it?, *The Public Health Engineer*, **9**, 1, January 1981, 11-13.

69. FIDDES D, The strategy for sewer rehabilitation, *Proceedings of symposium on deterioration of underground assets, the Institution of Water Engineers and Scientists*, 7th and 8th December 1983, Chameleon press, 9.1-9.9

70. FILLNOW R H et al, Development of remotely controlled devices for three mile island unit 2, *Nuclear Technology*, **87**, November 1989, 624-630.

71. FLEMONS K J, Maintaining our sewers, *Consulting Engineer*, September 1984, 13-14,17.

72. FOSTER J et al, Development of an expert vision system for automatic industrial inspection, *Proceedings of 4th International Conference on Robot Vision and Sensory Controls*, London, 1984, 303-311.

73. FOUNDATION FOR WATER RESEARCH, *Summary Report of the DOE Sewer Renovation Development Trials*, March, 1990.

74. FRAHM R B et al, Robots save money at PSE&G, *Nuclear Engineering International*, March 1989, 43-46.

75. FU, S., COOPER, D., PRIDMORE, T., TAYLOR, N., Determination of sewer structure using a moving camera, *Proceedings 12th International Symposium on Automation and Robotics in Construction, Warsaw*, May 1995, 539-546.

76. FURTHER EDUCATION UNIT, *Robotic Arms - A Contribution to the Curriculum: An Occasional Paper*, July 1984.

77. G B, *Robot Design Handbook*, SRI International, McGraw-Hill, 1988.

78. GALE J C, The renovation of sewerage systems, *The Public Health Engineer*, **9**, 1, January 1981, 24-41.

79. GALLIER E et al, *ICE Users Guide*, Thomson-C.S.F. Laboratoires Electroniques de Rennes, 15th July, 1991.

80. GELHAUS F e et al, Robotic applications in nuclear power plants, *Progress in Nuclear Energy*, **23**, 1, 1990, 1-33.

81. GIARRATANO R, *Expert Systems - Principles and Programming*, PWS-Kent.

82. GIEFER D L et al, Implementation of remote equipment at three mile island unit 2, *Nuclear Technology*, 87, November 1989, 641-647

83. GILMORE J F et al, Terrain navigation through knowledge-based route planning, *Proceedings of the Ninth International Joint Conference on Artificial Intelligence*, Los Angeles California, 18th - 23rd August, 1985, 2, 1086- 1088.

84. GINI M, The future of robot programming, *Robotica*, 5, 1987, 235-246.

85. GOOCH M N et al, Herne Bay sewerage improvements - the first pilot study goes underground, *Municipal Engineer*, 7, April 1990, 69-85.

86. GREEN D J, KA-TE goes underground, *Water Services*, September 1993, 60-62.

87. GREGORY P J et al, Knowledge based models for computer vision, *Proceedings of 4th International Conference on Robot Vision and Sensory Controls*, London, 1984, 325-330.

88. HARRIGAN R W, The role of model based control in robotics, *IEEE Transactions on Nuclear Science*, **37**, 3, June 1990, 1426-1431.

89. HAYWOOD D, Sonar sweep shows hidden sewer profile, *New Civil Engineer*, 12th November 1987, 40-42.

90. HEALTH AND SAFETY EXECUTIVE, *Blackspot Construction*, HMSO, 1988.

91. HEALTH AND SAFETY EXECUTIVE, *Injuries In Sewers*, Requested Statistical Data, 9th march 1993.

92. HEMAMI A, On a human-arm-like manipulator, *Robotica*, 5, 1987, 23-28.

93. HENDERSON T et al, A framework for distributed sensing and control, *Proceedings of the Ninth International Joint Conference on Artificial Intelligence*, Los Angeles California, 18th - 23rd August, 1985, 2, 1106-1109.

94. HENRY, R. AND LUXMOORE, A.R., A pipe-profiling adapter for CCTV inspection cameras: development of a pipe-profiling instrument, *Measurement Science and Technology*, 1996, **7**, 495-504.

95. HEWITT J R, Dynamic decoupled control of robot arms, *Cont of Manip & Robotic Devices*, Colloquium, 4, April 1980, 1-10.

96. HIROSE S et al, Design and control of a mobile robot with an articulated body, *The International Journal of Robotics Research*, **9**, 2, April 1990, 99-114 .

97. Hisatomi Yo, Introduction of construction robotics in Japan, *IABSE Journal*, **40**, 1990, 1-12.

98. HORAUD R, Spatial object perception from an image, *Proceedings of the Ninth International Joint Conference on Artificial Intelligence*, Los Angeles California, 18th - 23rd August, 1985, 2, 1116-1118.

99. Horn B K P, *Robot Vision*, MIT press, 1986

100. IWAHORI Y et al, Reconstructing shape from shading images under point light source illumination, *Proceedings of the 10th International Conference on Pattern Recognition*, 1990, 1, 83-87.

101. JARVIS R A, A perspective on range finding techniques for computer vision, *IEEE Transactions on Pattern Analysis and Machine Intelligence*, **5**, 2, March 1983, 122-139.

102. JARVIS R A, Range from brightness for robotic vision, *Proceedings of 4th International Conference on Robot Vision and Sensory Controls*, London, 1984, 165-172.

103. JENKINS O, Seeing to the defects, *Surveyor* , **170**, 521, 1988, 24-25.

104. JIANG X Y et al, An error analysis for surface normals determined by photometric stereo, *Signal Processing*, 23, 1991, 221-226.

105. JUMARIE G, A new class of PID parameter adaptation algorithms for robot manipulators, *Robotica*, 9, 1991, 107- 109.

106. JUMARIE G, On the use of deformation matrices in artificial vision systems, *Robotica*, 6, 1988, 13-21.

107. KAISTO I et al, Laser range finding techniques in the sensing of 3D objects, *SPIE*, 1260, 1990, 122-133.

108. KAMEI H et al, A method for reconstructing the shape of an object from two images taken under point light source illumination, *Systems and Computers In Japan*, **20**, 10, 1989, 75-84.

109. KANGARI R et al, Identification of factors influencing implementation of construction robotics, *Construction Management and Economics*, **8**, 1990, 89-104.

110. KARL W C et al, Reconstructing ellipsoids from projections, *Graphical Models and Image Processing*, **56**, 2, March 1994, 124 – 139

111. KEITZ H A E, *Light Calculations and Measurements, 2nd Ed*, Philips Technical Library, 1971.

112. KELLEY R B et al, Heuristic vision hole finder, *Proceedings of 4th International Conference on Robot Vision and Sensory Controls*, London, 1984, 341-350.

113. KENT E W et al, Real time co-operative interaction between structured light and reflectance ranging for robot guidance, *Robotica*, 3, 1985, 7-11.

114. KILLEN T S, Automation and robotic applications in North American construction, *Cost Engineering*, **33**, 7, July 1991, 9-13.

115. KOREN Y, *Robotics for Engineers*, McGraw-Hill, 1985.

116. KRUSTEV E et al, Kinematic path control of robot arms, *Robotica*, 4, 1986, 107-116.

117. KUO B C, *Automatic Control Systems*, Prentice-Hall Inc, 1987.

118. LEE C C, Fuzzy logic in control systems: fuzzy logic controller - part 1, *IEEE Transactions on Systems Management and Cybernetics*, **20**, 2, March-April 1990, 404-418.

119. LEE C C, Fuzzy logic in control systems: fuzzy logic controller – part 2, *IEEE Transactions on Systems Management and Cybernetics*, **20**, 2, March-April 1990, 419-435.

120. LEMBESSIS E, Dynamic leaning behaviour of a rule-based self organising controller, PHD THESIS, Queen Mary College, 1984.

121. LLOYD J G, Water supply and sewerage systems: a severe problem in the north west, *The Public Health Engineer*, **6**, 4, October 1978, 256-264.

122. LOCKE D, Modern hydraulic power, *2nd Technical Meeting of BAARC*, Lancaster University, 24th June 1992.

123. MANDIC N J et al, Practical application of a heuristic fuzzy rule-based controller to the dynamic control of a robot arm, *IEE Proceedings*, **132**, Pt D, 4, July 1985, 190- 203.

124. MEEGAN A V, Structural localised repairs without excavation, The Public Health Engineer, **14**, 4, October 1986, 21- 23.

125. MEIERAN H B et al, Mobile robots designed for hazardous environments, *Robotics Engineering*, March 1986, 10-16.

126. MEIERAN H B, How mobile robots have helped at Chernobyl and other accidents, *Nuclear Engineering International*, April 1988, 21-26.

127. MEIERAN H et al, Robots: l'embrras de richesses, *Nuclear Engineering International*, March 1989, 38-52.

128. MEIERAN H, Looking beyond the robot hype, *Nuclear Engineering International*, March 1989, 41-43.

129. MIRZAI A R et al, An overview of the applications of neural networks in process engineering, *Computing and Control Engineering Journal*, May 1992, 105-108.

130. MORAWSKI P, 2D object acquisition using circular scanning, *Pattern Recognition*, **17**, 3, 1984, 321-330.

131. MOSELLNI O et al, Robotics in construction: implementation and economic evaluation, *Canadian Journal of Civil Engineering*, 16, 1989, 678-683.

132. MOSS G F, Research and development in sewerage - 1. latest developments in sewer renovation, *The Public Health Engineer*, **11**, 2, April, 1983, 31-34.

133. MOSS G F, Sewerage rehabilitation: the way forward, *The Public Health Engineer*, **13**, 3, July 1985, 157-160.

134. MUEHLENFELD E, Robot vision by a contour sensor with associative memory, *Pattern Recognition*, **17**, 1, 1984, 169-176.

135. MUSPRATT M A, Hitech for engineering and implications for management decision making, *Applied Construction Management*, 1989, 89-101.

136. MUSPRATT M A, Robot ensembles for building construction, *Robotica*, 6, 1988, 275-284.

137. NAGHDY F., BALDWIN S. D., Simulation of locomotion on GRASP, *Automation In Construction*, **1**, 1, May 1992, 83-96.

138. NATIONAL WATER COUNCIL, *Manual of Sewer Condition Classification*, London, May 1980.

139. NATIONAL WATER COUNCIL, *Sewers and Water Mains - A National Assessment*, London, June 1977.

140. NICHOLLS H R et al, Virtual devices and intelligent gripper control in robotics, *Robotica*, 7, 1989, 199-204.

141. NORTH R C, Economic approach (finance options), *Proceedings of Symposium on Deterioration of Underground Assets, the Institution of Water Engineers and Scientists*, 7th and 8th December 1983, Chameleon press, 11.1-11.10

142. NOYCE K W et al, Maintenance of sewers - is it worth it?, *The Public Health Engineer*, **7**, 1, January 1979, 24-27.

143. NYMAN D H, Meeting the challenge of hostile environments, *Robotics Today*, October 1987, 23-24.

144. OHTA Y et al, Stereo by two-level dynamic programming, *Proceedings of the Ninth International Joint Conference on Artificial Intelligence*, Los Angeles California, 18th-23rd August 1985, 1120-1126.

145. PALER K et al, Local ordered grey levels as an aid to corner detection, *Proceedings of 4th International Conference on Robot Vision and Sensory Controls*, London, 1984, 351-360.

146. PARKINSON J, Dirty work in Mineheads sewers, *New Civil Engineer*, 15th April 1985, 32-34

147. PAVELEK I M D, Operations and achievements of remote equipment at three mile island unit 2, *Nuclear Technology*, 87, November 1989, 1122-1133 .

148. PETTIPHER, M., Tapping knowledge, *New Civil Engineer*, 1993, 17th June, 21.

149. PINKAVA J, Towards a theory of sensory robotics, *Robotica*, 8, 1989, 254-256.

150. PLANT M G, Sewers for adoption: developers viewpoint, *The Public Health Engineer*, **14**, 4, October 1986, 11-12.

151. POLLARD, S. B., PRIDMORE, T., PORRILL, J., MAYHEW, J. E. W., FRISBY, J. P., Geometrical modelling from multiple stereo views, *The International Journal of Robotics Research*, **8**, 4, August 1989, 3-32.

152. PORRILL, J., POLLARD, S.B., PRIDMORE, T.P., BOWEN, J., MAYHEW, J.E.W. AND FRISBY J.P., TINA: a 3d vision system for pick and place, *Image and Vision Computing*, 1988, **6**, 2, 91-99.

153. POULSON B C et al, Simulating construction robot agents and their knowledge environment, *ASCE Journal Comp in Civil Engineering*, **3** , 4, October 1989, 303-319.

154. POULSON C B, Automation and robotics for construction, *Journal of Construction Engineering and Management*, 111, **3**, 1985, 190-207.

155. PRIDMORE T P et al, Exploiting image-plane data in the interpretation of edge-based binocular disparity, *Computer Vision Graphics and Image Processing*, 52, 1990, 1-25.

156. PRIDMORE T P et al, Segmentation and description of binocularly viewed contours, *Image and Vision Computing*, **5**, 2, May 1987, 132-138.

157. PRIDMORE T P, *Understanding Images - An Introduction to Computer Vision*, a short course, School of Engineering I T, Sheffield Hallam University, (1992).

158. PRIDMORE, T.P., COOPER, D., AND TAYLOR, N, Estimating camera orientation from vanishing point location during sewer surveys, *Automation In Construction*, 1997, 5, 407-419.

159. PRIDMORE, T.P., PORRILL, J. AND MAYHEW, J.E.W., Segmentation and description of binocularly viewed contours, *Image and Vision Computing*, 1987, **5**, 2, 132-138.

160. PROCYK T J et al, A linguistic self-organising process controller, *Automatica*, 15, 1979, 15-30.

161. PROCYK T J, A self organizing controller for dynamic processes, PhD THESIS, University of London, 1977

162. READ G F, Sewer renovation and reconstruction in Manchester, *Municipal Engineer*, June 1984, 27-38.

163. REED E C, The assessment of the problem in the UK, *Restoration of Sewerage Systems*, ICE, Thomas Telford Ltd, London, 1982, 3-8.

164. REES D F, The state of the nations sewers, *The Public Health Engineer*, **7**, 1, January 1979, 29-30.

165. ROBERTS L G, Machine perception of three dimensional solids, *Optical and Electro-Optical Information Processing*, ma : MIT press, 1965.

166. ROSENFELD A, Machine vision for industry: concepts and techniques, *Robotics Today*, December 1985, 19-22

167. ROSIN P L et al, Segmentation of edges into lines and arcs, *Image and Vision Computing*, **7**, 2, May 1989, 109-114.

168. RUSHBROOKE J N et al, Classification of defects observed in sewer systems, *The Public Health Engineer*, **9**, 1, January 1981, 14-17.

169. RUSSELL A., CANT J., A robotic workout, *Surveyor*, 22nd July 1993, 19-21.

170. SALAGNAC J L, A general purpose positioning system for construction robotics, Proceedings 6th International Symposium on Automation and Robotics in Construction, June 1989, 396-403.

171. SCHREIBER R R, Reaping the benefits of vision, *Robotics Today*, December 1985, 26-27.

172. SHERIDAN T B, Telerobotics, *Automatica*, **25**, 4, 1989, 487-507.

173. SHIOKAWA T et al, Navigation / positioning control of mobile robots for construction, *Proceedings of the 5th International Symposium on Robotics in Construction*, 6th-8th June, Tokyo, 1988, 589-598.

174. SIAS F R JR et al, Mobile robot survival, *IEEE*, 8, 1988, 497-501.

175. SILVERMAN E B, Robotic and remotely operated technology in hazardous waste sites, Robotics Engineering, March 1986, 22-24.

176. SKEAL W O, editor, *Manual of British Water Engineering Practice*, 4th Edition, The Institution of Water Engineers, London, 1969.

177. SKIBNIEWSKI M J et al, Robotic applications to construction, *Cost Engineering*, **31**, 6, June, 1989, 10-18.

178. SKIBNIEWSKI M J, *Robotics in Civil Engineering*, Van Nostrand Rheinhold, 1988.

179. SLIWINSKA D et al, Some problems of the shape of fuzzy sets and the dimension of a model with respect to its adequacy, *Fuzzy Sets and Systems*, **26**, 1, April, 1988, 63-83.

180. SMITH D J, Robots reduce radiation exposure in nuclear maintenance, *Power Engineering*, July 1989, 22-28.

181. SMITHSON M, Fuzzy set theory and the social sciences: the scope for applications, *Fuzzy Sets and Systems*, **26**, 1, April 1988, 1-21.

182. SOBECK R P, A robot planning structure using production rules, *Proceedings of the Ninth International Joint Conference on Artificial Intelligence*, Los Angeles California, 18th - 23rd August 1985, 2, 1103-1105.

183. SOCKMAN G, Object recognition and localisation via pose clustering, *Computer Vision Graphics and Image Processing*, 40, 1987, 361-387.

184. STAUFFER R N, Robotics technology being drafted for combat and support functions, *Robotics Today*, December 1985, 31- 33.

185. STAUNTON R C et al, A comparison between square and hexagonal sampling methods for pipeline image processing, *SPIE Optics Illumination and Image Sensing for Machine Vision IV*, 1989, 142-151.

186. STONECIPHER K, *Industrial Robotics Machine Vision and Artificial Intelligence*, Howard W Sams & Company, 1989.

187. SUTTON R, A design study of a self-organising fuzzy autopilot for ship control, *Proceedings Institution of Mechanical. Engineers*, Part 1, **205**, 1991, 35-47.

188. SWONGER C W, Machine vision, *Robotics Today*, December 1986, 14-15.

189. TAGARE H D et al, A theory of photometric stereo for a class of diffuse non-lambertian surfaces, *IEEE Transactions on Pattern Analysis and Machine Intelligence*, **13**, 2, February 1991, 133-151.

190. TAGARE H D et al, Non-lambertian shading and photometric stereo, *SPIE*, 1260, 1990, 100-111.

191. TAYLOR N et al, Automatic visual detection of lateral junctions in sewers, *Proceedings Institution of Civil Engineers, Water, Marine and Energy*, 130, June 1998, 56-69.

192. TAYLOR N, Dover's smart bridge, *Proceedings of the Institution of Mechanical Engineers*, **206**, 1992, 9-18.

193. TAYLOR N, *The Discrete Methods of Structural Analysis*, PhD THESIS, UCL, 1974.

194. TAYLOR, N., DRAPER, R., BROADHURST, S. J., MALLINDER, P. A., Static and kinematic limit states of masonry vaults, *The Centenary Year Bridge Conference Proceedings*, University of Wales College of Cardiff, Elesvier, 1994, 181-186.

195. THE INSTITUTION OF CIVIL ENGINEERS, *Restoration of Sewerage Systems*, Thomas Telford Ltd, London, 1982.

196. TONG R M, A retrospective view of fuzzy control systems, *Fuzzy Sets and Systems*, 14, 1984, 199-210.

197. TURNER R, *Logics For Artificial Intelligence*, Ellis Horwood Limited, 1984.

198. VARLEY J, End to the clean-up programme in sight, *Nuclear Engineering International*, March 1989, 27-33.

199. VARLEY J, No easy answers to Chernobyl questions, *Nuclear Engineering International*, June 1991, pp 34-37.

200. VEPA R, The architecture of knowledge bases required for implementing expert control systems, *IEE Colloquium on Knowledge-Based Control: Principles and Applications*, 1991.

201. VERTUT J et al, *Robot Technology - Teleoperation and Robotics: Evolution and Development*, Kogan Page, London, 1984

202. WALLACE A M, Industrial applications of computer vision since 1982, *IEE Proceedings*, **135**, Part E, 3, May 1988, 117-135.

203. WALLACE R et al, First results in robot road-following, *Proceedings of the Ninth International Joint Conference on Artificial Intelligence*, Los Angeles California, 18th - 23rd August 1985, 2, 1089-1095.

204. WANG K et al, Structure design and kinematics of a robot manipulator, *Robotica*, 6, 1988, pp 299-309.

205. WARD C R et al, Examples of robots and teleoperators at the savannah river site, IEEE Transactions on Nuclear Science, **37**, 3, June 1990, 1437-1442 .

206. WARING JR G E, *Sewerage and Land Drainage*, 3rd Edition, E & F N Spon, London, 1891.

207. WARSZAWSKI A, Robots in the construction industry, *Robotica*, **4**, (1986), 181-188.

208. WATER INDUSTRY TRAINING ASSOCIATION, *Training Course Manual For Sewerage Rehabilitation - Structural Assessment and Sewer Renovation*, **4**, March 1987.

209. WATER RESEARCH CENTRE, *Sewer Rehabilitation Manual*, Swindon, 1983.

210. WATER RESEARCH CENTRE, *Sewer Renovation*, Swindon, 1978.

211. WATSON R, Futuristic fisheye camera takes Pearpoint forward, *Underground*, March 1989, 14-16

212. WATSON R, Northern liner, *New Civil Engineer*, 18th January 1990, 36-38

213. WATSON R, Nuclear industry repairs lead way for utility robotics, *Underground*, December 1988, 25-27.

214. WATTS I L, Recent sewer renovation at oxford using semi-remote drain reconnection, *The Public Health Engineer*, **10**, 1, January 1982, 41-44.

215. WEHE D K et al, Intelligent robotics and remote systems for the nuclear industry, *Nuclear Engineering and Design*, 113, 1989, 259-267.

216. WHITE J B, *Wastewater Engineering*, 3rd Edition, Edward Arnold, 1987.

217. WHITE J, Surbot surveys browns ferry, *Nuclear Engineering International*, March 1989, 52.

218. WING R D, Robots in the construction industry - a state of the art review, *Proceedings of the Institution of Civil Engineers Part 1*, **86**, October 1989, 937-952.

219. WINNEY M, New sonar survey cracks flooded pipe problems, *Underground*, March 1989, 18-19

220. WITKIN A P, Intensity based edge classification, *Proceedings AAAI-82*, 1982, 36 to 41

221. WOODHAM, R J, Photometric method for determining surface orientation from multiple images, *Optical Engineering*, January / February 1980, **19**, 1, 301 – 306.

222. WOODHAM, R. J., Analysing images of curved surfaces, *Artificial Intelligence*, **17**, 1981, 117-140.

223. ZIEGLER J G, N B NICHOLS, Optimum settings for automatic controllers, *Transactions of the ASME*, November 1942, 759-768.

224. ZUECH N, Machine vision, *Robotics Today*, April 1986, 35-36.